12-2016

Modeling the impact of land surface feedbacks on post landfall tropical cyclones

Subashini Subramanian
Purdue University

Graduate School Form
30 Updated 12/26/2015

PURDUE UNIVERSITY
GRADUATE SCHOOL
Thesis/Dissertation Acceptance

This is to certify that the thesis/dissertation prepared

By Subashini Subramanian

Entitled

MODELING THE IMPACT OF LAND SURFACE FEEDBACKS ON LAND FALLING TROPICAL CYCLONES

For the degree of Doctor of Philosophy

Is approved by the final examining committee:

Harshvardhan
Chair

Dev Niyogi

Rao S. Govindaraju

Sundararaman Gopalakrishnan

To the best of my knowledge and as understood by the student in the Thesis/Dissertation Agreement, Publication Delay, and Certification Disclaimer (Graduate School Form 32), this thesis/dissertation adheres to the provisions of Purdue University's "Policy of Integrity in Research" and the use of copyright material.

Approved by Major Professor(s): Dev Niyogi

Approved by: Indrajeet Chaubey 10/13/2016

Head of the Departmental Graduate Program Date

MODELING THE IMPACT OF LAND SURFACE FEEDBACKS ON POST LANDFALL TROPICAL CYCLONES

A Dissertation

Submitted to the Faculty

of

Purdue University

by

Subashini Subramanian

In Partial Fulfillment of the

Requirements for the Degree

of

Doctor of Philosophy

December 2016

Purdue University

West Lafayette, Indiana

To Appa.

ACKNOWLEDGEMENTS

There is certainly quite a long list of people whom I am thankful for. Special thanks to my advisor Dev Niyogi. I would like to acknowledge the support of my committee members Sundararaman Gopalakrishnan, Harshvardhan and Rao S. Govindaraju. Without the encouragements and collaboration from Frank Marks of HRD, Vijay Tallapragada and Mike Ek at NCEP/ EMC and U.C. Mohanty of IIT Bhubaneswar this dissertation wouldn't have been possible. Further acknowledgement to NSF CAREER grant (NSF CAREER – 0847472) and NSF R2O (Research to Operations) supplement, Indo-US Science and Technology Foundation (IUSTF), NOAA's Hurricane Forecast Improvement Program (HFIP) and Earth System Science Organization, Ministry of Earth Sciences, Government of India (Grant no./ 259 Project no MM/SERP/CNRS/2013/INT-10/002).

I started this research work without a formal training in atmospheric science and I would be amiss if I did not acknowledge Krishna Osuri (India team) for getting me started on my research topic and being around night or day to answer any of my questions. I would also like to thank Samuel Trahan at EMC for answering the innumerable questions that I had on HWRF and for his help in putting a roof over my head during my stint at NCEP. Thanks also to my friends and fellow lab mates especially Xing Liu and Elin Karlsson. They have always been there for me whenever I wanted to bounce off ideas or simply to

ramble on about life. For me, it was a huge source of strength just knowing my friends, Nithya, Pooja and Manasi will be around no matter what. I will be whacked if say thanks. All these people have become my family away from my home in India.

Finally, I am truly grateful and thank my stars for my family, my mother Geetha, who has supported me in all of my endeavors (good ones and the nutty one), my brother Srikanth, my alter ego and the calm head I need during troubled times, and my husband Girish, who makes me look beyond, into the future, makes me believe and dream.

TABLE OF CONTENTS

Page

Page

Page

APPENDICES

LIST OF TABLES

LIST OF FIGURES

Figure Page

Figure Page

Figure Page

Figure Page

Figure Page

Figure Page

Figure Page

Figure Page

LIST OF ABBREVIATIONS

HWRF	Hurricane Weather Research and Forecasting Model
TC	Tropical Cyclone
SST	Sea Surface Temperature
TS	Tropical Storm
WRF	Weather Research and Forecasting Model
ARW	Advanced Research WRF
LHF	Latent Heat Flux
SHF	Sensible Heat Flux
PBL	Planetary Boundary Layer
ABL	Atmospheric Boundary Layer
SM	Soil Moisture
ST	Soil Temperature
IMR	Indian Monsoon Region
LSM	Land Surface Model
GFDL	Geophysical Fluid Dynamics Laboratory
DTC	Development Testbed Center
NCEP	National Centers for Environmental Predictions
CAPE	Convective Available Potential Energy
LCLUC	Land Cover Land Use Change
NWP	Numerical Weather Prediction

ABSTRACT

Subramanian, Subashini. Ph.D., Purdue University, December 2016. Modeling the Impact of Land Surface Feedbacks on Post Landfall Tropical Cyclones. Major Professor: Dev Niyogi.

The land surface is an important component of numerical models. The land surface models are modules that control energy partitioning, compute surface exchange coefficients and form the only physical boundary in a regional scale numerical model. Thus, an accurate representation of land surface is critical to compute surface fluxes, represent the boundary layer evolution and affect changes in weather systems. Land surface can affect landfalling tropical cyclones in two ways: (i) when the cyclone is offshore and land can influence cyclones by introducing dry (or moist) air that can weaken (or strengthen) the organized convective structure of cyclones, and (ii) land can affect the evolution of cyclones post landfall by modifying the surface heat fluxes and introducing additional surface drag. In this dissertation, the hypothesis that improved representation of land surface conditions will improve the prediction of landfalling tropical cyclones is tested. To that effect, a comprehensive review of land surface effects on tropical cyclones was undertaken and an idealized study was conducted to study the impact of antecedent soil temperature on the sustenance/reintensification of tropical cyclones over land. Rainfall verification for cyclone events over the Atlantic Ocean was conducted and a comparison study between land models – GFDL Slab and Noah, also

considers the sensitivity of tropical cyclone models to land surface parameterizations. The recent adoption of Noah land model with hydrology products in HWRF offers a unique opportunity to couple a river routing model to HWRF to provide streamflow estimations from the HWRF model and this dissertation has outlined techniques to real time predict streamflow for United States with HWRF forcing.

Results from this dissertation research indicate antecedent land surface conditions can affect tropical cyclone evolution post landfall and high soil temperature and thermally diffusive soil texture of land surface are critical factors contributing to re-intensification/ sustenance of tropical cyclones. This idealized study, in addition to enabling improved understanding of the land surface effects on cyclones, has also led to a developmental effort to incorporate landfalling capability in the idealized framework of HWRF model and is available for use for the wider tropical cyclone community. The development of river routing coupled HWRF model could also be used in the operational mode to improve flooding and streamflow predictions and efforts are underway to integrate this new capability in HWRF. Study findings contribute to the understanding regarding the effects of land surface on landfalling cyclones and helps translate research products into HWRF's operational framework for predicting tropical cyclones.

CHAPTER 1. INTRODUCTION

1.1 Motivation

There has been considerable push in the last decade to harness the scientific and technological advancements to understand and model complex issues of land approaching and post landfall evolution of TCs. Most of the recent efforts in modeling TCs have justifiably focused on achieving high accuracy in cyclone track and intensity predictions while second order, albeit highly critical rainfall forecasts, landfall studies have taken a back stage. With considerable gains now in track and intensity predictions, the focus has shifted to rainfall prediction, and in particular to the land surface effects on landfalling TCs and inland rain and floods have emerged as critical aspects to coordinate risk and disaster management operations. This issue has attained greater urgency after Superstorm Sandy (2012) where considerable damage was caused by coastal flooding complicated by both inland rainfall and storm surge. The need for improved TC landfall prediction is a top priority for hazard communities to provide accurate forecasts for dissemination to the general public, disaster management and mitigation authorities.

1.2 Dissertation Objective

Study objective is to investigate the role of antecedent land conditions on the post-landfall characteristics of TCs. The study seeks to understand how landfalling TCs are

modulated by antecedent land conditions, and if rainfall predictions over land can be improved by incorporating improved land models in hurricane models.

The study hypothesis that "*Enhanced representation of land surface conditions will improve the prediction of landfalling TCs, particularly their track and inland precipitation*" will be tested.

This dissertation will specifically seek to answer the following questions –

1. How does land surface affect TC systems? What is the available body of research?
2. How does the antecedent land state cause TC sustenance/ re-intensification over land?
3. What is the ability of current TC prediction models to accurately simulate the land surface processes and does enhanced representation of land surface in numerical models improve track, intensity and rainfall predictions?
4. By implementing an enhanced land model in a tropical cyclone model, can we achieve seamless integration of hydro-meteorological forecast for flood and inundation?

This research topic is quire unique in the sense that much of the research revolved around the express belief that research should be effectively transitioned into operations and products generated through this dissertation could be used by the larger community. To this effect, with a strong collaborative partnership with tropical cyclone research and operations community in both USA and India, most of the research components in this dissertation have a foundation on requirements and needs of the tropical cyclone operational community. Much of the effort described in the following chapters are

directly transferable into an operational setting and can be adapted to improve the understanding of landfalling tropical cyclones.

1.3 Structure of the Dissertation

The dissertation is organized as follows: the following chapter provides a comprehensive literary review of land surface models, land surface physics and some of prior studies that have focused on the impact of land state on convective systems and tropical cyclones. Chapter 3 contains a primer on tropical cyclones and will discuss the genesis, structure, energetics and the life cycle of tropical cyclones. Chapter 4 provides an overview of the Hurricane Weather and Forecasting Model (HWRF), the main modeling tool used for the PhD research. It also contains a primer on the landfalling capability that was developed for the idealized HWRF framework to specifically study the impact of land surface on tropical cyclones. Chapter 5 discusses an idealized study to assess the impact of land state on tropical cyclones and specially focusses on the antecedent soil temperature and soil moisture feedback on post landfall sustenance of tropical cyclones. This chapter will also discuss a case study to test the hypothesis. Chapter 6 is a rainfall verification study that compares two different land surface models on simulating landfalling tropical cyclones over the north Atlantic basin. Chapter 7 provides a research to operations application to couple streamflow model to HWRF for real time flooding and inundation models. A concluding chapter provides a summary, research implications and limitations and lay down the way for future research.

CHAPTER 2. THE ROLE OF LAND SURFACE PROCESSES ON TROPICAL CYCLONES: INTRODUCTION TO LAND SURFACE MODELS

2.1 Introduction

The role of land surface processes in land falling TCs is an area of emerging interest. TCs are formed as organized convection over warm water (typically 26.5°C, Gray 1968) packing tremendous amounts of energy. TCs have a typical size of 200-2000 km with a life span of about one to two weeks. The cyclone and its environment are interlinked. There are a number of environmental factors that are important for sustaining and intensifying a TC including low humidity, cooler sea surface temperature (SST), or higher tropopause temperatures, dry air intrusion from land masses, and large vertical wind shear (Gray, 1968; McBride and Zehr, 1981). However, a number of environmental conditions can change the evolution of a landfalling storm.

As TCs approach land, the situation becomes more complex. There are a multitude of inland heterogeneities such as soils, land use, and topography that can affect the boundary layer and mesoscale processes which can affect TC evolution. Additionally, landfalling storms have major socio-economic impacts which are dependent not just on wind and intensity but, also on the rainfall/flood potential. As stated in Emanuel et al. (2006), rainfall, storm water flooding, storm surges, and damaging winds associated with TCs and depressions over land continue to be the greatest threat to loss of life and

property in regions prone to them. While cyclone track prediction has improved considerably over the past few decades due to advances in numerical weather prediction, enhanced atmospheric observations, and data assimilation, the skill in prediction of TC intensity has not similarly improved (Marks and Shay, 1998). Track prediction often depends on the large-scale environment, with intensity being a function of multi-scale interactions that include processes that are active at inner-core/ cloud scale, mesoscale, sub-synoptic, and synoptic (large) scales. Some possible scenarios in cyclone evolution as it approaches land/coastal areas are shown in Figure 2.1.

TCs typically decay as they approach land by encountering unfavorable synoptic conditions such as depletion of its energy source and friction across the surface distorting inflow which leads to weakening of the eye (Kaplan and DeMaria, 1995; Emanuel, 2000). Some storms can also transition into an extratropical cyclone and develop a cold core. In rare instances, the storms can redevelop or reintensify after making landfall by sustaining the necessary convection to maintain TC characteristics and in each of these scenarios, there is a distinct threat of rainfall and inundation over land. Heterogeneities in the land surface characteristics (e.g., soil moisture, surface roughness, albedo, vegetated land cover) can create mesoscale boundaries that can impact the related convection (Pielke, 2001; Emanuel et al., 2004). Whether the storm decays quickly after landfall or sustains its intensity over land, the land surface and its interaction with the TC and atmospheric environment is an important component of a landfalling TC research efforts. There are many studies highlighting the need for accurate representation of land-atmosphere interactions in models that affect atmospheric weather predictions and this

continues to be a critical issue as well. Numerical models lack the ability to accurately model converging overland tracks even though great strides have been made in ocean basin track forecasts (Marks and Shay, 1998).

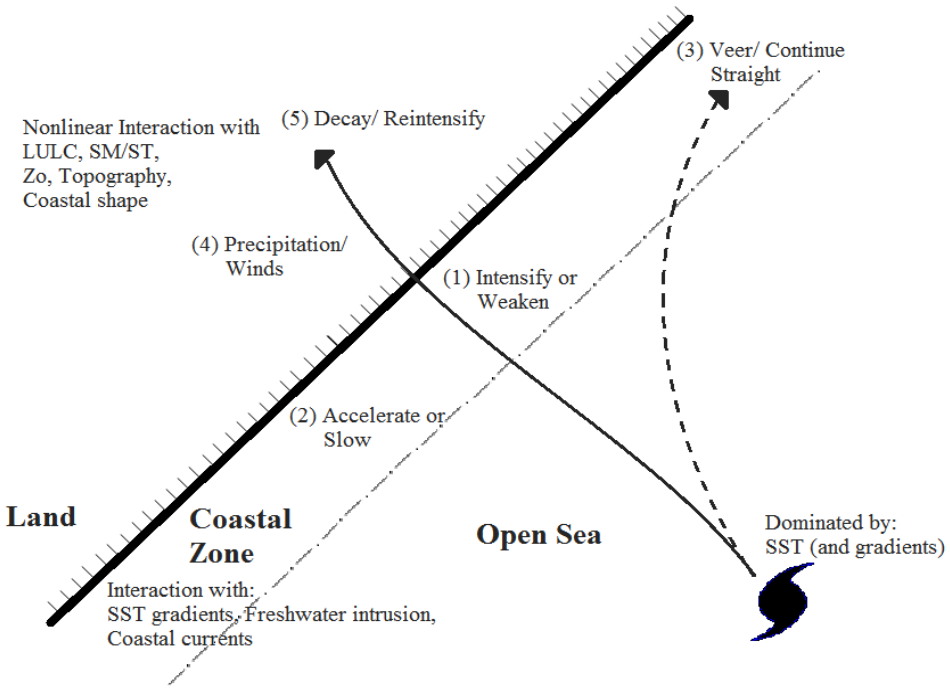

Figure 2.1 Illustration of some possible outcomes and factors in the evolution of a TC as it approaches land.

Numerical models continue to be important forecasting tools employed by the operational community to determine track movement and landfall location. However, uncertainty still exists since atmospheric models are not developed enough to capture and simulate the whole range of land-atmosphere interactions particularly at finer scales. Schade and Emanuel (1999) identified potential areas of improvement needed to enhance the overall quality of TC prediction including the storm's initial intensity and structure, the thermodynamic state of the storm's environment, and energy exchange between the

boundary layer and the storm. Recent modeling efforts by Emanuel et al. (2008) over Australia and Chang et al. (2009) over India suggests that the antecedent land surface settings can affect post landfall tropical cyclone structure because of the heat and moisture fluxes provided from warm (cold) and wet (dry) land surfaces. Numerous studies have contributed to the understanding of the role that large scale conditions play in the evolution of TCs (Zehnder, 1991; Breigel and Frank, 1997; Frank and Roundy, 2006).

Recent works have shown the importance of landscape processes in weather and climate (Werth and Avissar, 2005; Feddema, 2005; Alpert et al., 2006). Many studies have concluded that land surface characteristics such as topography, land use and land cover, soil temperature and moisture, albedo, emissivity and land surface roughness have considerable influence on convective systems (e.g., Pielke, 2001). Different land surface conditions result in different boundary layer structures and mesoscale atmospheric circulations. Numerous studies have acknowledged the influence of surface conditions on drylines, fronts, low-level jets, capping inversions, and convective storms (Mahfouf et al., 1987; Pielke et al., 1991; Avissar and Liu, 1996; Chase et al., 1999). Although a few studies suggest realistic representation of landscape heterogeneities have no bearing on boundary layer characteristics (Zhong and Doran, 1998; Doran and Zhong, 2000), observational and modelling work by Weaver and Avissar (2001) document that landscape heterogeneity does produce organized cumulus convection using the same model applied by Doran and Zhong. In summary, over the last decade, accurate

representation of land surface feedbacks has become a critical component of state-of-the-art NWP models.

A broad objective of this chapter is to summarize some of the recent scientific progress made on land surface processes and landfalling TCs. Beginning with global surface energy budgets, a brief primer on the atmospheric boundary layer is included with an introduction to land surface schemes used in weather models.

2.2 Surface Energy Budget

Weather and climate in general is fueled by solar radiation and controlled by the amount and distribution of energy radiation. Incoming radiation is scattered, reflected, and absorbed by clouds, atmospheric gases and aerosols. The radiation transmitted by the atmosphere may either be absorbed or reflected back by the Earth's surface. The land surface partitions shortwave radiation into sensible heat flux, latent heat flux and ground heat flux to be stored by the surface before being reflected back as longwave radiation (see Figure 2.2). Energy may be stored in various forms and converted to different types, giving rise to a broad variety of weather or turbulent phenomena in the atmosphere. The important interaction between the land surface and atmosphere is the exchange of radiation, sensible heat, latent heat, and momentum fluxes. Land-surface feedback mainly impacts the surface energy and water budgets from the boundary layer perspective.

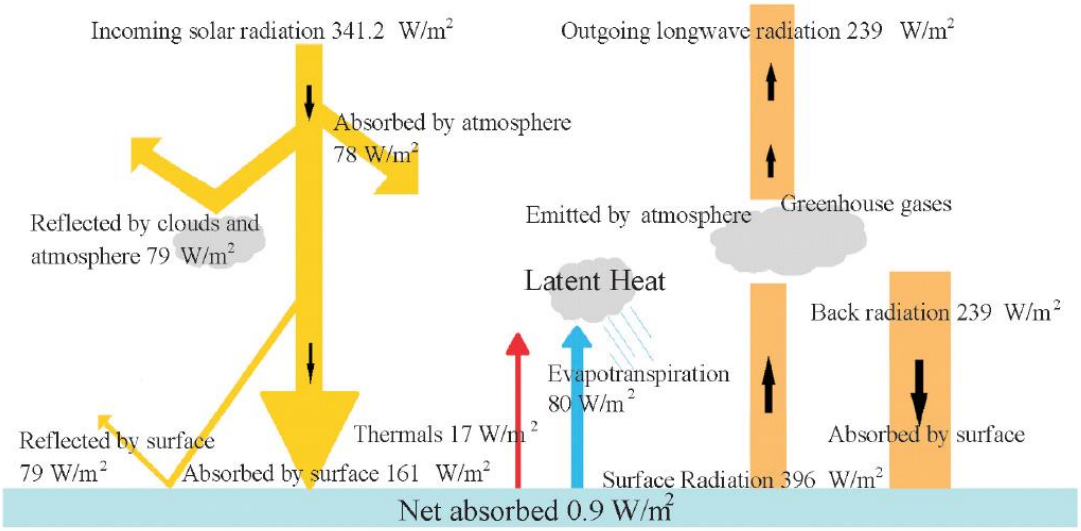

Figure 2.2 The global annual mean Earth's energy budget. The broad arrows indicate the schematic flow of energy in proportion to their importance. (Modified from Trenberth et al., 2009)

The energy budget is not the only component driving the Earth's system. The global water cycle also plays an important role in transporting energy and moisture to the atmosphere from the surface. The total radiation absorbed by the land surface is balanced by emissions of thermal, infrared radiation to the atmosphere, latent heat associated with evaporation and transpiration, and sensible heat and diffusion of energy into soil. At the idealized land surface (e.g., if the land surface is flat, bare, and opaque to radiation), the surface net radiation can be expressed as the sum of sensible, latent, and ground heat fluxes. However, in reality, the surface is covered by vegetation, buildings, and water, which are opaque to radiation and has a significant heat capacity.

At the idealized surface, the net downward radiative flux (shortwave and longwave),

R_n *= Sensible heat flux (*H_S*) +Latent heat flux (*H_L*) + Ground heat flux (*H_G*)*

or

$R_n = H_S + H_L + H_G$

The ***Bowen ratio,*** $B = H_S/H_L$

Under real surface conditions, the land surface with plant canopy or other features can store some energy. When considering canopy, it is more appropriate to define an interfacial layer which includes such features. W(t) is the energy stored within this layer per unit area. The revised energy budget is:

$R_n = H_S + H_L + H_G + dW/dt$

The sensible heat flux, H_s, describes the heat flux from or to the land surface. The latent heat flux, H_L, describes the vertical transfer of moisture (water vapor) required for evaporation at the surface. Radiation and energy fluxes are considered positive if they transfer energy away from the Earth's surface (into the atmosphere), otherwise they are considered negative. All the terms in the above equation show strong variations in response to the diurnal cycle of heating and cooling at the surface. The turbulent (latent and sensible) fluxes and the ground heat flux are considered positive during daytime and negative during evening/night. During daytime, the land surface receives energy ($R_n > 0$) and is partitioned into the above mentioned three fluxes out of which the sensible and latent heat fluxes are directed upward (into the atmosphere) and the ground heat flux into the surface. The partitioning of the energy fluxes depends on many factors such as land surface characteristics (soil texture, type, vegetation, soil moisture, etc.), geographical

location (latitude), season, thermal properties (albedo and emissivity), time of day and of course, local weather (Noilhan and Planton, 1989). For example, in an irrigating field, due to an abundance of soil moisture, the latent heat flux increases due to evaporative cooling of the wet surface and sometimes may exceed the net radiation. The sensible and ground heat fluxes may become negative under such conditions. In contrast, the latent heat flux will be less and sensible heat flux will be greater in a desert region. During the evening/night, the surface loses energy as outgoing radiation which is compensated by the heat from the atmosphere/soil during the formation of dew as latent heat of condensation. Thus, these terms become negative. Comparing the magnitudes of latent and sensible heat fluxes, the energy balance terms are larger during the day and smaller during night time. However, ground heat flux can be assumed typically 10% of the net radiation. Over land, there is significant diurnal variation in surface energy budget and associated surface variables such as humidity and temperature (see Figure 2.3). Over large oceans, the large heat capacity of water and radiation absorption over large ocean depths reduce the diurnal variability of sea surface temperatures. Thus H_S and H_L varies little. The sea surface temperature of a tropical ocean varies as little as 3°C under normal conditions (Barale, 2010) while land surface the temperatures can vary an order of magnitude higher.

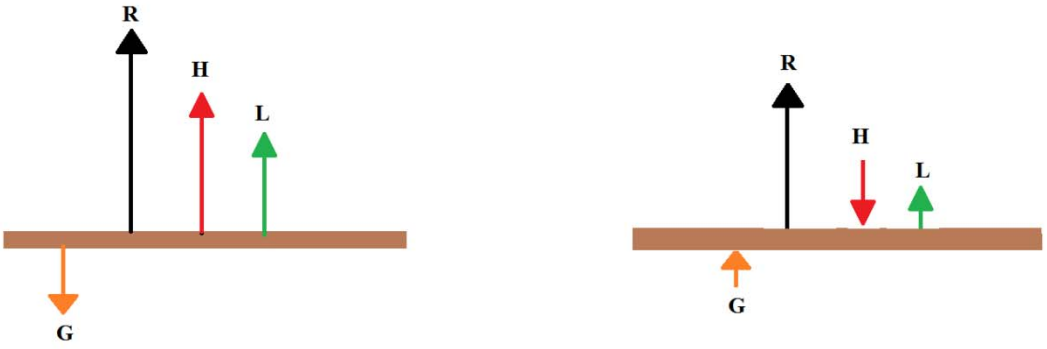

Figure 2.3 Schematic representation of typical surface energy budgets for daytime (left) and night time (right). (Adapted from Arya, 1988)

2.2.1 Examples of Energy Balance over Different Landscapes

The energy budget measured over a dry shrub land for a typical cloud free day in January and April is shown in Figure 2.4. In this case, latent heat fluxes are very small. During the day, as high amounts of sun's radiation gets absorbed by the earth's surface, the surface temperature rapidly increases. In the beginning, most of this heat is transferred into the deep layers of the soil, but as more radiation bears down on the surface, H_S dominates and the energy is transferred to the air thus, increasing the air temperature. The large differences in the surface and the air temperature allows for the flux transfer. Later at night, surface radiative cooling is balanced by increased outgoing ground heat flux. As the nocturnal boundary layer is comparatively stable (to daytime conditions), the sensible heat flux H_S is small.

The energy budget of a corn and soybean field for a day in January and April is shown in Figure 2.5. During the daytime, latent heat fluxes due to evaporation and transpiration

dominate i.e. (evapotranspiration). The increased latent heat fluxes can also help in cooling the surface when the sensible heat flux is downwards (during early morning and late afternoon). At night, both latent and sensible heat components are small and radiative cooling is balanced by ground heat flux.

Another example is for an evergreen needle leaf forest (Figure 2.6). Here, the latent heat and sensible heat diurnal profiles are similar during the day. The storage and ground heat flux become important and for deeper soil, the storage term dominates. At night, the release of heat from the trees and condensation (dew) balance the radiative energy loss.

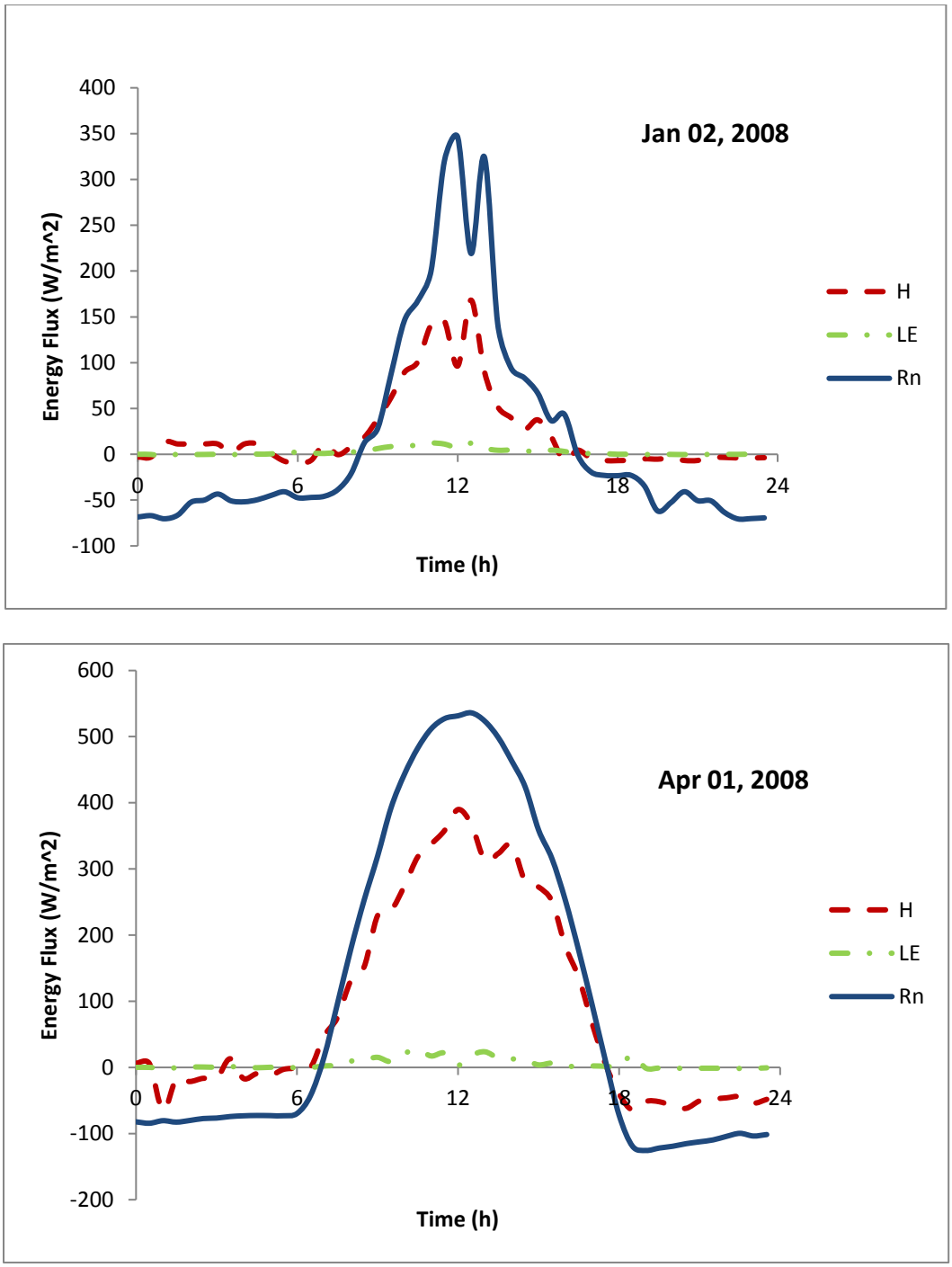

Figure 2.4 Observed diurnal energy balance over Sevilleta Desert shrub land in New Mexico USA Jan 02, 2008 (top) and Apr 01, 2008 (bottom). (Data source: Ameriflux)

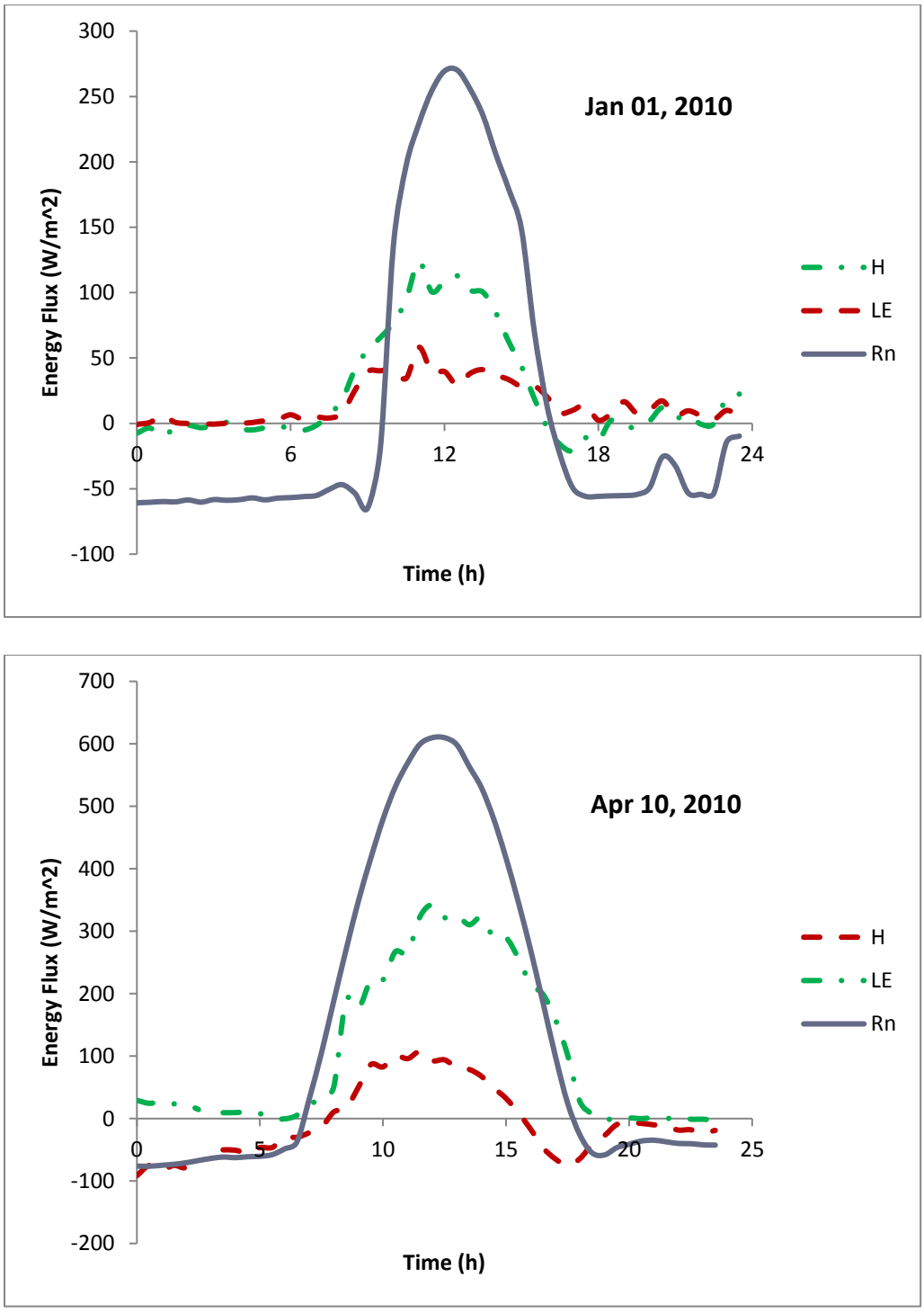

Figure 2.5 Observed diurnal energy budget of an agricultural field in Oklahoma, USA, on Jan 01, 2010 (top) and Apr 10, 2010 (bottom). (Data source: Ameriflux)

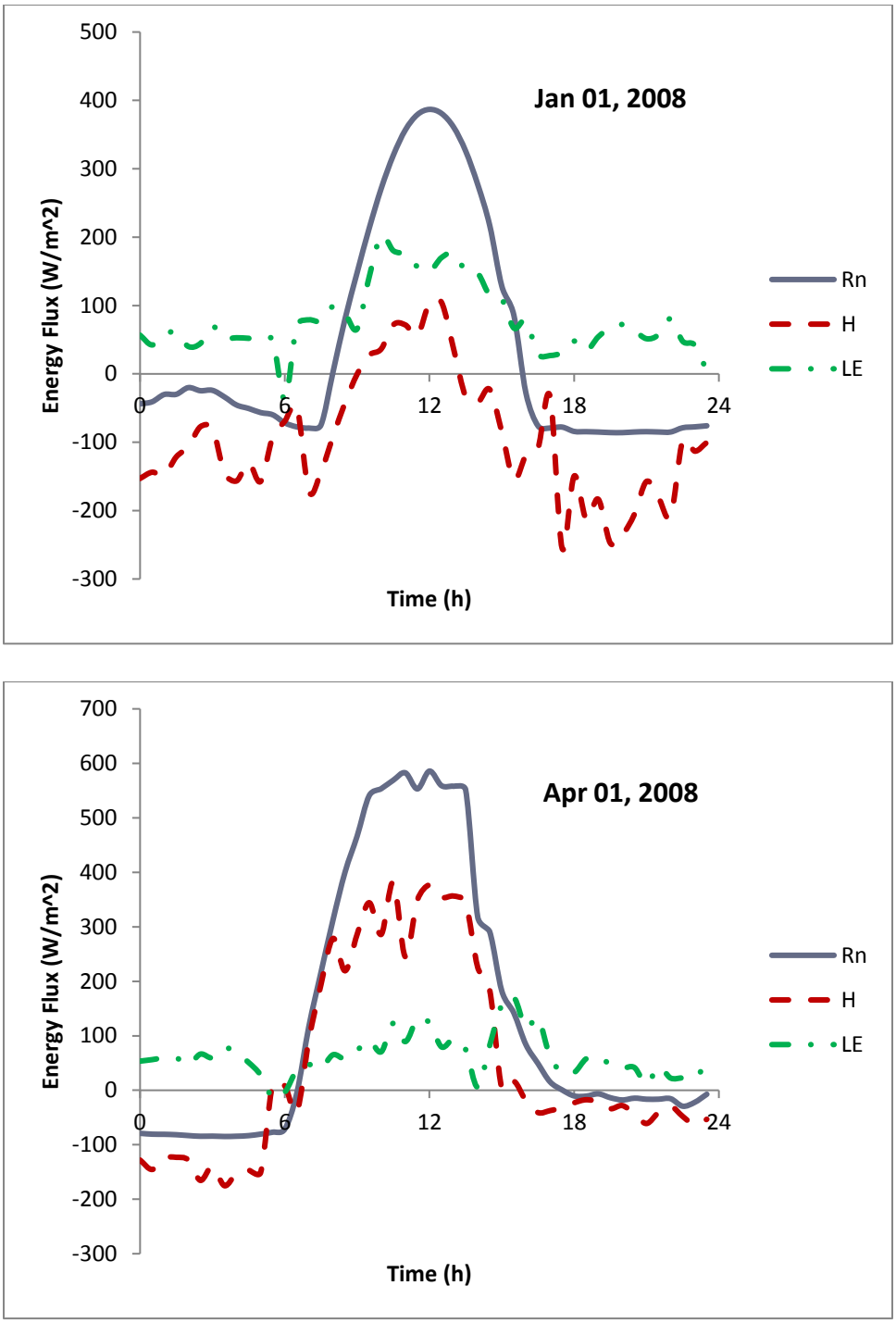

Figure 2.6 Observed diurnal energy budget of a needle leaf forest in Niwot Ridge, Colorado, USA, on Jan 01, 2008 (top) and Apr 01, 2008 (bottom). (Data source: Ameriflux)

2.2.2 Net Radiation at the Surface

The net radiation R_n is considered as the difference between incoming and outgoing short and longwave radiative fluxes. The net longwave flux depends upon the incoming longwave radiation $R_{L\downarrow}$, the surface emissivity ε_s. The net shortwave radiation depends on the surface incident solar radiation $R_{S\downarrow}$ and on albedo a_s, and the radiating temperature T_s-

$$R_n = R_{S\downarrow} - R_{S\uparrow} + R_{L\downarrow} - R_{L\uparrow} = (1 - a_s)R_{S\downarrow} + R_{L\downarrow} - \{(1 - \varepsilon_s)R_{L\downarrow} + \varepsilon s\sigma_s T_s^4\}$$

$$= (1 - a_s)R_{S\downarrow} + \varepsilon_s(R_{L\downarrow} - \sigma_s T_s^4)$$

... (2.1)

Thus, the surface characteristics critically influence R_n. Albedos vary considerable depending upon the surface, while emissivities normally approach 1.

2.2.3 Soil temperature and Surface Heat Flux

The surface or skin temperature is important for calculating the radiative balance of surface and for predicting moisture processes. The skin or surface temperature can be rather different from the air temperature, and is conventionally measured at 2 m from the surface. If there is a plant canopy or high surface heterogeneity, one cannot define a single surface temperature for that particular land surface. An apparent surface temperature can be obtained from the outgoing longwave flux if the surface emissivity is known. Large diurnal variations in surface temperature are achieved for bare, dry surfaces for clear calm conditions. Under stable conditions, surface temperatures can even each 50°C (under extremely dry conditions), while daybreak or dawn skin temperatures can drop to very low values. The surface temperature is related to the

temperature profile in the sub-surface medium, as illustrated in Figure 2.7. In a solid medium, the sub-surface temperature profile is governed by heat conduction. Deeper in the soil, the diurnal temperature cycle variability decreases and lags the skin temperature cycle.

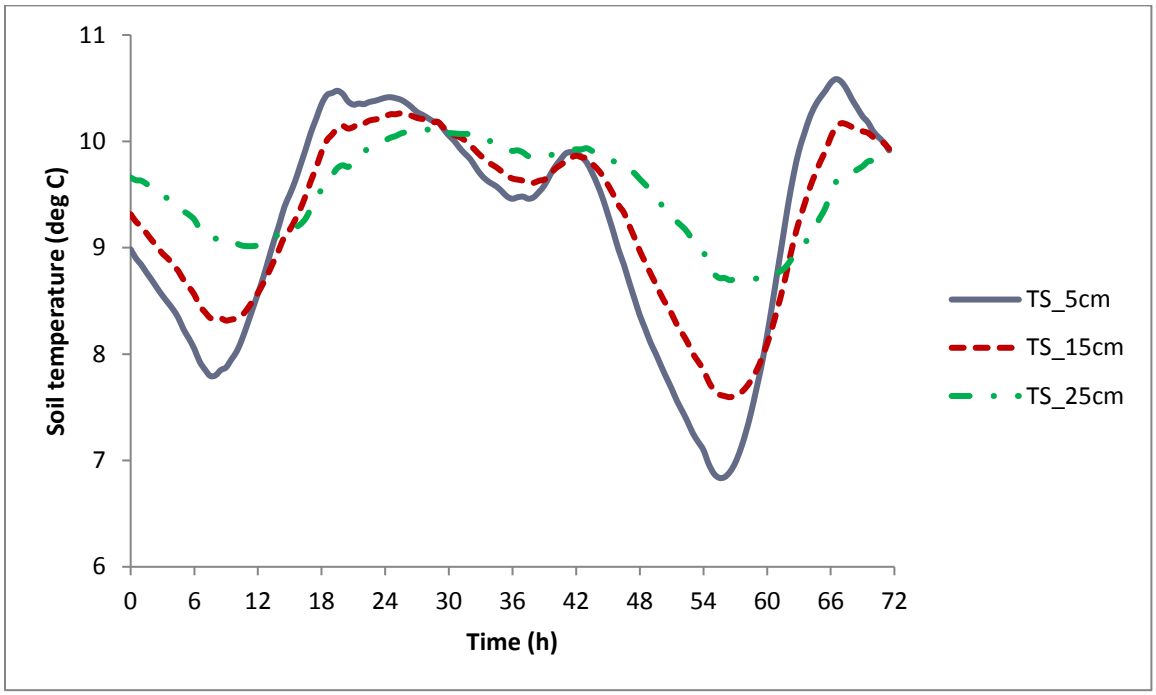

Figure 2.7 Observed diurnal course of subsurface soil temperatures at various depths in ARM SGP Main Ameriflux site (Vegetated Cropland) in Oklahoma USA, on Apr 01- 03, 2008 (data source: Ameriflux).

2.3 Boundary Layer

The land surface affects the surface energy balance, which in turn affects the eddies and the turbulent energy exchange within the atmosphere. The atmospheric layer in the vicinity of the land surface is affected by the surface energetics and has detectable turbulence exchanges. This layer can be considered as the atmospheric boundary layer and consists of the lower troposphere. The chief energy source for the Earth's water cycle

and the driving force behind boundary layer processes is incoming solar radiation. During daytime and under clear sky conditions, shortwave radiation heats up the Earth's surface creating rising and sinking parcels/plumes of warm air (also called eddies). This causes rapid expansion of the boundary layer height as the surface warms during the day and reaches a maximum height a few hours after solar noon. The height of a typical daytime boundary layer is between 1-2 km. During nighttime, the land cools at a faster rate than the air in the atmosphere resulting in lowering of turbulence consequently causing a collapse in boundary layer height (between 100-200 m). This is also the time when weak mixing occurs. The turbulence is considered to be present only within the boundary layer. Alternately, boundary layer height is also defined as the height of the largest eddy present in the layer.

Over the oceans, the diurnal variation in temperature is small. The boundary layer does not evolve much during the day and largely depends on synoptic conditions (high pressure or low pressure). This is also due to the fact that water has a large thermal capacity and absorbs most of the incoming radiation. Large-scale conditions, to an extent, also affect the boundary layer structure over land but evolution of boundary layer processes is largely influenced by diurnal variations in ground temperature. The major components of the ABL evolution are a surface layer that is over laid by (i) the mixed layer, (ii) the residual layer, and (iii) the stable boundary layer. The surface layer is typically considered 10% of the depth of the entire boundary layer and has roughly constant flux values or no flux divergence. The layer above the surface layer or the constant flux layer is dominated by vertical exchanges and mixing. There is also a thin

layer called the micro layer or the interfacial layer which is the lowest few centimeters of the air just above the ground where molecular transport is more significant than turbulent transport.

The mixed layer is convectively driven and occurs due to heating near the land surface and radiative cooling at the top. Warm air rises, mixes with the atmosphere, and cooling occurs at the top sending the cold air parcels back to the surface aiding the turbulent mixing. Heat, momentum and water vapor are well mixed leading to scalar quantities such as temperature and humidity is almost constant (see Figure 2.8).

Just before sunset, due to a decrease in incoming radiation, eddy thermals cease to form and turbulence weakens in the formerly well-mixed layer. The resulting layer is called a residual layer (see Figure 2.9) and is called so because the initial mean state variables and concentration variables such as humidity resemble the recently decayed mixed layer. Sometimes, over a period of a few days, additional moisture can accumulate in the residual layer through mixing during the day and storage during the night which can lead to formation of clouds in areas where they may normally not form.

As night progresses, the lower part of the residual layer which is in contact with the ground is transformed into a stable boundary layer characterized by very low turbulence and highly stable air. A stable boundary layer has a poorly defined top in contrast to the daytime mixed layer and blends smoothly into the residual layer. The profile of variables for daytime and night time are given in Figure 2.10.

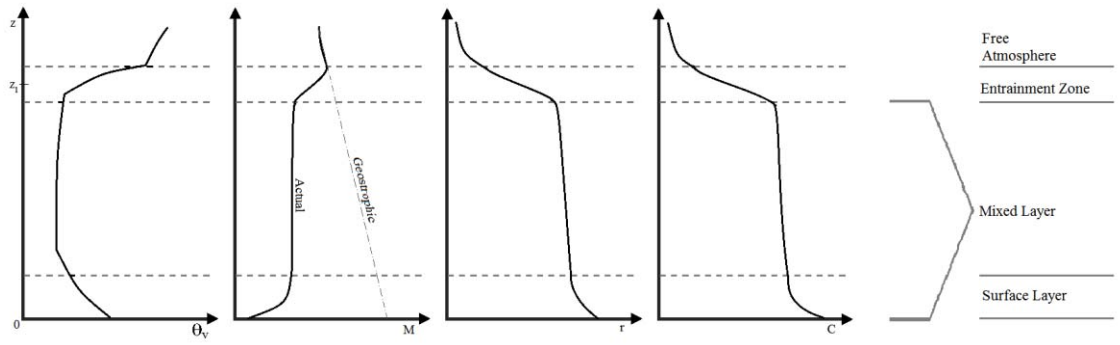

Figure 2.8 Typical daytime profiles of mean virtual potential temperature θ_v, wind speed M (where $M^2 = u^2+v^2$), water vapor mixing ratio r, and pollutant concentration C. (Redrawn from Stull 2012.)

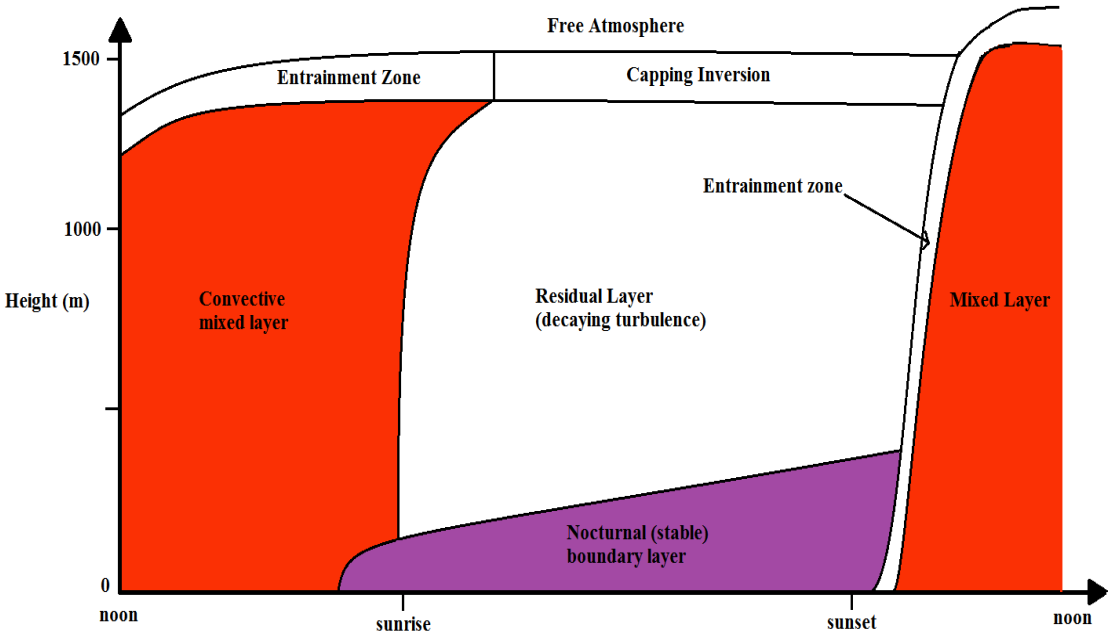

Figure 2.9 ABL evolution during a diurnal cycle. (Adapted from Stull, 2012)

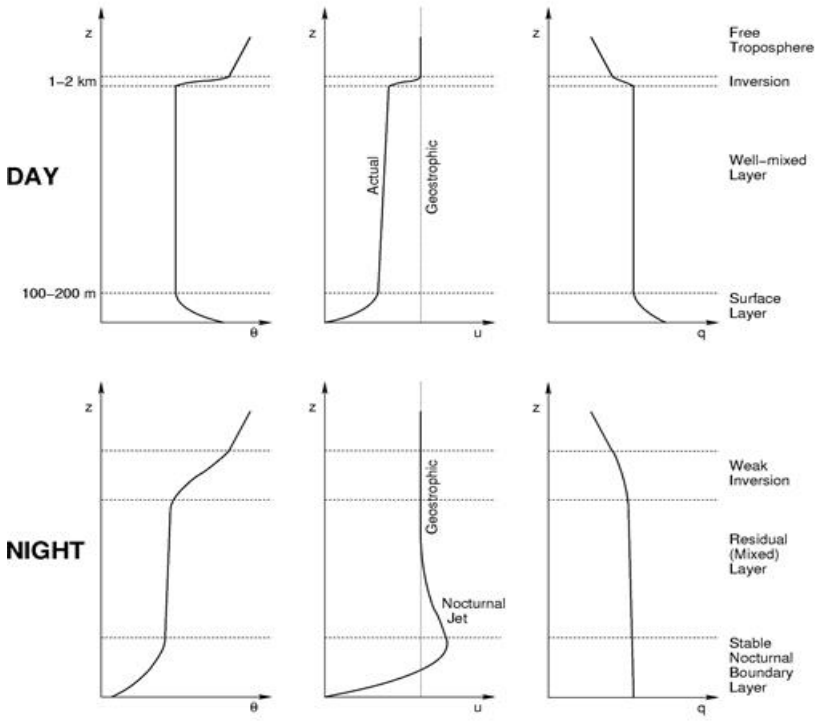

Figure 2.10 Typical day and nighttime profiles for potential temperature θ, mean winds *u*, and specific humidity *q*. The boundary layer and mixed layer are marked.

In fluid dynamics, a boundary layer is the layer next to a surface in which surface drag associated with friction is important (term introduced by Prandtl, 1905). Such boundary layers can be laminar or turbulent in nature, and are often very thin with only a few millimeters in thickness. In atmospheric models, a similar definition is used. The atmospheric boundary layer or planetary boundary layer is the vertical layer above the Earth's land surface in which momentum, heat and moisture fluxes are transferred through turbulent currents or eddies whose vertical extent is comparable to boundary layer depth, and whose circulation timescales extend to a few hours. A similar definition works for the boundary layer over the ocean. The complexity of this definition is due to several complex features when compared to classical fluid dynamics.

(i) Thermal convection due to surface heat exchange from the surface to the boundary layer.

(ii) Convection impacted by moisture and its related feedbacks in the boundary layer.

(iii) Rotation of earth and the effect of Coriolis force.

(iv) heterogeneous land surface and relief features.

In broad terms, the atmospheric boundary layer provides the surface and mixed layer which in turn provide the link and coupling for the land surface and the atmosphere. The BL is assumed to encompass surface-driven buoyancy, shear and convection.

2.4 Air-surface Exchange

The interactions between the atmosphere and the land surface are important across a wide variety of space and timescales. Energy from the Sun is converted at the land surface into sources of heat and moisture for the lowest part of the atmosphere (ABL), and the land acts to slow down the surface wind leading to atmospheric turbulence. The ABL is strongly modulated by exchanges of heat, moisture and momentum with the underlying land surface. These exchanges also affect the variations of wind, temperature and humidity in the ABL. As a result, the characterization of land surfaces to predict these heat fluxes accurately becomes important for broader prediction rather than just the boundary layer depth.

Compared to the scale of the atmosphere, the ABL is a shallow layer, albeit an important one. Most of the small-scale processes often occur within this layer, particularly in the surface layer (the lowest 10% of the ABL). These processes are responsible for

exchanges of most of the energy and moisture between the surface and the atmosphere which are considered to be important for the evolution of local and large-scale weather phenomena. In addition, the friction at the surface and ABL is primarily responsible for the low-level convergence and divergence of wind and moisture. Thus, an accurate representation of land surface processes and ABL exchange processes becomes an important part of the state-of-the-art weather and climate models.

Representing land surface processes in a numerical weather prediction model involves linking the model's atmospheric boundary layer scheme with its surface schemes and determining the structure of the lowest part of the boundary layer, or the surface layer. A prerequisite for improving the representation of these processes in models is building a good physical representation of the land surface. Observational studies play a prominent role in this research, but detailed process models, such as the Large Eddy Simulations, are also used.

2.5 Land Surface Models

The total radiation absorbed by the land surface is balanced by emissions of thermal, infrared radiation to the atmosphere, latent heat loss associated with evaporation and transpiration, and sensible heat losses and diffusion of energy into the soil. The basic task of any LSM is to simulate the partitioning of net radiation at the land surface into corresponding energy fluxes, when provided with the relevant information on land surface and meteorological forcing. Land covers approximately 30% of the Earth's surface and as stated earlier, the variability of weather above land is greater than the one

above oceans. As part of the water cycle, land provides a link (through surface water and ground water) between atmospheric and hydrological models (Boone et al., 2004).

LSMs based on a solving the equations for energy balance at the land surface have been subject of ongoing research. Since 1980's, a large number of LSMs containing enhanced vegetation representation (through parameterizations) and root zone have been developed.

A commonly used method to land surface modeling is to consider the turbulent energy exchange between the surface and the atmosphere as an electrical equivalent. Penman (1948) assumed that the resistance between the surface and the atmosphere above. The atmospheric resistance is representative of the ability of the air to transport a given quantity away from the surface. Under unstable conditions, such as those occurring when there is strong convection or excessive surface heating, buoyancy will augment the vertical motions allowing rapid exchange which results in lowering the resistance. Under stable conditions, vertical motion is dampened by the stable layers of atmosphere near the surface and a shallow boundary layer above the surface, leading to higher resistance. A schematic of Penman's model is illustrated in Figure 2.11.

One of the earliest LSMs using the Penman approach was the so-called 'bucket' model (Manabe, 1969). The bucket model assumes the soil surface holds and evaporates moisture at the same rate as a wet surface. Excess water that the bucket cannot hold was termed as run-off. The bucket model does not take into account vegetation or canopy and was the first generation LSM.

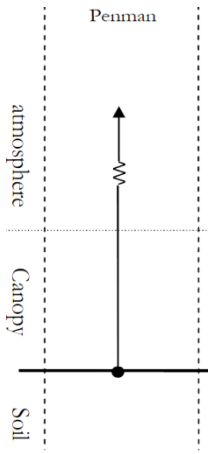

Figure 2.11 Penman's electrical analogue approach.

However, the land surface can act as a water surface only during and immediately after a rainfall event. At all other times, evapotranspiration can be altered by two things. (i) bare soil evaporation can be reduced when the top soil layer become dry and; (ii) when the vegetation influences the transpiration rate due to stomatal resistance under stress conditions. Monteith (1965) further developed the Penman equation by taking the land surface influences on evaporation into consideration and introducing an additional surface resistance. This resistance depends surface vegetation, soil wetness and local weather and climate.

Models of the Penman-Monteith type are referred as 1-layer, or big-leaf models because they do not differentiate between evaporation and transpiration, but consider the surface as one functionally homogeneous surface by parameterizing the different land surface controls. Their simplicity and physically-sound basis has led to the wide application of

big-leaf models. In densely vegetated regions, ‘big-leaf’ models have proved adequate to represent and model evapotranspiration (Monteith and Unsworth, 2007).

Deardorff (1978) modified the land surface energy consideration thus incorporating a prognostic temperature feedback with vegetation. These second generation LSMs included the interaction of vegetation impacts on energy, water and momentum budgets. These models included more than two soil layers and also considered multilayer soil water interactions.

A common model now in use is the NOAH LSM which is an enhancement of and is fundamentally based upon Deardorff (1978), Dickinson’s (1983) BATS model, and the SiB model (Sellers, 1986). An advancement introduced in these models over the bucket model was to explicitly consider temporal changes in soil moisture (in addition to soil temperature). Some of these models also included snow effects and more realistic land surface interactions. These models outperformed the first generation bucket model improving the modelling of surface-atmosphere interaction on the time scale of days as shown by Beljaars et al. (1996) and Viterbo et al. (1999). The corresponding electrical analog is shown in Figure 2.12.

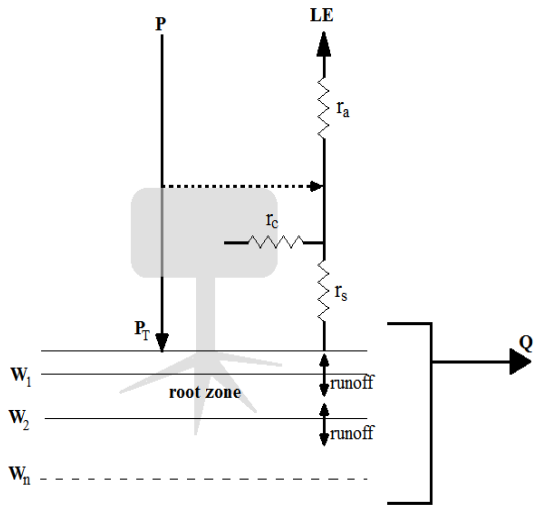

Figure 2.12 Illustration of a second-generation LSM. P and P_T are the total precipitation above the canopy and through-fall respectively, r_a is the aerodynamic resistance, r_s is the soil resistance, r_c is the canopy resistance, and Q is the collective runoff. (Adapted from Gascoin, 2009)

The third generation of LSMs added more complexity by including a semi-empirical representation of vegetation conductance (ET) and considered plant physiology based on how leaf photosynthesis interactions are believed to function (Figure 2.13). The evapotranspiration process is considered along with leaf and canopy photosynthesis and conductance. These models have been labeled as BATS2, and SiB2 (e.g., Sellers et al., 1992, 1996; Bonan, 1995).

The level of details being considered as 'adequate' in a LSM appears to depend on the applications and regions being simulated. For instance, for climate studies there have been an early adaptation of more detailed photosynthesis and carbon feedbacks along with increased complexity in the land representation. For the weather forecast community, there has been a general necessity for simplicity and computational

efficiency (Niyogi et al. 2009). As a result, while great advances are made in land surface modeling to realistically capture surface variables, the NWP community has continued the use of either the "Bucket"/SLAB model (enhanced first generation model) or the NOAH LSM (second generation, Noilhan and Planton, 1989) in NWP models.

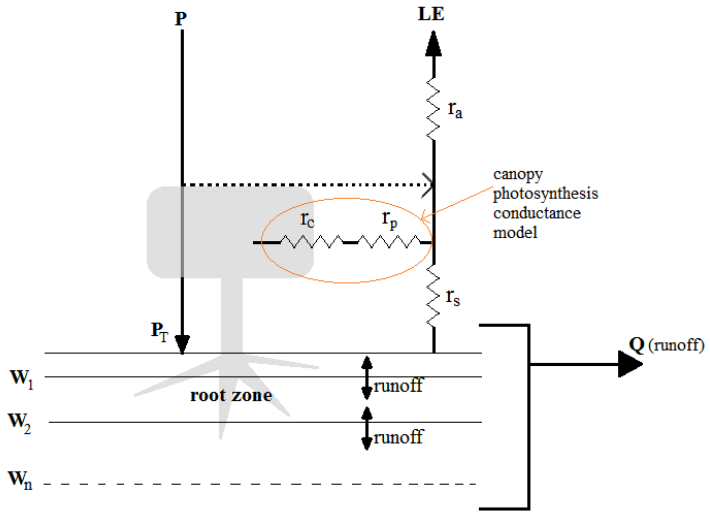

Figure 2.13 Illustration of a third-generation LSM. P and P_T are the total precipitation above the canopy and throughfall respectively, r_a is the aerodynamic resistance, r_s is the soil resistance, r_c is the canopy resistance in series with the resistance from the leaf stomata/photosynthesis, and Q is the collective runoff. (Adapted from Pitman, 2003; Bonan, 2008)

The SLAB model that is still operationally used in many regions for its simplicity or for the lack of observations to verify a detailed model, uses the modified force-restore method in the calculation of soil temperature and the soil moisture and heat capacity of soil is set as a seasonally varying function of land-use type (supplied to the model as a look-up table) without explicitly considering the role of vegetation. Soil layers are

typically 1, 2, 4, 8 and 16 cm thick, and the temperature below these layers is fixed as the daily average.

The governing equations in Noah LSM (Chen et al. 1996) are

Soil Moisture

$$\frac{\partial \theta}{\partial t} = \frac{\partial}{\partial z}\left(D\frac{\partial \theta}{\partial z}\right) + \frac{\partial K}{\partial z} + F_\theta$$

- "Richard's Equation for soil water movement
- D, K functions (soil texture, soil moisture)
- F_θ represents sources (rainfall) and sinks (evaporation)

Soil Temperature

$$C(\theta)\frac{\partial T}{\partial t} = \frac{\partial}{\partial}\left(K_t(\theta)\frac{\partial T}{\partial z}\right)$$

- C, K_t functions (soil texture, soil moisture)
- Soil temperature information used to compute ground heat flux

The NOAH land model that is typically adopted for daily weather forecasts has four soil layers at 10 cm, 30 cm, 60 cm, and 100 cm respectively. The root zone extends through the first three or all four layers depending on the vegetation class. Desert and shrub land has three layers while forest and crop land has four soil layers. Vertical diffusion, latent heat release from soil freezing/ thawing, and surface heat fluxes in the soil column are modeled in the soil thermodynamic equation which governs the soil and surface temperature and in turn the sensible heat fluxes. Precipitation, hydraulic conductivity

(including soil drainage), infiltration capacity and depth, and surface evaporation and transpiration by vegetation are all responsible for moisture changes in the soil column. The surface evaporation and surface infiltration of precipitation are influenced by the vegetation canopy. Weather forecast models continue to adopt second generation LSMs which have Penman-Monteith equation as the base framework (e.g., Chen and Dudhia, 2001; Ek et al., 2003). Niyogi et al. (2009) showed that photosynthesis-based gas exchange models (GEM) integrated within a prognostic soil moisture and soil temperature model similar to that developed by Noilhan and Planton (1989) can be efficiently coupled to weather forecast models. The core component of GEM is the surface resistance scheme and uses the relative humidity approach (Ball-Berry model, Ball et al., 1987). Evaluation of this model suggests that it performs better than the Jarvis-based approach (Niyogi et al., 2009; Charusombat, 2012). A more comprehensive review of the evolution and developments in land surface modeling can be found in Pitman (2003).

2.5.1 Land Surface Models within Tropical Cyclone/ Hurricane Models

There are at least three categories of LSMs being used in TC modelling studies. The first is a simple diagnostic model described in Emanuel et al. (2008). Here, the soil model consists of a series of 1D columns set along the track of the storm. There are a number of soil layers that extend from the surface to 2 m below the surface. Each column integrates a set of two equations of the form (Flerchinger and Saxton, 1989; Chen et al., 1997).

$$\frac{\partial T_{soil}}{\partial t} = \frac{\partial}{\partial z}\left(\kappa \frac{\partial T_{soil}}{\partial z}\right) - I \frac{\partial T_{soil}}{\partial z} \qquad \ldots (2.2)$$

κ is the thermal diffusivity of the soil

T_{soil} is the soil temperature

$$I = \frac{hydraulic\ conductivity\ \times soil\ porosity}{soil\ heat\ capacity \times density}$$

This is the measure of the downward flux of water through the soil. The first term on the right hand side of the equation represents the thermal diffusion through the soil and the second term represents the heat transport by hydraulic conductivity through the soil. The above layer is solved for all layers except the topmost layer. The top soil layer interacts with the atmosphere above and is represented by the following equation which when solved is the upper boundary condition for the solution of equation (2.2).

$$\delta z C_z \rho_z \frac{\partial T_1}{\partial z} = C_s \rho_s \kappa \frac{(T_2 - T_1)}{\delta z} - C_k \rho_a |V|(k_0^* - k_b) - \rho_l P C_l (T_1 - T_{rain}) + \dot{Q}_{rad} \quad \ldots (2.3)$$

where δz is the depth of the uppermost soil layer, T_1 and T_2 are the temperature of first (top) and the second soil layer, ρ_s is the soil density and C_s is the heat capacity per unit mass of the soil. C_k is the transfer coefficient of surface enthalpy and ρ_a is the air density at the surface, $|V|$ is the 10 m wind speed, k_0* and k_b are the enthalpy of air in equilibrium with the soil surface and the enthalpy of air at 10 m respectively, C_1 is the heat capacity per unit mass of liquid water, ρ_1 is the liquid water density, P is the precipitation rate (m/s), T_{rain} is the temperature of rain as it reaches the ground, and Q_{rad} is the net radiative heating of soil surface.

The above two equations conserve energy and efficiently represent a surface boundary for a landfalling hurricane system that evolved over highly porous, sandy soil at high surface temperatures (Emanuel et al. 2008).

The second category of model – the Slab model (Tuleya 1994) – is the most common model and has been used in operational models such as WRF, Hurricane WRF (HWRF) and GFDL (Geophysical Fluid Dynamic Laboratory) model. The SLAB model follows Deardorff (1978) to assume a surface energy balance equation of the form

$$\sigma T_L^4 + H + LE - (S + F\downarrow) = G \quad \ldots (2.4)$$

$$H = \rho c_p C_e V (T_L - \theta_{va}) \quad \ldots (2.5)$$

$$LE = (WET)\rho L C_e V [R_s(T_L) - R_a] \quad \ldots (2.6)$$

where G is the net ground heat flux, H is the sensible heat flux, LE is the evaporative flux, σT^4_L is the longwave emission from the surface, (S+F↓) is the net downward surface flux. C_e is the drag coefficient of heat and moisture calculated from the Monin Obukhov framework similar to Kurihara and Tuleya (1974), where V is the surface wind speed (normally 10 m winds), θ_{va} is the virtual potential temperature of air just above the surface, WET is soil water coefficient(representative of soil moisture availability), R_s and R_a are the mixing ratios of saturated land-surface temperature and the low-level air, L is the latent heat of condensation, ρ is the density of near-surface air, and c_p is the specific heat of air. The land-surface temperature can then be computed using the tendency equation

$$\frac{\partial T_L}{\partial t} = \frac{-\sigma T_L^4 - H - LE + (S + F\downarrow)}{\rho_s c_s d} - c\left(T_L - T_{gref}\right) \quad \ldots (2.7)$$

where $\rho_s c_s$ is the soil heat capacity and d is the damping depth, $c=2\pi/\tau$ (τ is the period of forcing). The last term in (iv) is used to "force-restore" the model's surface temperature to a reference value to avoid spurious trends. This sub-surface scheme can adequately represent and simulate the thermal evolution (temperature only) of a more complex multi-level land model and is being used as an operational land-surface model to this day. Transitional efforts are currently underway to adapt the NOAH land model (prognostically predict both surface temperature and moisture) within the hurricane WRF. The NOAH model has a long history of development beginning with the adoption of the OSU (Oregon State University) land model into NCEP's Eta model as the NOAH model and its continuing upgrades. A brief history of NOAH's land model evolution is summarized in Table 2.1.

Another enhanced version of NOAH LSM is the NOAH LSM with multi-parameterization options (NOAH-MP) which is customizable based on the application for which the land model is being run. This development improves biophysical realism based on Ball-Berry photosynthesis surface resistance with a dynamic vegetation model that allocates carbon to various parts of vegetation (leaf, stem, wood and root) and soil carbon pools (fast and slow). A multi-layer snowpack for improved cold season processes and unconfined aquifer model to accurately represent surface runoff are some of the parameterization options available through this model enhancement. This updated multi-parameterization based version of NOAH LSM improves on deficiencies identified in treating interactions among vegetation, soil, hydrology, snow and long-term soil state evolution in the current NOAH LSM (Niu et al., 2011; Yang et al., 2011). There are sub

models that incorporate urban land surface (Chen et al., 2011), crop land and agricultural feedback (Liu et al., 2014).

Table 2.1. History of evolution in development of NOAH LSM

Date	Development/ Upgrade description	Reference(s)
	Original OSU land model	
	Potential evaporation	Mahrt and Ek (1984)
	Surface fluxes, soil hydraulics	Mahrt and Pan (1984)
	and soil thermodynamics	Pan and Mahrt (1987)
	NOAH LSM implementation	
1996	OSU land model introduced into Eta model	Chen et al. (1996)
	Surface runoff and infiltration	Schaake et al. (1996)
1996	ISLSCP vegetation greenness changes	
1997	NESDIS vegetation greenness	Gutman and Ignatov (1998)
	Bare soil evaporation changes	Betts et al. (1997)
	Snow melt changes	Betts et al. (1997)
	Thermal roughness length changes	Chen et al. (1997)
1998	Increase from 2 to 4 soil layers	
	Self-cycling Eta-EDAS soil moisture and temperature	Ramsay (1998)
	NESDIS snow cover and sea ice analysis	
	NOAH LSM Upgrades	
2001	Frozen soil physics	Koren et al. (1999)
	Snow pack physics upgrade	Koren et al. (1999)
	Max. snow albedo climatology	Robinson and Kukla (1985)
	Shallow snow thermal conductivity	Lunardini (1981)

Table 2.1 continued

	Bare soil evaporation refinement	
	Bare soil thermal conductivity changes	Peters-Lidard et al. (1998)
	Vegetation-reduced soil thermal conductivity	Peters-Lidard et al. (1997)
2002	Transpiration refinements	
2003	Patchy shallow snow thermal conductivity	
	Improvements to cold season processes	Ek et al. (2003)

2.6 Challenges in Land Surface Modeling

Without a doubt, LSMs have benefited from collective efforts across varied disciplines and have proved to perform well at different spatial and temporal scales. The NOAH LSM requires key input such as land use/land cover (vegetation type), soil texture, initial soil moisture and temperature, slope and other secondary variables that are functions of the above primary variables (Chen et al., 2007). Variations in soil moisture may be caused by factors such as rainfall, irrigation patterns, soil texture and floods. While most LSMs applied in distributed frameworks include a detailed description of vegetation and root zone, the interactions between different levels of the soil and various components of soil water and ground water as well as the surface, lateral and baseflow flows are normally neglected. Consequently, these models have larger uncertainty in results in regions where such interactions are important. Typically, only three of the land components (soil, snow and vegetation) are explicitly treated while lakes and land ice are neglected (Yang et al., 2004). Vegetation is treated as ‘big leaf’ and scaling linearly from the size of a normal leaf to grids measuring 10 km and 100 km can pose problems when dealing with land-surface heterogeneities at smaller scales. The increasing quantity as

well as improved quality and resolution of land surface and near-surface climate data obtained from remote sensing in conjunction with the ability to assimilate remotely-sensed data and in-situ data (e.g., NDVI and LAI) into a gridded form has significantly improved the performance of LSMs. From the operational perspective, optimizing the efficiency of LSMs in capturing the multitude of processes and yet retaining simplicity is the continued quest that the land community embarks itself on. The challenges in representing LSMs are even more dominant as post landfall hazards continue causing increasing socio-economic losses in the coastal zones.

2.7 References

Alpert, P., D. Niyogi, R. Pielke, J. Eastman, Y. Xue, and S. Raman, 2006: Evidence for carbon dioxide and moisture interactions from the leaf cell up to global scales: Perspective on human-caused climate change. *Global and Planetary Change*, **54,** 202-208.

Avissar, R., and Y. Liu, 1996: Three-dimensional numerical study of shallow convective clouds and precipitation induced by land surface forcing. *Journal of Geophysical Research: Atmospheres*, **101,**7499-7518.

Ball, J. T., I. E. Woodrow, and J. A. Berry, 1987: A model predicting stomatal conductance and its contribution to the control of photosynthesis under different environmental conditions. *Progress in photosynthesis research*, Springer, 221-224.

Barale, V., J. Gower, and L. Alberotanza, 2010: *Oceanography from Space: Revisited.* Springer Science & Business Media.

Beljaars, A. C., P. Viterbo, M. J. Miller, and A. K. Betts, 1996: The anomalous rainfall over the United States during July 1993: Sensitivity to land surface parameterization and soil moisture anomalies. *Monthly Weather Review*, **124,** 362-383.

Betts, A. K., F. Chen, K. E. Mitchell, and Z. I. Janjic, 1997: Assessment of the land surface and boundary layer models in two operational versions of the NCEP Eta model using FIFE data. *Monthly Weather Review*, **125,** 2896-2916.

Bonan, G., 2015: *Ecological climatology: concepts and applications.* Cambridge University Press.

Bonan, G. B., 1995: Land-atmosphere COz exchange simulated by a land surface process model coupled to an atmospheric general. *Journal of Geophysical Research*, **100,** 2817-2831.

Boone, A., and Coauthors, 2004: The Rhone-Aggregation land surface scheme intercomparison project: An overview. *Journal of Climate*, **17,** 187-208.

Briegel, L. M., and W. M. Frank, 1997: Large-scale influences on tropical cyclogenesis in the western North Pacific. *Monthly Weather Review*, **125,** 1397-1413.

Chang, H.-I., 2009: Effect of land-atmosphere interactions on mesoscale convection and precipitation over the Indian monsoon region.

Charusombat, U., and Coauthors, 2012: Noah-GEM and Land Data Assimilation System (LDAS) based downscaling of global reanalysis surface fields: Evaluations using observations from a CarboEurope agricultural site. *Computers and electronics in agriculture*, **86,** 55-74.

Chase, T. N., R. A. Pielke, T. G. Kittel, J. S. Baron, and T. J. Stohlgren, 1999: Potential impacts on Colorado Rocky Mountain weather due to land use changes on the adjacent Great Plains. *Journal of Geophysical Research: Atmospheres*, **104,** 16673-16690.

Chen, F., and J. Dudhia, 2001: Coupling an advanced land surface-hydrology model with the Penn State-NCAR MM5 modeling system. Part I: Model implementation and sensitivity. *Monthly Weather Review*, **129,** 569-585.

Chen, F., Z. Janjić, and K. Mitchell, 1997: Impact of atmospheric surface-layer parameterizations in the new land-surface scheme of the NCEP mesoscale Eta model. *Boundary-Layer Meteorology*, **85,**391-421.

Chen, F., and Coauthors, 1996: Modeling of land surface evaporation by four schemes and comparison with FIFE observations. *Journal of Geophysical Research: Atmospheres*, **101,** 7251-7268.

——, 2011: The integrated WRF/urban modelling system: development, evaluation, and applications to urban environmental problems. *International Journal of Climatology*, **31,** 273-288.

Deardorff, J., 1978: Efficient prediction of ground surface temperature and moisture, with inclusion of a layer of vegetation. *Journal of Geophysical Research: Oceans*, **83,** 1889-1903.

Dickinson, R. E., 1983: Land surface processes and climate—Surface albedos and energy balance. *Advances in geophysics*, **25,** 305-353.

Doran, J. C., and S. Zhong, 2000: A study of the effects of sub-grid-scale land use differences on atmospheric stability in prestorm environments. *Journal of Geophysical Research: Atmospheres*, **105,**9381-9392.

Ek, M., and Coauthors, 2003: Implementation of Noah land surface model advances in the National Centers for Environmental Prediction operational mesoscale Eta model. *Journal of Geophysical Research: Atmospheres*, **108**.

Emanuel, K., 2000: A statistical analysis of tropical cyclone intensity. *Monthly Weather Review*, **128,** 1139-1152.

Emanuel, K., J. Callaghan, and P. Otto, 2008: A Hypothesis for the Redevelopment of Warm-Core Cyclones over Northern Australia*. *Monthly Weather Review*, **136,** 3863-3872.

Emanuel, K., C. DesAutels, C. Holloway, and R. Korty, 2004: Environmental control of tropical cyclone intensity. *Journal of the atmospheric sciences*, **61,** 843-858.

Emanuel, K., S. Ravela, E. Vivant, and C. Risi, 2006: A statistical deterministic approach to hurricane risk assessment. *Bulletin of the American Meteorological Society*, **87,** 299-314.

Feddema, J. J., K. W. Oleson, G. B. Bonan, L. O. Mearns, L. E. Buja, G. A. Meehl, and W. M. Washington, 2005: The importance of land-cover change in simulating future climates. *Science,* **310,**1674-1678.

Flerchinger, G., and K. E. Saxton, 1989a: Simultaneous heat and water model of a freezing snow-residue-soil system I. Theory and development. *Transactions of the ASAE*, **32,** 565-0571.

Frank, W. M., and P. E. Roundy, 2006: The role of tropical waves in tropical cyclogenesis. *Monthly Weather Review*, **134,** 2397-2417.

Gascoin, S., 2009: Etude des paramétrisations hydrologiques d'un modèle de surface continentale: importance des aquifères et des premiers centimètres du sol, Université Pierre et Marie Curie-Paris VI.

Gray, W. M., 1968: Global view of the origin of tropical disturbances and storms. *Monthly Weather Review*, **96,** 669-700.

Gutman, G., and A. Ignatov, 1998: The derivation of the green vegetation fraction from NOAA/AVHRR data for use in numerical weather prediction models. *International Journal of remote sensing*,**19,** 1533-1543.

Kaplan, J., and M. DeMaria, 1995: A simple empirical model for predicting the decay of tropical cyclone winds after landfall. *Journal of applied meteorology*, **34,** 2499-2512.

Koren, V., J. Schaake, K. Mitchell, Q. Y. Duan, F. Chen, and J. Baker, 1999: A parameterization of snowpack and frozen ground intended for NCEP weather and climate models. *Journal of Geophysical Research: Atmospheres*, **104,** 19569-19585.

Kurihara, Y., and R. E. Tuleya, 1974: Structure of a tropical cyclone developed in a three-dimensional numerical simulation model. *Journal of the Atmospheric Sciences*, **31,** 893-919.

Liu, X., 2015: Noah-MP-Crop: Enhancing cropland representation in the community land surface modeling system. *2015 AGU Fall Meeting*, Agu.

Lunardini, V. J., 1981: *Heat transfer in cold climates.* Van Nostrand Reinhold Company.

Mahfouf, J.-F., E. Richard, and P. Mascart, 1987: The influence of soil and vegetation on the development of mesoscale circulations. *Journal of Climate and Applied Meteorology*, **26,** 1483-1495.

Mahrt, L., and H. Pan, 1984: A two-layer model of soil hydrology. *Boundary-Layer Meteorology*, **29,** 1-20.

Mahrt, L., and M. Ek, 1984: The influence of atmospheric stability on potential evaporation. *Journal of Climate and Applied Meteorology*, **23,** 222-234.

Manabe, S., 1969: Climate and the ocean circulation. *PartI: The atmospheric circulation and the hydrology of the*.

Marks, F. D., and L. K. Shay, 1998: Landfalling tropical cyclones: Forecast problems and associated research opportunities. *Bulletin of the American Meteorological Society*, **79,** 305-323.

McBride, J. L., and R. Zehr, 1981: Observational analysis of tropical cyclone formation. Part II: Comparison of non-developing versus developing systems. *Journal of the Atmospheric Sciences*, **38,**1132-1151.

Monteith, J., 1964: Evaporation and environment. *Symposia of the society for experimental biology*, 205-234.

Monteith, J., and M. Unsworth, 2007: *Principles of environmental physics.* Academic Press.

Niu, G. Y., and Coauthors, 2011: The community Noah land surface model with multiparameterization options (Noah-MP): 1. Model description and evaluation with local-scale measurements. *Journal of Geophysical Research: Atmospheres*, **116**.

Niyogi, D., K. Alapaty, S. Raman, and F. Chen, 2009: Development and evaluation of a coupled photosynthesis-based gas exchange evapotranspiration model (GEM) for mesoscale weather forecasting applications. *Journal of Applied Meteorology and Climatology*, **48,** 349-368.

Noilhan, J., and S. Planton, 1989: A simple parameterization of land surface processes for meteorological models. *Monthly Weather Review*, **117,** 536-549.

Pan, H.-L., and L. Mahrt, 1987: Interaction between soil hydrology and boundary-layer development. *Boundary-Layer Meteorology*, **38,** 185-202.

Penman, H. L., 1948: Natural evaporation from open water, bare soil and grass. *Proceedings of the Royal Society of London A: Mathematical, Physical and Engineering Sciences*, The Royal Society, 120-145.

Peters-Lidard, C., E. Blackburn, X. Liang, and E. Wood, 1998: The effect of soil thermal conductivity parameterization on surface energy fluxes and temperatures. *Journal of the Atmospheric Sciences*,**55,** 1209-1224.

Peters-Lidard, C., M. Zion, and E. Wood, 1997: A soil-vegetation-atmosphere transfer scheme for modeling spatially variable water and energy balance processes. *Journal of Geophysical Research: Atmospheres*, **102,** 4303-4324.

Pielke, R. A., 2001: Influence of the spatial distribution of vegetation and soils on the prediction of cumulus convective rainfall. *Reviews of Geophysics*, **39,** 151-177.

Pielke, R. A., G. Dalu, J. Snook, T. Lee, and T. Kittel, 1991: Nonlinear influence of mesoscale land use on weather and climate. *Journal of Climate*, **4,** 1053-1069.

Pitman, A., 2003: The evolution of, and revolution in, land surface schemes designed for climate models. *International Journal of Climatology*, **23,** 479-510.

Prandtl, L., 1904: On fluid motions with very small friction. *Verhldg*, **3,** 484-491.

Ramsay, B. H., 1998: The interactive multisensor snow and ice mapping system. *Hydrological Processes*, **12,** 1537-1546.

Robinson, D. A., and G. Kukla, 1985: Maximum surface albedo of seasonally snow-covered lands in the Northern Hemisphere. *Journal of Climate and Applied Meteorology*, **24,** 402-411.

Schaake, J. C., V. I. Koren, Q. Y. Duan, K. Mitchell, and F. Chen, 1996: Simple water balance model for estimating runoff at different spatial and temporal scales. *Journal of Geophysical Research: Atmospheres*, **101,** 7461-7475.

Schade, L. R., and K. A. Emanuel, 1999: The ocean's effect on the intensity of tropical cyclones: Results from a simple coupled atmosphere-ocean model. *Journal of the Atmospheric Sciences*, **56,** 642-651.

Sellers, P., Y. Mintz, Y. e. a. Sud, and A. Dalcher, 1986: A simple biosphere model (SiB) for use within general circulation models. *Journal of the Atmospheric Sciences*, **43,** 505-531.

Sellers, P., J. Berry, G. Collatz, C. Field, and F. Hall, 1992: Canopy reflectance, photosynthesis, and transpiration. III. A reanalysis using improved leaf models and a new canopy integration scheme. *Remote sensing of environment*, **42,** 187-216.

Sellers, P., and Coauthors, 1996: A revised land surface parameterization (SiB2) for atmospheric GCMs. Part I: Model formulation. *Journal of climate*, **9,** 676-705.

Stull, R. B., 2012: *An introduction to boundary layer meteorology*. Vol. 13, Springer Science & Business Media.

Trenberth, K. E., J. T. Fasullo, and J. Kiehl, 2009: Earth's global energy budget. *Bulletin of the American Meteorological Society*, **90,** 311.

Tuleya, R. E., 1994: Tropical storm development and decay: Sensitivity to surface boundary conditions. *Monthly Weather Review*, **122,** 291-304.

Viterbo, P., and A. K. Betts, 1999: Impact on ECMWF forecasts of changes to the albedo of the boreal forests in the presence of snow. *Journal of Geophysical Research: Atmospheres*, **104,** 27803-27810.

Weaver, C. P., and R. Avissar, 2001: Atmospheric disturbances caused by human modification of the landscape. *Bulletin of the American Meteorological Society*, **82,** 269-281.

Werth, D., and R. Avissar, 2005: The local and global effects of Southeast Asian deforestation. *Geophysical Research Letters*, **32**.

Yang, Z.-L., 2004: *Modeling land surface processes in short-term weather and climate studies.* Vol. 3, World Scientific Series on Meteorology of East Asia.

Yang, Z. L., and Coauthors, 2011: The community Noah land surface model with multiparameterization options (Noah-MP): 2. Evaluation over global river basins. *Journal of Geophysical Research: Atmospheres*, **116**.

Zehnder, J. A., 1991: The interaction of planetary-scale tropical easterly waves with topography: A mechanism for the initiation of tropical cyclones. *Journal of the atmospheric sciences*, **48,** 1217-1230.

Zhong, S., and J. Doran, 1998: An evaluation of the importance of surface flux variability on GCM-scale boundary-layer characteristics using realistic meteorological and surface forcing. *Journal of climate*, **11,** 2774-2788.

CHAPTER 3. LANDFALLING TROPICAL CYCLONES – AN INTRODUCTION

3.1 Introduction

Tropical Cyclones are nature's one of the most dangerous and hazardous destructive force. Every year, they cause heavy damage to property and considerable loss of life. Nearly 800,000 people have died due to TCs between 1970 and 2009 (EMDAT, 2010) and approximately 130 million people are under the threat of cyclones (Peduzzi et al. 2012). The large numbers are explained by the fact that more than half the world population live 200 kilometers of a coastline. TCs today cause more than $26 billion in global damages every year and set to increase in the future (Mendelsohn et al. 2012). TCs cause heavy rains, winds, storm surge during landfall, inland flooding and spawn tornadoes. Erosion and changes in coastal geomorphology are serious environmental concerns. Nevertheless, they are also important part of the earth's energy and hydrological cycle. TCs are an efficient system to transfer heat and energy from the tropic to the colder regions in the midlatitudes and poles (Emanuel et al. 2001; Sriver et al. 2007; Korty et al. 2008; Jansen et al. 2009). They also bring much needed precipitation to rain parched regions around the world and are critical to ensure enough agricultural water (Landsea 1993, Kellner et al. 2015). Important rainmakers, TCs account for 25% of the rainfall in India and South East Asia (Prat and Nelson 2013). In

Australia, significant amount of precipitation comes from inland TCs (Ryan 1993) and typhoons in China have known to increase grain production for farmers (Liu et al. 2006). Most of rainfall over the Coromandel coast of India (east coast) is due to the TCs during the region's winter monsoon. They are an important component of the bio-geochemical cycle by stirring up and circulating nutrients from the ocean floor to the surface increasing ocean productivity and marine life (Sugg 1968). Thus, it is only important to study, analyze and minimize the risk and threat that the world population faces and maximize the benefits from TCs. This chapter will discuss the TC genesis, structure and energetics of a TC and the changes in TC dynamics post landfall which is the main focus of this dissertation.

3.2 Tropical Cyclone Genesis

A TC is a warm core, low pressure system with organized convection that form over the warm waters of the tropics (Frank 1977). Gray (1968) analyzed features of the large scale tropics that are conducive to TC genesis. They are

i. Sufficient sea surface temperature (ocean heat content) higher than 26°C
ii. Enhanced mid troposphere moisture (relative humidity)
iii. Conditional instability that supports convective initialization
iv. Enhanced relative vorticity in the lower troposphere (circulation tendency)
v. A weak vertical wind shear
vi. Slight displacement away from the equator for sufficient Coriolis force.

The first three conditions are thermodynamics based to sustain convection and the others are dynamical that supports organization of convective cells (McBride and Zehr 1981). The ability of the initial convection to survive and organize into a depression depends on the local vorticity, stability and the vertical depth of the convective cells and is defined by Rossby radius of deformation (when rotation of the system becomes as important as the buoyancy of the system; Simpson et al. 1997). They generally form between latitudes 2° and 30° on either side of the equator (Chang et al. 2003) and monsoon troughs are the most common regions in the tropics where TCs where genesis is observed. The monsoon trough is characterized by enhanced lower tropospheric vorticity derived from westerlies and enhanced rainfall. Monsoon depressions, African easterly wave and subtropical cyclones have been known to provide the necessary disturbance for TCs to develop under appropriate and supporting thermodynamic conditions. Regardless of the how the initial vortex develops, it must remain stable until a favorable environment for the storm the intensify. Strong vertical wind shear will disturb the organization of the vertical structure of the vortex while the absence of wind shear will be detrimental to the original vortex by suppression of convection due to development of cold pools. Dry air entrainment can evaporate the rain in downdrafts delivering cool and dry downdraft air into the convective boundary layer (Emanuel 1995) thus weakening the cyclone spin up process. With warm waters and enhanced evaporation, low pressure convective cells organize, the depression grows into a tropical storm and then a hurricane or a typhoon or a TC.

3.3 Tropical Cyclone Structure

TCs are areas of low pressure, characterized by cyclonic tangential and inflowing radial winds. The cyclonic winds associated with a TC can extend out to over 1000 km from its center in the lower troposphere; this radial extent decays with increasing height. TCs are warm core features, meaning that their intensity (as measured by the cyclonic tangential wind) decreases with increasing height. A TC is most intense just above the top of the boundary layer, where frictional dissipation is minimized and weakest in the upper troposphere, where winds become anti-cyclonic and exhibit mass divergence. Radial inflow is typically maximized within the boundary layer with weaker inflow observed into the middle troposphere. The radial inflow rapidly decelerates upon reaching the eyewall of the TC. The resultant convergence leads to strong updrafts/ ascending motion over a deep vertical layer within the eyewall. Compensatory descent for such strong ascent occurs in a concentrated manner within the eye and in a diffuse manner in the outer regions over the cyclone away from the center of the storm (subsidence). A schematic vertical cross section of a cyclone structure and circulation is given in Figure 3.1. This is typically for offshore unsheared cyclone.

The warm core structure of a TC can be viewed as the hydrostatic response to a radially constrained warm potential temperature anomaly near the center of the TC. This warm anomaly primarily results from latent heat energy extracted from the underlying surface that is released in the upper troposphere by convective updrafts. A small but non-negligible contribution to this warm anomaly is also observed from subsidence warming within the eye. In planar view (Figure 3.2), a mature TC is characterized by a nearly

cloud free region near its center, termed as the “eye”. The minimum sea level pressure is found at the center of the eye. For weaker TCs without eye features, the minimum sea level pressure is found at the location of the greatest vertically integrated potential temperature (warm anomaly is strongest).

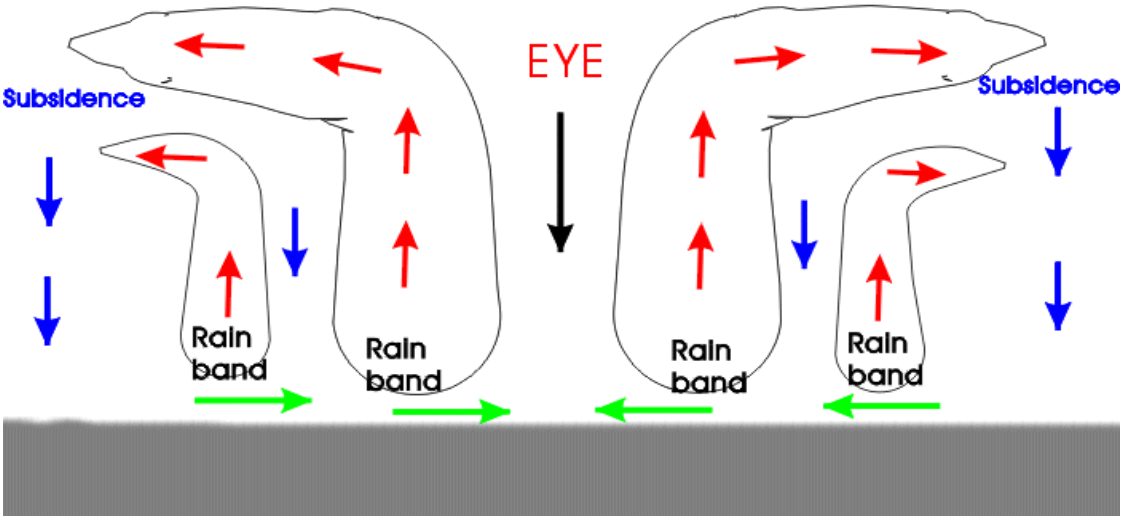

Figure 3.1 Vertical cross section of a mature TC

The primary eyewall is found at the outermost radius of the eye. Here, intense convection and modestly strong updrafts are often found. The eyewall is often the location of the radius of maximum winds. The eyewall region of a TC is characterized by a local maximum in equivalent potential temperature. The eyewall and the radius of maximum winds within a mature TC slope outward with increasing height at an angle approaching 45°. This implies that the outward displacement of the eyewall in the upper troposphere (relative to its location at the surface) is approximately equivalent to its height above the

sea surface. The physical reasoning behind this sloping structure lies with the conservation of angular momentum is approximately conserved.

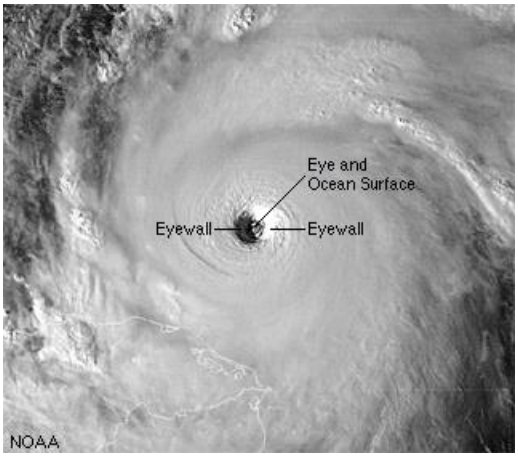

Figure 3.2 Visible satellite imagery of a mature TC (Source: NOAA)

A moat region, or region of predominantly stratiform precipitation, is found radially outward of the eyewall. Secondary eyewalls are also observed in mature TCs outside of the moat region. Secondary eyewall often forms in response to accumulation of heat energy, angular momentum and vertical velocity (Kossin and Sitkowski 2009). The formation of a secondary eyewall temporarily halts the intensification of TC by effectively cutting off radial inflow into the inner eyewall. As the secondary eyewall matures and contracts or moves inwards to replace the eroding inner eye wall. This process is called eyewall replacement cycle and the resulting broadened TC wind field results in a stronger storm.

Beyond the eyewall region, are found the rain bands of the TC. The primary rain band lies within the TC's inner core region and are stationary (storm-relative) and do not rotate around the cyclone. This rain band is characterized by new convection upwind, mature

convection in its core and more stratiform like precipitation in the downwind region. Primary rain band are also regions of secondary horizontal wind maximum (Houze 2010). Beyond this region, are distant rain bands composed of deep, moist convection along confluence lines. Often regions of large CAPE, they are regions of burst of intense rain and lightning. Tornadic activity is also possible in rain bands in the right front quadrant of landfalling TCs.

3.4 Secondary Circulation

The dynamics and energetics of a TC can be explained by primary circulation and secondary circulation. The primary circulation is the rotational part of the flow and results from the conservation of angular momentum. The secondary circulation is characterized by radial inflow at low levels, ascent near its center and radial outflow near the troposphere. This is also referred to as "in-up-and-out". These terms were coined by Ooyama (1982) and this circulation is thermally direct in nature; i.e., as a TC associated with localized warmth at its core, ascent occurs where it is warm. Compensating descent occurs at larger radii where it is relatively cooler.

The axisymmetric circulation of the cyclone can be analyzed by the Sawyer-Eliassen non-liner balance framework and outlined in Appendix A. Localized heat and cyclonic momentum sources within the upper troposphere act to enhance the secondary circulation of a TC (Shapiro and Willoughby 1982). Strengthening of secondary circulation of a TC enhances the rate of heat energy accumulation within the upper troposphere. Hydrostatically, this leads to intensification of the primary circulation via reduced surface

pressure and with gradient balance adjustment, enhanced surface winds (Pendergrass and Willoughby 2009). More specifically, a localized heat source (center of the storm) leads to enhanced cyclonic tangential flow near and just inside the radius of maximum heating. Weakened cyclonic tangential flow is found closer to the center of the TC. A localized cyclonic momentum source results in enhanced cyclonic tangential flow radially inward of the radius at which the cyclonic momentum is found.

3.5 Tropical Cyclone Intensity

Potential intensity is the maximum possible surface wind speed or minimum sea level pressure that can be attained any individual storms given the thermodynamics of the environment. Two theories have competed to explain potential intensity. (i) Conditional Instability of the Second Kind (Ooyama 1963; Charney and Eliassen 1964), and (ii) Wind Induced Surface Heat Exchange.

3.5.1 Conditional Instability of the Second Kind (CISK) for Cyclone Intensity

This theory was developed in the 1960 by Ooyama (1963) and Charney and Eliassen (1964). According to CISK, the frictional convergence of warm and moist air (high θ_e) via the hurricane boundary layer into the TC determines its intensity through latent heat release in the eyewall. This theory states that the boundary layer convergence provides all of the moisture for the latent heat release. Friction, however has a dual role to play in CISK. (i) surface winds decelerate due to friction but, (ii) also increases moisture convergence into the boundary layer. Thus, for a TC to intensify, latent heat energy

release should exceed the energy lost due to surface friction (Fraedrich and McBride 1989).

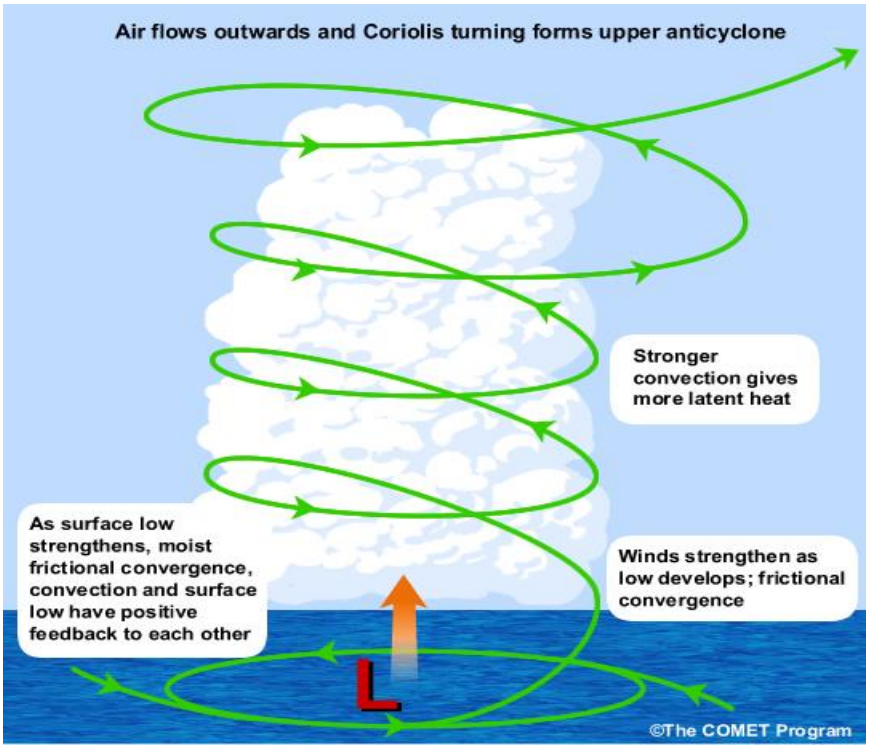

Figure 3.3 Schematic of CISK theory for TC intensity. (Source: The COMET PROGRAM)

3.5.2 Wind Induced Surface Heat Exchange (WISHE) for Tropical Cyclone Intensity

An alternative theory was put forward by Emanuel (1986; 1988) to consider the energetics of the system as an idealized atmospheric Carnot engine (Figure 1.4). The inflow air acquires energy and heat due to evaporation of water (latent heat flux). The warm air rises and cools within the eyewall and condenses while conserving total heat content. This air eventually outflows and loses heat near the tropopause and finally subsides and warms at the outer edge of the storm. The first (A→B) and the third (C→D) part of the cycle are nearly isothermal and second (B→C) and fourth (D→A) part of the

cycle are nearly isentropic. The Carnot perspective provides an upper bound on maximum wind speed that a storm can attain. Stronger circulation leads to larger heat fluxes transported aloft by organized convection that further strengthen the storm. Surface fluxes are the primary means by which a system intensifies and convection is only a pathway by which heat is supplied to the TC.

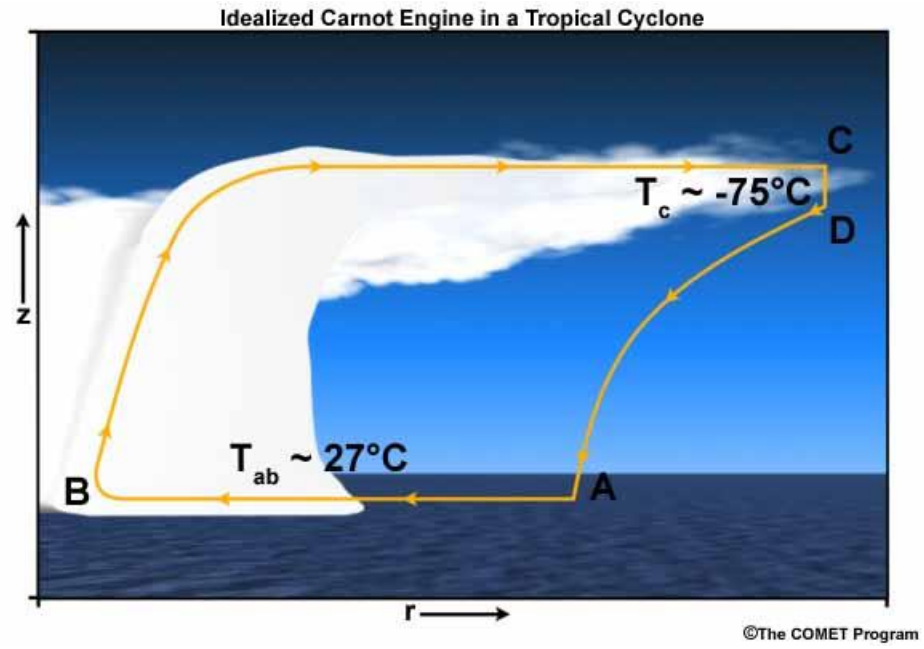

Figure 3.4 Schematic of a TC idealized as a Carnot engine (Source: The COMET Program)

3.6 Post Landfall Tropical Cyclone Structure

The TC structure changes when TCs make landfall, i.e. when the center of the storm eye crosses land. These changes critically affect the intensity of the TC, rainfall distribution and possibly tornadic activity over land. Since major impacts from a TC occurs over land, it is important to understand the evolution and structure of storms post landfall and is the focus of this work.

With landfall, the TC encounters two things (Tuleya 1978; Emanuel 1995) -

i. Loss of surface flux energy compared to the ocean heat energy.

ii. Increased friction.

The loss of surface energy fluxes is the primary cause for TC decay post landfall. The loss of evaporative and sensible heat fluxes results in weakening of the warm core structure through reduction in convection and subsidence. The surface pressure increases and surface winds decrease as a result.

Surface friction effects significantly increase after landfall. Compared to the drag experienced by the system over ocean, TCs experience higher orders of surface roughness. The increased roughness alters the hurricane boundary layer and introduces asymmetries into the cyclone structure disrupting the organized convection over land and, weakening the storm.

Ultimately, the impact of landfall on intensity of TCs depends on a variety of factors. Surface heterogeneities and land use of regions play a significant role in post landfall TC evolution. In addition to friction, the land surface conditions such as soil moisture, soil temperature, topography and the size of land mass, all play a critical role (Shen and Tuleya 2002; DeMaria and Kaplan 2006; Wong and Chan 2006; Emanuel et al. 2004, 2008; Kimball 2008) and the focus of this dissertation will be to identify the impact of land surface on landfalling TCs. The schematic figure (Figure 2.1) shown in previous chapter summarized the impact, the different land features can have on TC evolution post (and approaching) landfall.

3.7 References

Chang, C. P., C. H. Liu, and H. C. Kuo, 2003: Typhoon Vamei: An equatorial tropical cyclone formation. *Geophysical research letters*, **30**.

Charney, J. G., and A. Eliassen, 1964: On the growth of the hurricane depression. *Journal of the Atmospheric Sciences*, **21,** 68-75.

DeMaria, M., J. A. Knaff, and J. Kaplan, 2006: On the decay of tropical cyclone winds crossing narrow landmasses. *Journal of applied meteorology and climatology*, **45,** 491-499.

EM-DAT, C., 2010: The OFDA/CRED international disaster database. *Université catholique*.

Emanuel, K., 2001: Contribution of tropical cyclones to meridional heat transport by the oceans. *Journal of Geophysical Research: Atmospheres*, **106,** 14771-14781.

Emanuel, K., J. Callaghan, and P. Otto, 2008: A Hypothesis for the Redevelopment of Warm-Core Cyclones over Northern Australia*. *Monthly Weather Review*, **136,** 3863-3872.

Emanuel, K., C. DesAutels, C. Holloway, and R. Korty, 2004: Environmental control of tropical cyclone intensity. *Journal of the atmospheric sciences*, **61,** 843-858.

Emanuel, K. A., 1986: An air-sea interaction theory for tropical cyclones. Part I: Steady-state maintenance. *Journal of the Atmospheric Sciences*, **43,** 585-605.

——, 1988: The maximum intensity of hurricanes. *Journal of the Atmospheric Sciences*, **45,** 1143-1155.

——, 1995: Sensitivity of tropical cyclones to surface exchange coefficients and a revised steady-state model incorporating eye dynamics. *Journal of the Atmospheric Sciences*, **52,** 3969-3976.

Fraedrich, K., and J. L. McBride, 1989: The physical mechanism of CISK and the free-ride balance. *Journal of the Atmospheric Sciences*, **46,** 2642-2648.

Frank, W. M., 1977: The structure and energetics of the tropical cyclone II. Dynamics and energetics. *Monthly Weather Review*, **105,** 1136-1150.

Gray, W. M., 1968: Global view of the origin of tropical disturbances and storms. *Monthly Weather Review*, **96,** 669-700.

Harr, P. A., M. S. Kalafsky, and R. L. Elsberry, 1996: Environmental conditions prior to formation of a midget tropical cyclone during TCM-93. *Monthly weather review*, **124,** 1693-1710.

Hebert, P. H., and K. O. Poteat, 1975: A satellite classification technique for subtropical cyclones. *NOAA TECHNICAL MEMORANDUM NWS SR-83, JULY 1975. 6 FIG, 7 TAB, 8 REF*.

Houze Jr, R. A., 2010: Clouds in tropical cyclones. *Monthly Weather Review*, **138,** 293-344.

Jansen, M., and R. Ferrari, 2009: Impact of the latitudinal distribution of tropical cyclones on ocean heat transport. *Geophysical Research Letters*, **36**.

Kimball, S. K., 2008: Structure and evolution of rainfall in numerically simulated landfalling hurricanes. *Monthly Weather Review*, **136,** 3822-3847.

Korty, R. L., K. A. Emanuel, and J. R. Scott, 2008: Tropical cyclone-induced upper-ocean mixing and climate: Application to equable climates. *Journal of Climate*, **21,** 638-654.

Kossin, J. P., and M. Sitkowski, 2009: An objective model for identifying secondary eyewall formation in hurricanes. *Monthly Weather Review*, **137,** 876-892.

Landsea, C. W., 1993: A climatology of intense (or major) Atlantic hurricanes. *Monthly Weather Review*, **121,** 1703-1713.

Liu, J. P., 2006: Actions towards Typhoon-related disasters reduction in China. *IFNet Action Report 2006 for The 2nd General Meeting of International Flood Network (IFNet)*, Kobe, Japan.

McBride, J. L., and R. Zehr, 1981: Observational analysis of tropical cyclone formation. Part II: Comparison of non-developing versus developing systems. *Journal of the Atmospheric Sciences*, **38,**1132-1151.

Mendelsohn, R., K. Emanuel, S. Chonabayashi, and L. Bakkensen, 2012: The impact of climate change on global tropical cyclone damage. *Nature Climate Change*, **2,** 205-209.

Ooyama, K. V., 1963: Hurricane development. *Proc. Technical Conference on Hurricanes and Tropical Meteorology*, Mexico, 6-12 June, 1963.

Peduzzi, P., and Coauthors, 2012: Global trends in tropical cyclone risk. *Nature climate change*, **2,** 289-294.

Pendergrass, A. G., and H. E. Willoughby, 2009: Diabatically induced secondary flows in tropical cyclones. Part I: Quasi-steady forcing. *Monthly Weather Review*, **137,** 805-821.

Prat, O. P., and B. R. Nelson, 2013: Mapping the world's tropical cyclone rainfall contribution over land using the TRMM Multi-satellite Precipitation Analysis. *Water Resources Research*, **49,** 7236-7254.

Ryan, C. J., 1993: Costs and benefits of tropical cyclones, severe thunderstorms and bushfires in Australia. *Climatic change*, **25,** 353-367.

Shapiro, L. J., and H. E. Willoughby, 1982: The response of balanced hurricanes to local sources of heat and momentum. *Journal of the Atmospheric Sciences*, **39,** 378-394.

Shen, W., I. Ginis, and R. E. Tuleya, 2002: A numerical investigation of land surface water on landfalling hurricanes. *Journal of the atmospheric sciences*, **59,** 789-802.

Simpson, J., E. Ritchie, G. Holland, J. Halverson, and S. Stewart, 1997: Mesoscale interactions in tropical cyclone genesis. *Monthly weather review*, **125,** 2643-2661.

Sugg, A. L., 1968: Beneficial aspects of the tropical cyclone. *Journal of Applied Meteorology*, **7,** 39-45.

Tuleya, R. E., and Y. Kurihara, 1978: A numerical simulation of the landfall of tropical cyclones. *Journal of the Atmospheric Sciences*, **35,** 242-257.

Wong, M. L., and J. C. Chan, 2006: Tropical cyclone motion in response to land surface friction. *Journal of the atmospheric sciences*, **63,** 1324-1337.

Zehnder, J. A., 1991: The interaction of planetary-scale tropical easterly waves with topography: A mechanism for the initiation of tropical cyclones. *Journal of the atmospheric sciences*, **48,** 1217-1230.

CHAPTER 4. MODELING TOOLS

This research is primarily numerical modeling based. In the model, dynamic meteorology provides the equations to describe the evolution of the atmosphere and solving those equations using numerical approximations and by parameterizing other atmospheric, ocean and land surface quantities, the future state of circulation is predicted.

Accurate forecasts and simulation of TCs depends on a realistic theoretical model that incorporates the key physics of the tropics and the evolution of TCs. In this chapter, the primary modeling tool Hurricane Weather Research and Forecasting Model will be introduced and outlined. In addition to the HWRF and key LSM components within HWRF will be described. Also, the development of an idealized framework with landfall capability in HWRF as part of NOAA/NSF Research2Operations (R2O) and DTC Visiting Student Program that was implemented in the community HWRF maintained by Developmental Testbed Center (DTC) is also described.

4.1 Hurricane Research and Forecasting Model

The hurricane research and forecasting model (HWRF)[1] is an operational model designed and implemented by National Centers for Environmental Prediction to provide numerical

[1] This summary as presented builds off Tallapragada et al. (2015) – HWRF Scientific Documentation.

TC guidance to National Hurricane Center (NHC) for cyclone track, intensity and structure forecasts.

The HWRF model is a primitive-equation, non-hydrostatic, coupled ocean-atmospheric model. The Non-hydrostatic mesoscale model is HWRF's atmospheric core and is coupled with the Message Passing Interface Princeton Ocean Model–TC (MPIPOM-TC) through NCEP Coupler. This limited area model or regional dynamical model facilitates higher resolution leading to increased accuracy and cover a large enough domain such that TCs do not approach the domain boundaries in the model. To realize higher efficiency in forecasting and resolving the intricate structures of TCs, a triple nest is employed within HWRF and the two inner nests are two way interactive telescopic nests that move along the storm. The operational model's static parent domain covers 80°×80° area at 0.135° grid spacing (~ 18 km), the moving nests - middle nest spans 12°×12° area at 0.045° (~ 6 km) and the inner nest covers an area of 7.5°×7.5° at 0.015° resolution (Figure 4.1). The location of the parent domain depends on the initial observed position of the storm (from NHC and Joint Typhoon Warning Center (JTWC) and the ocean basin in which the storm is observed. The model top and the number of vertical levels in the model is also dependent on the ocean basin in which the model is configured in. In the north Atlantic (AL), north Eastern Pacific (EP) and north Central Pacific (CP) ocean basins, there are 61 vertical levels and the top boundary is at 2 hPa. In all other domains, there are 43 vertical sigma pressure levels and the model tops out at 50 hPa. The model is also customizable to modify the number of levels and the model's vertical boundary settings along with the size and area of each domain.

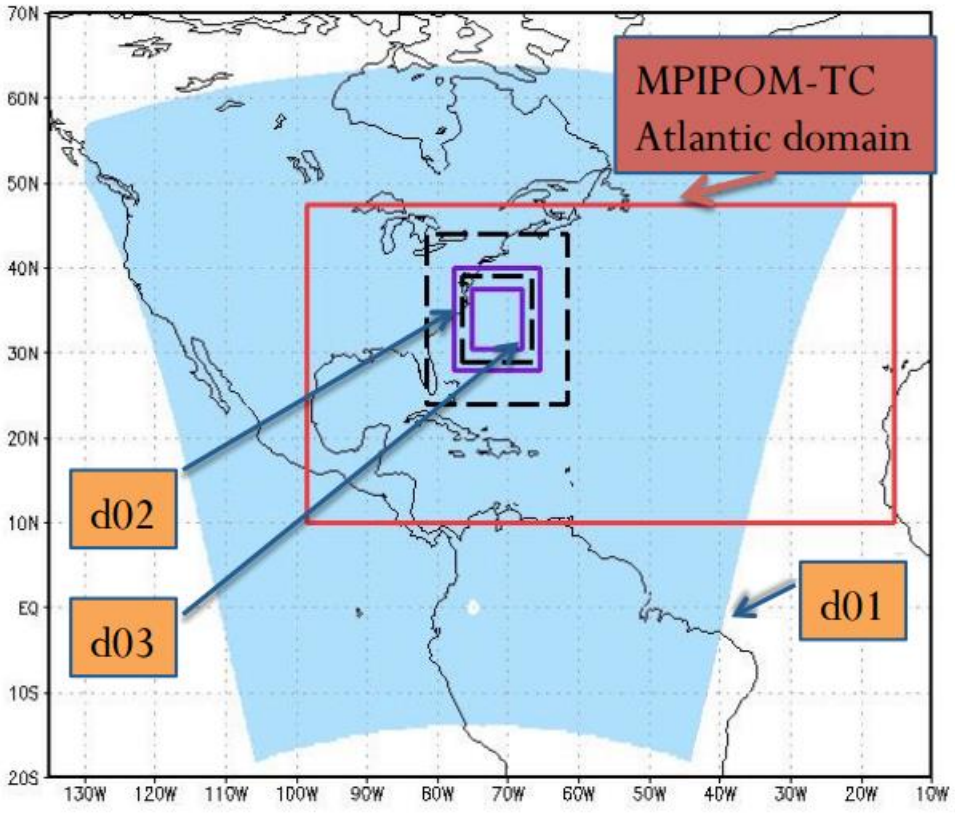

Figure 4.1 Illustration of domain configuration over north Atlantic Ocean Basin. The domains are labeled.

4.1.1 WRF-NMM Dynamics

The HWRF contains the WRF-NMM core. The dynamic non-hydrostatic mesoscale model is a fully compressible model with terrain following hybrid sigma-pressure vertical levels (Janjic et al. 2002; Janjic 2003 a, b). It uses the staggered Arakawa E grid (Arakawa and Lamb 1977). The term staggered or unstaggered represents the choice with which prognostic variables are distributed or arranged in the model's grid (Figure 4.2). When all the prognostic variables are defined at the same point in the grid, it called an unstaggered grid. On the other hand, when the predictive variables are defined at more

than one point on the grid, it is called a staggered grid. Arakawa E grid is staggered and also rotated 45° with relative to other grid orientations. First order and second order quantities such as energy and enstrophy is conserved in the model.

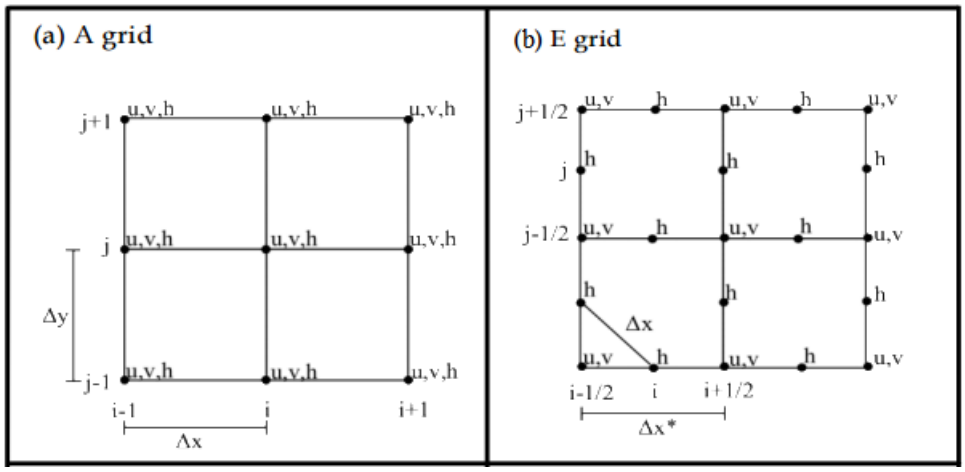

Figure 4.2 Grid types based on horizontal staggering. (a) unstaggered Arakawa A grid and (b) staggered Arakawa E grid. Δx is the west-east resolution and Δy is the south-north resolution. u, v represents the velocity points and h represents the mass or thermodynamic points such as temperature and humidity.

4.1.1.1 Time Stepping and Advection (Space) of T, U, V

WRF-NMM uses “forward-backward” scheme for horizontally propagating fast waves, implicit scheme for vertically propagating sound waves, Adams-Bashforth scheme (AB scheme aka two step method) for horizontal advection (Bashforth 1883; Goldstine 1977), and Crank-Nicholson scheme for vertical advection. The same time step is used for all the terms. Total Kinetic Energy (TKE), water species are solved explicitly, iteratively every alternate time steps and are flux-corrected and positive definite. A number of quantities like energy, enstrophy are conserved (Janjic 1984).

4.1.1.2 Diffusion and Divergence Damping

WRF-NMM categorizes diffusion as lateral and vertical diffusion. The vertical diffusion is handled by the planetary boundary layer scheme (Janjic 1996a, 1996b, 2002, 2003a) and determines the turbulence or mixing of the atmosphere. The lateral diffusion is modeled using the Smagorinsky non-linear approach (Smagorinsky 1963; Janjic 1990). The divergence damping terms are essentially used to the computational modes or in other words used to damp gravity waves that make the model very unstable. The horizontal component of divergence in WRF-NMM is damped by using the technique described in Sadourny (1975). This helps in conserving mass and potential enstrophy and aids in maintaining realistic energy spectrum within the model.

4.1.2 HWRF Physics

WRF-NMM offers a variety of physics options that are appropriate for different atmospheric problems. The broad idea of these options is that they can be combined in many ways to efficiently and effectively solve the evolution of an atmospheric event. It varies from simple and computationally inexpensive to sophisticated and computationally intensive and detailed physics modules. The choice depends on the user, the weather phenomena being studied and the geographical region of interest. HWRF uses a specific set of physics options that are customized to the tropics and simulating realistic TC environment.

The operational HWRF configuration employs the modified Ferrier-Aligo (FA) microphysics scheme (Rogers et al. 2001, Ferrier et al. 2002) with separate species (cloud

water, rain, snow, ice, graupel, sleet) which was developed to enhance convective cloud simulations in high resolution model domains and explicitly handle the behavior of hydrometeors. The cumulus parameterization schemes solve sub-grid scale effects of clouds and represent the updrafts, downdrafts and other motions inside that cloud that are not explicitly solved by the microphysics parameterization. HWRF uses the Simplified Arakawa-Schubert (SAS) scheme (Pan and Wu 1995; Hong and Pan 1998; Pan 2003; Han and Pan 2011) for cumulus parameterization. Surface layer parameterizations calculate the frictional velocities and exchange coefficients for momentum and heat. These variables enable LSMs to calculate the surface temperature, moisture and heat fluxes in the model. The HWRF surface layer physics is based on GFDL surface layer scheme and follows the Monin-Obukhov similarity theory (Sirutis and Miyakoda 1990; Kurihara and Tuleya 1974). This module has been modified over water (Kwon et al. 2010, Powell et al. 2003 and Black et al. 2007) and is parameterized using Coupled Boundary Layers Air-Sea Transfer (CBLAST) observation data and is very closely coupled to the POM-TC ocean model. The surface roughness over water is calculated using stability functions and formulations for drag coefficients. On the other hand, over land the surface roughness length is specified through a land parameter and vegetation table and thermal and momentum roughness length are assumed to be equal. The surface layer physics is closely tied to the LSM. The operational land surface physics used in HWRF is a 4 layer NOAH LSM that predicts both soil temperature and soil moisture (Mahrt and Ek, 1984; Mahrt and Pan, 1984; Pan and Mahrt, 1987; Chen et al., 1996; Schaake et al., 1996; Chen et al., 1997; Koren et al., 1999; Ek et al., 2003). Extensive review of NOAH LSM has been provided in chapter 2. Both land surface physics and

surface layer physics are closely tied in with the boundary layer model that HWRF uses and provides the surface fluxes to the boundary layer scheme. The HWRF's planetary boundary layer scheme is based off Troen and Mahrt (1986) and is also employed in the Global Forecast System (GFS) model and Geophysical Fluid Dynamics Laboratory (GFDL) operational hurricane model (Hong and Pan1996). The HWRF PBL scheme uses bulk Richardson approach to determine the planetary boundary layer height and eddy diffusivity parameter. To close out the physics package, radiation schemes provide forcing due to radiative fluxes and energy budget is computed from the surface downward shortwave and longwave radiation. The RRTMG longwave and shortwave schemes are the standard radiation schemes used in HWRF. The schemes are modified RRTM for Global Climate Models (RRTMG; Iacono et al. 2008) and is effective in its treatment of sub-gridscale cloud variability. Absorption of different gases are included in the longwave and shortwave schemes. The optical depth, scattering albedo and asymmetry parameter are parameterized and optical properties of ice particles are calculated through ice particle parameterization. Table 4.1 summarizes the default physics options used in the operational HWRF.

Table 4.1 Physics options used in operational HWRF configuration

Physics	**Options**
Microphysics	Ferrier-Aligo Scheme
Cumulus Parameterization	Simplified Arakawa and Schubert (SAS) scheme
Surface Layer	HWRF surface layer scheme
Land Surface	NOAH land surface model
Planetary boundary layer	HWRF PBL scheme
Long wave Radiation	RRTMG long wave radiation scheme
Short wave Radiation	RRTMG short wave radiation scheme

4.1.3 Other HWRF features

HWRF is a suite of techniques and models combined together to produce the best possible TC forecast. In addition to the WRF-NMM atmospheric component, HWRF also consists of an ocean model to create an accurate and realistic sea surface temperature (SST) dataset. HWRF is initialized using data assimilation and vortex improvement procedures (vortex initialization and relocation techniques based off NHC observed TC position and intensity). Initial conditions are provided by GFS and Global Data Assimilation System (GDAS) dataset can used to initialize the inner nests. In addition to GDAS dataset, HWRF Data Assimilation System (HDAS) provides vortex level assimilation of TC fly through dropsondes and flight observations when available. A comprehensive post processing package within HWRF such as gfdl-vortex tracker and HRD's diagnostic package – DiaPost enables accurate visualization and diagnostics of HWRF simulations.

4.2 Idealized HWRF Framework

In this research for studying the different processes, an idealized HWRF modeling framework was used. The use of idealized conditions conducive to intense TC development allows for model results to be viewed without the confounding of case specific conditions. Emanuel (1995) for example, utilizing an idealized hurricane model, investigated the sensitivity of simulated TC intensity to the ratio C_k to C_d. Montgomery et al. (2010) furthered the understanding of the role of C_d on hurricanes by using a three dimensional idealized MM5 model. While the former modeling study suggested that the intensity of TCs decreases with increase in frictional forces due to increase in C_d, the

newer study points to a dual role that frictional forces play in hurricane dynamics. Gopalakrishnan et al. (2013) using the idealized version of HWRF characterized the effect of the vertical diffusion coefficient on the structure and intensity of TCs. In this study, they calibrated the HWRF modeled eddy diffusivities to best match flight level observation data gathered during Hurricane Allen (1980) and Hurricane Hugo (1989). Halliwell et al. (2015) used an idealized version of HWRF to obtain an improved understanding of the sensitivity of the HWRF model to ocean cooling and enhance understanding of the dynamical processes that contribute to change in intensity of storms and resulting asymmetries. The Halliwell et al. (2015) study also stressed the importance of idealized studies in advancing the forecasting competencies in more complex and detailed models. While there are many studies involving the idealized model that deepen the understanding of the fundamental processes that affect TCs over the ocean, there are a relatively limited number of studies available to study the land impact. Thus, an additional capability in the already existing idealized HWRF framework to realize landfall was developed. This capability has subsequently been implemented in the community repository of HWRF and released via the Developmental Testbed Center.

4.2.1 Design and Configuration

The baseline source code was obtained from the DTC consistent with the latest version of HWRF and the code modules for the landfall capability was added following the HWRF code management protocols (as followed by all HWRF developers). In the typical idealized HWRF, the domain is all ocean. The vortex is added to the center of the HWRF domain and kept stationary. The conventional method to realize landfall is to introduce a

mean wind in the domain and move the storm towards a predefined land surface in the domain. While this method is more physical, the closed domains of ideal HWRF can cause spurious convective towers near the boundaries making the model unstable due to reflection of gravity waves. This is particularly more pronounced when land is introduced and higher land surface temperature is prescribed. To overcome this limitation, a technique was developed in which land was moved underneath the centered storm to realize relative landfall. A land/ sea mask was used as control variable to define the land points and the domain was redefined for every time step and based on the domain resolution, the speed of the land moving underneath can be controlled.

Land characteristics are based on the land use, soil and vegetation table and different land use/ land cover parameters including SM ranges, surface roughness, emissivity, albedo was defined through a separate namelist file specifically created for idealized HWRF. Heterogeneities in land surface can also be built both longitudinally and latitudinally. A schematic of the land relative to storm motion is shown in Figure 4.3a, b at different time steps. The namelist file also define an on/ off switch for landfalling studies and the direction in which the land surface moves (west-east or east-west direction). As of now, the landfall capability is configured to use GFDL LSM and HWRF surface layer scheme only.

The code changes to the base idealized HWRF code and the configuration namelist file is given in Appendix B.

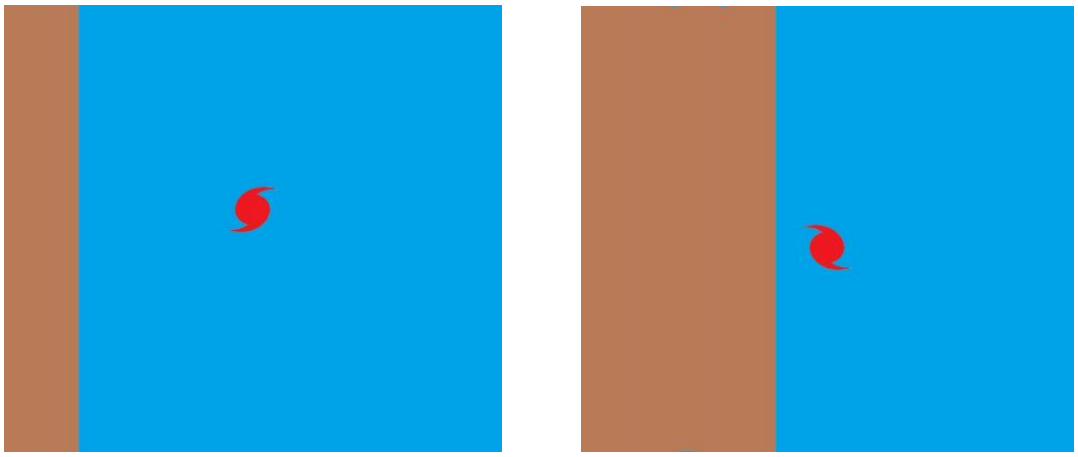

Figure 4.3 Idealized Domain with landfalling capability at (a) T hours, and (b) T+ΔT hours

4.3 References

Arakawa, A., and V. R. Lamb, 1977: Computational design of the basic dynamical processes of the UCLA general circulation model. *Methods in computational physics*, **17,** 173-265.

Bashforth, F., and J. C. Adams, 1883: *An attempt to test the theories of capillary action: by comparing the theoretical and measured forms of drops of fluid.* University Press.

Black, P. G., E. A. D'Asaro, W. M. Drennan, and J. R. French, 2007: AIR-SEA EXCHANGE IN HURRICANES: Synthesis of Observations from the Coupled Boundary Layer Air-Sea Transfer Experiment. *Bulletin of the American Meteorological Society*, **88,** 357.

Center, E. M., 2003: The GFS atmospheric model. *National Center for Environmental Prediction Office Note*, **442**.

Chen, F., and Coauthors, 1996: Modeling of land surface evaporation by four schemes and comparison with FIFE observations. *Journal of Geophysical Research: Atmospheres*, **101,** 7251-7268.

Crank, J., and P. Nicolson, 1947: A practical method for numerical evaluation of solutions of partial differential equations of the heat-conduction type. *Mathematical Proceedings of the Cambridge Philosophical Society*, Cambridge Univ Press, 50-67.

Dudhia, J., Z. Janjic, and M. Baldwin, 1997: Coupling a land--surface model to the NCEP mesoscale Eta model. *Preprints, lath Conf. on Hydrology, Long Beach, CA, Amer. Meteor. Soc*.

Ek, M., and Coauthors, 2003: Implementation of Noah land surface model advances in the National Centers for Environmental Prediction operational mesoscale Eta model. *Journal of Geophysical Research: Atmospheres*, **108**.

Emanuel, K. A., 1995: Sensitivity of tropical cyclones to surface exchange coefficients and a revised steady-state model incorporating eye dynamics. *Journal of the Atmospheric Sciences*, **52,** 3969-3976.

Ferrier, B., Y. Jin, Y. Lin, T. Black, E. Rogers, and G. DiMego, 2002: Implementation of a new grid-scale cloud and precipitation scheme in the NCEP Eta model. *CONFERENCE ON WEATHER ANALYSIS AND FORECASTING*, AMS, 280-283.

Gopalakrishnan, S. G., F. Marks Jr, J. A. Zhang, X. Zhang, J.-W. Bao, and V. Tallapragada, 2013: A study of the impacts of vertical diffusion on the structure and intensity of the tropical cyclones using the high-resolution HWRF system. *Journal of the Atmospheric Sciences*, **70,**524-541.

Halliwell Jr, G., S. Gopalakrishnan, F. Marks, and D. Willey, 2015: Idealized study of ocean impacts on tropical cyclone intensity forecasts. *Monthly Weather Review,* **143,** 1142-1165.

Han, J., and H.-L. Pan, 2011: Revision of convection and vertical diffusion schemes in the NCEP global forecast system. *Weather and Forecasting,* **26,** 520-533.

Hong, S.-Y., and H.-L. Pan, 1996: Nonlocal boundary layer vertical diffusion in a medium-range forecast model. *Monthly weather review*, **124,** 2322-2339.

——, 1998: Convective trigger function for a mass-flux cumulus parameterization scheme. *Monthly weather review*, **126,** 2599-2620.

Iacono, M. J., J. S. Delamere, E. J. Mlawer, M. W. Shephard, S. A. Clough, and W. D. Collins, 2008: Radiative forcing by long-lived greenhouse gases: Calculations with the AER radiative transfer models. *Journal of Geophysical Research: Atmospheres*, **113**.

Janjic, Z., 1996a: The Mellor-Yamada level 2.5 scheme in the NCEP Eta model, paper presented at 11th Conference on Numerical Weather Prediction. *Am. Meteorol. Soc., Norfolk, Va***,** 19-23.

——, 1996b: The surface layer parameterization in the NCEP Eta Model. *World Meteorological Organization-Publications-WMO TD***,** 4.16-14.17.

——, 2003a: The NCEP WRF core and further development of its physical package. *5th International SRNWP Workshop on Non-Hydrostatic Modeling, Bad Orb, Germany*, 27-29.

——, 2003b: A nonhydrostatic model based on a new approach. *Meteorology and Atmospheric Physics*, **82,** 271-285.

Janjic, Z. I., 1984: Nonlinear advection schemes and energy cascade on semi-staggered grids. *Monthly Weather Review,* **112,** 1234-1245.

——, 1990: The step-mountain coordinate: physical package. *Monthly Weather Review*, **118,** 1429-1443.

Janjić, Z. I., 2002: Nonsingular implementation of the Mellor–Yamada level 2.5 scheme in the NCEP Meso model. *NCEP office note*, **437,** 61.

Koren, V., J. Schaake, K. Mitchell, Q. Y. Duan, F. Chen, and J. Baker, 1999: A parameterization of snowpack and frozen ground intended for NCEP weather and climate models. *Journal of Geophysical Research: Atmospheres*, **104,** 19569-19585.

Kurihara, Y., and R. E. Tuleya, 1974: Structure of a tropical cyclone developed in a three-dimensional numerical simulation model. *Journal of the Atmospheric Sciences*, **31,** 893-919.

Kwon, Y. C., S. Lord, B. Lapenta, V. Tallapragada, Q. Liu, and Z. Zhang, 2010: Sensitivity of air-sea exchange coefficients (Cd and Ch) on hurricane intensity. *29th Conf. on Hurricanes and Tropical Meteorology*.

Mahrt, L., and H. Pan, 1984: A two-layer model of soil hydrology. *Boundary-Layer Meteorology*, **29,** 1-20.

Mahrt, L., and M. Ek, 1984: The influence of atmospheric stability on potential evaporation. *Journal of Climate and Applied Meteorology*, **23,** 222-234.

Montgomery, M. T., R. K. Smith, and S. V. Nguyen, 2010: Sensitivity of tropical-cyclone models to the surface drag coefficient. *Quarterly Journal of the Royal Meteorological Society*, **136,** 1945-1953.

Pan, H., and W.-S. Wu, 1995: Implementing a mass flux convection parameterization package for the NMC medium-range forecast model. *NMC office note*, **409,** 20,233-9910.

Pan, H.-L., and L. Mahrt, 1987: Interaction between soil hydrology and boundary-layer development. *Boundary-Layer Meteorology*, **38,** 185-202.

Powell, M. D., P. J. Vickery, and T. A. Reinhold, 2003: Reduced drag coefficient for high wind speeds in tropical cyclones. *Nature*, **422,** 279-283.

Rogers, E., T. Black, B. Ferrier, Y. Lin, D. Parrish, and G. DiMego, 2001: Changes to the NCEP Meso Eta Analysis and Forecast System: Increase in resolution, new cloud microphysics, modified precipitation assimilation, modified 3DVAR analysis. *NWS Technical Procedures Bulletin*, **488,** 21.

Sadourny, R., 1975: The dynamics of finite-difference models of the shallow-water equations. *Journal of the Atmospheric Sciences*, **32,** 680-689.

Schaake, J. C., V. I. Koren, Q. Y. Duan, K. Mitchell, and F. Chen, 1996: Simple water balance model for estimating runoff at different spatial and temporal scales. *Journal of Geophysical Research: Atmospheres*, **101,** 7461-7475.

Sirutis, J., and K. Miyakoda, 1990: Subgrid scale physics in 1-month forecasts. Part I: Experiment with four parameterization packages. *Monthly weather review*, **118,** 1043-1064.

Smagorinsky, J., 1963: General circulation experiments with the primitive equations: I. the basic experiment*. *Monthly weather review*, **91,** 99-164.

Tallapragada, V., and Coauthors, 2015: Hurricane Weather Research and Forecasting (HWRF) model: 2015 scientific documentation.

Troen, I., and L. Mahrt, 1986: A simple model of the atmospheric boundary layer; sensitivity to surface evaporation. *Boundary-Layer Meteorology*, **37,** 129-148.

CHAPTER 5. IMPACT OF ANTECEDENT LAND STATE ON POST LANDFALL TROPICAL CYCLONE SUSTENANCE

5.1 Introduction

While the majority of TCs (TC) decay rapidly post landfall, there are cyclones that have maintained intensity or even re-intensified inland. Recent examples of post-landfall sustenance include TS Erin (2007) and TS Fay (2008) in the Atlantic basin, TC Abigail (2001) in Northern Australia, and TC Phet (2010) over the Indian Monsoon Region. The availability of antecedent wet conditions and surface latent heat flux has been thought to be the primary signatures for post-landfall TC intensification [e.g., Chang et al. 2009; Anderson et al. 2013]. Evans et al. [2011] and Kellner et al. [2012] analyzed the re-intensification of TS Erin (2007) over the U.S. Southern Great Plains and concluded that anomalously wet land conditions can help sustain the storm inland. Similarly, it has been observed that monsoon depressions respond to high antecedent soil moisture (SM) conditions and their intensity was maintained for a longer duration [Chang et al. 2009; Kishtawal et al. 2013]. Thus, a growing number of studies highlight the role of anomalously wet land surface conditions aiding TC sustenance over land.

An outstanding question remains within the literature regarding whether the soil wetness or soil temperature (ST) contributes to post-landfall evolution. For example, Tuleya [1994] highlights the influence of soil thermal properties and particularly ST on storm

sustenance. Emanuel et al. [2008] studied TC Abigail (2001) that re-intensified twice after landfall in Northern Australia in a warm and sandy (high thermal diffusivity) region and concluded that the surface characteristics played an important role in intensifying the storm inland. Kishtawal et al. [2012] in their climatological study of TCs over the North Atlantic region also established a positive correlation between post-landfall hurricane intensity and thermal heat capacity of soils. These studies seem to indicate that warm land ST and hence sensible heat flux (SHF) may play a larger role in determining the fate of a storm post landfall. However, an earlier study by Shen et al. [2002] concluded that the post landfall decay rate depends on the water content over land as well as, on the surface cooling that controls the potential evaporation. Thus the chief motivation for this study is to contribute to the debate on the relative role of antecedent wet and warm land surfaces on TC post-landfall evolution.

Post-landfall impacts such as flooding from hurricane Sandy (2012) over New York in addition to parallel improvements in LSMs (LSM) and hurricane models such as the Hurricane Weather Research and Forecasting (HWRF) model, are providing momentum for the study of the effects of land surface on TC post-landfall characteristics. As stated, there is still limited understanding of what contributes to the decay, re-intensification or sustenance of a TC over land. Additionally, land feedbacks are at multiple scales (i.e., local boundary layer energetics to mesoscale convergence due to gradients in surface fluxes) and involve multiple parameters as well as processes. In this study, utilizing the realistic processes simulated by the ideal HWRF, understanding the role of land surface characteristics on post-landfall storm evolution is the priority. Building off prior studies,

the hypothesis that under favorable synoptic settings, a warm land surface is a necessary condition to aid post landfall TC sustenance or re-intensification will be tested. The synergetic relationship between warm and wet soils is also studied.

5.2 Model Configuration and Experimental Setup

This study uses the idealized framework of the operationally adopted HWRF (HWRFX2013) with domain settings and physics options (Table 4.1) similar to that of Gopalakrishnan et al. [2013]. The initial cyclonic vortex strength was set to 20 ms^{-1}. A typical tropical sounding was used for temperature and humidity following Gray et al. [1975]. The HWRFX2013 system configuration uses the HWRF surface layer parameterization scheme [Tallapragada et al. 2013] to represent surface layer fluxes and boundary layer processes. In order to individually study the ST and SM feedbacks, the bulk Slab land surface parameterization was used for all simulations.

To simulate landfall, a vortex was introduced and kept fixed at the center of the domain and the land surface was advected at a constant rate. The approach of ignoring the basic environmental flow and its interaction with the surface is ignored similar to Tuleya and Kurihara [1978] and Halliwell et al. [2015]. The model was integrated for 120 hours with landfall around the 56th hour. GFDL LSM was used for the idealized experiment. As stated in the previous chapters, it is a single layer LSM with explicit prognostic temperature prediction. This model does not predict soil moisture and is initialized manually. A homogeneous land surface is defined using the model default soil and the vegetation lookup tables and is initialized to dry, bare sandy soil. To extract the feedback

processes and interactions in these idealized simulations, land temperature is held constant and diurnal variation effects are eliminated. The model was initialized to the default setting with the following parameters held constant. The ST was set to 308 K and SM at 0.02 m^3/ m^3 (10% of field capacity) along with land surface roughness (z_0) of 0.01 m. The radius of maximum winds that defines the size of the storm was set to 90 km to simulate a moderate-sized storm. To maintain the ocean temperature higher than the threshold value favoring cyclone genesis and evolution, the sea surface temperature (SST) was held at a constant 302 K throughout the simulations. A number of experiments were conducted and a subset of 16 experiments was selected to study warm and wet land surfaces as shown in Table 5.2. These experiments seek to isolate the SM and ST impacts on TC evolution following a factor separation (FacSep) approach [Stein and Alpert, 1993]. Further, experiments were performed to assess the impact of soil moisture content, surface roughness and size of storm. These experiments are outlined later in this chapter. To further evaluate the primary hypothesis, a real case [TS ERIN (2007)] was run using operational HWRF (HWRF v3.7). The three nested grids were configured with 18:6:2 km. The physics options are the same as in Table 5.1 (similar to the operational configuration) except Noah LSM with GFDL surface physics was used to make it as realistic as possible with diurnal and spatial soil moisture, soil temperature evolution.

Table 5.1 Physics options used in the idealized HWRF experiments.

Physics schemes	**Options**
Microphysics	Ferrier Scheme
Cumulus Parameterization	Simplified Arakawa and Schubert (SAS) scheme
Longwave Radiation	GFDL longwave radiation scheme
Shortwave Radiation	GFDL shortwave radiation scheme
Surface Layer	GFDL surface layer scheme
Planetary boundary layer	GFS PBL scheme
Land Surface	GFDL Slab model, Noah land model (For TS Erin runs)

Table 5.2 List of experiments conducted in the idealized HWRF2013

Variable	Sensitivity experiments
Soil Temperature	300 K, 302 K, 304 K, 306 K, 308 K (default), 310 K, 312 K, 314 K
Factor separation experiments	
Experiment	Factors included (Idealized experiments)
F0	default run: ST = 308 K, default SM
F1	Soil temperature only; ST=314 K
F2	Soil moisture only; SM+50%
F12	Soil temperature and soil moisture; ST=314 K and SM+50%
Real Case (TS ERIN 2007) Cycle 2007081600 UTC	
F0r	Default run
F1r	Initial soil temperature increased by 6°C
F2r	Initial soil moisture increased by 50% throughout the domain
F12r	Soil temperature and soil moisture increase

5.3 Results and Discussion

The results are presented in two contexts – first for the impact of ST on post-landfall TC evolution; and then for ST and SM interactions from the FacSep analysis. The model results are analyzed using a number of typical dynamic and thermodynamic features that are typically used [Gopalakrishnan et al. 2012; Halliwell et al. 2015]. The Hovmöller diagrams are used summarize the fields (winds, surface fluxes, rainfall) with radial

distance on the abscissa and the simulation time on the ordinate (e.g. Figure 5.1). The Hovmöller of axisymmetric mean tangential winds is used as the measure of intensity and the discussion is complemented by time series plots of minimum mean sea level pressure (MSLP) and 10 m maximum wind speeds (Vmax).

5.3.1 Soil Temperature Impacts

To investigate the impact of land surface temperature on TC intensity, a sensitivity study was undertaken by varying the surface temperature from 300 K to 314 K and experiments are named accordingly. The Hovmöller diagram of intensity evolution is presented in Figure 5.1 and supplemented by Figure 5.2 for time series plots of central pressure and winds. In all the experiments, steady state (maximum tangential wind speed is approximately constant) was achieved after around 48 hours from the start of run. A fully mature TC landfall was noted around the 56^{th} hour. For surface temperatures up to 302 K, simulations show a notable drop in intensity immediately after landfall. Similar to SST thresholds for TCs over the ocean (299 – 300 K), 302 K emerged as the threshold ST over land in the simulation. The post-landfall storm evolution remains much stronger when surface temperatures were between 304 and 308 K and re-intensification signatures are noted (i.e., strengthening after initial drop in intensity post landfall). For surface temperatures between 308 and 314 K, sustenance in TC (maintaining landfall intensity) patterns was noted. The wind swaths of cyclones are also significantly larger (45 km for 302 K and 60 km for 308 K after landfall) and likely enable the storm system to draw in heat and moisture to maintain circulation. Convective precipitation also increased for warmer land surfaces and is shown in Figure 5.3.

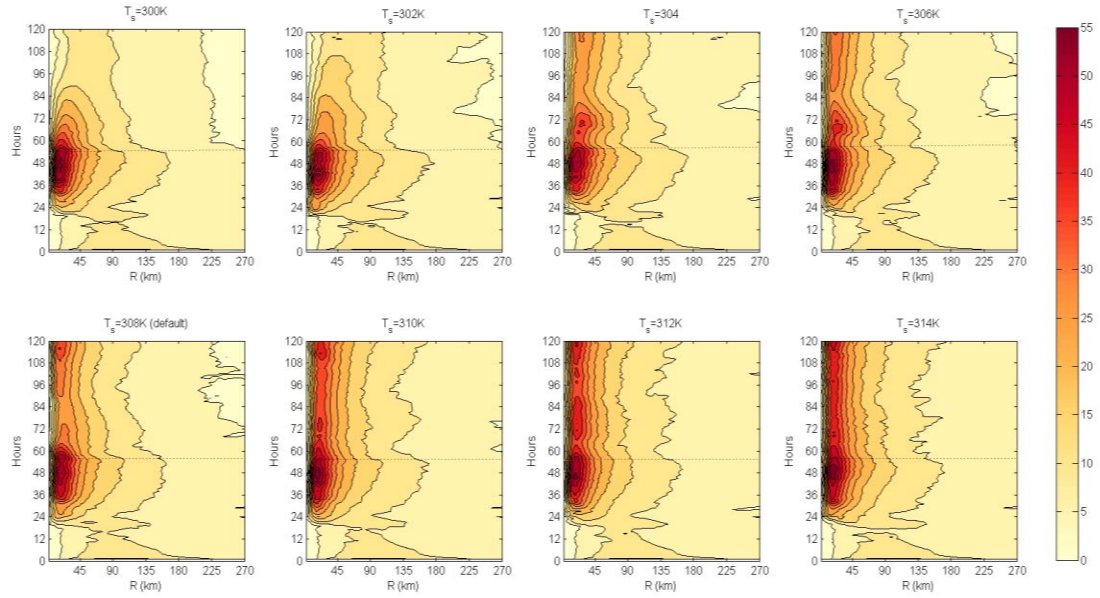

Figure 5.1 Time evolution (Hovmöller diagram) of azimuthally-averaged axisymmetric 10 m winds (m s^{-1}) for different land temperatures (300 K to 314 K). The sea surface temperature was 302 K for all experiments.

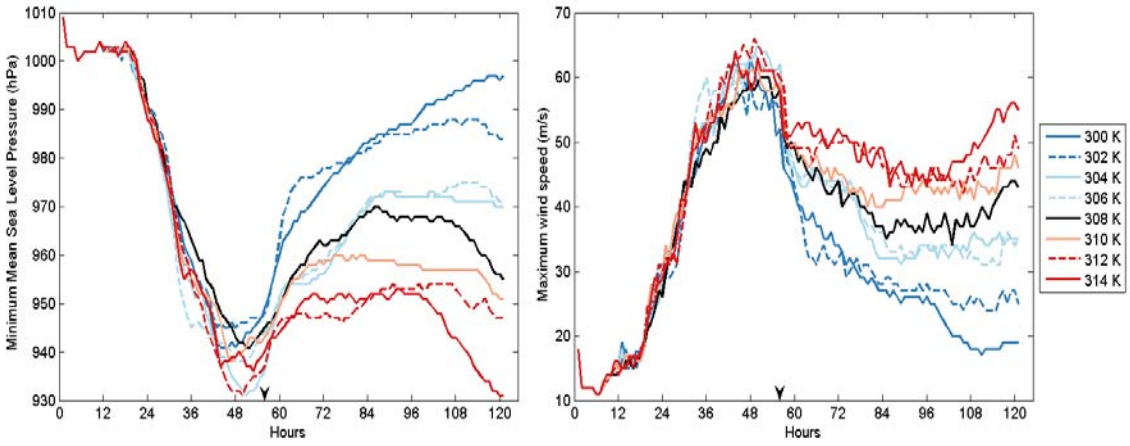

Figure 5.2 Time series of mean sea level pressure in hPa (left) and maximum wind speed in (m/s) (right) for different surface temperatures.

Rainfall has a two primary effects on the soil. While precipitation cools the surface, it also increases the soil heat capacity, neither of which is modelled in HWRF. Rainfall also increases the soil moisture, thus effecting the coefficient of evaporation. Thus, depending on the type of land-surface, the fall in ST may be offset by the higher heat capacity which slows cooling. Note that in the current model configuration, this is simulated by higher surface temperatures for soils with higher thermal diffusivity [cf. Emanuel et al., 2008; Kishtawal et al., 2013]. Sandy soil being highly diffusive, supports instantaneous heat transfer which results in higher SHF. The results suggest that storms are stronger when the land is warmer and SHF is higher. Between 80-85% of the net surface heat flux is comprised of SHF (Figure 5.4). Through evaporation, precipitation is also recycled back into the storm system increasing latent heat fluxes (LHF) which could further intensify the storm.

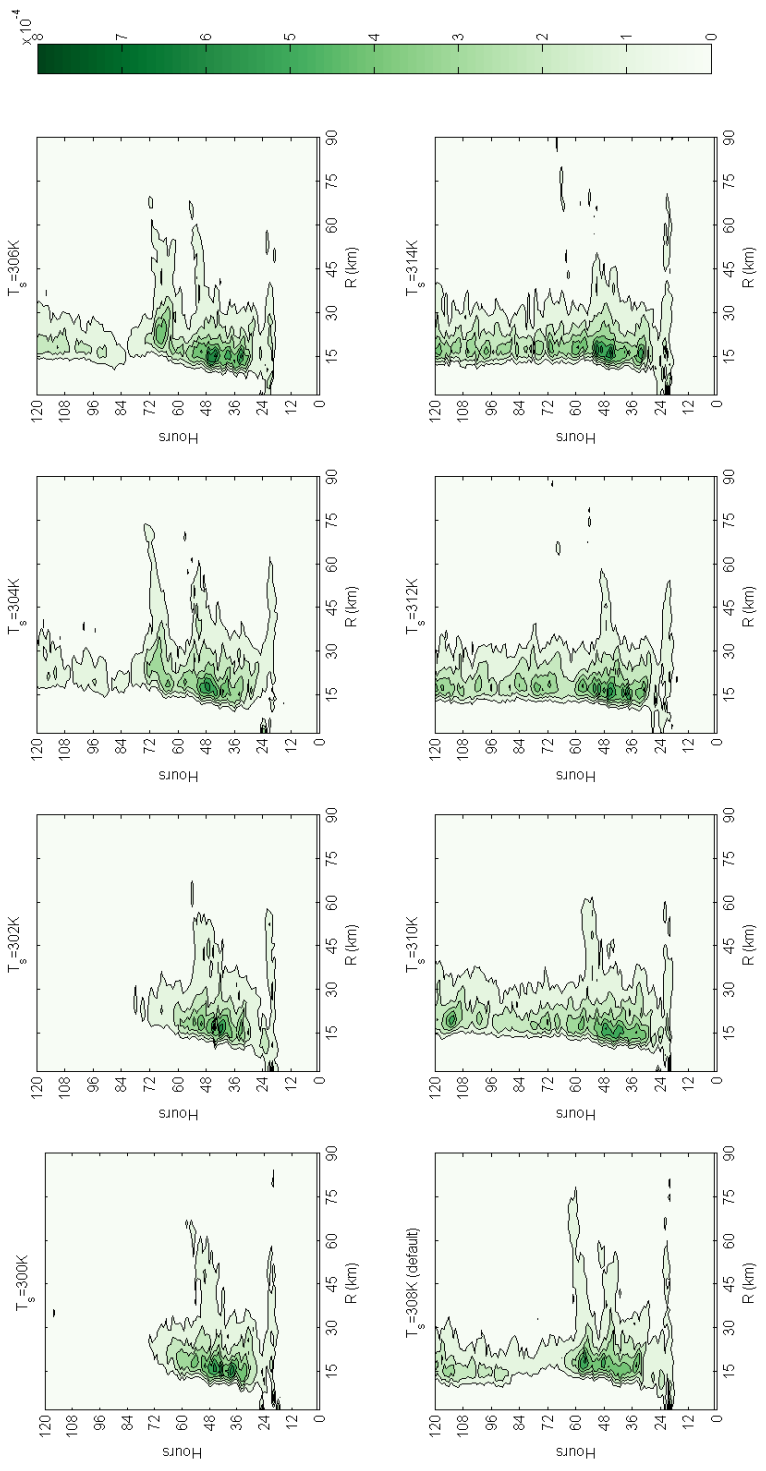

Figure 5.3 Hovmöller of instantaneous precipitation (m) corresponding to different soil temperatures (300 K to 314 K).

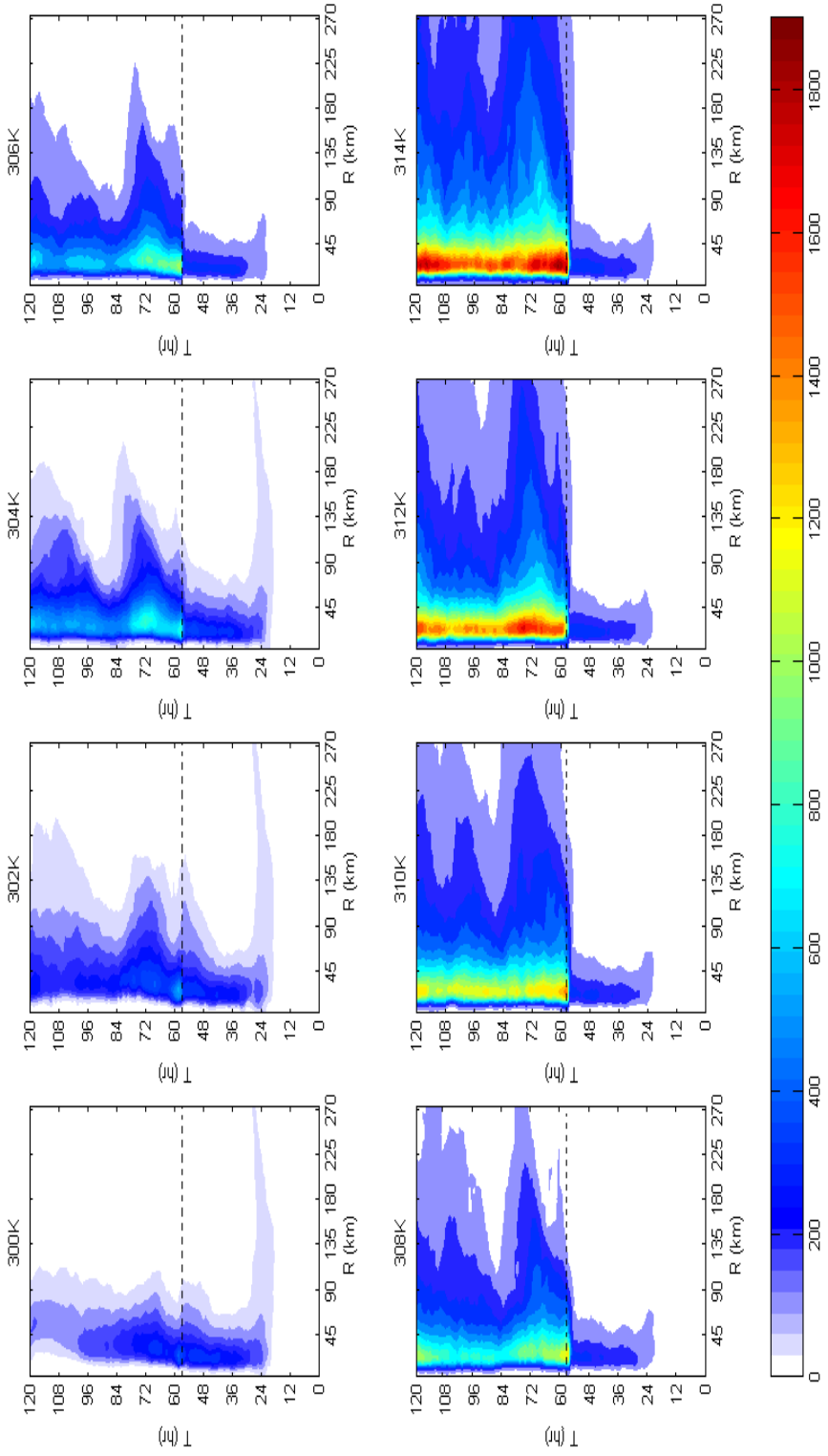

Figure 5.4 Hovmöller of sensible heat flux (W m^{-2}) corresponding to different soil temperatures (300 K to 314 K).

In order to isolate the relative importance of SHF over LHF, an analysis of the total enthalpy fluxes ($\overline{Q_E}$) was done. Enthalpy analysis is a comprehensive and an integrative method to apply to TC intensity studies since it contains both surface fluxes and wind component in the analysis governing equations. Halliwell et al. [2015] outlined a set of equations to define enthalpy flux ($\overline{Q_E}$) for a storm system as

$$\overline{Q_E}(r,t) = \overline{Q_L}(r,t) + \overline{Q_S}(r,t) = \rho_a L_v C_k \bar{v}_{10}(r,t)\Delta\bar{q}(r,t) + \rho_a c_p C_k \bar{v}_{10}(r,t)\Delta\overline{T}(r,t) \quad \text{... (5.1)}$$

$\overline{Q_L}$ and $\overline{Q_S}$ are the azimuthally averaged latent heat and the sensible heat flux components. $\Delta\bar{q} = \bar{q}_s - \bar{q}_{10}$, where $\bar{q}_s$ is the surface specific humidity and $\bar{q}_{10}$ is the specific humidity at 10 m, $\Delta\overline{T} = \overline{T}_S - \overline{T}_{10}$, where $\overline{T}_S$ is the surface temperature and $\overline{T}_{10}$ is the air temperature at 10 m, C_k is the surface exchange coefficient for heat and moisture, L_v is the latent heat of vaporization, and c_p is the specific heat capacity of air. The difference between enthalpy of the system over the ocean and over land can be attributed to changes in $\Delta\overline{T}$, $\Delta\bar{q}$, and $\bar{v}_{10}$. The change in enthalpy, $\overline{Q_E}$ (r,t) – $\overline{Q_E}$(r,56) is expressed as

$$\delta\overline{Q_E} \approx \rho_a L_v C_k \bar{v}_{10}(r,t)\delta\Delta\bar{q}(r,t) + \rho_a c_p C_k \bar{v}_{10}(r,t)\delta\Delta\overline{T}(r,t)$$
$$+\rho_a L_v C_k \Delta\bar{q}(r,t)\delta\bar{v}_{10}(r,t) + \rho_a c_p C_k \Delta\overline{T}(r,t)\delta\bar{v}_{10}(r,t) \quad \text{… (5.2)}$$

The reference enthalpy was calculated at landfall (t=56 hours). The sum of first two terms is referred to as the ‘land-air part’ and the sum of the other two terms is termed the ‘wind part’. The enthalpy analysis results are presented as Hovmöller diagrams in Figure 5.5. The difference in enthalpy is negative indicating that the storm is always more intense over the ocean as compared to land. Thus, when the relative difference in the enthalpy is

smaller, the post-landfall storm is stronger. The changes in wind speed (δv_{10}) and specific humidity ($\delta \Delta q$) are negative but the temperature difference between land and sea ($\delta \Delta T$) is positive. Thus, the 'wind part' of the enthalpy contributes to a spinning down of the storm and the thermodynamic part consisting of the $\delta \Delta T$ term (part of the sensible heat component) aids in strengthening the storm. For surface temperatures up to 302 K, the difference in enthalpy for the storm decreases with time. This is because at relatively lower temperatures, the storm decays immediately post landfall and the enthalpy approaches zero which is indicative of storm dissipation. For warmer land, $\delta \Delta T$ is positive compared to cooler land surfaces and the relative difference in $d\overline{Q_E}$ reduces thus increasing the total enthalpy of the system. Difference in $\overline{Q_E}$ is almost constant at warmer surface temperatures suggesting sustenance of landfall intensity.

This analysis suggests that warmer land drives higher SHF to increase enthalpy fluxes of the storm ultimately enabling sustenance. These results show that warm soils affect post-landfall storm evolution suggesting that the moisture cutoff after landfall may not be the only reason for post-landfall sustenance of a TC system. The questions then arise, regarding the necessary surface conditions and what surface condition is optimal for storm sustenance. To answer these questions, additional analysis was conducted to isolate the effect of wet and warm soils on post-landfall TCs.

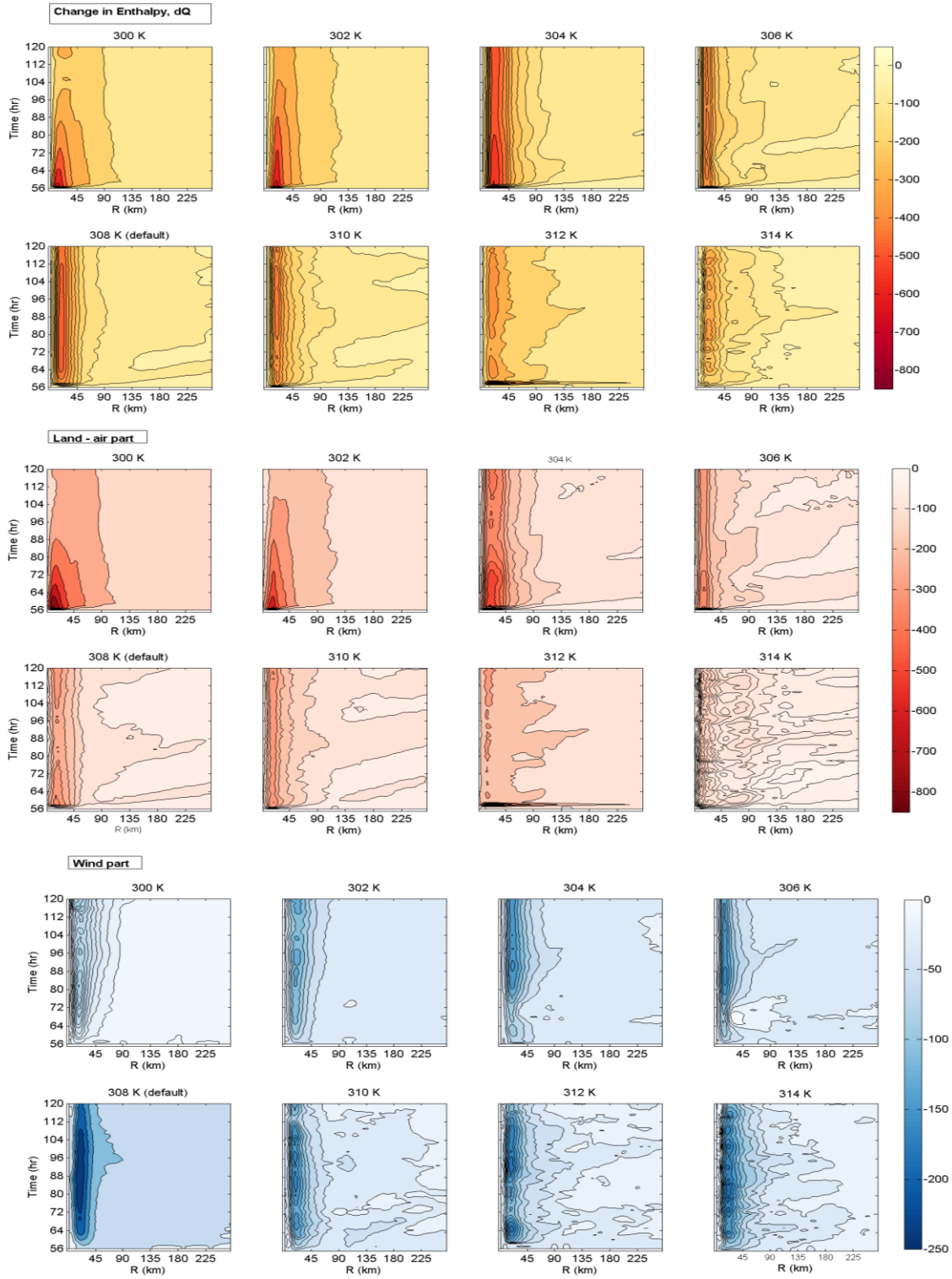

Figure 5.5 Hovmöller diagrams of $\overline{Q_E}(r,t)$- $\overline{Q_E}(r,56)$ in Wm^{-2} (top panel) and its two primary components from Equation (5.2): the air-sea part due to changes in Δq and ΔT (middle panel) and the wind part due to changes in wind speed (bottom panel) for different soil temperature experiments.

5.3.2 Impact of Soil Moisture Content

To assess the impact of land surface soil moisture content a second set of sensitivity experiments (Table 5.3) were performed to assess the impact of SMC of the land surface on the intensity after landfall by changing the SMC to ±50%, ±25% of the default value. The HD of axisymmetric mean winds is given in Figure 5.6. All simulations show a sudden drop in intensity at around 56 hours when landfall occurs but a systematic increase in post landfall intensity is noticed as SMC of LS increases. This is due to the increase in LHF that is available for the storm and this result is aligned with past studies on SM impact on TCs (Tuleya 1994, Chang et al. 2009, Evan et al. 2011, Kellner et al. 2012). The maximum intensity reached by a storm over ocean also changes with varying SM which reiterates the importance of land impacts on tropical systems both offshore and inland.

Table 5.3 Additional experiments for SM, Z_0, size of storm.

Variable	**Sensitivity experiments**
Soil Moisture	SM-50%, SM-25%, SM (default), SM+25%, SM+50%
Roughness length	Z0-50%, Z0-25%, Z0 (default), Z0+25%, Z0+50%, Z0x3, Z0x5, Z0x7, Z0x10
Radius of maximum winds	60 km, 75 km, 90 km (default), 105 km, 120 km, 135 km

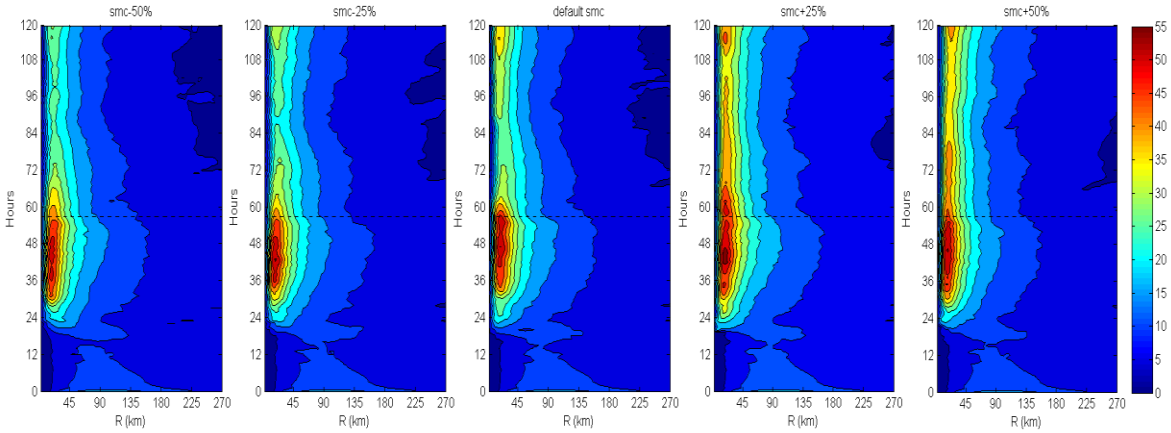

Figure 5.6 Hovmöller of axisymmetric 10m mean winds (m/s) azimuthally averaged around the center of the cyclone for different soil wetness. Landfall is at 56 hours.

5.3.3 Soil Moisture – Soil Temperature Interactions

Four representative simulations were analyzed (Table 5.2) using a control run (F0), one with warmer soil surfaces (F1), another with wetter land (F2), and a run with both warmer and wetter land (F12). This experimental setup is used to extract post-landfall intensity changes occurring with an increase in ST from 308 K to 314 K (f1), and an increase in SM by 50% (f2) as well as the contribution from both higher ST and SM (f12), discussed previously. The experimental design follows the factor separation method outlined by Stein and Alpert [1993] and the equations are outlined in Table 5.4. Intensity contributions through f0, f1, f2, and f12 as calculated from the equations in Table 5.4 is given in Figure 5.7. It is evident that increasing both SM and ST enhances post-landfall TC intensity. However, the impact of warmer soil is observed almost immediately after landfall whereas the effect of an increase in SM is noted almost 15 hours later. The delayed response of a TC to an increase in SM is consistent with other studies noting the positive impact of antecedent SM conditions on TCs [Kellner et al.

2011; Evans et al. 2008; Chang et al. 2009]. The f1 panel in Figure 5.7 also shows that the ST effect is relatively high compared to the SM impact on TC intensity. These results suggest that high ST is a dominant and necessary condition for TC sustenance over bare and sandy land. Results for the f12 field suggest that not only warm and wet surfaces favor TC sustenance over land, there also exists a synergism where the effect of the combination of the two factors is greater than the individual factors alone.

Table 5.4 Interaction terms and equations for the factor separation analysis.

Interaction term	**Factor Separation Equation**
f0	F0
f1	F1 – F0
f2	F2 – F0
f12	F12 – (F1 + F2) + F0

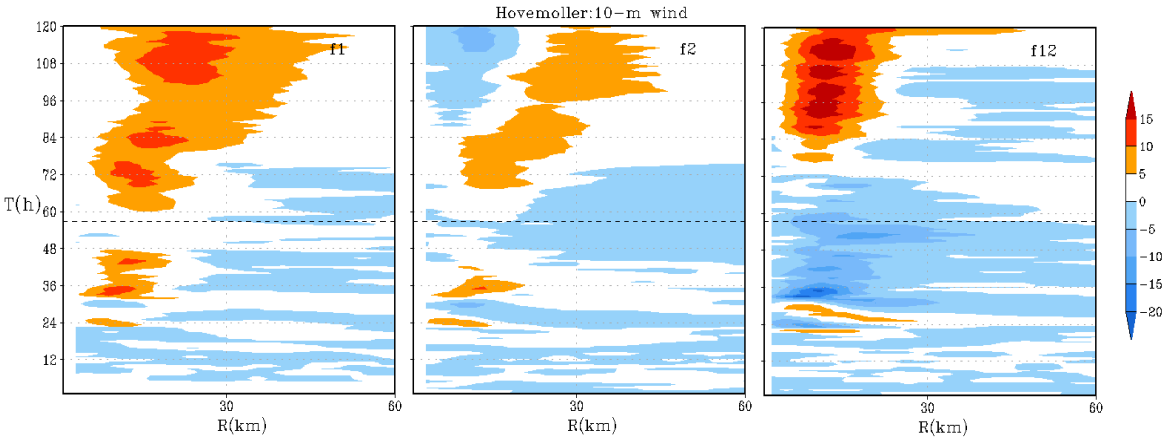

Figure 5.7 Time evolution of mean winds (ms^{-1}) around the center of the cyclone to depict the contribution of individual and the interaction of factors in the factor separation analysis.

To further analyze and verify the above results, a similar FacSep analysis was conducted for a real TC case. TS Erin (2007) was chosen for its distinct strengthening and formation of a post-landfall eye early on 19 August 2007 over Oklahoma. Four experiments were performed using the operational HWRF (v3.7) similar to the idealized FacSep experiments with ST and SM. The experiments were initialized for the 1600 UTC cycle. The physics options are also similar except that real cases uses Noah land model. For the FacSep analysis, the SM and surface temperatures needed to be modified. This was done by increasing the initial fields from National Centers for Environmental Prediction's Final (FNL) Operational Global Analysis dataset by 50% for SM and by 6 K for ST for the four layer Noah LSM that prognostically predicts both ST and SM. These chosen values are guided by multiple idealized sensitivity experiments conducted that show clean signature of both SM and ST. This will enable the model to capture diurnal soil temperature variations as well as surface cooling and soil moisture changes caused by precipitation. The track simulated by these experiments are given in Figure 5.8.

Due to the relative coarse resolution of the FNL data used to initialize the model, there are significant track errors and the tracks of all experiments consistently show a clear westward bias compared to the observed best track data for TS ERIN. The track errors do not however invalidate the land surface effects observed by the storm mainly because of the large swath of land region that the storm encounters. The results are presented as time series plots for MSLP and Vmax (Figure 5.9) for F0r, F1r, F2r, and F12r. The results obtained are similar to those from the idealized runs from the previous section. While the experiments capture the broad features well there are notable difficulties in capturing the

observed intensity changes, and experiments F1r and F12r shows nominal over land intensification after 84 hours of simulation. Despite the model limitation, in the current context, the model does serve its role as a detailed analysis tool to extend the idealized work and study post landfalling systems. When ST was increased initially by 6°C (F1r), the system evolved with lowering of storm central pressure, consistent with the idealized experiments. Increase in SM, in fact, shows increased weakening of storm post landfall compared to observed. F12r shows significant increase in intensity and continues to deepen through 20th of August similar to what was noted in the idealized experiments. The combination of increased soil moisture and soil temperature acts synergistically to setup conditions for post landfall intensification. This result from the TS Erin simulation again highlights that warmer soil emerges as the primary factor supporting re-intensification over land and confirms that the availability of SM helps sustenance. These results also highlight the importance of accurate representation of the land surface, especially antecedent ST and SM in hurricane models to improve prediction of TC landfall characteristics and warrants attention. It is also acknowledged that more detailed analysis of real cases is necessary and results from a few real cases will be presented in the next chapter.

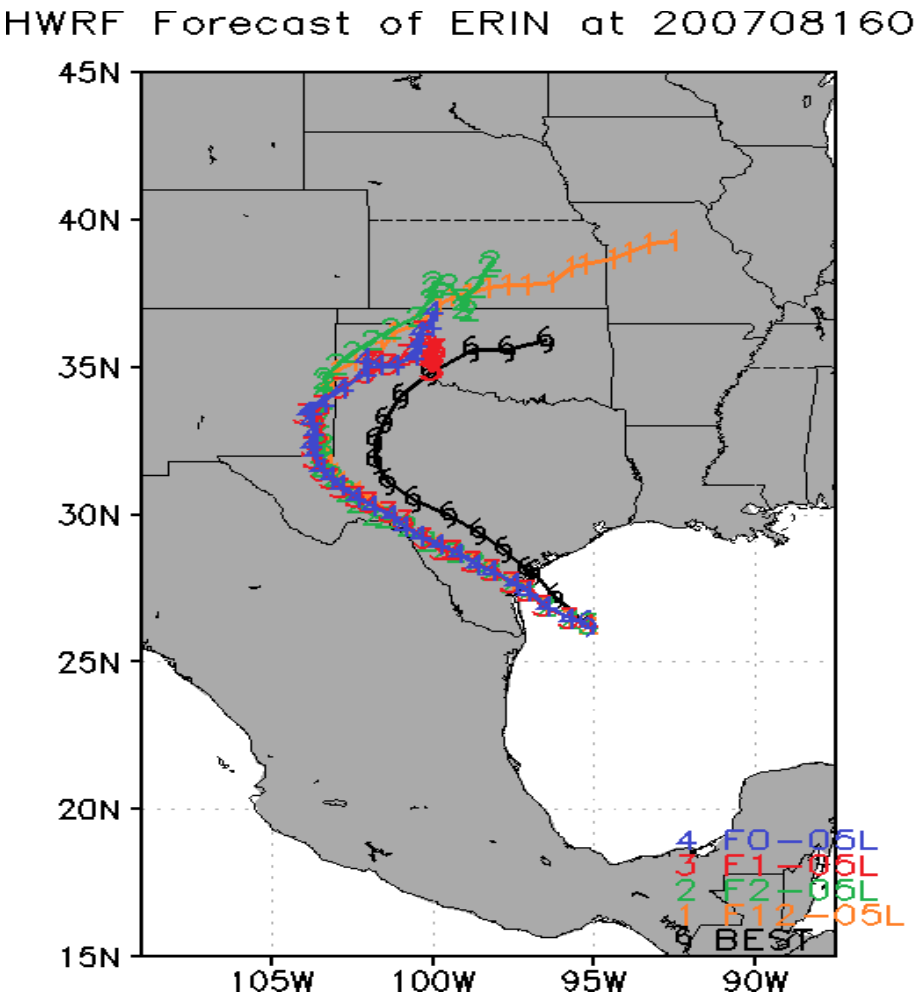

Figure 5.8 Simulated and best track for TS ERIN 2007 initialized at 1600 UTC. The tracks are color coded for experiments F0r (Blue), F1r (Red), F2r (Green), F12r (Orange)

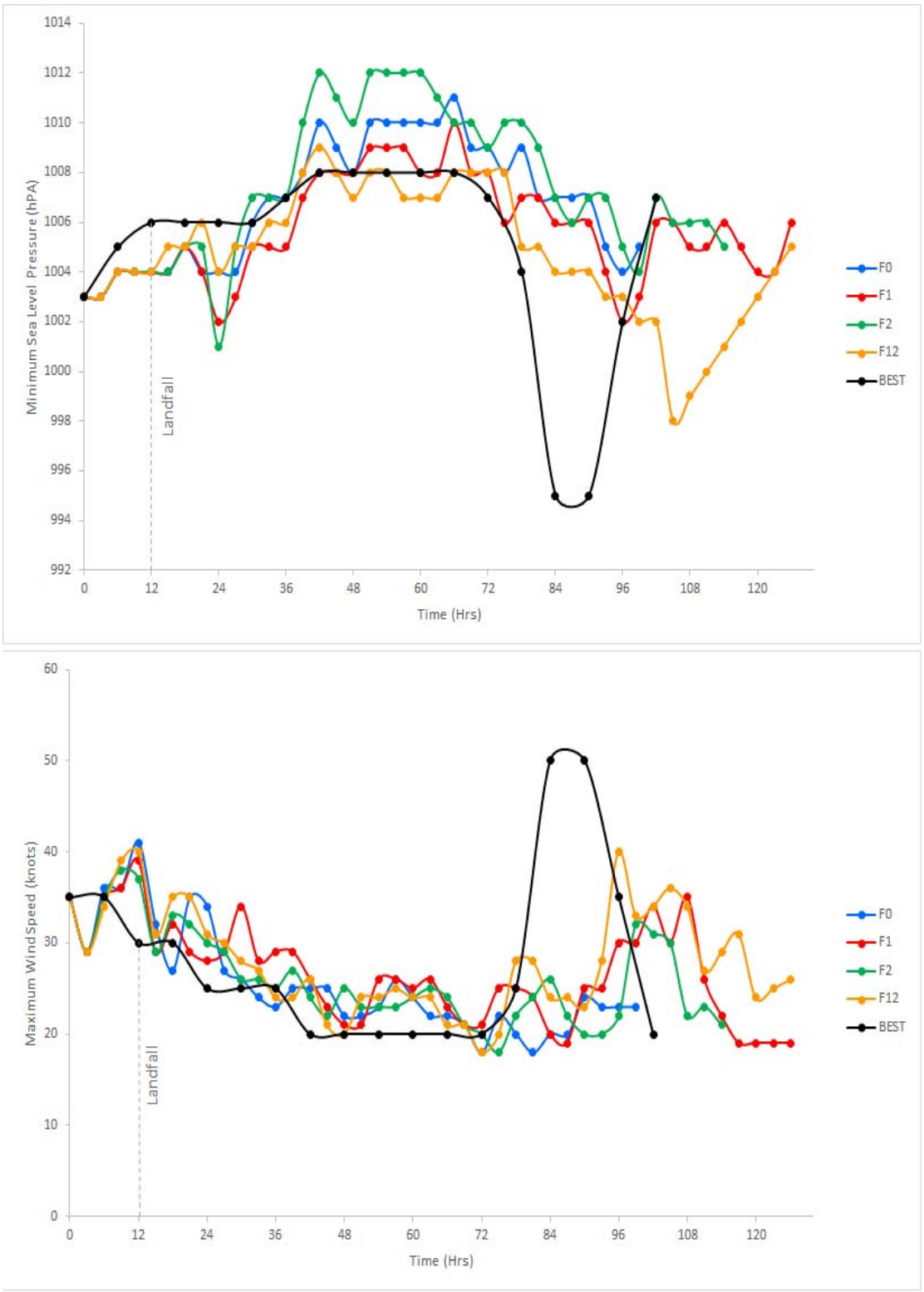

Figure 5.9 Minimum sea level pressure (hPa) (top) and maximum sustained 10 m wind speeds in knots (bottom) for TS Erin (2007) in the factor separation experiments.

5.3.4 Impact of Surface Roughness Length

Roughness length (Z_0) of a surface has a two-way interaction with the BL (Montgomery and Smith 2010). Change in roughness length for momentum (Z_{0m}) which is prescribed over land increases the land associated frictional velocity and decreases tangential wind speed. This can negatively impact the intensity of a cyclone by disrupting the primary circulation and thus structure. On the other hand, increased friction also increases the inflow in the secondary circulation within the hurricane boundary layer (HBL). As the velocity in the inflow layer increases, it favors greater convergence and subsequently divergence aloft. Over land, Z_{0m} is much higher than over the ocean (~ 0.0001m) and thus, the balance over oceans is disrupted. Frictional forces along with drop in surface fluxes cause the TC to decay post landfall.

To study the impact of Z_0, the variable was varied from Z_0-50% to 10 times default Z_0. (Note that since winds show logarithmic variations to Z_0, the changes are 1 order of magnitude) The list of experiments is given in Table 5.3. The results over land indicate that as Z_0 increases, the intensity of hurricanes decrease due to increase in frictional force (Figure 5.10). The pressure drop that is seen with increasing Z_0 may be explained by the increasing inflow and the higher temperature over land. As Z_0 increases, radial wind in the inflow layer increases the extent of convergence there by creating a local low that is enhanced by the high surface temperature (308 K). At lower Z_0, Vmax after is high immediately after landfall but is comparable to other experiments later in the simulations. These results follow past studies (Tuleya 1994; Zhu 2008) and thus highlight the validity of this idealized model setup to simulate TC's response to LS accurately.

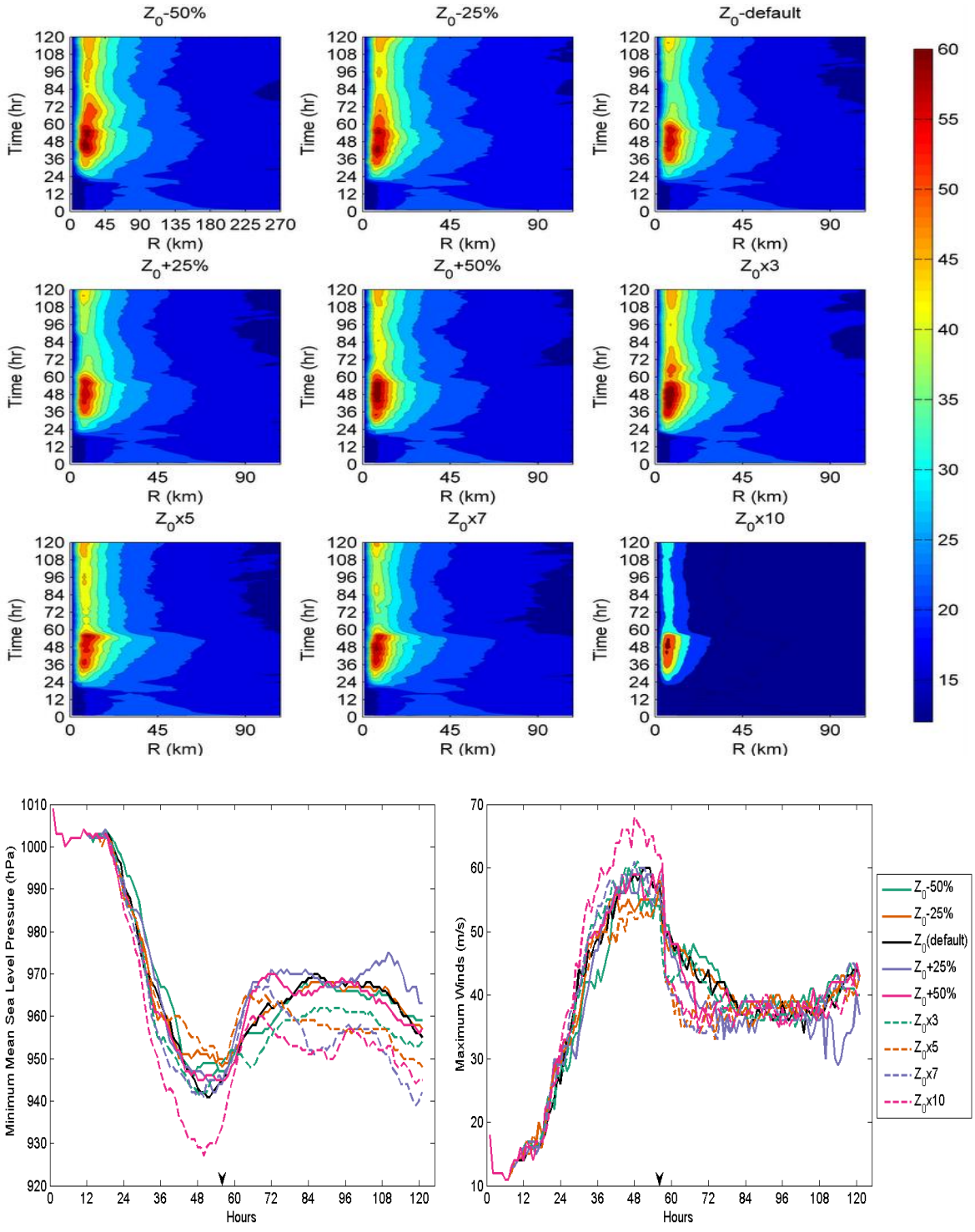

Figure 5.10 Hovmöller of axisymmetric 10m mean winds (m/s) azimuthally averaged around the center of the cyclone for varying roughness length (top). The time series plot for central pressure (hPa) [bottom right] and maximum 10m wind speed (m/s) [bottom left]. Default momentum roughness length is 0.01m.

5.3.5 Impact of Size of Storm

The size of storm was altered by varying the radius of maximum winds from 60 km to 135 km with 90 km as the default size (Figure 5.11). Smaller storms are less intense over the ocean as well as over land after landfall. The storm is less intense but sustains longer over land compared to the default size storm that re-intensifies. The larger storm has a larger wind swath that enables higher moisture and heat convergence at the lower level. Thus, rate of re-intensification post landfall in larger storms is much higher when compared to the smaller storms and there is a definite two-way interaction between land and cyclones.

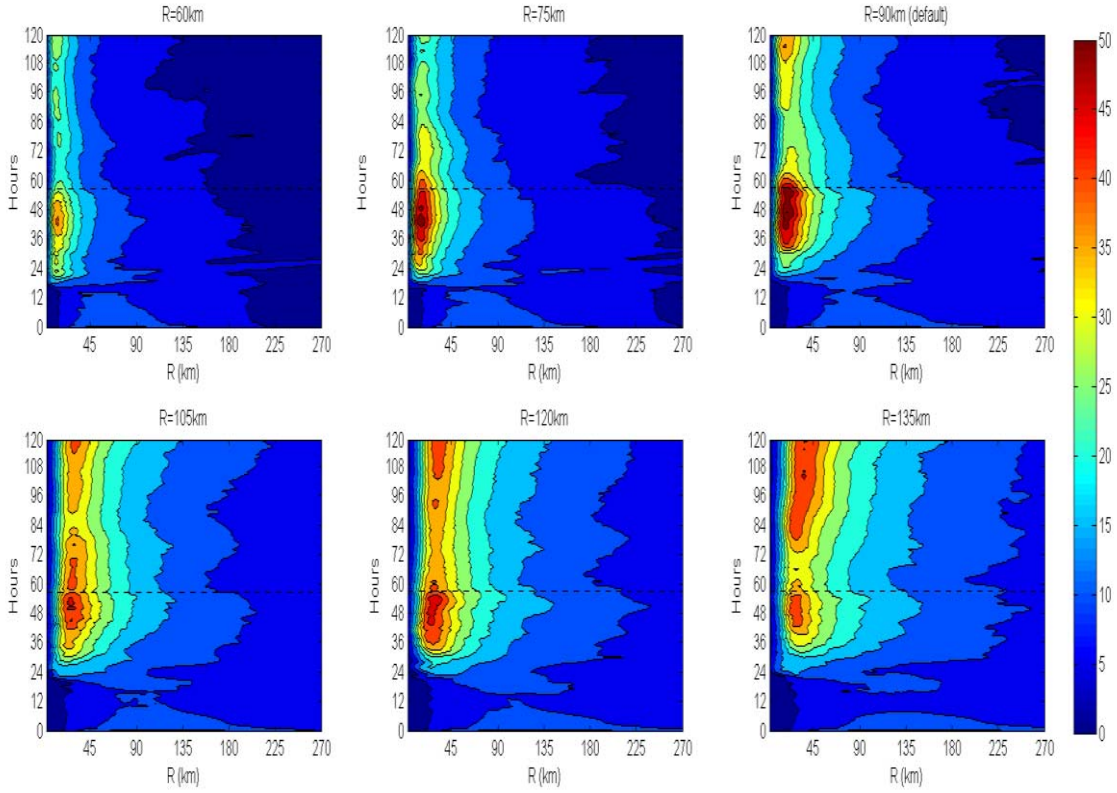

Figure 5.11 Hovmöller of axisymmetric 10m mean winds (m/s) azimuthally averaged around the center of the cyclone for different storm sizes. Default storm size is 90 km and Landfall is at 56 hours.

5.4 Conclusions

This study focused on understanding the effect of land surfaces on post-landfall TCs. Results indicate that warmer land surfaces support TC sustenance by enhancing system enthalpy. The soil characteristics of the land surface are also important to counteract evaporative cooling and increase energy exchange into the boundary layer. It is evident that under certain conditions for TCs over warm sandy soil, if warm soils can be maintained, and moistened by preceding rains, the TCs can sustain or re-intensify through rapid transfer of surface heat flux into the atmosphere.

Results from SM experiments are in line with other studies conducted by Kellner et al. (2012), Chang et al. (2009) and others. By increasing soil moisture content of the LS, the moisture convergence and latent heat fluxes also increase resulting in stronger storms. Larger storms have better chance of surviving inland when compared to smaller storms because stronger circulations are established and land interaction may be a significant factor in its evolution. In addition to this, when LS favors intensification (as it does in the simulations), and the storm interacts with a larger such surface area, the LS interaction only further the already strong system to remain active over land.

Roughness length is a complex parameter to assess and it is known to interact with a hurricane in two ways. Increased roughness affects the primary circulation thereby reducing the intensity, whereas inflow velocity is increased that contributes to larger convergence and strengthen the storm. The results indicate that by increasing Z_0 over land, the cyclone intensity decreases. Drop in surface pressure is observed at higher Z_0

values but the gusting winds remain fairly unchanged and these results are similar to past studies.

To investigate the relative importance of ST and SM effects on TC evolution over land, experiments were designed to isolate their impacts and the impact of the interaction between the factors. This was also followed by a real case analysis of TS Erin (2007) using the quasi-operational version of the model. TC response to higher land temperature is relatively rapid as compared to an increase in SM. The magnitude of intensity changes induced by warmer soils is also greater than the intensity changes due to increased soil wetness. This highlights that a warm surface is a necessary condition for TC sustenance post landfall and the SM adds to the increase in energy of the system. A dominant synergism also emerges from the interaction term between these two parameters suggesting that a warm-wet land surface is more favorable for TC sustenance over land than a cold-dry land surface.

Although opinions differ on the extent of influence of LS on a large system such as TC that is mostly dominated by synoptic conditions, one cannot ignore the contributions of LS on generating small scale features as well as how these LS features drive large scale conditions. Similar to how the SST affects the evolution of the storm, this study brings out the importance of the role that surface temperature plays in the evolution post landfall. The results from this study lay an emphasis on the complex land atmosphere interaction achieved through surface parameters that ultimately plays a significant role in affecting the fate of a landfalling TC and require additional attention and research efforts.

5.5 References

Andersen, T. K., D. E. Radcliffe, and J. M. Shepherd, 2013: Quantifying surface energy fluxes in the vicinity of inland-tracking tropical cyclones. *Journal of Applied Meteorology and Climatology*, **52,** 2797-2808.

Chang, H. I., and Coauthors, 2009: Possible relation between land surface feedback and the post-landfall structure of monsoon depressions. *Geophysical Research Letters*, **36**.

Emanuel, K., J. Callaghan, and P. Otto, 2008: A Hypothesis for the Redevelopment of Warm-Core Cyclones over Northern Australia*. *Monthly Weather Review*, **136,** 3863-3872.

Evans, C., R. S. Schumacher, and T. J. Galarneau Jr, 2011: Sensitivity in the overland reintensification of Tropical Cyclone Erin (2007) to near-surface soil moisture characteristics. *Monthly Weather Review*, **139,** 3848-3870.

Gopalakrishnan, S. G., F. Marks Jr, J. A. Zhang, X. Zhang, J.-W. Bao, and V. Tallapragada, 2013: A study of the impacts of vertical diffusion on the structure and intensity of the tropical cyclones using the high-resolution HWRF system. *Journal of the Atmospheric Sciences*, **70,** 524-541.

Gray, W. M., E. Ruprecht, and R. Phelps, 1975: Relative humidity in tropical weather systems. *Monthly Weather Review*, **103,** 685-690.

Halliwell Jr, G., S. Gopalakrishnan, F. Marks, and D. Willey, 2015: Idealized study of ocean impacts on tropical cyclone intensity forecasts. *Monthly Weather Review*, **143,** 1142-1165.

Kellner, O., D. Niyogi, M. Lei, and A. Kumar, 2012: The role of anomalous soil moisture on the inland reintensification of Tropical Storm Erin (2007). *Natural hazards*, **63,** 1573-1600.

Kishtawal, C., D. Niyogi, B. Rajagopalan, M. Rajeevan, N. Jaiswal, and U. Mohanty, 2013: Enhancement of inland penetration of monsoon depressions in the Bay of Bengal due to prestorm ground wetness. *Water Resources Research*, **49,** 3589-3600.

Kishtawal, C. M., D. Niyogi, A. Kumar, M. L. Bozeman, and O. Kellner, 2012: Sensitivity of inland decay of North Atlantic tropical cyclones to soil parameters. *Natural hazards*, **63,** 1527-1542.

Pielke, R. A., 2001: Influence of the spatial distribution of vegetation and soils on the prediction of cumulus convective rainfall. *Reviews of Geophysics*, **39,** 151-177.

Shen, W., I. Ginis, and R. E. Tuleya, 2002: A numerical investigation of land surface water on landfalling hurricanes. *Journal of the atmospheric sciences*, **59,** 789-802.

Stein, U., and P. Alpert, 1993: Factor separation in numerical simulations. *Journal of the Atmospheric Sciences*, **50,** 2107-2115.

Tallapragada, V., and Coauthors, 2014: Hurricane Weather Research and Forecasting (HWRF) model: 2013 scientific documentation.

Tuleya, R. E., 1994: Tropical storm development and decay: Sensitivity to surface boundary conditions. *Monthly Weather Review*, **122,** 291-304.

Tuleya, R. E., and Y. Kurihara, 1978: A numerical simulation of the landfall of tropical cyclones. *Journal of the Atmospheric Sciences*, **35,** 242-257.

CHAPTER 6. IMPACT OF IMPROVED LAND SURFACE REPRESENTATION ON TROPICAL CYCLONE RAINFALL

6.1 Introduction

Numerical models are useful tools in capturing the micro and macro scale interactions, the planetary boundary layer (PBL) have with the environment and studying the two-way feedback between landfalling TC and land surface characteristics. The models are particularly important because of our current inability to measure these variables in a direct way. Numerous studies suggest that numerical models predict a TC track reasonably well, but most often fail to accurately capture the intensity and evolution of a storm post landfall. Evans et al. (2011) and Kellner et al. (2012) simulated the re-intensification of tropical storm (TS) Erin (2007) over Oklahoma using WRF-ARW and concluded that intensity of the storm and the vortex was dependent on development and maintenance of PBL. They also found that the storm was sensitive to soil moisture (SM) changes and the high soil moisture condition over Oklahoma before the landfall contributed to the re-intensification of storm.

In their study of land falling typhoon Sepat (2007), Zhang et al. (2011) showed that both latent and sensible heat fluxes (LHF and SHF) helped sustain intensity over land along with the spiral structure of rain bands. In addition, they also found that SM initialization impacted storm prediction over land. This conclusion continues to emerge from studies

such as Bozeman et al. (2012) and many others. Kishtawal et al. (2012) used observational datasets and analytical techniques to study the factors influencing the post landfall characteristics of tropical storms over the Atlantic Ocean basin. Their results identify surface roughness and soil heat capacity as two dominant parameters. Model simulations were unable to capture these feedbacks thus highlighting the need to improve the land surface representation for improved post landfall TC characterization. Emanuel et al. (2008) studied the TC Abigail (2001) over Western Australia which underwent a significant period of re-intensification twice over land and concluded that surface and boundary layer interactions play an important role in the life cycle of a storm in intensifying the TC. Over the Indian monsoon region (IMR), it has been observed that monsoon depressions over land sustain themselves longer post landfall, if the 7-day antecedent soil moisture availability was high (Chang et al., 2009; Kishtawal et al., 2013).

Bister and Emanuel (1998) concluded that the bulk of dissipative heating occurs near the atmospheric boundary layer and positively influences the storm centric wind speed maxima. Emanuel (1998) developed an asymmetric hurricane model in which the maximum winds increase with C_k and decrease C_d similar to the Malkus-Riehl and Ooyama models and the hurricane intensity depended on the ratio of transfer coefficients. Braun and Tao (2000) studied a combination of boundary layer schemes with identical values of C_k/ C_d, and concluded that the intensity is not only related to the magnitude of C_k/C_d but also on 'the wind speed dependence of roughness parameter Z_0. These results call for a better representation of the surface processes that govern intensity predictions

of hurricane and their dependence (or lack thereof) on exchange coefficients. Montgomery et al. (2010) conducted numerical experiments in which the intensification rate and vortex intensity increases with additional surface drag until a certain threshold value is attained after which intensification rate decreases. This emphasizes the importance of surface friction in increasing radial inflow into the hurricane boundary layer and thereby creating a zone of convergence for surface fluxes to fuel the cyclone. The turbulence mixing processes within the hurricane boundary layer plays an important role in regulating the radial and vertical distribution of enthalpy and momentum (from the sea surface to the atmosphere and vice-versa) and, consequently, the TC intensity changes (Gopalakrishnan et al., 2013; Emanuel, 1986, 1995). Classical studies like Smith (1968) have concluded that insufficient information and understanding of turbulence hindered a more realistic understanding and representation of the boundary layer. To this day, even with the availability of high resolution TC prediction models it is quite challenging to realistically represent the boundary layer processes. The transfer and diffusion of fluxes from the land surface to the atmosphere and vice versa are dependent on at least four key parameters - surface exchange coefficients for momentum (C_d), moisture and heat (C_k) and eddy diffusivity for moisture and heat (K_h) and momentum (K_m). Nevertheless, there is a large degree of uncertainty in the estimates of these variables. Thus, the structure and intensification processes of TCs simulated by high-resolution numerical models are dependent on the parameterizations used in the surface layer and the boundary layer (e.g., Braun and Tao, 2000; Nolan et al., 2009a, b; Montgomery et al., 2010; Smith and Thomsen, 2010).

Gopalakrishnan et al. (2013) used an idealized framework of the HWRF system to gain additional understanding of the variability in TC structure and intensity with respect to vertical diffusion. Decrease of eddy diffusivities, K_m (and K_h), to 25% of its original value produced comparable diffusion coefficients consistent with observations (from CBLAST) in the HWRF surface parameterization scheme (GFS scheme). Reduction of K_m had notable influence on the structure, size, and evolution of the cyclone vortex. With K_m set to 25% of its original value, the inflow layer depth decreased more consistent with the observations. The inflow velocity increased with decreased in inflow layer depth. Stronger inflow not only increased the primary circulation of the storm by increased the Coriolis term, but also increased the equivalent potential temperature in the boundary layer resulting in a stronger and warmer core.

Other studies that have highlighted the role of boundary layer feedbacks are Anthes and Chang (1978), Emanuel (2003), Smith and Thomsen (2010) and Wang and Wu (2004). Pielke (2001) has shown that underlying surface characteristics such as topography, vegetation characteristics, soil temperature and soil moisture, roughness and emissivity have great influence on convective systems that pass over areas with surface heterogeneities. Numerous studies have acknowledged the influence of surface conditions on drylines, fronts and low-level jets. Hence accurate representation of land surface is becoming increasingly important in this world of rapidly changing landscapes.

As highlighted in Subramanian et al. (2014) and previous chapter, TCs are impacted by surface enthalpy fluxes. TCs behave like large heat engines and in the absence of moisture fluxes, they usually decay rapidly. But there are storms that are known to have

passed over extremely dry and hot conditions and sustained or even re-intensified after landfall (e.g. TC Abigail, Emanuel et al. 2008). TC Abigail made landfall on the southern coast of the Gulf of Carpentaria in Australia around 1200 UTC 26 February 2001 with an estimated maximum sustained 10-min mean wind speed of 33 m/s (Figure 6.1). The cyclone weakened while moving in a general westward direction but later anomalously re-intensified over land. Emanuel et al. (2008) conducted idealized simulations and concluded that the warm and thermally diffusive soil in northern Australia after being wetted by initial rains from the extended rain bands of TC, may be able to rapidly transfer heat upwards to maintain and in some cases even re-intensify storms over land. This finding is of interest but emphasizes that underlying soil must be quite hot and have a large enough heat conductivity when wet to support some storms. The simulations also demonstrate the storm intensification may also depend on antecedent moisture availability as well as the translational speed of storm a feature confirmed in Subramanian et al. (2014).

One of the major challenges that operational community faces is to estimate the post landfall precipitation and flood threat associated with a cyclone. To predict the rainfall patterns accurately, track forecast accuracy becomes a primary factor. Bozeman et al. (2012) conducted a series of simulation on TS Fay (2008) using the HWRF modeling systems with two land surface parameterizations – the simple GFDL SLAB model and the more detailed NOAH LSM (Figure 6.2). The study focused on TS Fay because the storm developed an eye-like structure only after landfall over South Florida (Stewart and Beven, 2009). The Bozemann et al. (2012) study summarized three important results. (i)

land surface representation and the choice of land model is important to simulate storm track but did not affect the intensity. The improved track predictions from Noah land model (Figure 6.2) improved the predicted rainfall distributions and is in line with past studies that have suggested a similar relationship (Lonfat, 2004; Marchok et al., 2007; Rodgers et al., 2009); (ii) initial and boundary conditions are important for simulating the development of TCs as is important the representation of boundary layer processes, and; (iii) heterogeneity in land surface did not play as big a role in simulating the TCs but slight influences were noted. The study also noted that the presence of a large water body caused a decrease in surface pressure, but does not affect the TC intensity prediction much.

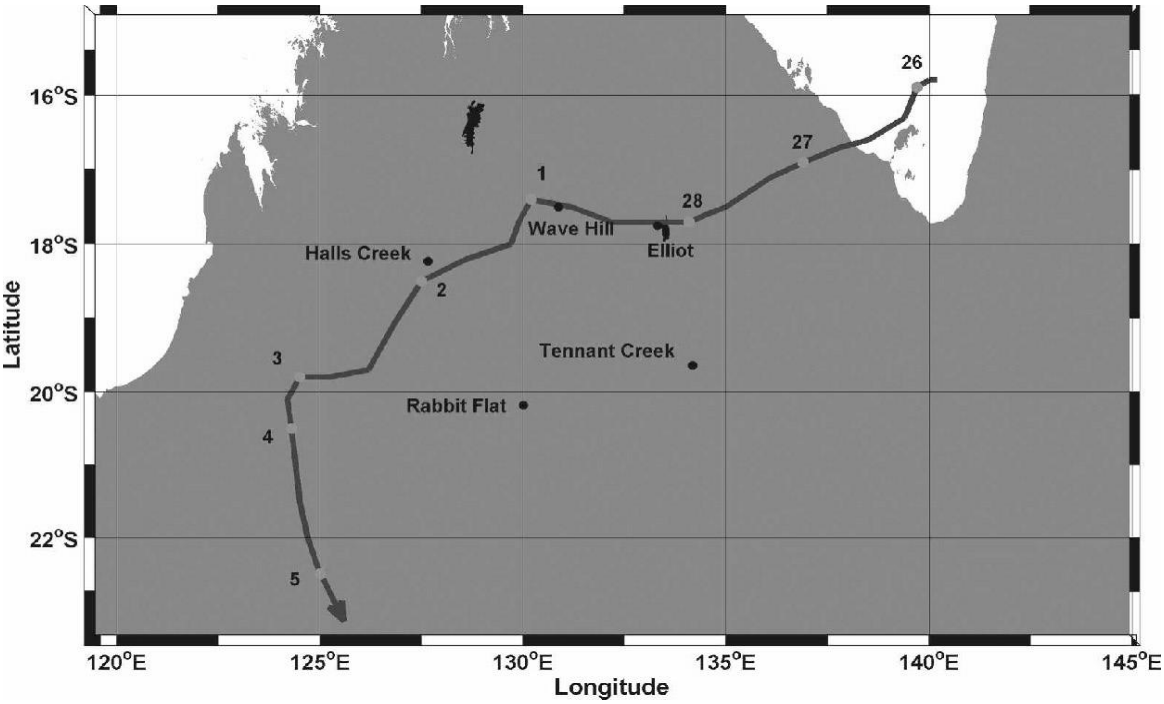

Figure 6.1 Track of Abigail following landfall on the southern Gulf of Carpentaria coastline from 1100 UTC 27 Feb 2001 (271100 UTC on map) to 0632 UTC 3 Mar 2001 (030632 UTC on map).

A number of studies now make a case for a more realistic land surface representation in numerical weather prediction (NWP) models (e.g Holt et al., 2006; Niyogi et al., 2006; Trier et al., 2004; Kellner et al., 2012). Studies (Tuleya 1994; Kellner et al., 2012) have shown that land surface heterogeneity and feedback could influence convective structure of tropical systems and sustain landfalling storms. Chang et al. (2009) isolated the effect of antecedent soil moisture, storms' rainfall and latent heat release, to provide evidence that warm, wet antecedent soil conditions can lead to more intense and sustained post-landfall TCs. The validity of these results and findings are further strengthened by the analysis of 183 landfalling monsoon TCs by Kishtawal et al. (2012). The hypothesis that, antecedent soil moisture conditions affect post landfall storm sustenance seems to be viable because of similar results found in a global model used over the Indian region (Dastoor and Krishnamurti, 1991) and Northern Australia (Emanuel et al., 2008). While the impact of land surface heterogeneity on convection has been the topic of research for several years (Pielke, 2001), how land surface heterogeneity and antecedent soil moisture conditions affect synoptic scale systems remains to be investigated.

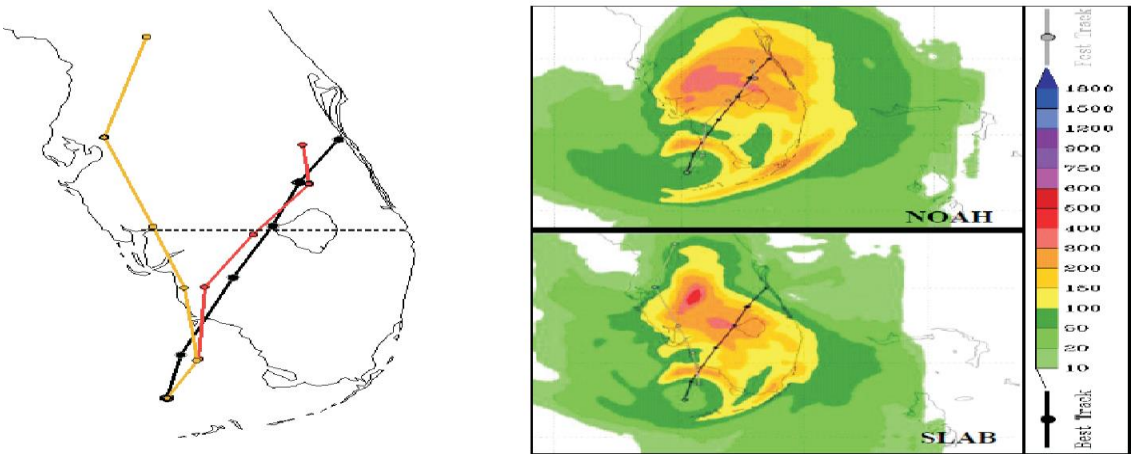

Figure 6.2 Left: Dotted line indicates the location of the cross section for the GFDL Slab (S) and Noah (N) LSM tracks for TS Fay (2008). Right: Noah (top) and GFDL Slab (bottom) LSM accumulated rainfall (mm) from 00Z Aug 19 until 06Z Aug 20. (Source: Bozeman et al. 2012)

6.2 Impact of Improved Land Surface Representation in Tropical Cyclone Simulations

As noted previously, while track prediction of TC (TC) has much improved over the past few years, the skill in TC intensity prediction has not similarly improved. Tropical systems typically weaken rapidly after landfall due to lack of surface moisture fluxes. The broad premise of land surface characteristics bearing an impact on convective events becomes even more important when simulating landfalling TCs. This section investigates the impact of two land surface schemes – SLAB and NOAH schemes on the antecedent land conditions that may influence the landfall and post landfall characteristics of TCs using the HWRF modeling tool. SLAB is the simpler single layer land model with prognostic soil temperature scheme and a constant soil moisture availability and no explicit vegetation scheme while NOAH land surface scheme is a 4-layer model with prognostic soil temperature and soil moisture and has a moderately complex vegetation representation. NOAH LSM is currently the operational LSM in HWRF (as of 2015). The soil

moisture/vegetation transpiration/evaporation feedbacks on the surface energy balance to develop different surface temperature and boundary layer characteristics and can interact with the regional mesoscale convergence and circulation patterns in the model leading to the modulation of the track inland precipitation and possibly, the intensity of the landfalling system. It is hypothesized here that NOAH land scheme with better representation of land surface conditions than SLAB would perform better in TC simulation than the SLAB model. In other words, the study builds off the work reported in Bozeman et al. (2012). The novelty is in the use of the most upto date version of the HWRF model, in the cases being considered and focus on the inland storm rainfall.

6.3 Experimental Setup

The WRF-NMM atmospheric component of HWRF (2015) was used to conduct these experiments. Ocean coupling with POM-TC and GSI that are part of the larger HWRF suite was disabled to avoid complexity and added feedback through coupling and assimilation. The results were notably different when results were considered for preliminary runs with and without atmospheric assimilation. Experiments using Noah LSM were labeled FY15 and experiments with GFDL-Slab model were labeled Slab.

Track, Intensity and Rainfall were considered to test the model. A comprehensive precipitation verification was conducted. Spatial analysis of precipitation was conducted for each NCEP verification region (Figure 6.3) and outlined under each cyclone. NCEP's Stage IV precipitation dataset is used as observation in addition to land surface observations from NCDC's US Climate Reference Network. NCEP's Stage IV

precipitation is a 4 km gridded analysis dataset that ingest radar and gauge data and produces hourly, 6 hourly and 24 hr accumulated rainfall dataset. USCRN dataset is an hourly dataset for soil moisture, soil temperature, and surface temperature.

The following cyclones were simulated and the effect of using an advanced Noah land model to GFDL Slab model were studied. These cyclones were selected for their uniqueness and because they had notable inland feedbacks.

a. Hurricane SANDY (18L, 2012) – CASES 2012102212 to 2012103100 (every 6 hours)

b. Hurricane IRENE (09L, 2011) – CASES 2011082100 to 2011082900 (every 6 hours)

c. Tropical Storm DON (04L, 2011) – CASES 2011072718 to 2011073006 (every 6 hours)

d. Tropical Storm BILL (02L, 2015) – CASES 2015061600 – 2015061706 (every 6 hours)

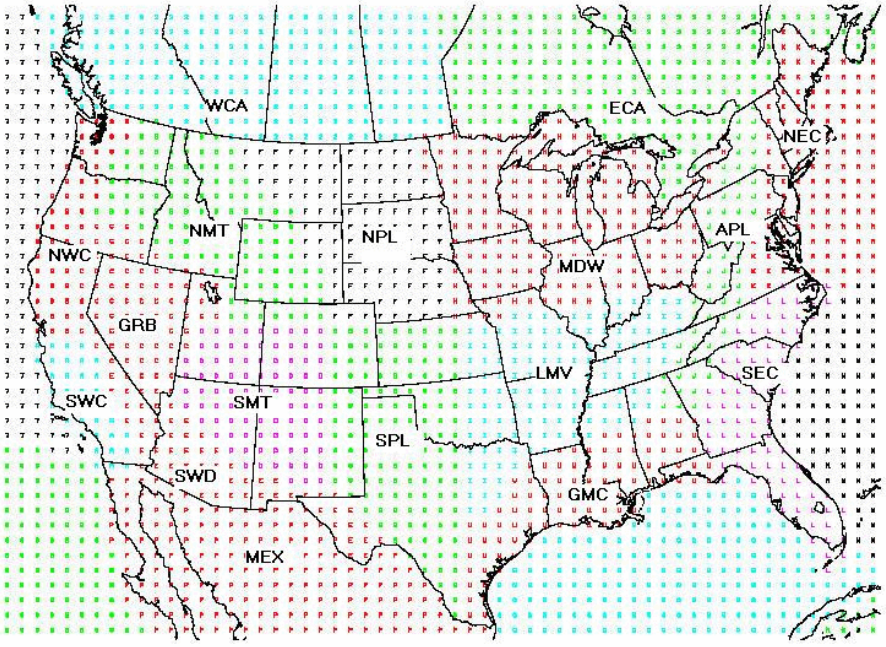

Figure 6.3 NCEP pre-defined verification regions (Source: NCEP)

Hurricane SANDY was one of the most catastrophic storms in the history of United States due to its size and associated storm surge and rainfall over New York and New Jersey. It was the second costliest hurricane since 1900.

Hurricane IRENE was chosen again for its size. It also remained cyclone intensity for days after landfall over North Carolina and stayed parallel to the eastern coast in the US after which it transitioned into an extratropical cyclone similar to SANDY

Tropical Storm DON was selected for its timing and impact on drought stricken Texas. The storm decayed well before landfall probably due to dry air intrusion and predominantly cold and dry land surface over Texas. The effect of LSM on this storm is especially interesting when compared to Tropical Storm ERIN (2007) studied in the previous chapter.

Tropical Storm BILL (2015) brought in notable rains over the Gulf region is Texas and Oklahoma and caused localized flooding. Although like TS Erin (2007), it was predicted to undergo re-intensification over Texas/ Oklahoma due to anomalous soil moisture conditions over land, it decayed post landfall. In addition to precipitation analysis, land surface temperature and soil moisture were compared to observations and initial analysis on why TS BILL did not re-intensify over land as predicted is conducted.

6.4 Surface Layer and Land Surface Model within HWRF

Before comparing Noah and Slab results, the surface layer formulation coupled with the land model as used within HWRF was analyzed. Hurricane Sandy was used as test case. The meteorological setting on Sandy's history and evolution will be discussed in the

section. The intent of this section is only to analyze the surface layer and LSM that is being used in operational HWRF. The operational HWRF model uses GFDL surface layer scheme and Noah land model. The function of the surface layer scheme is to interact with the land model and estimate surface exchange coefficients for heat and moisture (C_d and C_h). The GFDL surface layer uses the Monin-Obukhov similarity theory to calculate these values. If GFDL Slab model is used, the temperature prediction flag within the module is activated and the surface temperature is predicted explicitly without the use of the exchange coefficients calculated. When Noah land model is used, the temperature flag is switched off and the surface layer passes on the surface exchange coefficient values to the Noah land model. It was also noted that when Noah land model coupled with GFDL surface layer is used, the surface temperature predictions were abnormal for certain region and sometime quite high (in the order of 100 °C) which would make the model numerically unstable and crash. This error, it was discovered was due to the extremely high C_h calculated within the surface layer scheme. At very low wind speeds, the C_h values calculated over land were more than 10 times more than typical values observed over land. Typical values over land are around 0.012 -0.015 (Figure 6.4).

Note that within the GFDL surface layer the surface roughness length for momentum and heat are assumed equal which is also not physical. Analytical studies have placed the value of momentum roughness length (z_{0m}) to be one-tenth of roughness length for heat and moisture (z_{0h}). To overcome the high surface temperature values, the C_h values were capped at 0.05. The HWRF model was stable and the surface temperatures were plotted

to compare Slab, Noah-capped (HCAP) and GFS surface temperatures (assumed true values). It was observed that Slab predicted temperatures had an inherent cold bias when compared to GFS skin temperature values and Noah LSM was still showing points of high surface temperature (40-60 °C) (Figure 6.5).

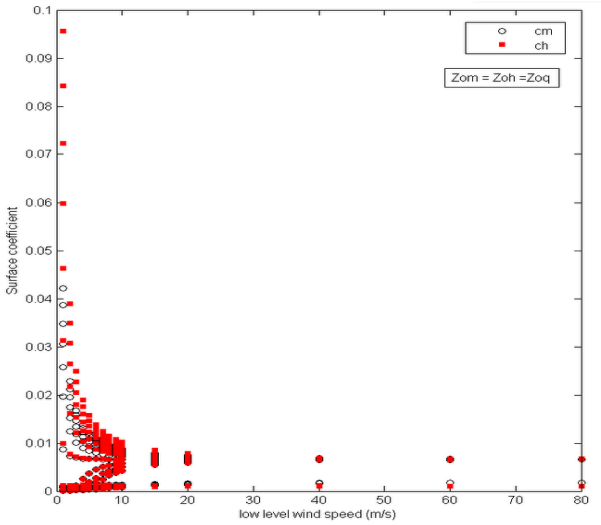

Figure 6.4 Surface exchange coefficient for heat (C_k) plotted against varying low level wind speeds (m/s).

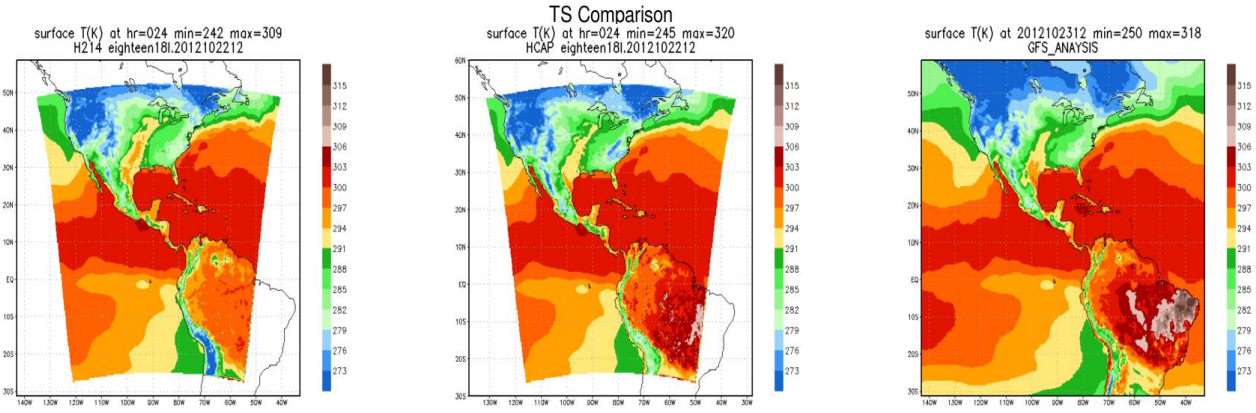

Figure 6.5 Surface temperature comparison between Slab, Noah (HCAP) and GFS (assumed true) data.

Another experiment was run with SANDY and the roughness length formulation was modified to reflect past studies where $z_{0m} \neq z_{0h}$ (MODZOT). The surface exchange coefficient for heat was plotted similar to Figure 6.4 and it was observed that its values were relatively damped and typical of C_h values over land (see Figure 6.6). The surface temperatures were plotted and compared again to GFS values (Figure 6.7). The points of temperature variations were absent in the MODZOT experiments. A time series plot for surface temperature was also reviewed at different grid points where high temperature was observed in the Noah experiment (see Figure 6.8) for every timestep within the model. It was concluded that the roughness length formulation did not solve the temperature fluctuation but the model missed capturing the fluctuations since only 3-hourly outputs are captured by the model.

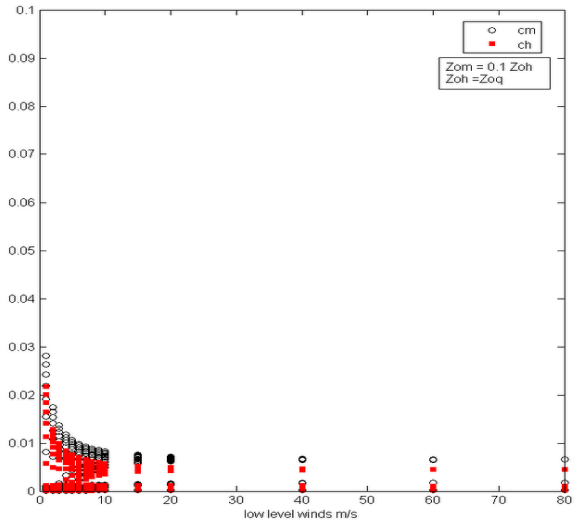

Figure 6.6 Surface exchange coefficients plotted against low level wind speeds (m/s)

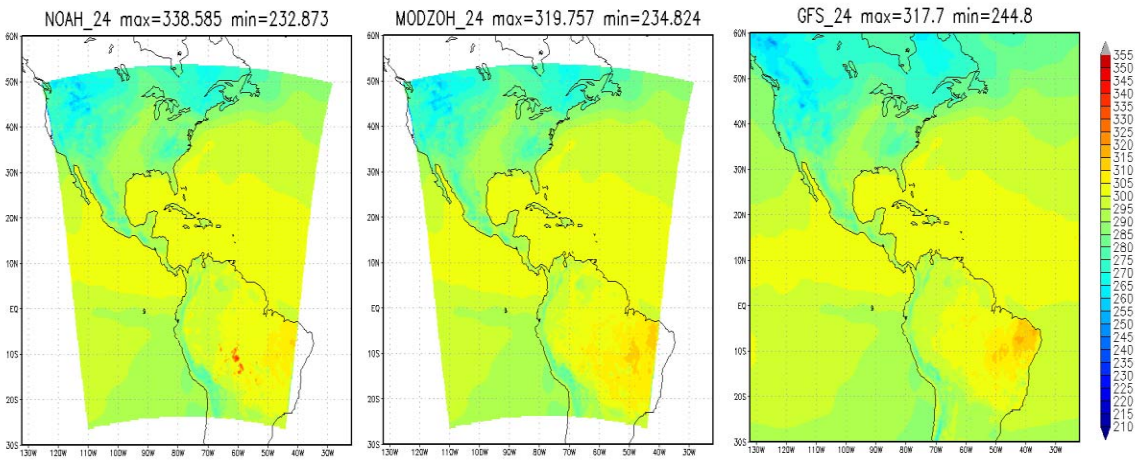

Figure 6.7 Surface temperature comparison between HCAP and MODZOT experiment with GFS skin temperature dataset.

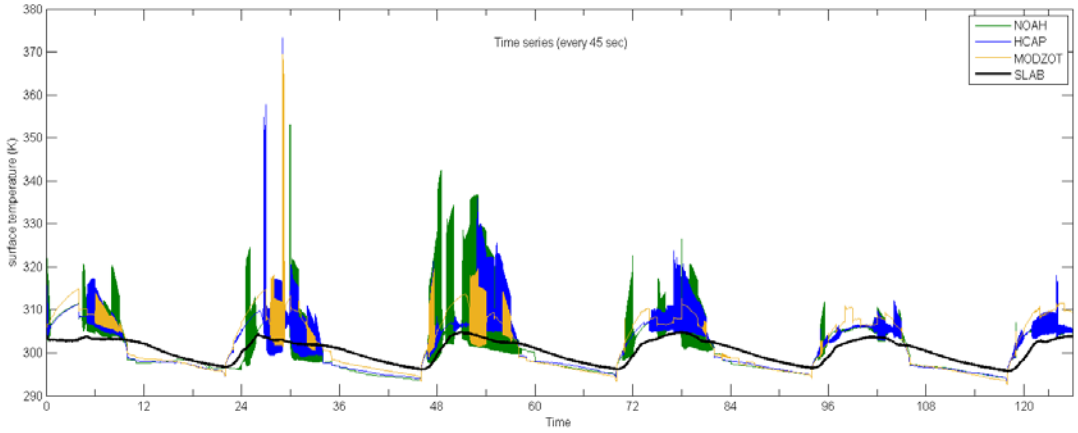

Figure 6.8 Time series for surface temperature model output captured every 45 secs in the model. The fluctuations are still observed even with modified surface roughness formulations.

These results have led us to conclude that C_h formulations within GFDL surface layer may not compatible with Noah LSM and has been highlighted within the NCEP community and significant research efforts are needed to make the GFDL surface layer work seamlessly with Noah LSM. Discussions with the operational and research HWRF

teams led to the conclusion that undertaking this modification would be beyond the scope of this dissertation.

This also means that the surface fluxes calculated within Noah LSM may be incorrect and boundary layer evolution have constraints in not capturing the full extent of land atmosphere interactions which could, in some cases cause errors in precipitation and other meso- and microscale features. A comprehensive precipitation evaluation is also required to test the hypothesis and the HWRF model was run with the HCAP formulation (herewith called Noah/ FY15/ CTRL) that is used in the operational configuration of HWRF. Both Slab and Noah experiments could have unknown errors in precipitation estimates and is expected to be so.

6.5 Impact of Improved Land Surface Model Formulations on Tropical Cyclone Simulations

6.5.1 Hurricane SANDY (2012)

Hurricane SANDY was a category 3 storm that underwent extratropical transition over the Atlantic Ocean. It made landfall over New Jersey as an extratropical storm. In spite of SANDY being in a high shear environment over the Atlantic Ocean, it continued to strengthen due to a favorable trough over southeastern US which continued to provide the baroclinic forcing for the storm to sustain and deepen. After landfall, the cyclone weakened and the remnants slowly moved west and northward into Canada.

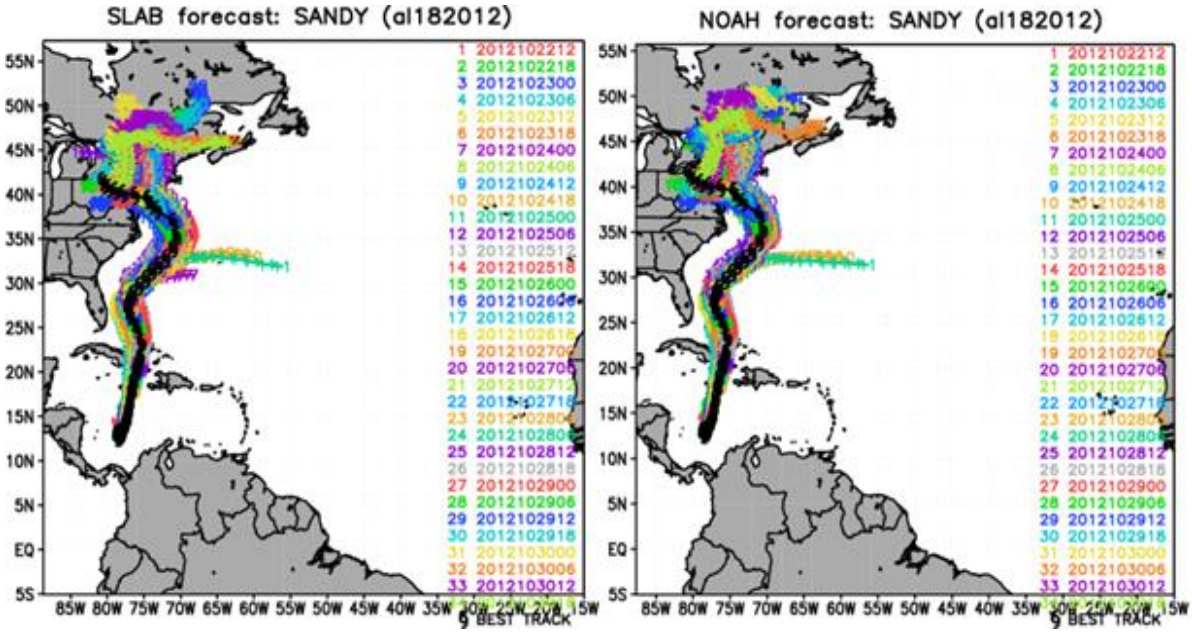

Figure 6.9 Composite track plots for Hurricane SANDY. Cycles run with GFDL-Slab land model are on the left and with Noah land model are on the right. The cycles are number and color coded.

The track of cyclone is given in Figure 6.9. Slab and Noah land model were used to run 68 simulations (34 each). The tracks largely converged and were found to be close to observations with a very small spread. Three cycles with Slab experiments (Cycles 7, 10, 11 in figure) and two with Noah LSM (Cycles 10, 11 in figure) diverged from the track and shows the storm track to lead eastward into the Atlantic Ocean instead of showing the observed recurvature. The composite plot of minimum sea level pressure and maximum winds are shown in Figure 6.10. The storm track, VMAX and MSLP of both Slab and Noah experiments compare well to observations large extent and not much of a difference can be ascertained between Slab and Noah experiments.

24 hour accumulated rainfall immediately after landfall was also compared (cycle – 2012102912) with Stage IV observed precipitation dataset and notable are seen. The spatial distribution of precipitation with both Noah and Slab are almost identical while the rainfall totals vary considerably. In general, precipitation in Noah experiments are under predicted compared to Slab though larger errors exist in both experiments in regions of interest. A statistical analysis was conducted and the results are tabulated in Table 6.1. Separate statistical analysis for the entire CONUS grid in addition to analysis for North Eastern Coast region, Appalachian region, Midwest, South eastern coast and Lower Mississippi Valley was conducted. The spatial correlation of rainfall estimate for the entire CONUS region is almost the same for both Noah (0.82) and Slab (0.855) but there is significant difference between the correlation values in the NEC region where SANDY made landfall. The spatial correlation for Slab rainfall is 0.76 compared to 0.65 for Noah rainfall. Both Noah and Slab perform relatively well for the Midwest region and the Appalachians with spatial correlation values around 0.95 and 0.88 respectively. The RMSE values are quite high at 28 mm and 34 mm with standard deviations of 34 and 27 mm (mean rainfall for NEC is 45 mm and 41mm) for Slab and Noah respectively for the NEC region and APL had slightly lower range at around 16 mm. These errors in precipitation may be due to inherent deficiencies in both Noah and Slab land surface parameterization. Slab has cold surface temperature bias and Noah's C_h formulations maybe incorrect resulting in correct surface heat fluxes (both sensible and latent heat components). The more complex model formulations in Noah may also be compounding to the errors already due surface layer parameterization resulting in degrading performances in precipitation estimates.

Table 6.1 Precipitation Statistics for Hurricane SANDY (Cycle 2012102912)

Region	Hurricane SANDY (2012) Ending 2012103012							
	Standard Deviation		RMSE		PR Correlation		Mean	
	Slab	Noah	Slab	Noah	Slab	Noah	Slab	Noah
FULL	15.16	14.04	8.14	8.71	0.86	0.82	5.26	4.92
LMV	2.83	1.58	0.84	0.89	0.98	0.93	0.50	0.20
NEC	34.27	27.11	28.26	33.85	0.77	0.65	45.16	41.22
APL	33.49	32.97	16.64	16.00	0.89	0.89	32.23	31.39
MDW	10.57	10.97	3.16	3.22	0.96	0.96	4.40	4.09
SEC	2.16	2.68	2.78	2.23	0.83	0.90	0.65	0.78

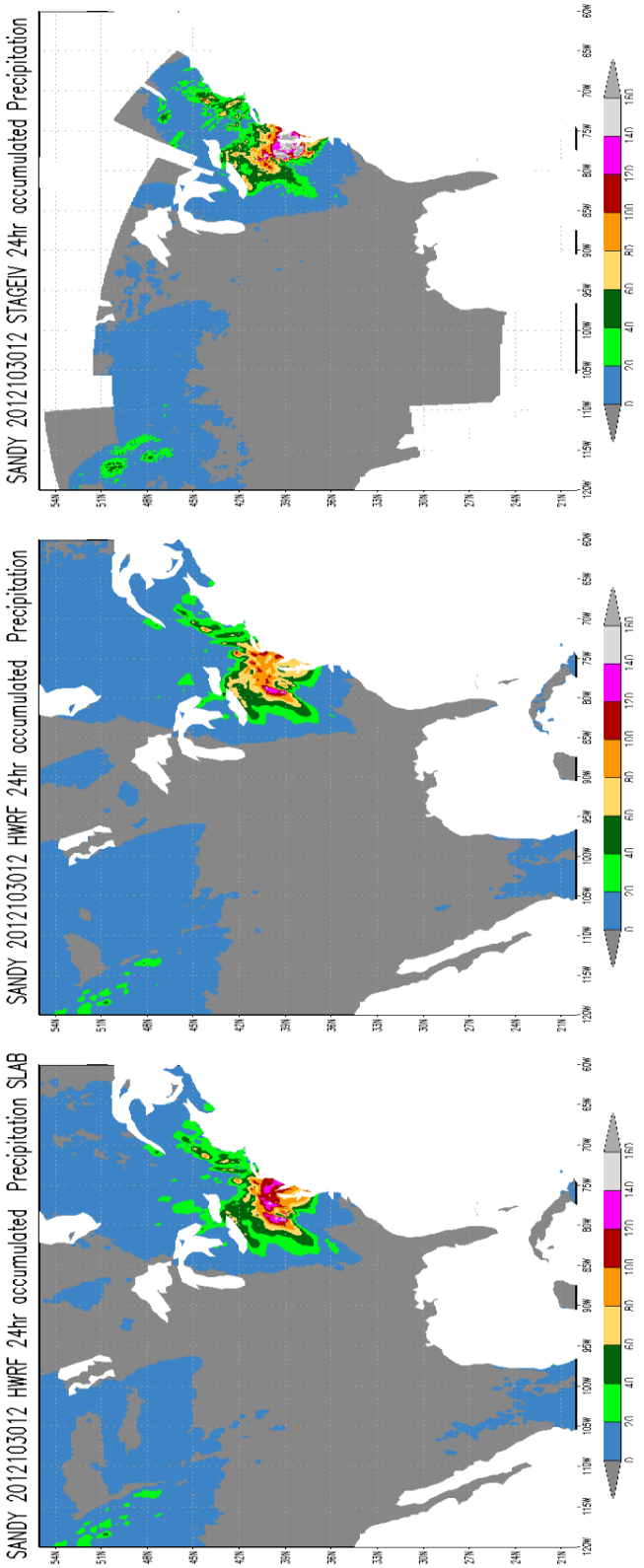

Figure 6.10 Accumulated precipitation ending at 2012103012 for Hurricane SANDY. The rainfall totals are in (mm) for Slab (top), Noah (middle) and STAGE IV observation (bottom)

Surprisingly, the track and intensity predictions using Noah and Slab land models do not show a lot of differences. This may be due to the HWRF being tuned to stay insensitive to lower boundary formulation and highly dependent on large scale dynamics and vortex initialization techniques used in HWRF. Despite the similarity in the tracks, the difference in the rainfall distribution is quite interesting.

6.5.2 Hurricane IRENE (2011)

Hurricane IRENE was a category 3 cyclone and made landfall over North Carolina, early on August 27 as a category 1 cyclone after undergoing an eyewall replacement cycle. In spite of making landfall and the winds slowing down, the central pressure of Irene was observed to be around 957 hPa indicative of category 3 hurricane. After tracking for over land for around10 hours after landfall, the intensity decreased but remained very close to the coast. It reemerged into the Atlantic Ocean later in the day and made a second landfall as a marginal category 1 hurricane over New Jersey early on Aug 28. It slowly weakened and moved over to the ocean again and made a third and final landfall over New York City (Brooklyn) as a tropical storm later on Aug 28. The storm thus stayed very close to the coast and stayed tropical until its third landfall after which cold core features started to emerge. Most severe impacts of this cyclone was catastrophic inland flooding in North Carolina, New York, Massachusetts and Vermont.

The tracks of Hurricane Irene are given in Figure 6.12 for both Slab and FY15 experiments. Like Hurricane SANDY, the two experiments do not exhibit differences in track and have largely been close to observed. The VMAX and MSLP plots are given in

Figure 6.13 and again largely similar in predictions. Both experiments do not capture the effects of the eyewall replacement cycle in dampening the intensity of the hurricane. The MSLP and VMAX are over predicted and the model predicts landfall as category 3 hurricane. The first 24 hr accumulated precipitation was plotted for both experiments for cycle 2012082712 (landfall over New Jersey) and the distributions have been largely similar (Figure 6.14).

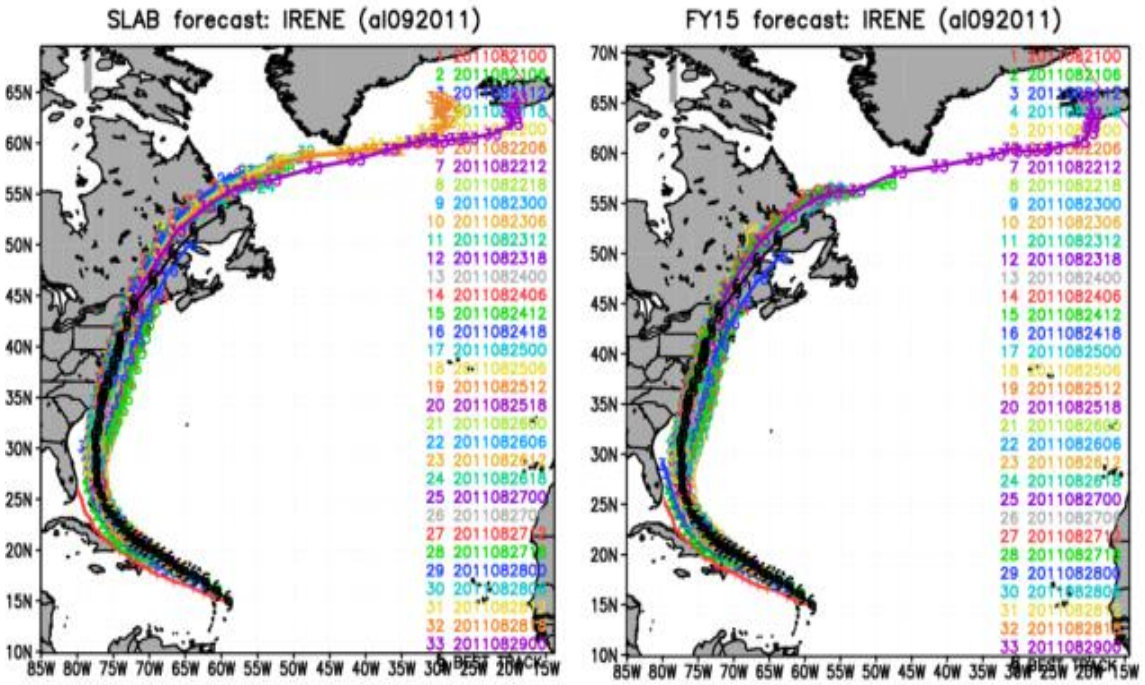

Figure 6.11 Composite plots for tracks for Hurricane Irene as modeled by Slab (left) and Noah (right) experiments. Best Track is marked in black.

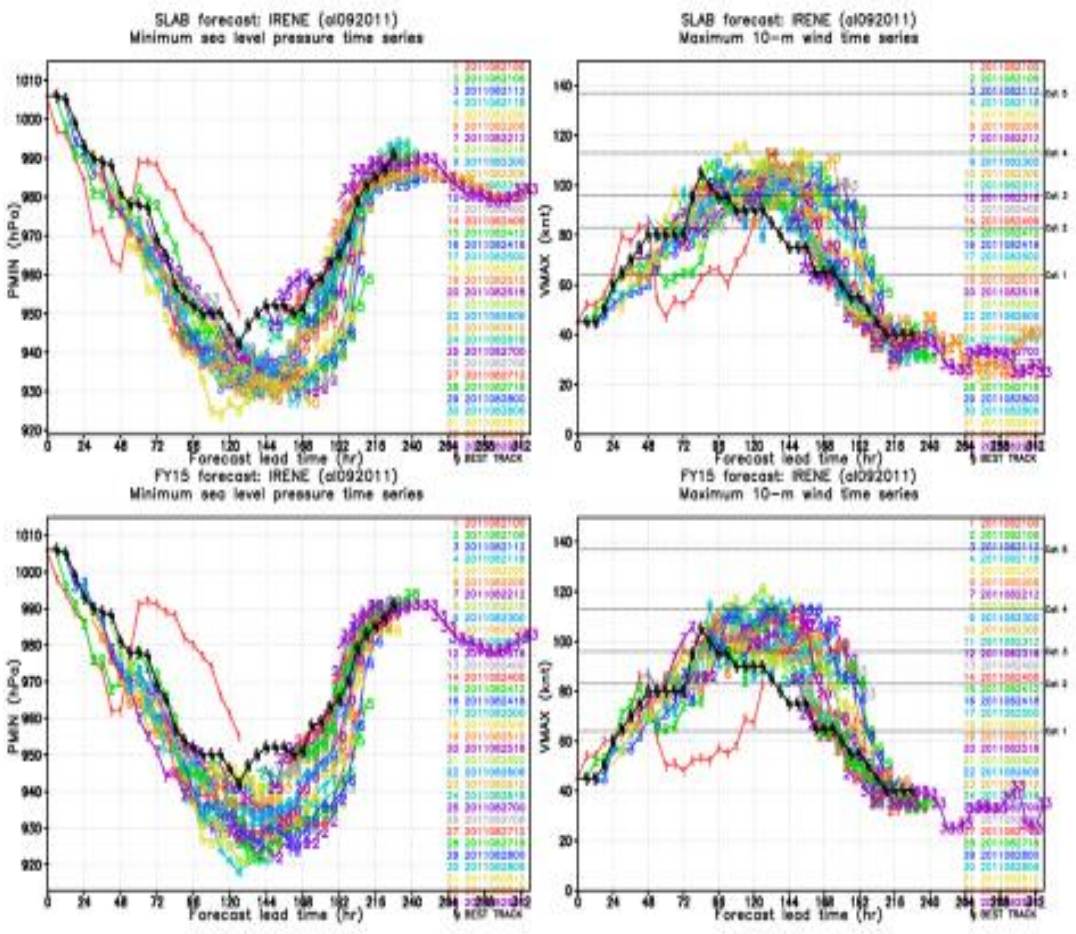

Figure 6.12 Composite plots for MSLP (hPa) and VMAX (knots) for hurricane Irene for Slab (left) and Noah (right) experiments.

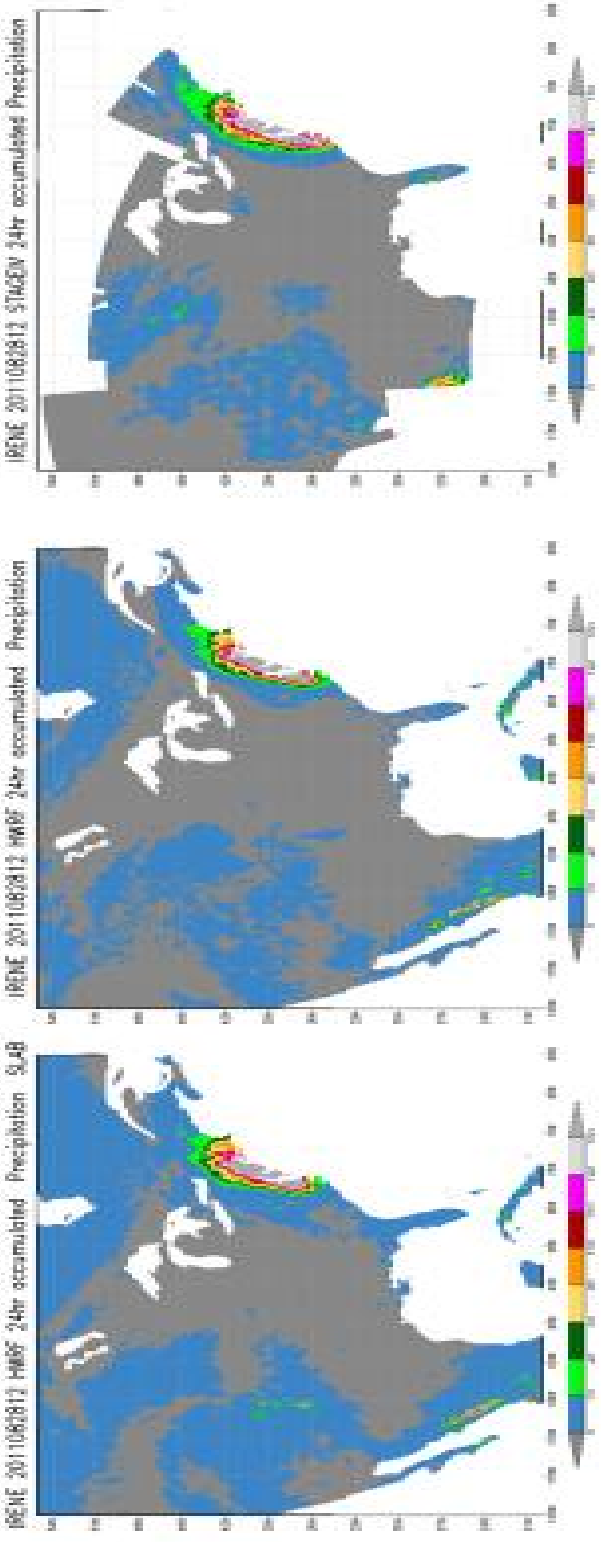

Figure 6.13 Accumulated 24 hr precipitation (mm) over the North East Coast region for Hurricane IRENE ending 2011082812 for experiments Slab (left), FY15 (center) and observations from Stage IV precipitation dataset (right).

The precipitation statistics is given in Table 6.2 for North East Coast, Appalachians and other regions along with the entire CONUS grid. The spatial correlation is very high at 0.95 for Slab experiments and Noah performs poorly compared to Slab at 0.92. The precipitation spatial distribution closely matches observed, the modeled rainfall totals have very high standard deviations and RMSE. Noah underperforms compared to Slab here as well. For the Appalachians, similar results are noted but the errors are substantially lower. The Midwest region in particular has very low Pearson correlation due to the inability of the model to capture any precipitation experienced near the Great Lakes region. Again, the precipitation from the two LSMs are notably different, even though the tracks are not.

Table 6.2 Precipitation statistics for Hurricane IRENE (2012)

Region	Hurricane IRENE (2011) Ending 2011082812							
	Standard Deviation		RMSE		PR Correlation		Mean	
	Slab	Noah	Slab	Noah	Slab	Noah	Slab	Noah
FULL	23.39	23.21	11.17	10.98	0.88	0.88	5.93	5.10
SPL	1.73	0.87	1.43	0.88	0.64	0.49	0.74	0.31
NEC	73.90	75.63	29.93	32.81	0.95	0.93	80.10	75.18
APL	19.97	13.43	7.43	7.73	0.94	0.92	11.25	5.74
MDW	0.23	0.11	0.30	0.23	0.05	0.06	0.05	0.01
SEC	18.83	25.31	26.88	22.69	0.75	0.81	7.59	8.28

6.5.3 Tropical Storm DON (2011)

Tropical Storm DON (27-30 July 2011) was a short lived storm that formed near the Yucatan Channel and tracked northwest ward into the Gulf of Mexico. The storm quickly weakened to moderate shear and dry air intrusion experienced by the storm vortex. The storm eventually made landfall in south Texas as a depression. Texas was under severe

drought and this storm was expected to bring rainfall to alleviate the situation but the weakened storm did not and the impacts were largely minimal.

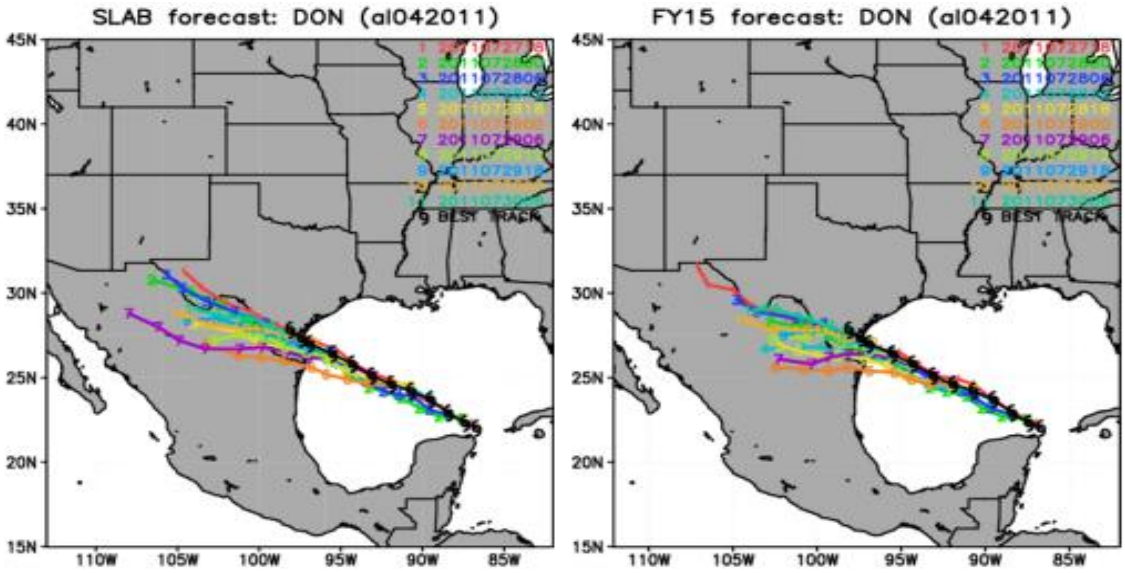

Figure 6.14 Composite plots for TS DON tracks for Slab (left) and FY15 (right) experiments. The observed storm track is in black.

The composite plots for two experiments Slab and Noah quite similar as expected through there are slight differences in positions relative to time (Figure 6.14). HWRF model does poorly in capturing the MSLP owing to the weak storm that DON was and the closed albeit elongated circulation center. The model relatively captures the VMAX estimated well and the composite intensity plots for both experiments are given in Figure 6.15.

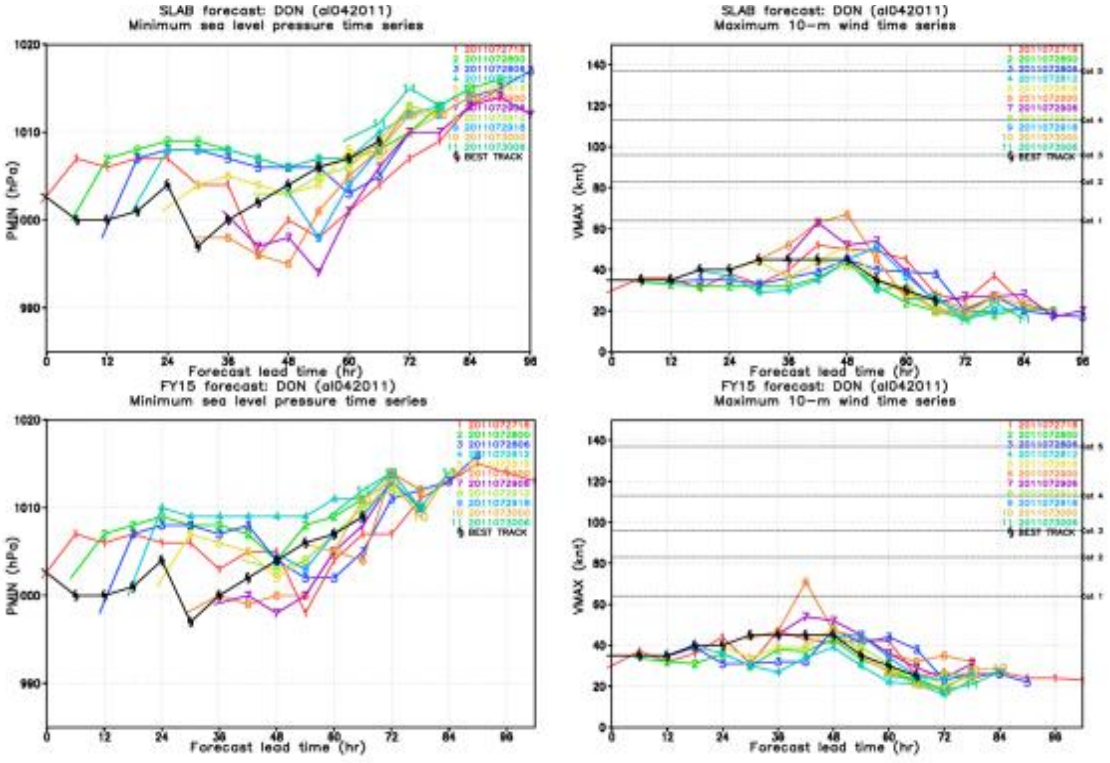

Figure 6.15 Composite intensity plots for tropical storm DON. The Slab experiment plots are on the top and the FY15 experiment plots are in the bottom. MSLP (hPa) on the left and VMAX (knots) on the right.

The precipitation distribution was plotted for both experiments. Accumulated 24 hr precipitation totals was plotted for 2011072912 cycle of the HWRF model (Figure 6.16). The precipitation statistics for accumulation for the 24 hr period ending 2011073012 is also given in Table 6.3. The HWRF model performed relatively poorly in capturing the observed spatial distribution. Both Slab and FY15 experiments consistently over predict the rainfall due to the landfalling storm. Statistics for other region apart from the Texas Gulf and Lower Mississippi Valley region are also poor. The HWRF does capture the rainfall experienced over the Midwest and the Appalachians but again similar to landfall region, over predicts it.

Table 6.3 Precipitation statistics for TS DON.

Region	TS DON (2011) Ending 2011073012							
	Standard Deviation		RMSE		PR Correlation		Mean	
	Slab	Noah	Slab	Noah	Slab	Noah	Slab	Noah
FULL	10.25	8.51	9.02	7.17	0.53	0.56	4.29	3.16
SPL	4.97	2.25	5.48	3.44	0.15	0.12	2.78	0.64
LMV	5.32	5.18	6.40	5.98	0.30	0.28	5.04	3.96
NEC	13.67	11.20	13.24	10.83	0.48	0.46	12.19	10.45
APL	11.60	9.89	10.16	8.44	0.53	0.54	5.91	4.88
GMC	13.18	11.25	13.80	11.11	0.22	0.29	8.35	5.99
MDW	10.51	9.62	8.93	8.01	0.56	0.57	3.79	3.36
SEC	2.13	1.37	2.22	1.45	0.24	0.29	1.10	0.65

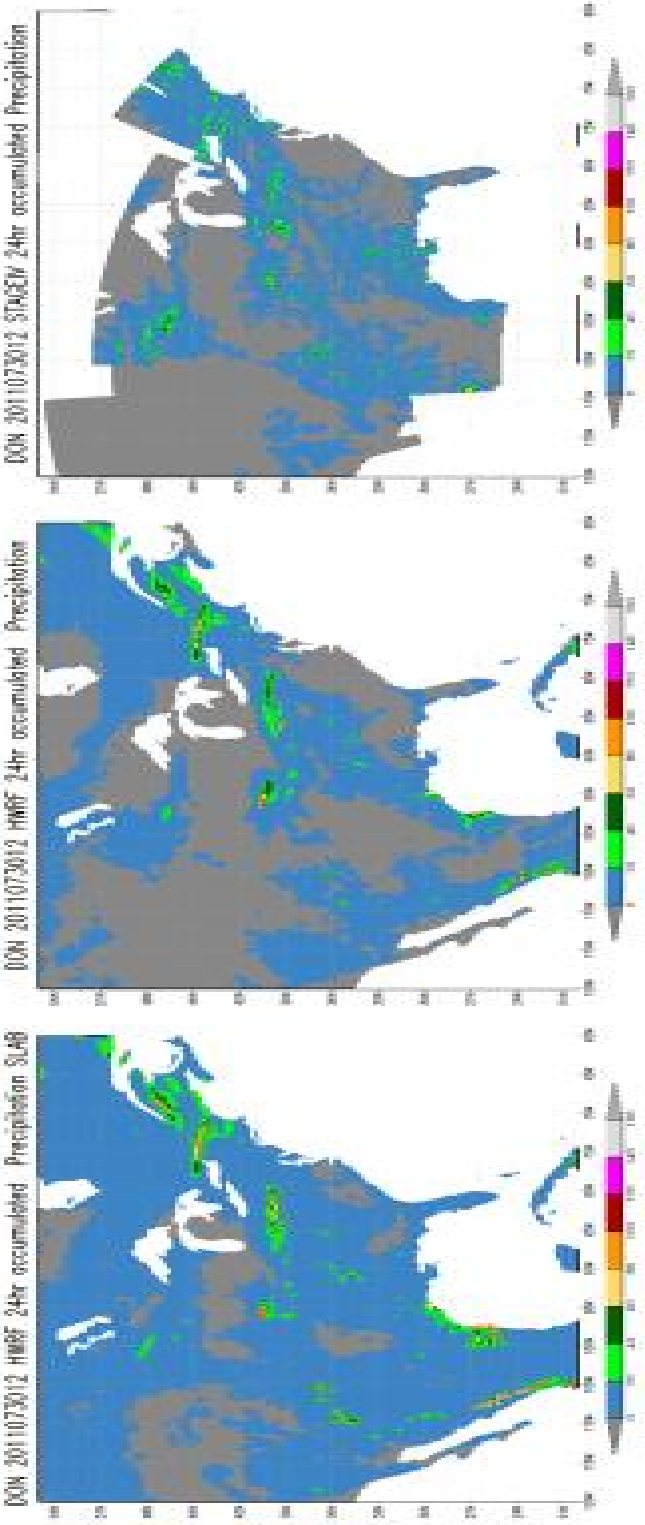

Figure 6.16 Precipitation plot for 24 hr accumulation totals for Slab (left) and FY15 (center) experiments with observed Stage IV precipitation values (right).

6.6 Impact of Improved Initial Conditions on Tropical Cyclone Simulations

Though hurricane models continue to be a subject of targeted research and have come a long way in the past few years, the results still remain dependent on initial conditions supplied to the model. Considerable uncertainty exists in model simulations because of the lack of accuracy in land surface input parameters. Among these, soil moisture and soil temperature (SM/ST) are perhaps the most crucial for BL modelling. The land models coupled with vegetative canopy sub-models (e.g., Noilhan and Planton, 1989; Chen and Dudhia, 2001) and rainfall have become more common to provide case-specific soil moisture profiles at high resolution (e.g., Chen et al., 1996, 2007; Chen and Dudhia, 2001). The rainfall significantly changes the underlying land surface characteristics, creating relatively wet and dry regions. The default climatologically nudged SM/ST may not be representative of these local rainfall changes and this in turn can result in poor simulation of boundary layer and cloud convection processes and resulting precipitation. Since direct ground-based SM measurements are not readily available or regionally representative, assimilation methods have been developed to create high resolution SM fields by providing realistic forcing of rainfall, near-surface (2 m above the ground level) air temperature and moisture, winds and remotely sensed radiances. Considerable progress has been made recently with such stand-alone approaches for hydrological balance and flux simulation using land data assimilation systems such as the North American land data assimilation system (NLDAS) and the high-resolution land data assimilation system (HRLDAS; Mitchell et al., 2004; Chen et al., 2007). Currently, initial land state for HWRF is typically obtained from GFS (Global Forecast System) input conditions. GFS soil moisture field is initialized through GDAS data and nudged to

climatological values and thus may not represent the true state of land surface. NLDAS (North American Land Data Assimilation System), on the other hand is initialized using observations in precipitation and thus accepted to be more realistic than GFS initial conditions. Hence, it is not only important to compare different land surface schemes and surface layer parameterization, but also the impact of improved initial conditions on the model outcome should also be analyzed.

To assess the effect of NLDAS land surface dataset as initialized in HWRF, experiments were conducted with TS BILL (2015) with Slab, Noah and NLDAS surface fields assimilated in HWRF (called LDAS) with Noah LSM. Track, intensity, precipitation, soil moisture, soil temperature and surface temperature datasets were compared with available observations. In the absence of gridded soil moisture and soil temperature observation dataset similar to Stage IV precipitation data, in-situ observations from US Climate Reference Network (USCRN) which has over 115 stations were used. In this study, the network's Texas and Oklahoma stations were considered. To compare the surface datasets from HWRF spatially, NCEP's NLDAS model datasets were considered true values.

6.6.1 Tropical Storm BILL (2015)

Tropical Storm BILL (June 16 – 21, 2015) formed as a low pressure area in the Gulf of Mexico and became sufficiently organized as a tropical system in the early hours of June 16. The storm did not have much time to strengthen over the warm waters in the Gulf and tracked north west toward the Texan Gulf Coast. The storm's organization stayed strong on approaching land and made landfall as a tropical storm over Matagorda Island in

Texas at 16.45 UTC on 16 June. The storm quickly lost its intensity and weakened to a depression on 17 June though it maintained its organized structure. The storm was responsible for heavy rainfall over Texas and Oklahoma and caused heavy inland flooding. Cyclone induced tornadoes were also observed across Missouri, Arkansas and lower regions of the Ohio Valley.

The tracks predicted by models were quite accurate and had very little uncertainty spread during the tropical storm phase of the storm. The composite plots for Slab, FY15 and LDAS experiments are given in Figure 6.17. Nevertheless, the extended tracks after the tropical storm traced northward and then east towards the north east coast, the tracks diverged. Slab here performs better showing a southward shift to exit into the ocean near New Jersey. Both Noah and LDAS experiments shows extended track in which the storm moved into the ocean near Massachusetts.

Earlier cycles of HWRF model in simulating the storm did not predict the central pressure as well as VMAX. The cycles after the storm made landfall was predicted well. The composite plots for each of the experiments are shown in Figure 6.18 and the ensemble plot for the cycle 2015061600 is shown in the Figure 6.19. The rest of the analysis on precipitation, soil moisture, soil temperature is for this cycle. Compared to observations, the modeled storm did not keep the organized circulation (Figure 6.20–Figure 6.23). After landfall, on June 17, 12Z as the observed storm moves over Houston, TX, models show that the storm stayed close to the coast and thus modeled precipitation is expected to be high near the gulf coast. The precipitation distribution was analyzed for the three experiments the statistics along with the 24hr accumulated precipitation valid

for 2015061712, 2015061812 and 2015061912 is given in Table 6.4 and Figure 6.24 – Figure 6.26. The models show moderate spatial comparison with the observed precipitation. The landfall regions, Lower Mississippi Valley (LMV), Southern Plains (SPL) and the Gulf of Mexico Coast (GMC) show low spatial correlation. The landfall area in Texas that falls under GMC shows large deviations of the order of 50 mm with mean around 45mm. The Appalachian region shows very poor performance where the model precipitation is quite high compared to observations. The 48-hour and 72-hour precipitation statistics for CTRL and LDAS experiments are improved and LDAS shows a correlation of 0.73 for Day 3 precipitation over Midwest. This is also in line with other studies (Osuri et al. 2015) where land surface data assimilation and improved surface representation has improved day 2 and day 3 precipitation when day 1 precipitation is comparable. Nevertheless, across the board all experiments over predict precipitation to a large extent and this is believed to be caused by the FA microphysics and the SAS cumulus physics schemes used in the model. More studies are need to quantify the effects of microphysics and cumulus parameterization in HWRF.

To analyze the structure, intensity and position of the storm, vorticity and winds were plotted for the 1612Z, 1700Z and 1712Z (Figure 6.27 – Figure 6.29). The plots show that the SLAB storm is the weakest and at 36 hours the cyclone vortex at the 200 mb level is displaced compared to the vortex at the lower levels. All the storms show a high cyclonic activity close to the coast and divergence atop. The vorticity plots also show that the storm was almost held stationary near the coast where it made landfall due to under prediction of the environmental flow in the model that caused model to over predict

precipitation. The LHF and SHF (Figure 6.30 and Figure 6.31) were analyzed at 1600Z, 1700Z and 1712Z and it was noted that SLAB experiments had higher LHF values over West Texas region and over the gulf coast compared to CTRL and LDAS experiments. This might be due to the model configuration where GFDL Slab land model assumes constant soil moisture throughout the simulation. The initial soil moisture values supplied to the model from GFS are also noted to be high as given in Figure 6.33. Thus, CAPE predicted by the SLAB experiment (see Figure 6.32) over these regions of West Texas and gulf coast is also high leading to high convective activity and is reflected in the precipitation plots.

Surface temperature was compared against in-situ dataset and is shown in Figure 6.34. Slab experiments exhibited a cold bias and discussions with Robert Tuleya confirmed this. Both Noah and LDAS experiments show improvement in surface temperature simulations compared to Slab but generally similar in performance when compared to each other. The diurnal variability was captured well in all the experiments. The domain top soil layer temperature was plotted against the NLDAS top soil temperature (considered true in the absence of gridded observation dataset) and is given in Figure 6.35 and time series plot for top soil temperature in USCRN observations stations are plotted in Figure 6.36. Both CTRL and LDAS experiments capture the high temperature region in the southwestern part of the north American landmass along with the temperature patterns in the Florida panhandle. Slab shows a cold bias all around as observed in Hurricane SANDY. Noah and LDAS experiments also show a negative temperature bias near the Gulf of Mexico Coast where the storm made landfall. The

observed surface temperatures were also quite low in this region and might account for the storm weakening in spite of high antecedent moisture observed due to heavy rains in the region before BILL. The domain plot for top soil moisture is given in Figure 6.33 and time series plot for top soil moisture against in-situ observations is given in Figure 6.37. Slab experiments are not plotted since GFDL Slab land model does not prognostically predict soil moisture and the initial soil moisture values are held constant throughout the simulation. The modeled soil moisture for both Noah and LDAS experiments show large differences. NLDAS initialized run shows spatial variability when compared to NCEP/ NLDAS model data. GFS initialized top soil moisture does not capture the variability in Southern and Lower and Upper Midwest. While LDAS experiment shows high spatial correlation to true values, the HWRF model over predicts the soil moisture field. The in situ observations also do not compare well against modeled soil moisture. This may be due to the mis match between the actual soil type and texture and the what the model considered to be the grid box's average soil type is. In order to confirm this, a normalized soil water content fraction was plotted for all the observation points. Normalized soil water content is defined as

$$w_{norm} = \frac{w - w_{wilting}}{w_{sat} - w_{wilting}} \quad \ldots (6.1)$$

where w is the absolute soil moisture, $w_{wilting}$ is the wilting point and w_{sat} is the saturation soil moisture. Both wilting point and saturation point of the soil depends on the soil type and texture. For observation data, wilting point and saturation point were obtained based on minimum and maximum soil moisture values for three years (2011, 2012, 2015)

where 2011 and 2012 were drought years and 2015 was a wet year for the region. The wilting point and soil saturation point for the modeled values were obtained from the soilparm table that is used in HWRF model to compute soil water content in the land model. Thus, normalized soil water content indicates the available soil water for evaporation and is a better index to compare than absolute soil moisture values.

The normalized soil water content Figure 6.38 shows that the soil moisture availability of these location compares well to the observed soil moisture availability if the precipitation in that location is captured well. Many points do not capture the precipitation in that region and hence soil moisture values are incorrect but wherever the modeled data shows variability similar to observations, the LDAS experiments slightly over predicts compared to Noah experiment. One should also bear in mind that the soil moisture is one of the hardest variable to measure and predict in an interactive model in both NLDAS dataset and the in-situ data sets will have errors. But the results are in line with the precipitation statistics where LDAS experiments over predict rainfall compared to CTRL in the GMC region.

An analysis of sounding profiles over Corpus Christi, TX (Figure 6.40 – Figure 6.42), Houston, TX (Figure 6.43 – Figure 6.45) and Norman, OK (Figure 6.46 – Figure 6.48) also revealed a similar result where Slab model sounding were more unstable than Noah and Slab and consistently showed high convective initialization (CI).

Table 6.4 Precipitation statistics for TS BILL.

Region	TS BILL (2015) Cycle 2015061600											
	Standard Deviation			RMSE			PR Correlation			Mean		
	SLAB	NOAH	LDAS	SLAB	NOAH	LDAS	SLAB	NOAH	LDAS	SLAB	NOAH	LDAS
day 1 precipitaion												
FULL	13.92	14.47	14.79	11.53	11.66	11.84	0.61	0.61	0.61	5.92	4.82	4.71
SPL	9.10	7.50	7.92	8.10	7.78	7.56	0.58	0.47	0.53	6.38	4.44	4.35
LMV	23.24	19.90	20.88	20.20	17.29	17.99	0.55	0.56	0.56	18.60	16.58	16.58
NEC	6.18	6.06	6.11	7.91	6.90	6.89	0.04	0.06	0.07	7.25	5.24	5.15
APL	8.42	8.02	4.81	9.27	7.85	4.76	0.24	0.36	0.46	7.15	5.31	4.38
GMC	37.75	47.19	49.20	30.72	39.25	41.42	0.63	0.60	0.58	22.41	25.95	25.66
MDW	7.09	4.81	4.98	6.28	5.22	5.24	0.50	0.42	0.43	2.98	2.07	2.15
SEC	2.41	2.06	1.71	2.80	1.77	1.55	0.52	0.55	0.49	2.41	0.89	0.67
day 2 precipitaion												
FULL	12.62	12.95	12.69	13.64	12.38	12.67	0.38	0.50	0.46	5.22	4.18	4.11
SPL	13.17	12.34	9.99	14.31	9.32	11.30	0.62	0.86	0.79	8.99	4.62	4.38
LMV	33.78	37.00	36.05	37.83	35.36	36.15	0.33	0.50	0.45	28.90	27.47	27.97
NEC	0.36	1.08	1.27	7.14	7.01	6.98	0.41	0.32	0.30	0.17	0.22	0.27
APL	4.51	6.73	6.65	8.27	6.94	6.56	-0.04	0.46	0.51	2.60	4.47	4.58
GMC	10.36	14.86	14.04	29.35	29.83	29.46	0.42	0.36	0.38	6.24	7.35	7.19
MDW	7.92	7.56	7.62	9.63	7.77	8.33	0.08	0.36	0.26	5.53	4.67	4.46
SEC	5.02	4.37	4.23	7.70	6.84	6.53	-0.18	-0.10	-0.02	4.58	2.65	2.30
day 3 precipitation												
FULL	15.58	12.17	10.62	16.37	11.63	9.67	0.17	0.38	0.47	6.82	4.56	4.34
SPL	24.01	3.78	2.18	26.72	6.34	5.52	-0.13	-0.01	0.12	12.24	2.04	1.15
LMV	14.19	25.86	24.33	21.36	27.63	24.49	0.09	0.22	0.34	10.80	16.08	17.63
NEC	9.71	4.70	5.62	11.09	4.01	4.85	-0.11	0.59	0.54	6.27	3.78	4.73
APL	14.07	6.91	7.48	16.19	6.66	7.90	-0.08	0.47	0.29	12.03	5.45	5.81
GMC	3.91	2.76	2.77	8.83	8.40	8.56	-0.06	-0.02	-0.05	2.00	1.37	1.12
MDW	31.18	22.38	15.35	32.33	20.41	12.13	0.39	0.59	0.73	16.93	9.66	6.88
SEC	3.95	2.76	3.15	7.34	7.26	7.61	0.21	0.29	0.19	3.66	2.32	2.30

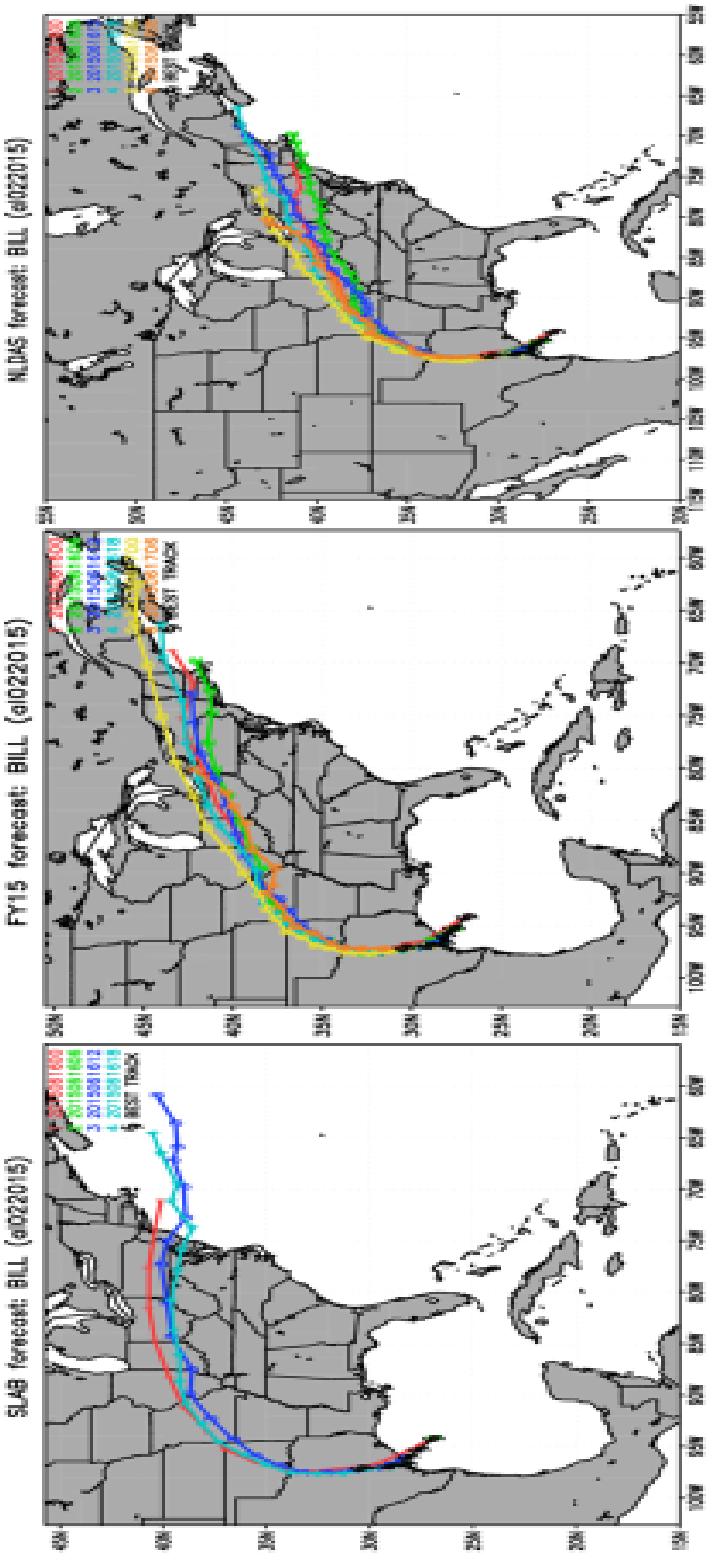

Figure 6.17 Composite plots for tropical storm BILL (2015) for all cycles for Slab (left), FY15 (center) and LDAS (right). The observed best track is marked in black.

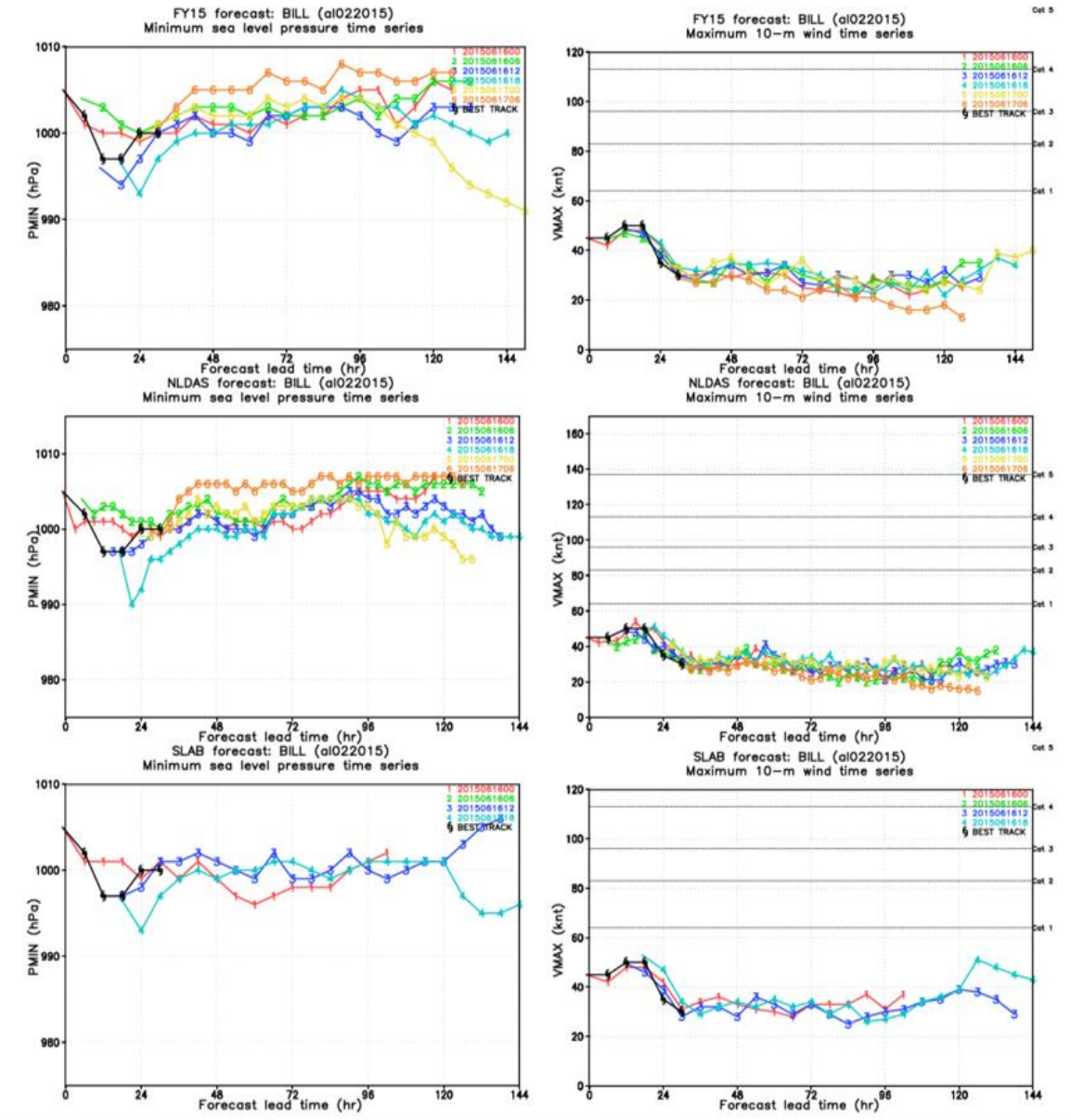

Figure 6.18 Composite plots for Slab (top), FY15 (center) and LDAS (bottom) experiments for MSLP (hPa) and VMAX (knots) on the left and right respectively.

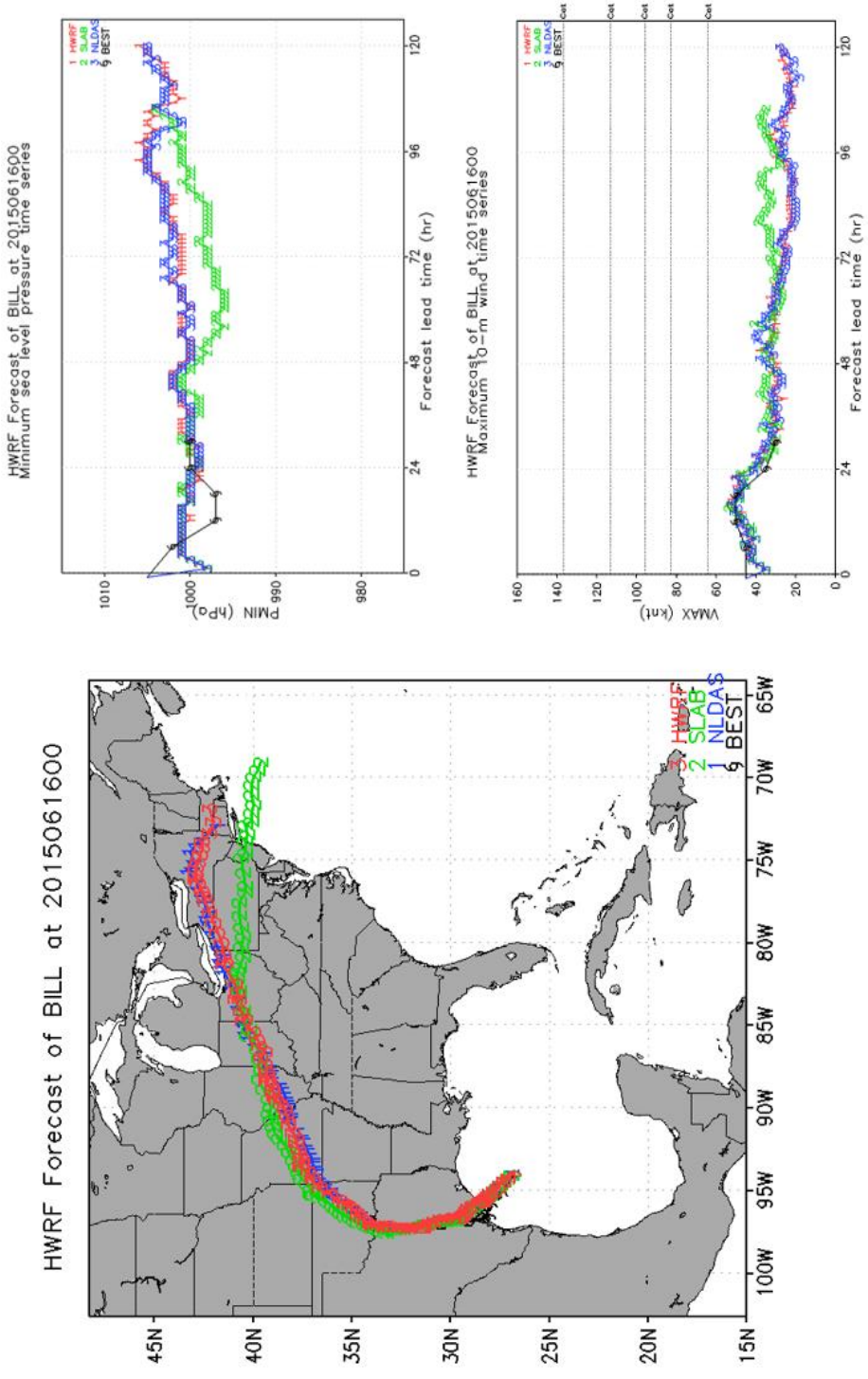

Figure 6.19 Ensemble plot for the HWRF cycle 2015061600.

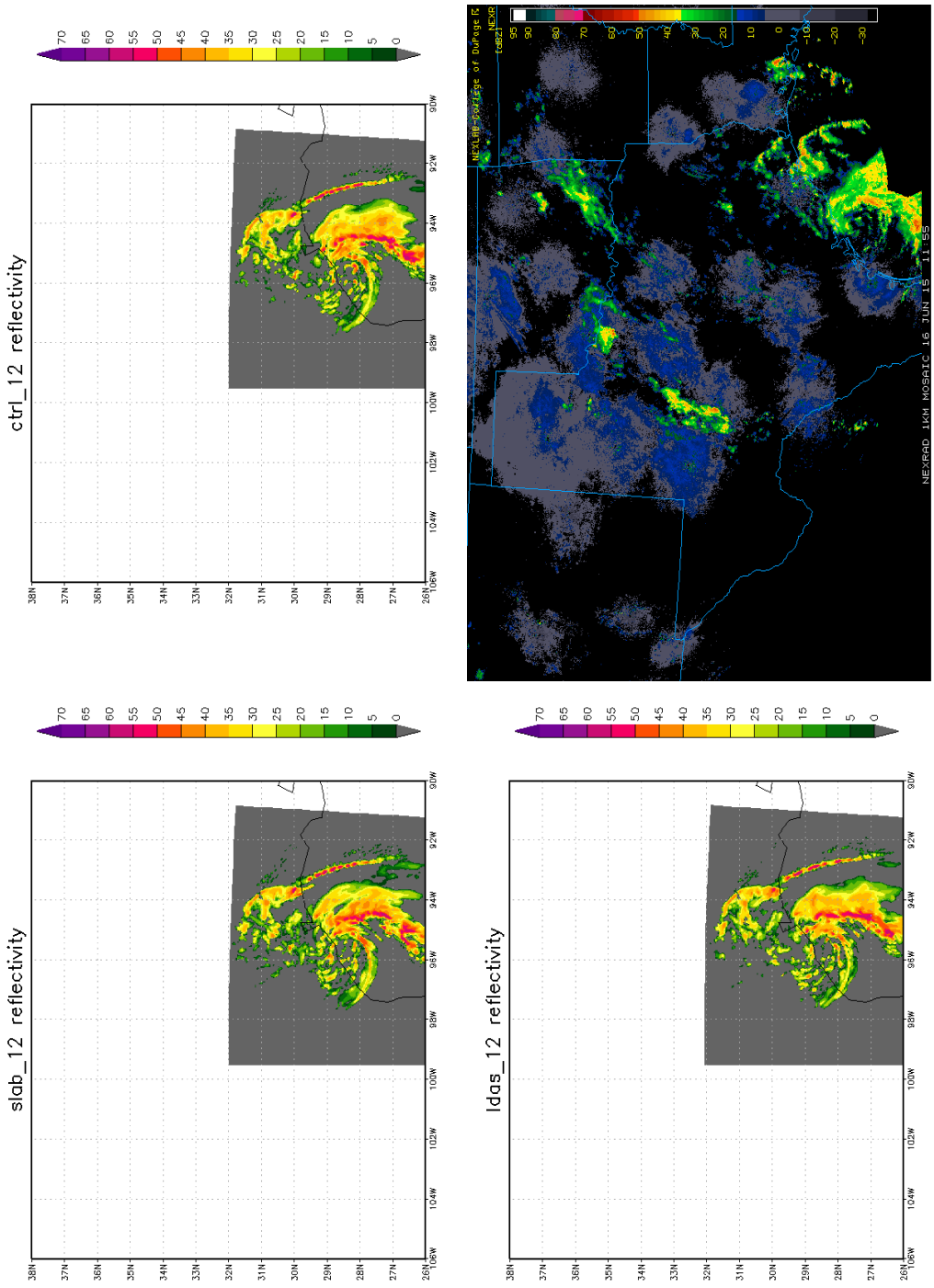

Figure 6.20 Radar reflectivity (dBz) at 20150616 12Z (before landfall), for three experiments Slab, CTRL and LDAS. Observation from NEXRAD radar composite product.

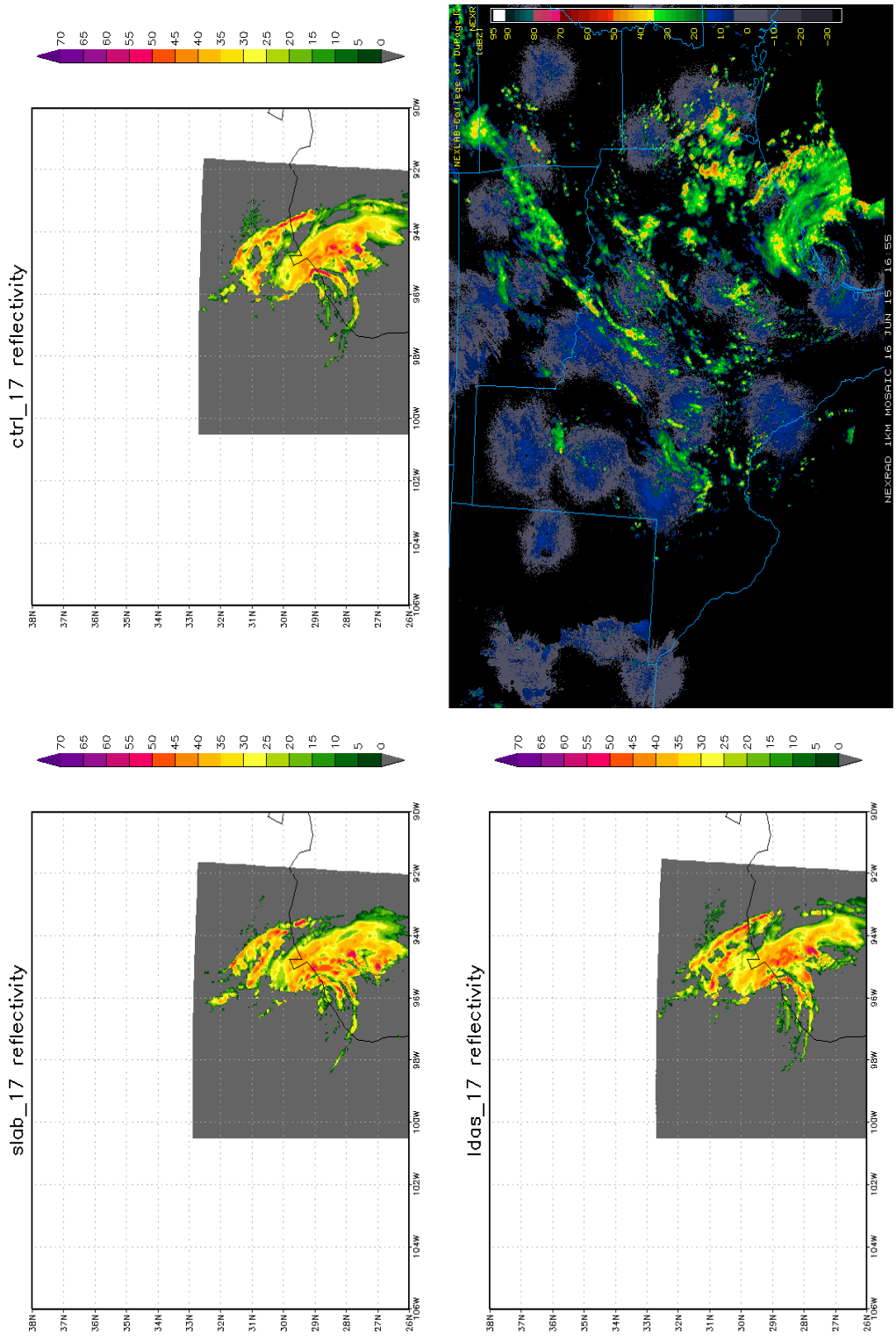

Figure 6.21 Radar reflectivity (dBz) at 20150616 17Z (at landfall), for three experiments Slab, CTRL and LDAS. Observation from NEXRAD radar composite product.

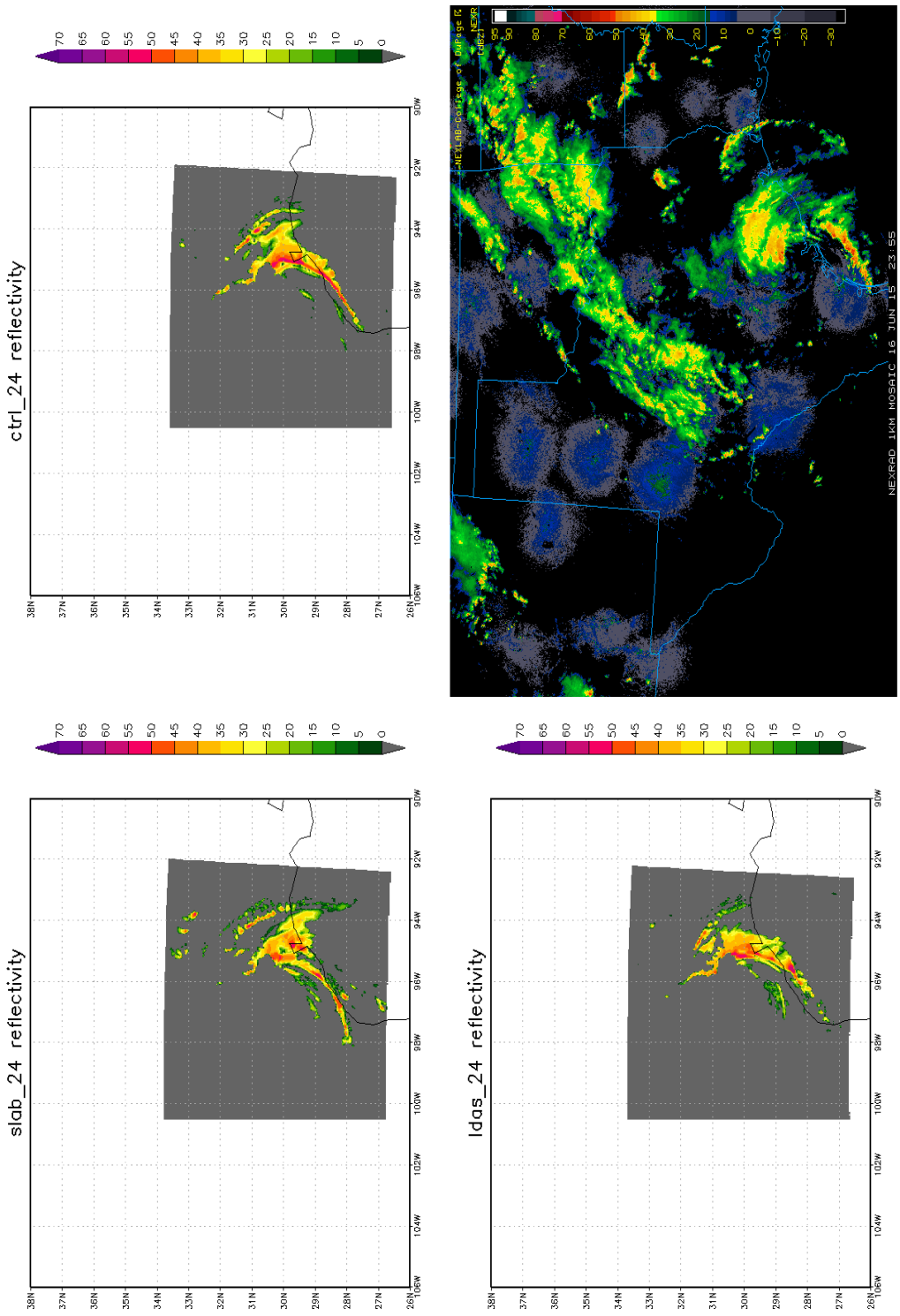

Figure 6.22 Radar reflectivity (dBz) at 20150617 00Z (after landfall), for three experiments Slab, CTRL and LDAS. Observation from NEXRAD radar composite product.

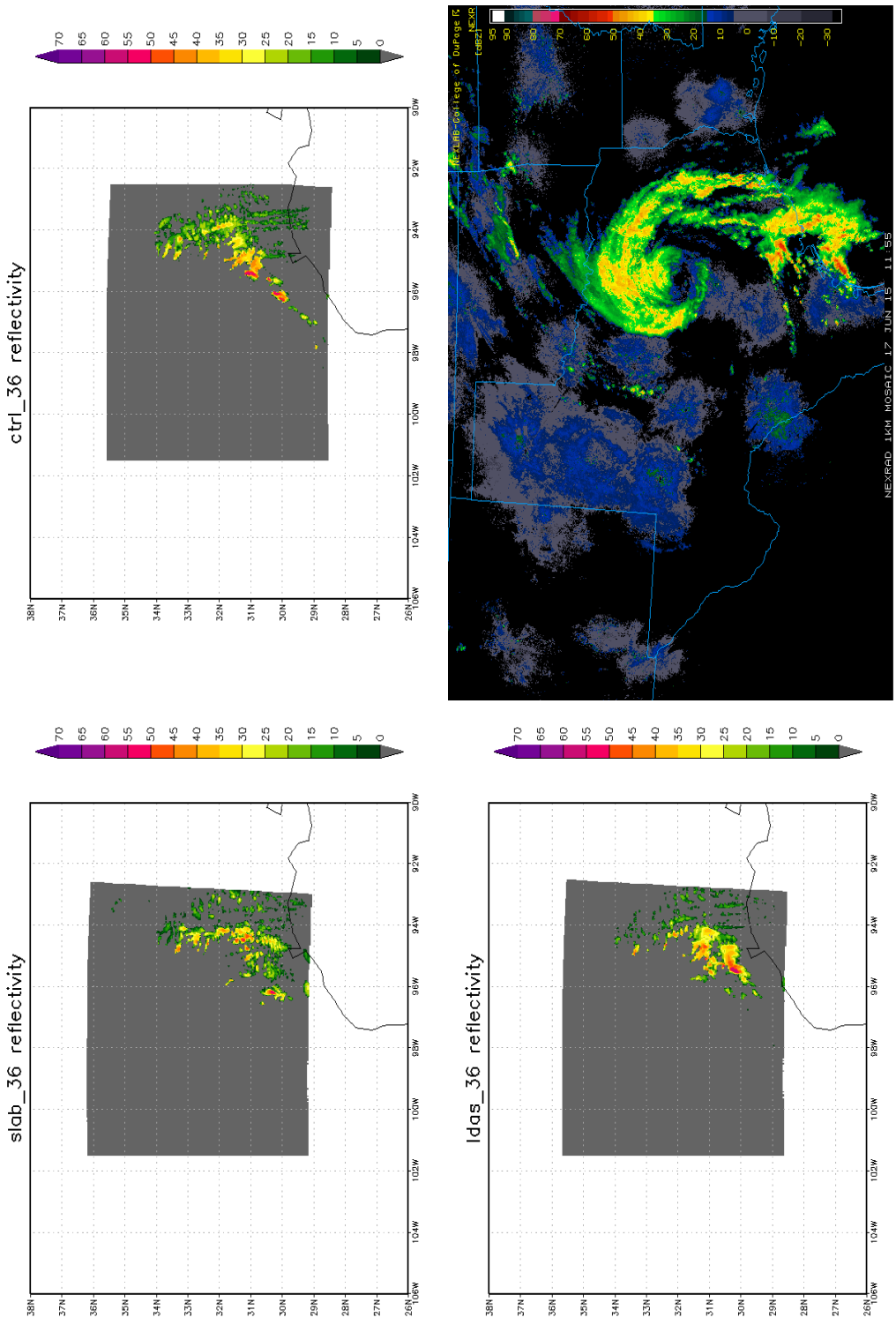

Figure 6.23 Radar reflectivity (dBz) at 20150617 12Z (after landfall), for three experiments Slab, CTRL and LDAS. Observation from NEXRAD radar composite product.

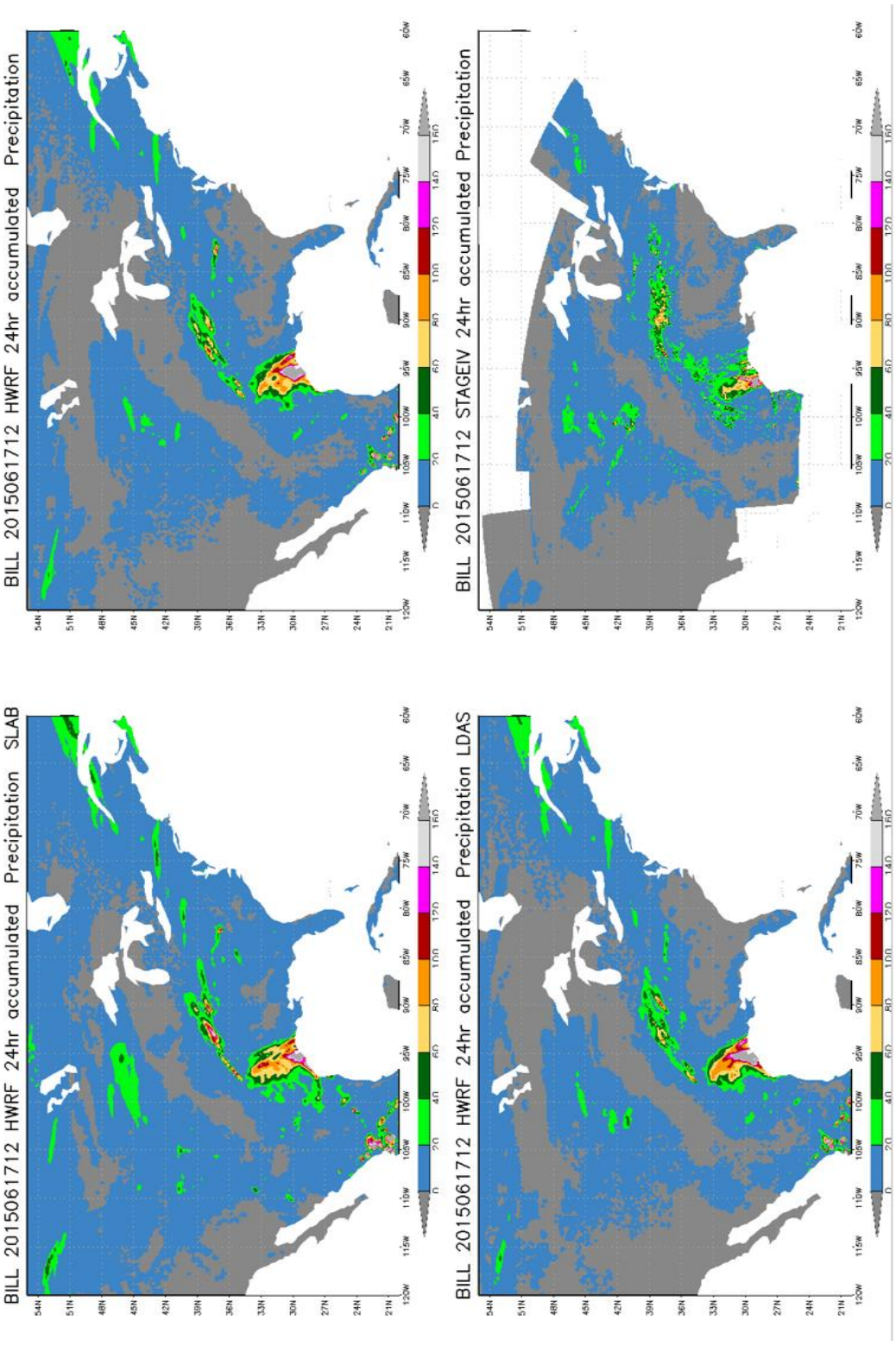

Figure 6.24 Accumulated 1-day precipitation valid for the day ending 2015061712 for Slab, FY15, LDAS and Stage IV dataset in mm.

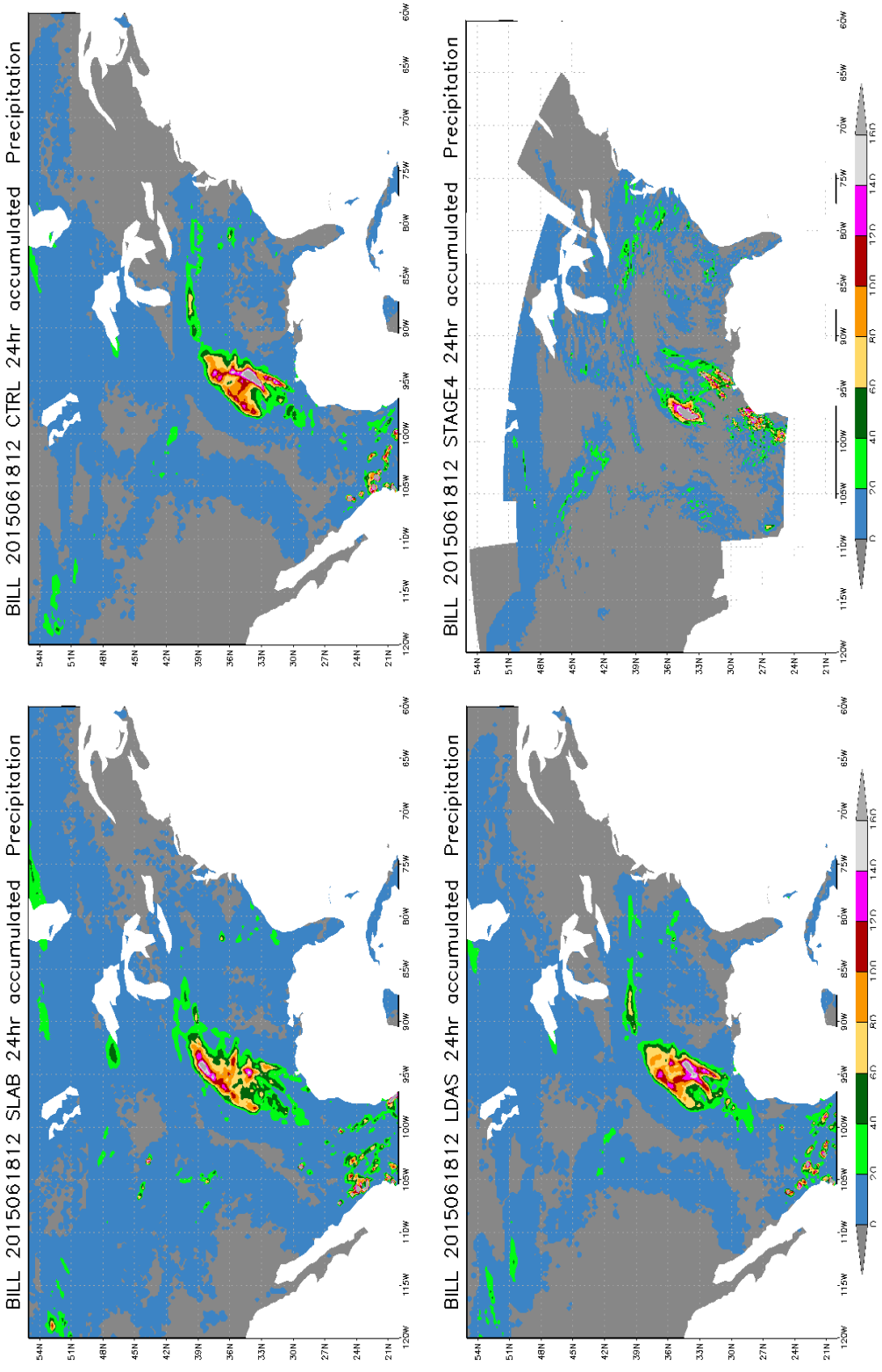

Figure 6.25 Accumulated 1-day precipitation valid for the day ending 2015061812 for Slab, FY15, LDAS and Stage IV dataset in mm.

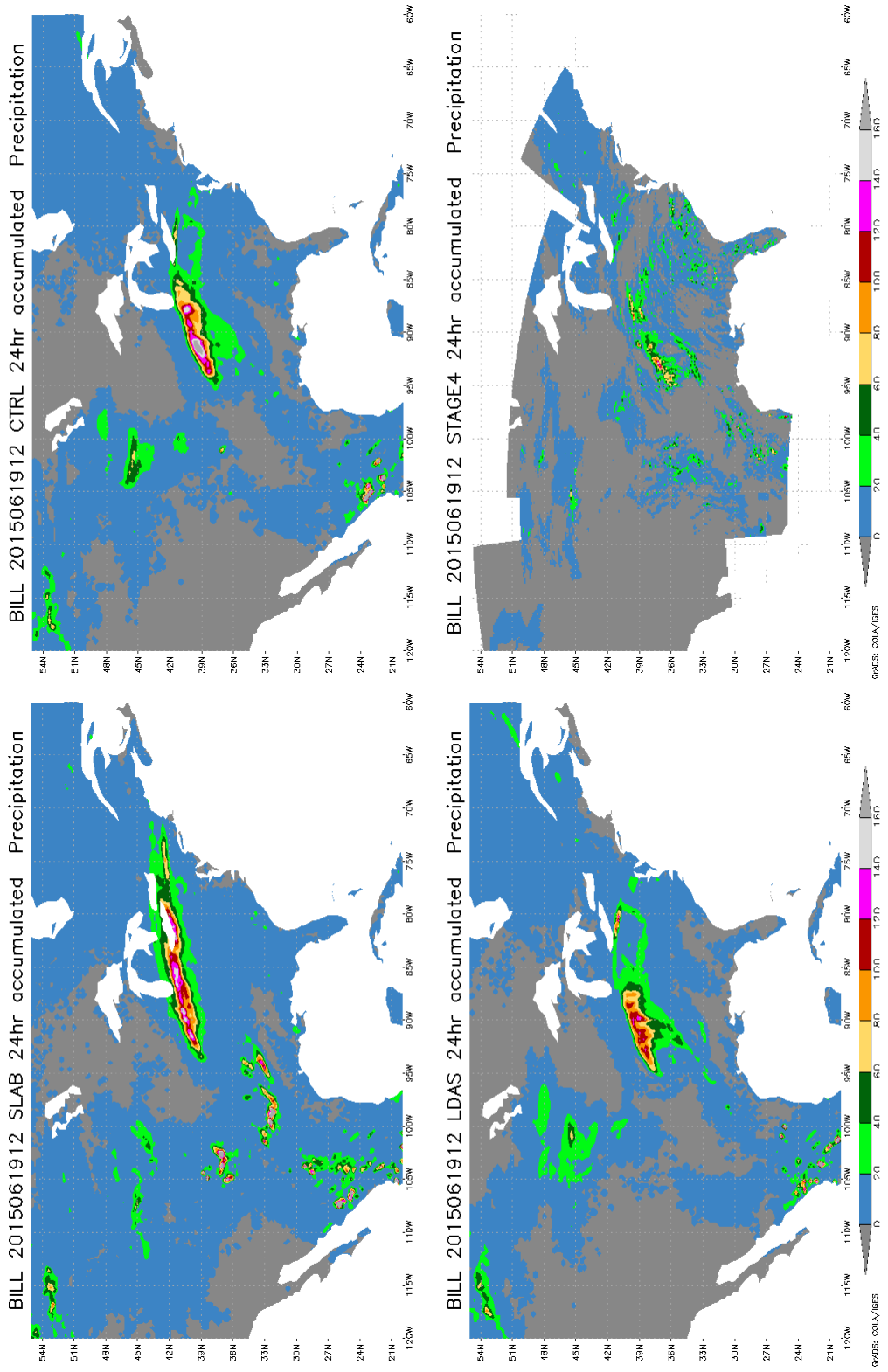

Figure 6.26 Accumulated 1-day precipitation valid for the day ending 2015061912 for Slab, FY15, LDAS and Stage IV dataset in mm.

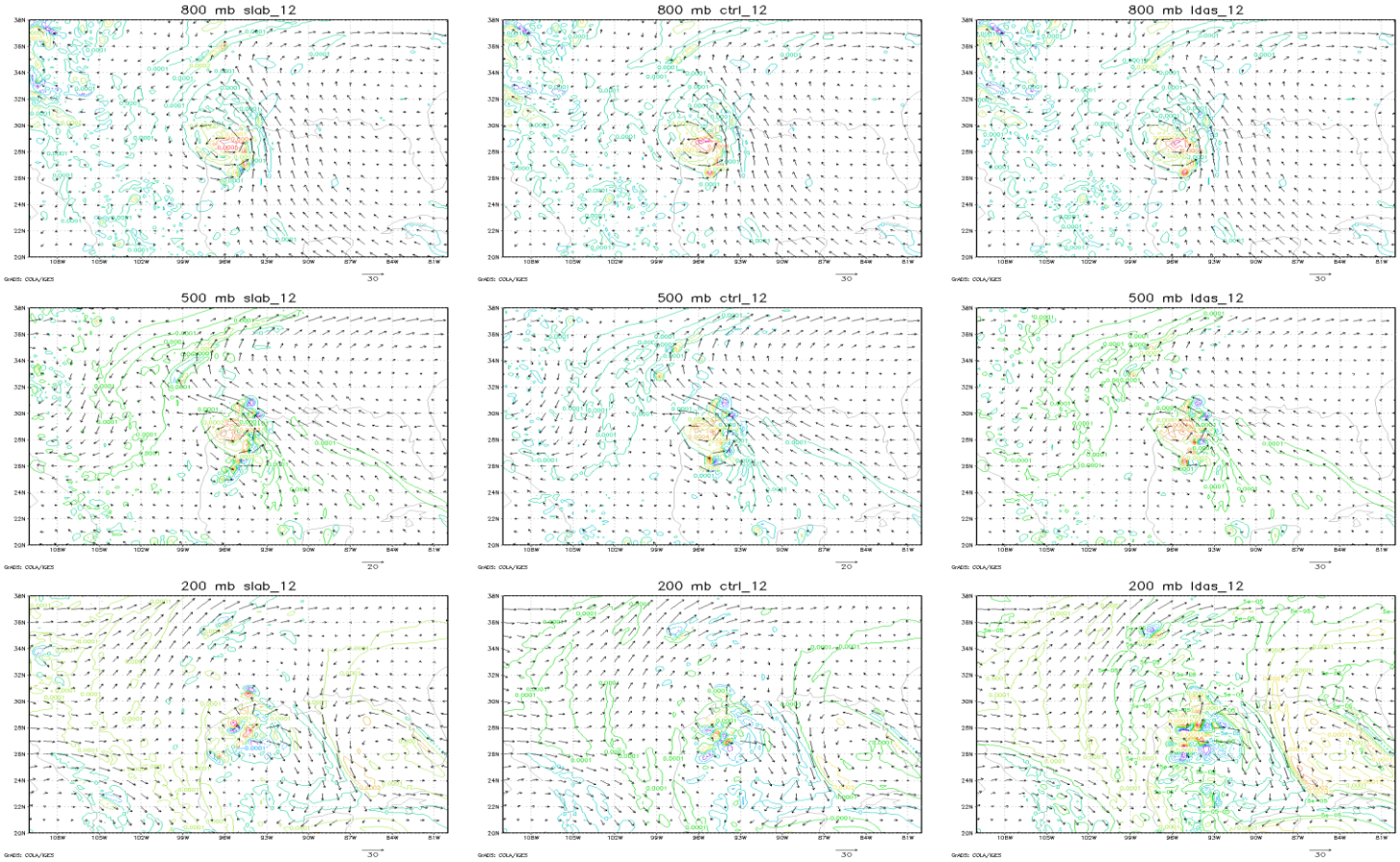

Figure 6.27 Vorticity and winds at different levels for SLAB, CTRL and LDAS experiments at 1612Z for 800mb, 500mb and 200mb levels. The storms in all experiments show a strong cyclonic flow at 800 mb and 500 mb levels and divergence in the upper level.

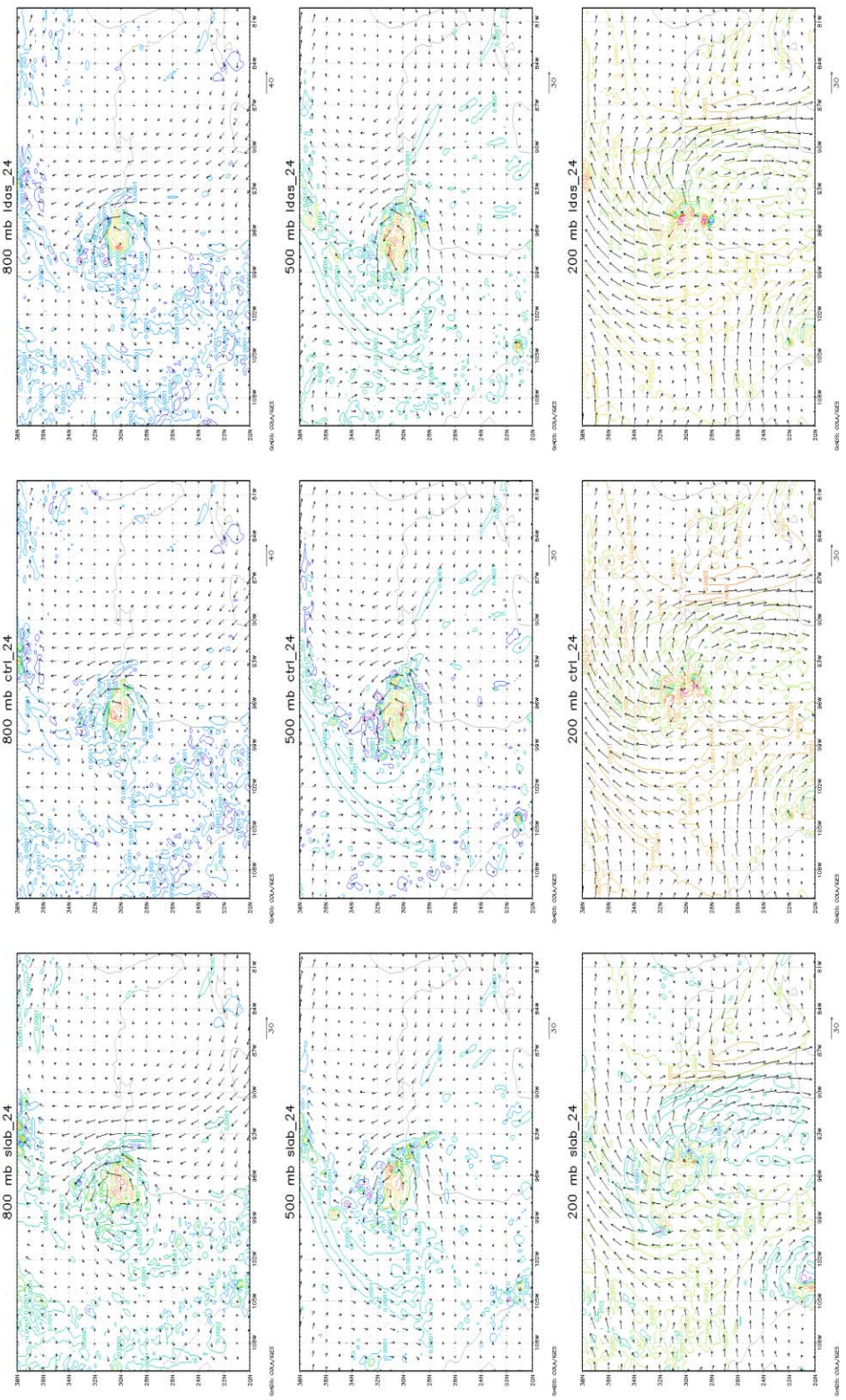

Figure 6.28 Vorticity and winds at different levels for SLAB, CTRL and LDAS experiments at 1700Z for 800mb, 500mb and 200mb levels. After landfall, SLAB experiment shows a weak storm compared to CTRL and LDAS and the SLAB storm vortex in 200 mb level is displaced slightly to north northwest of the coast compared to other experiments.

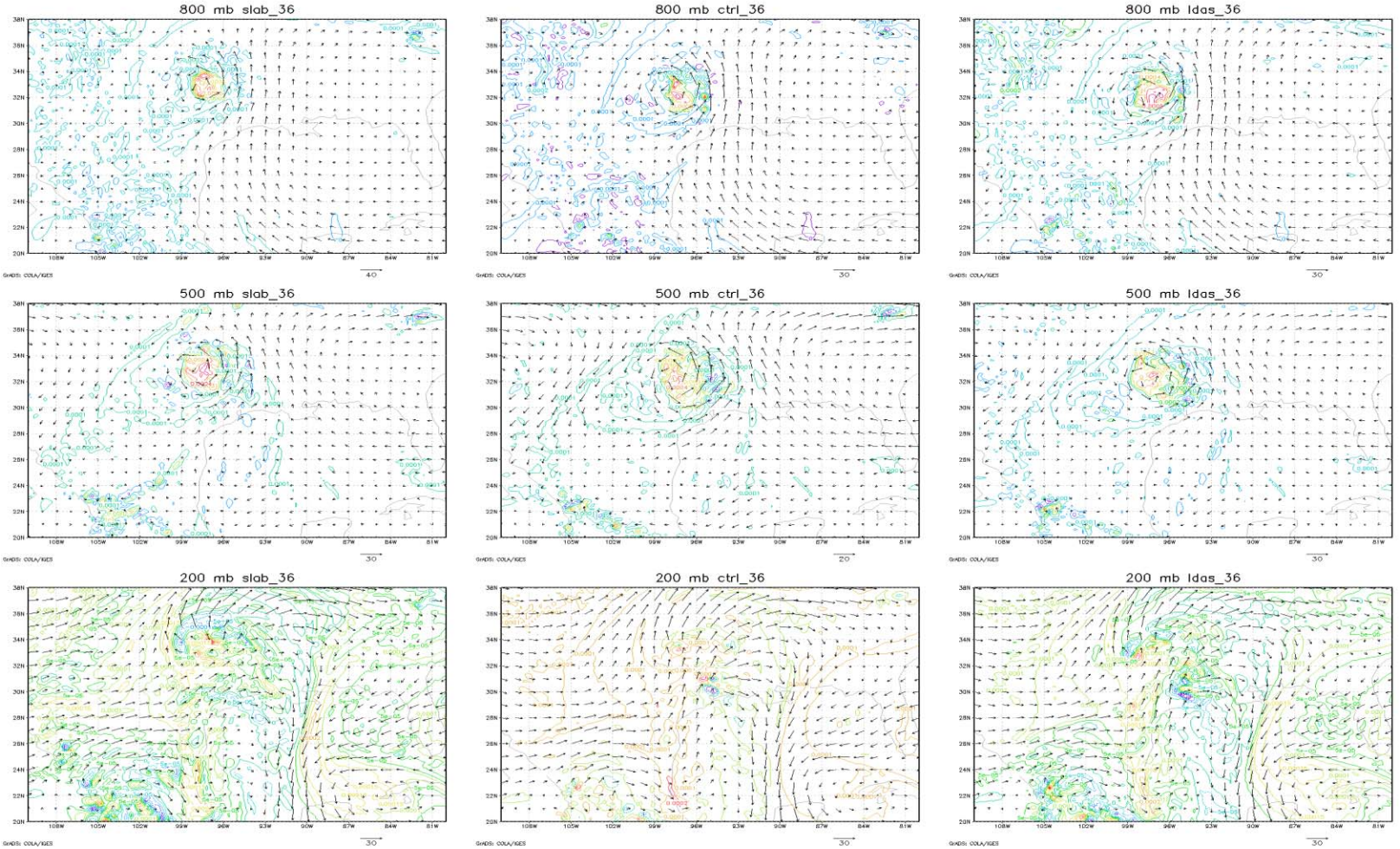

Figure 6.29 Vorticity and winds at different levels for SLAB, CTRL and LDAS experiments at 1712Z for 800mb, 500mb and 200mb levels. The storm is strongest for CTRL experiments and SLAB storm shows a sheared vortex at 200 mb. Strong upper level divergence exists in all experiments.

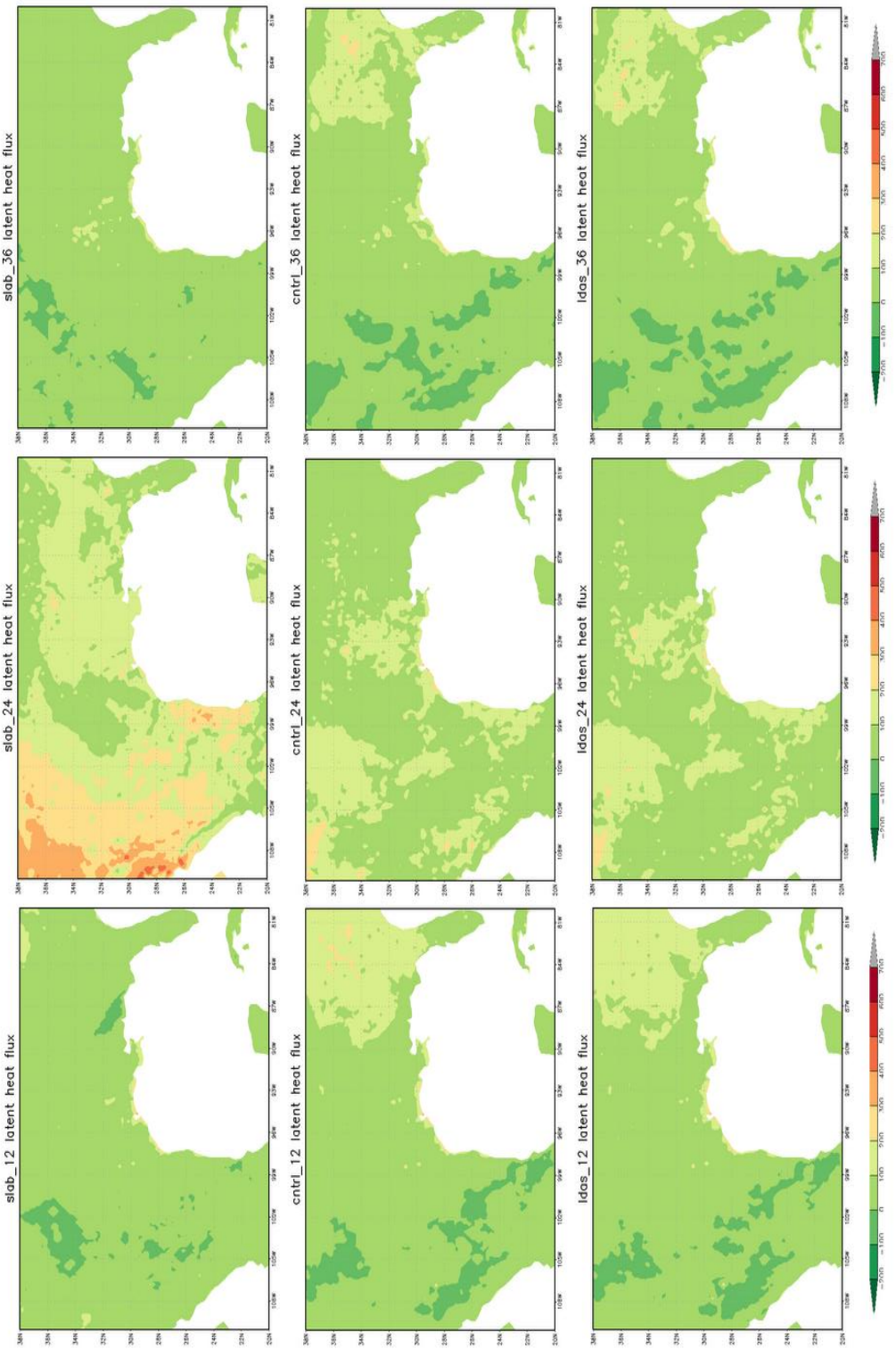

Figure 6.30 Spatial plot for latent heat flux (W/m^2) over the GMC region for Slab (top), Noah (middle) and LDAS (bottom) at 1612Z, 1700Z and 1712Z

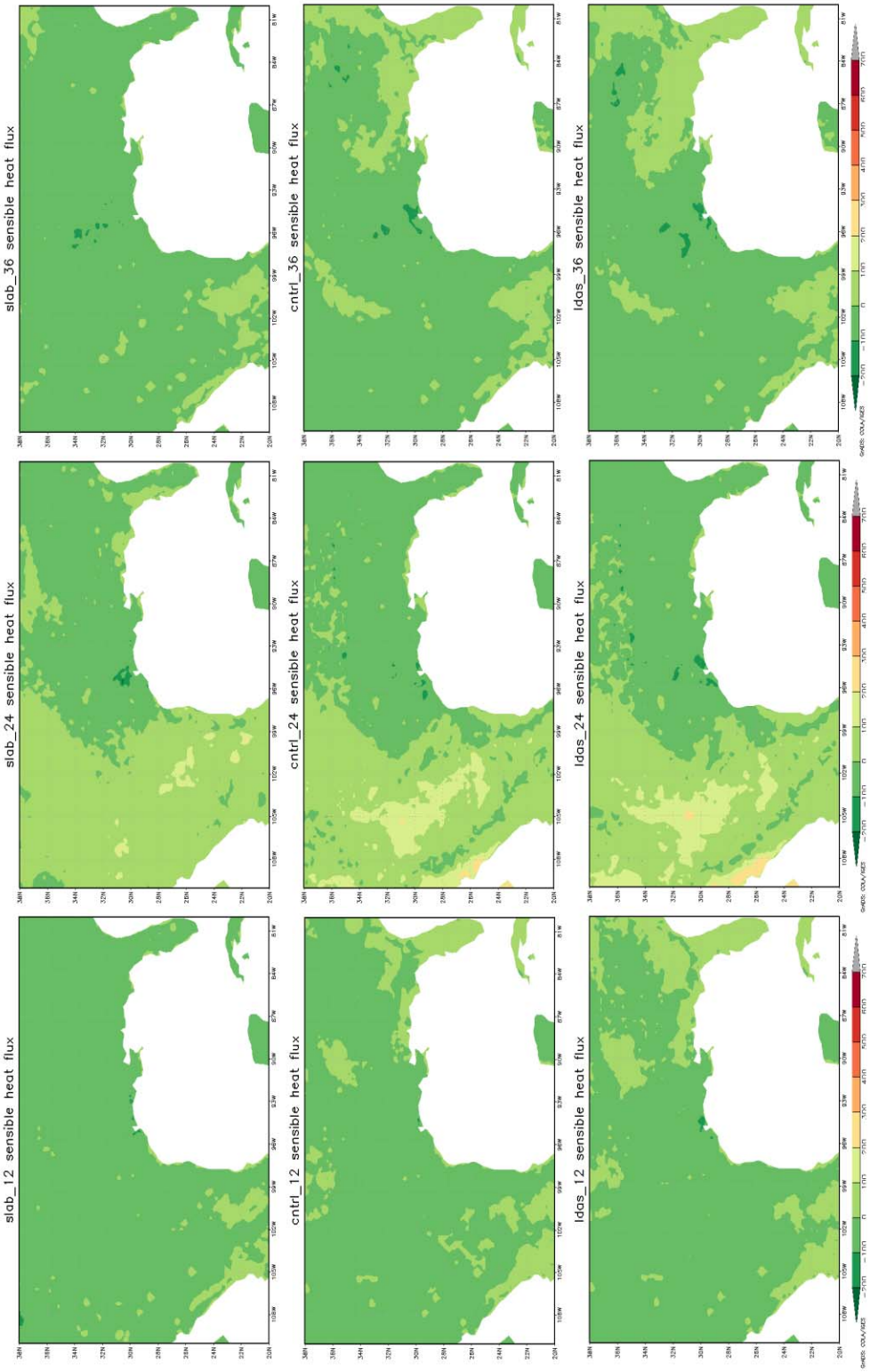

Figure 6.31 Spatial plot for sensible heat flux (W/m^2) over the GMC region for Slab (top), Noah (middle) and LDAS (bottom) at 1612Z, 1700Z and 1712Z.

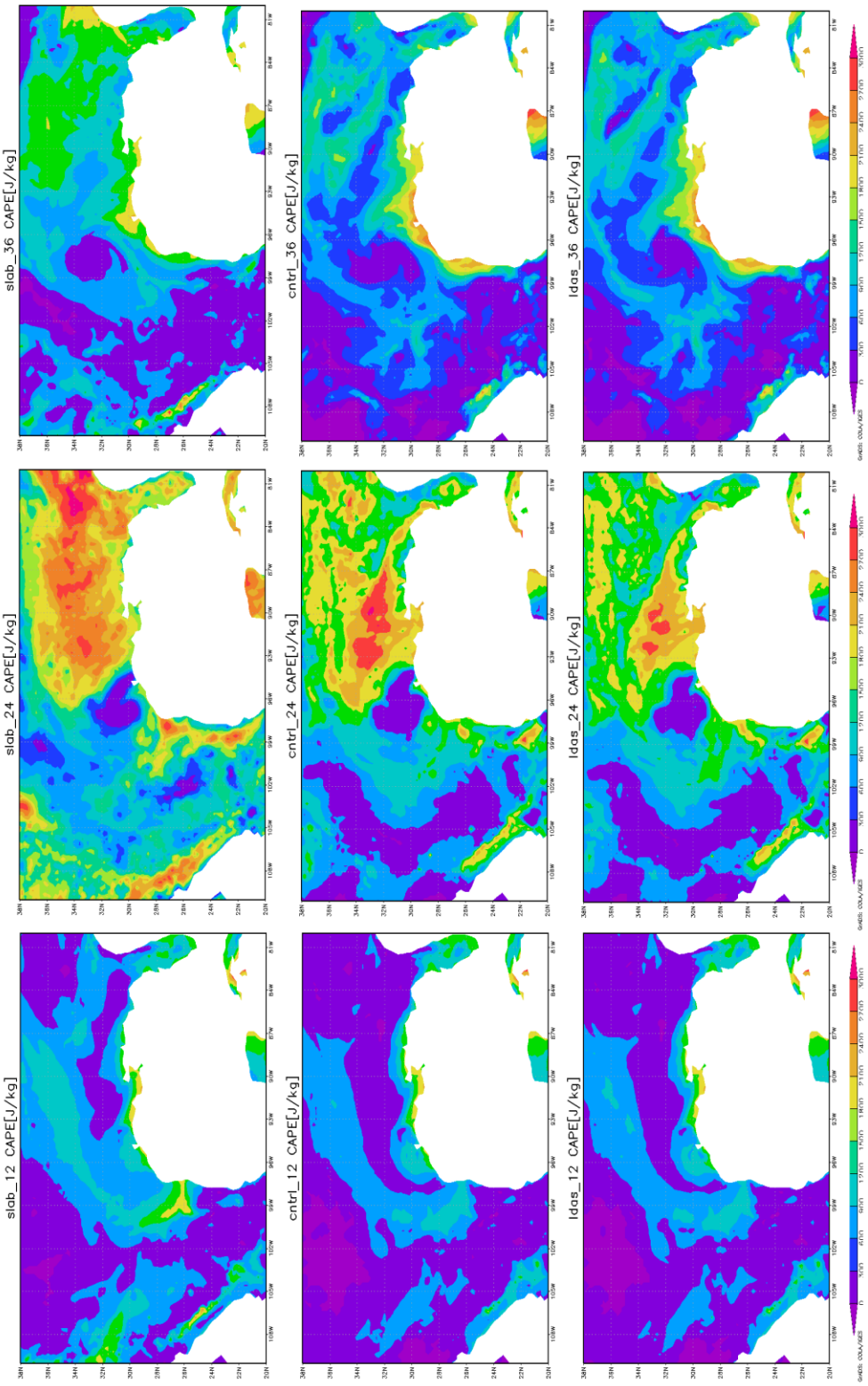

Figure 6.32 Spatial plot for CAPE (J/Kg) over the GMC region for Slab (top), Noah (middle) and LDAS (bottom) at 1612Z, 1700Z and 1712Z.

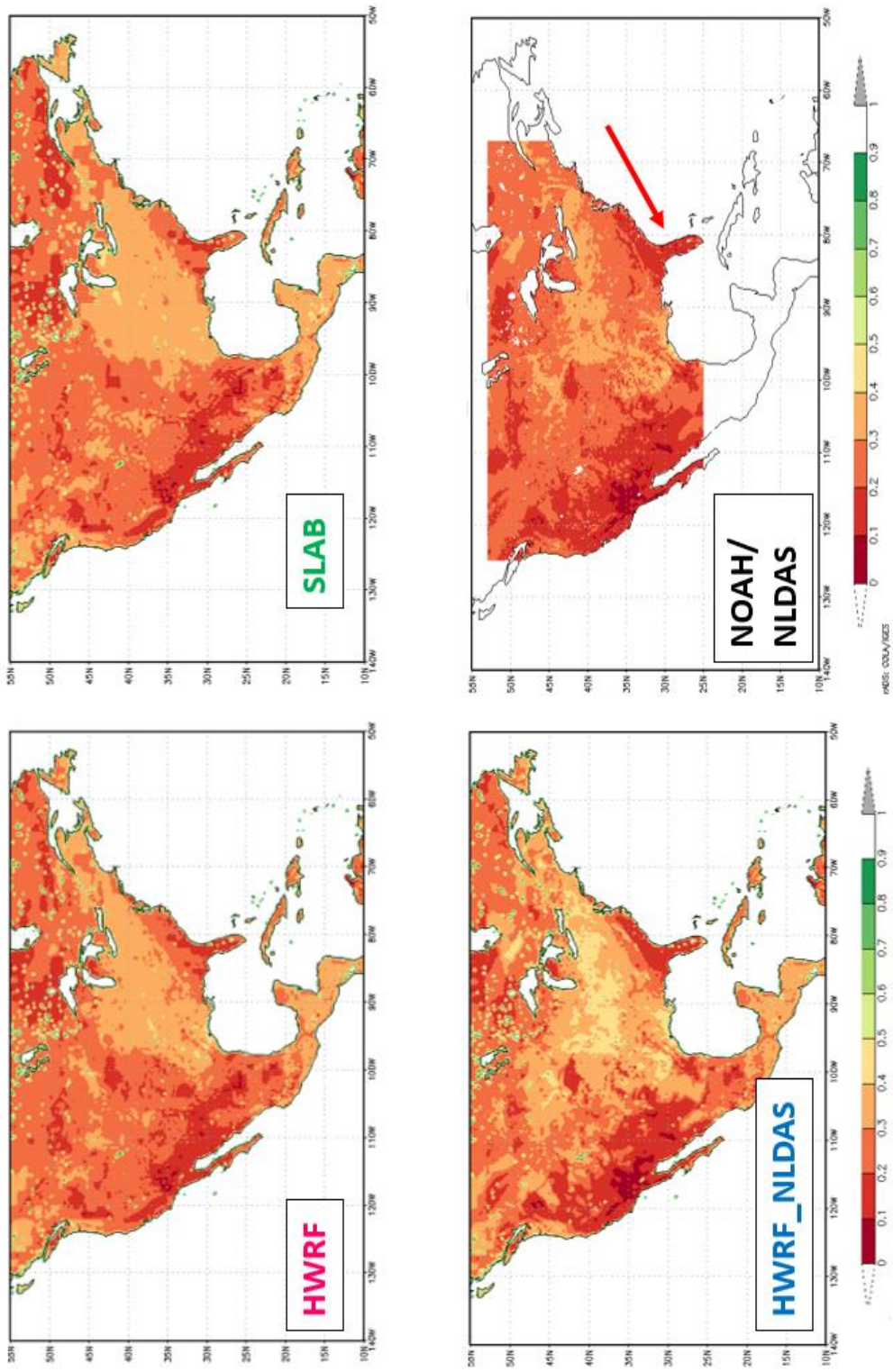

Figure 6.33 Top soil moisture (0-10 cm) in m^3/m^3 for different experiments on June 15, 2015 at 2100 UTC.

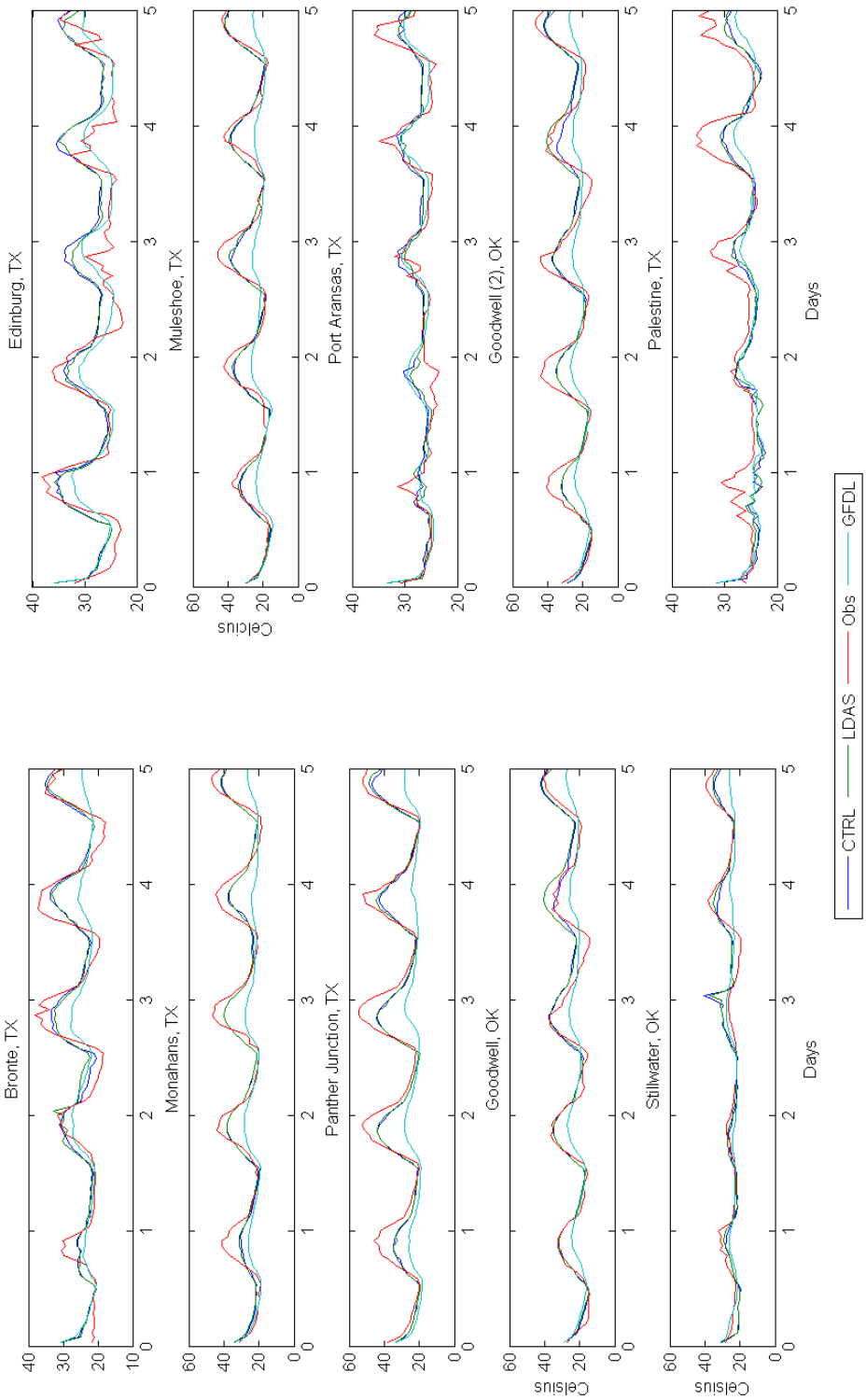

Figure 6.34 Time series plot for surface temperature for experiments against in-situ observations. The temperature values are in Celsius.

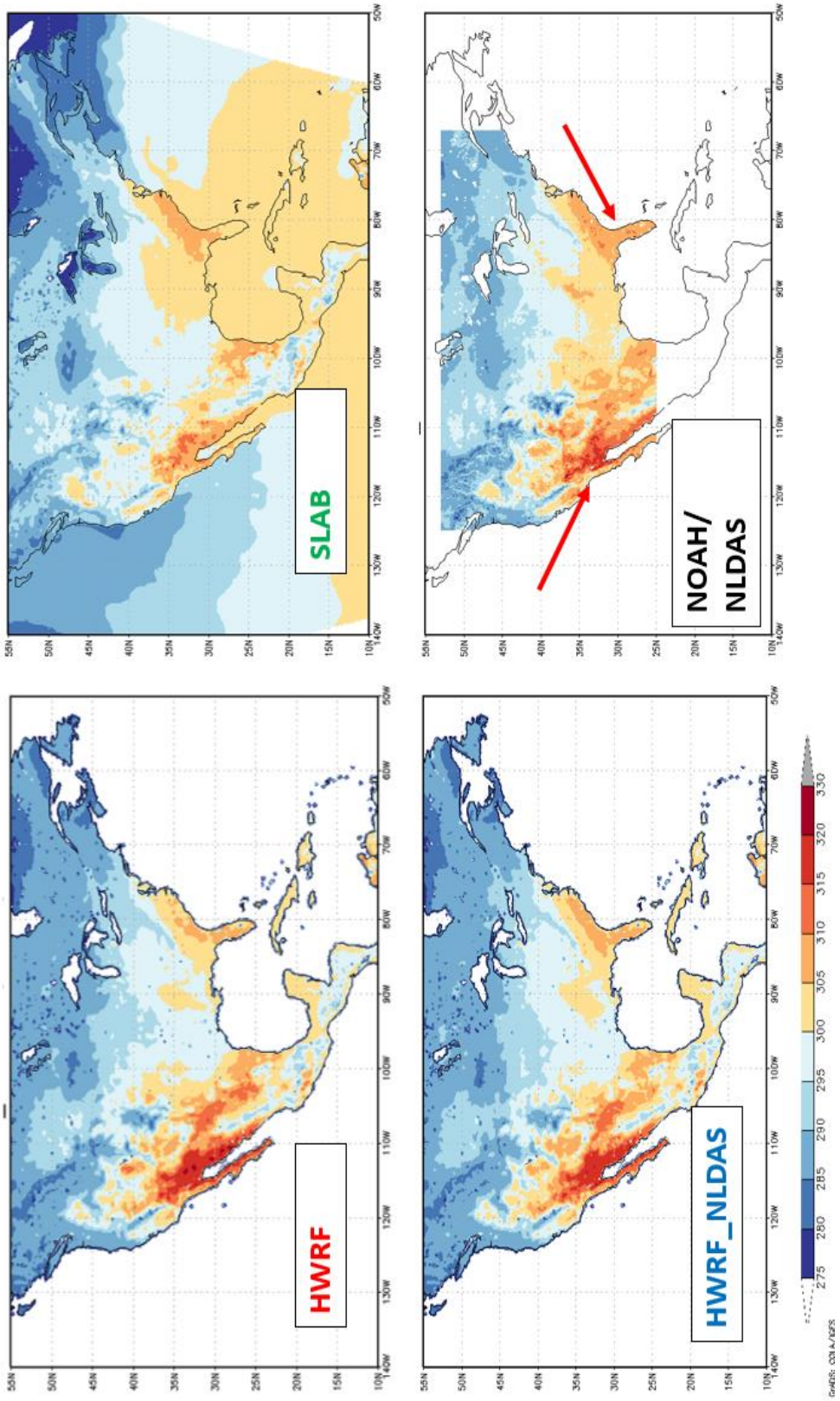

Figure 6.35 Top soil temperature for experiments on 26 June 2015 at 2100UTC in Kelvin. Both CTRL and LDAS experiments show high spatial correlation to true NLDAS dataset. SLAB experiment shows a cold bias in temperature.

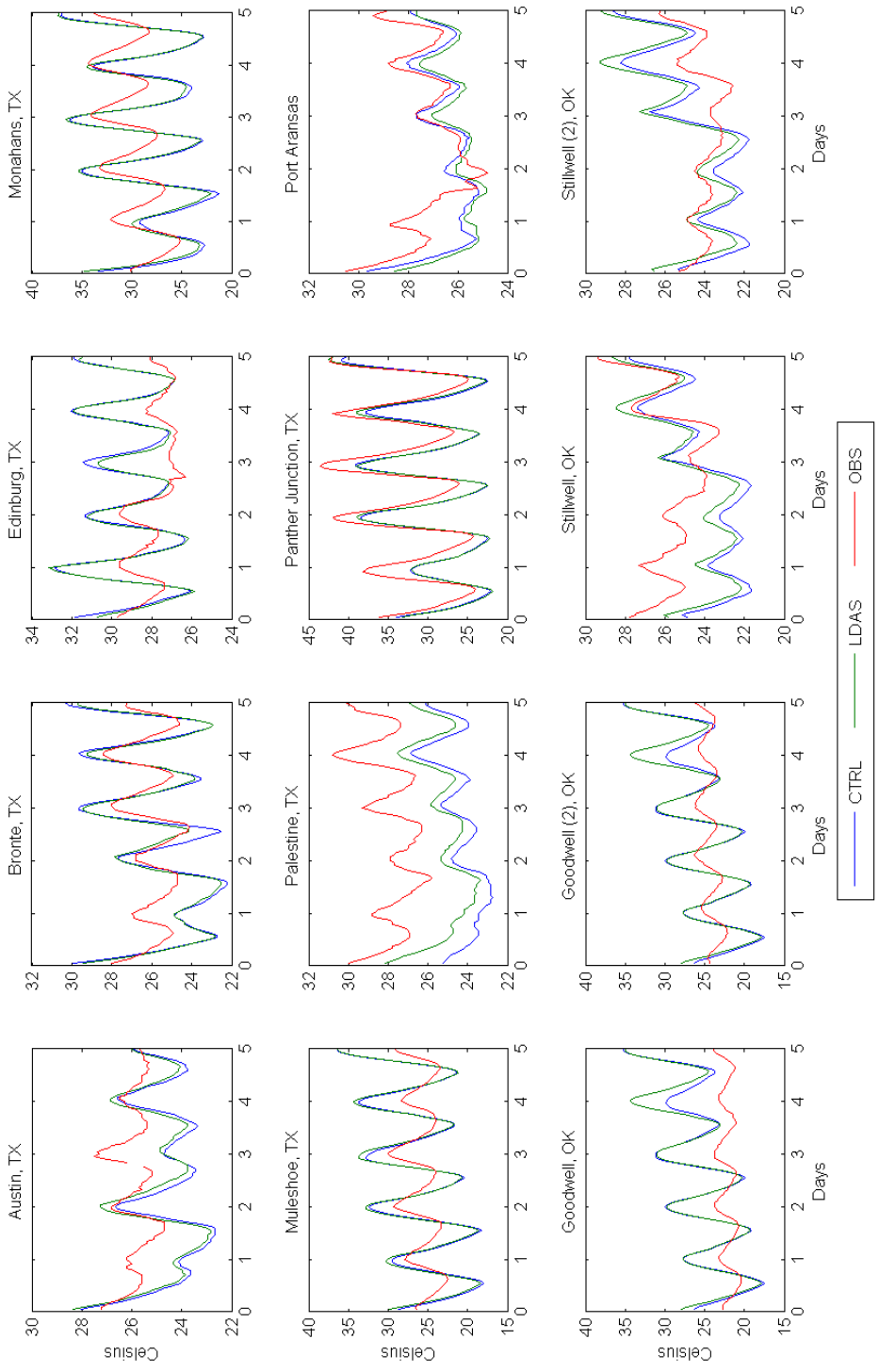

Figure 6.36 Time series plot for top soil temperature (0-10cm) for experiments against in-situ observations. The temperature values are in Celsius.

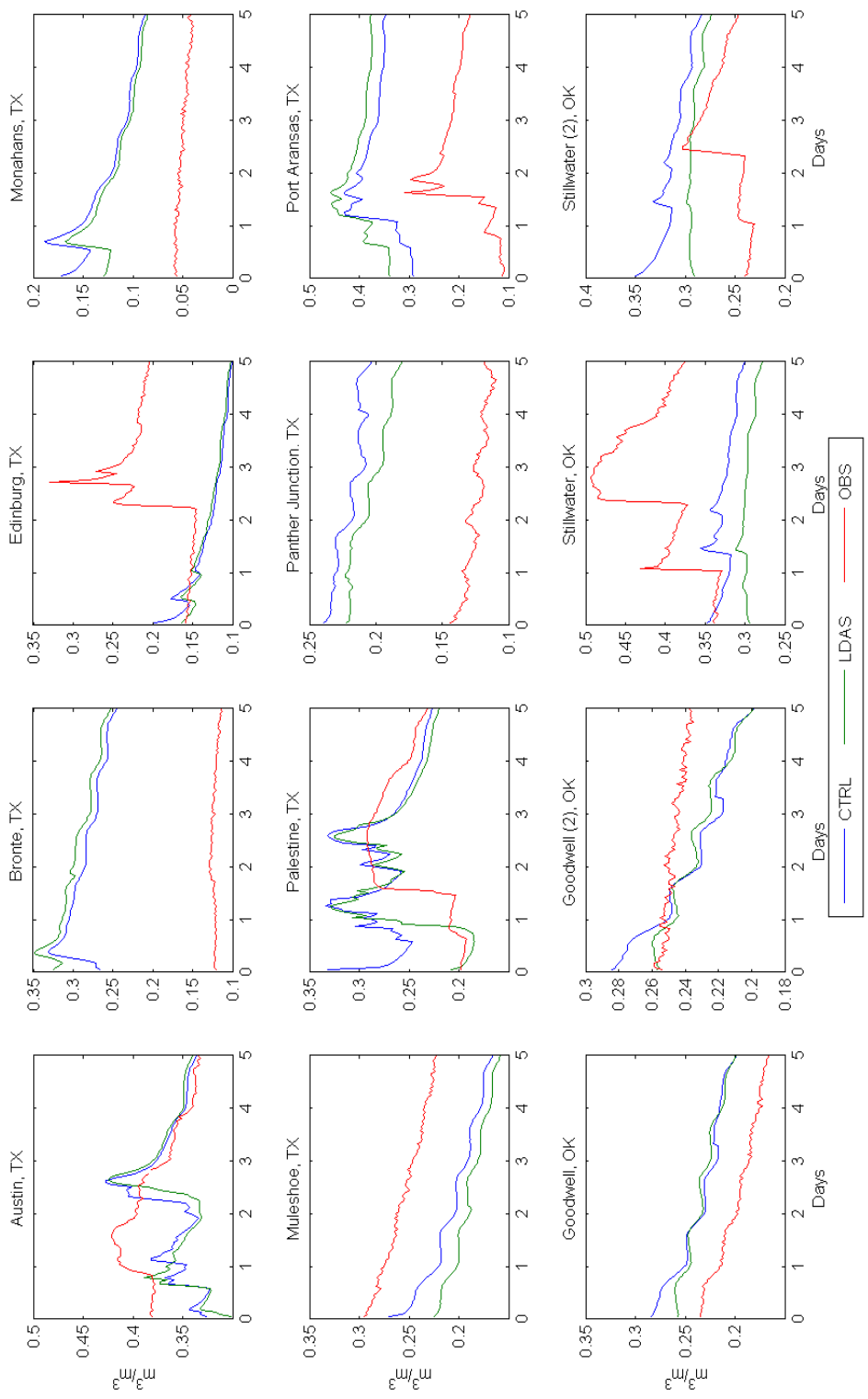

Figure 6.37 Time series plot of top soil moisture (0-10cm) in m^3/m^3 for HWRF cycle 2015061600 and experiment values are plotted against in-situ observations.

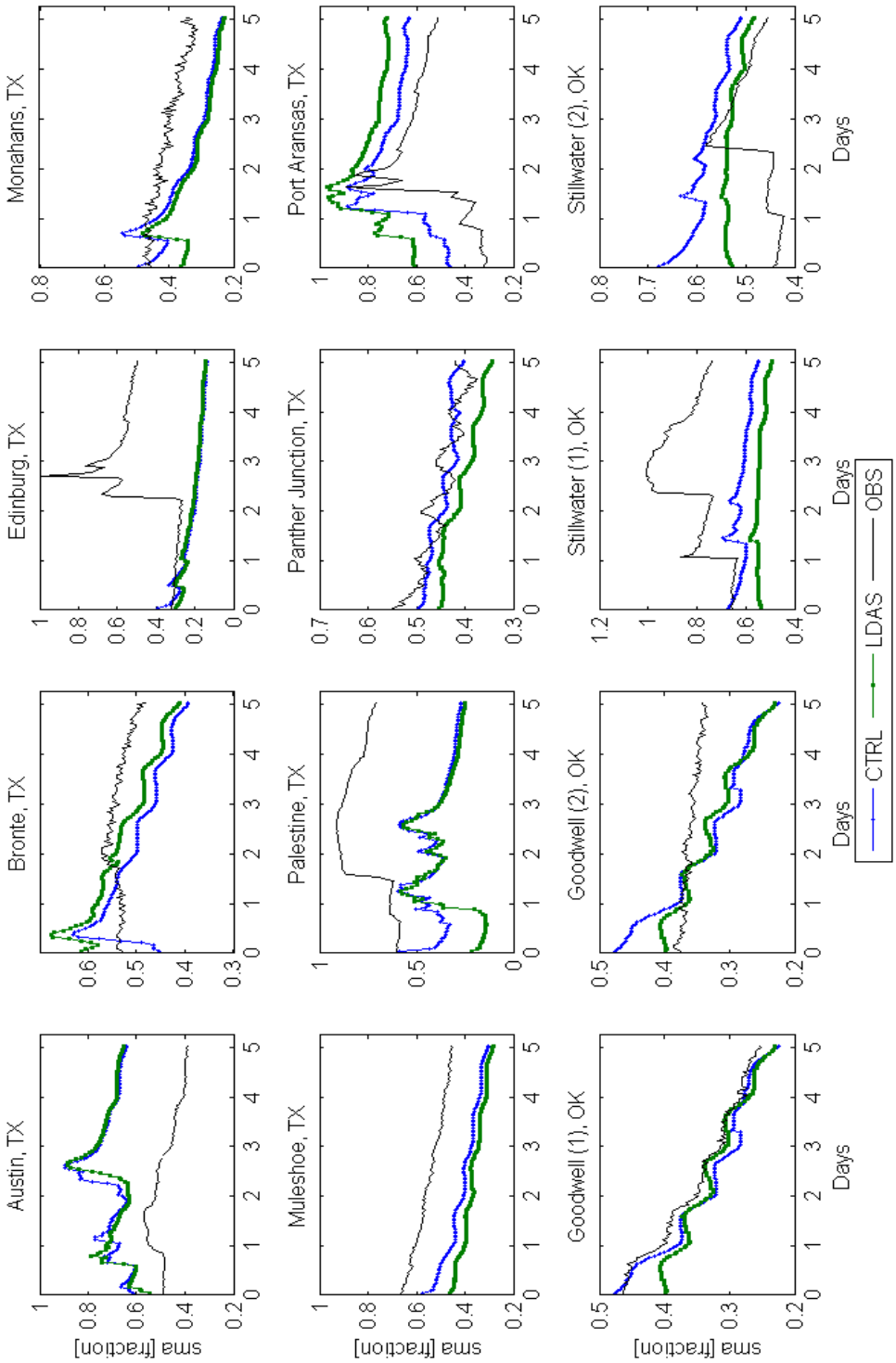

Figure 6.38 Time series plot of normalized soil water content (0-10cm) for HWRF cycle 2015061600 and experiment values are plotted against in-situ observations values.

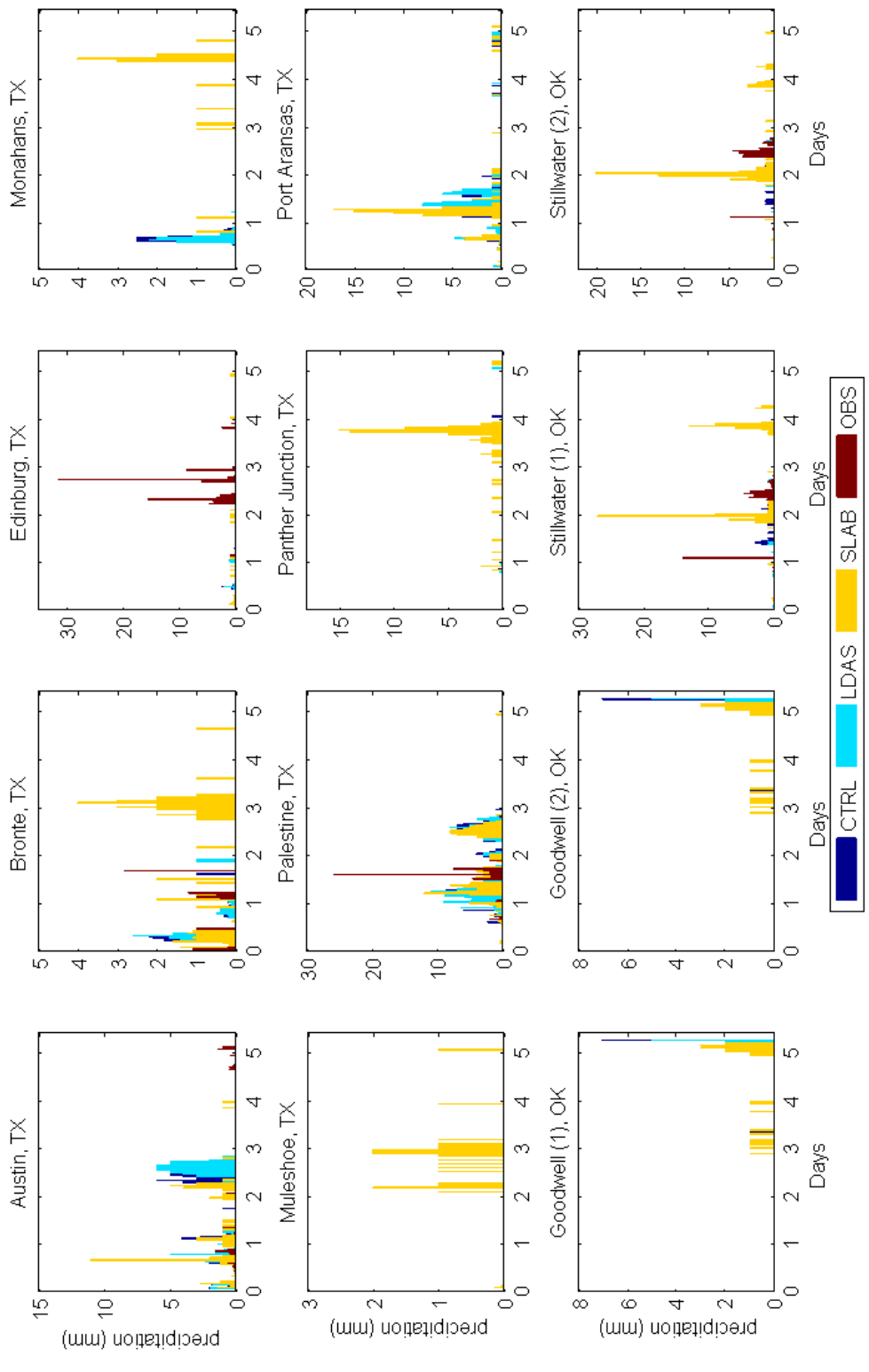

Figure 6.39 Bar graph of in situ precipitation for 120 hours for the cycle 2015061600 for SLAB, CTRL, LDAS and SLAB experiments. The soil moisture plot in Figure 6.38 varies based on precipitation modeled and observed at each of the points.

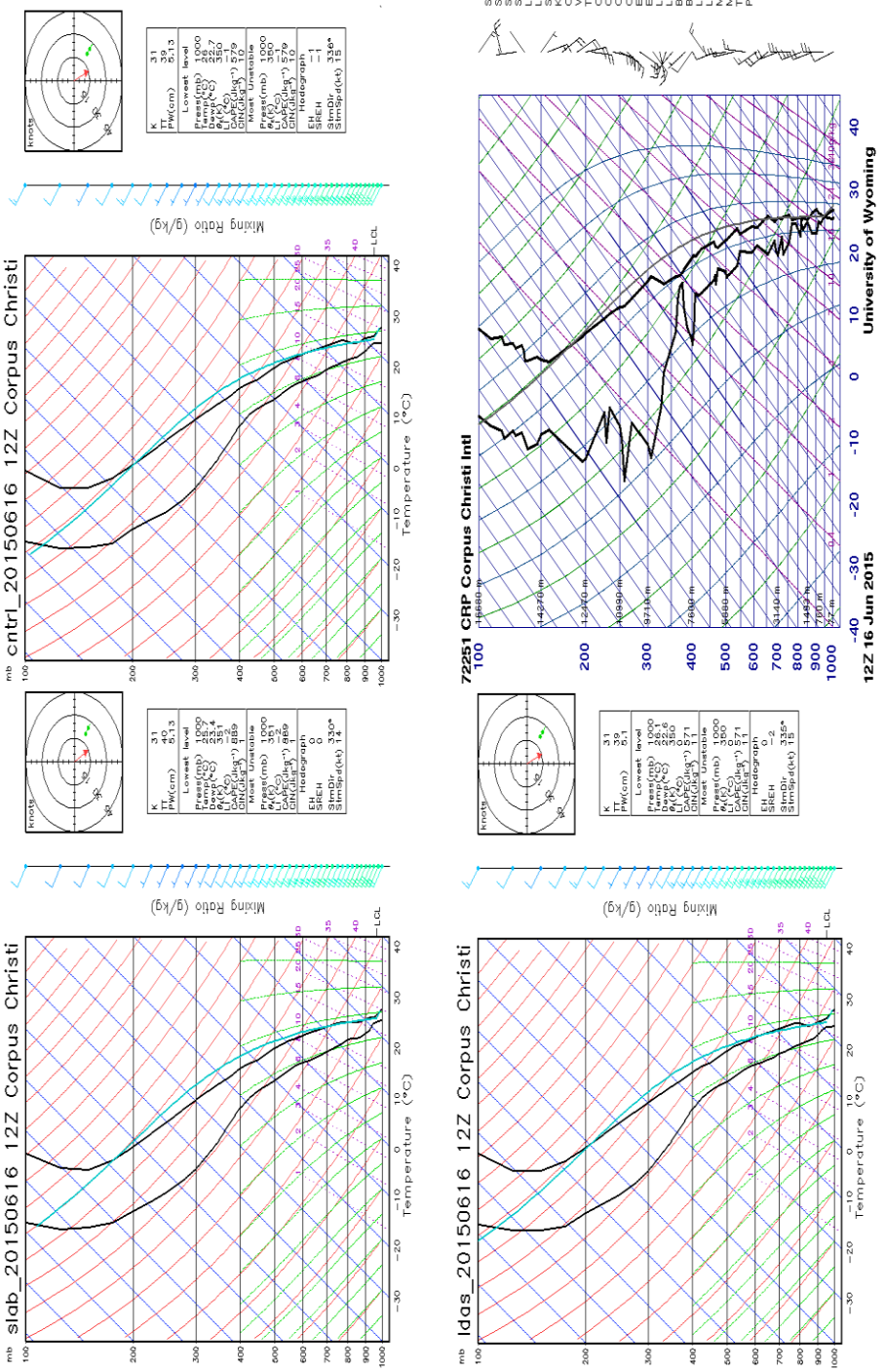

Figure 6.40 Sounding profiles at Corpus Christi, TX at 1612Z for Slab, CTRL and LDAS and compared with University of Wyoming sounding data.

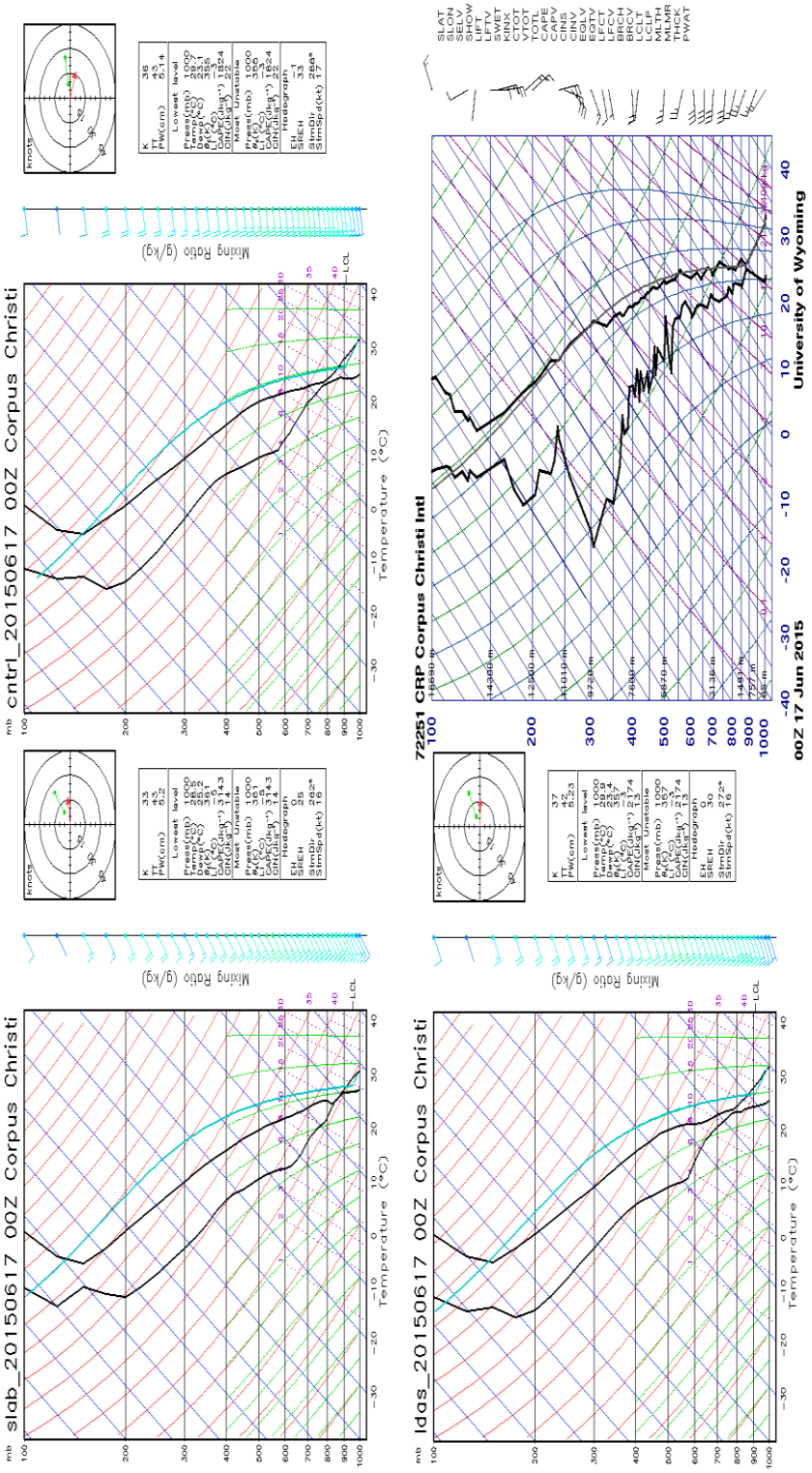

Figure 6.41 Sounding profiles at Corpus Christi, TX at 1700Z for Slab, CTRL and LDAS and compared with University of Wyoming sounding data.

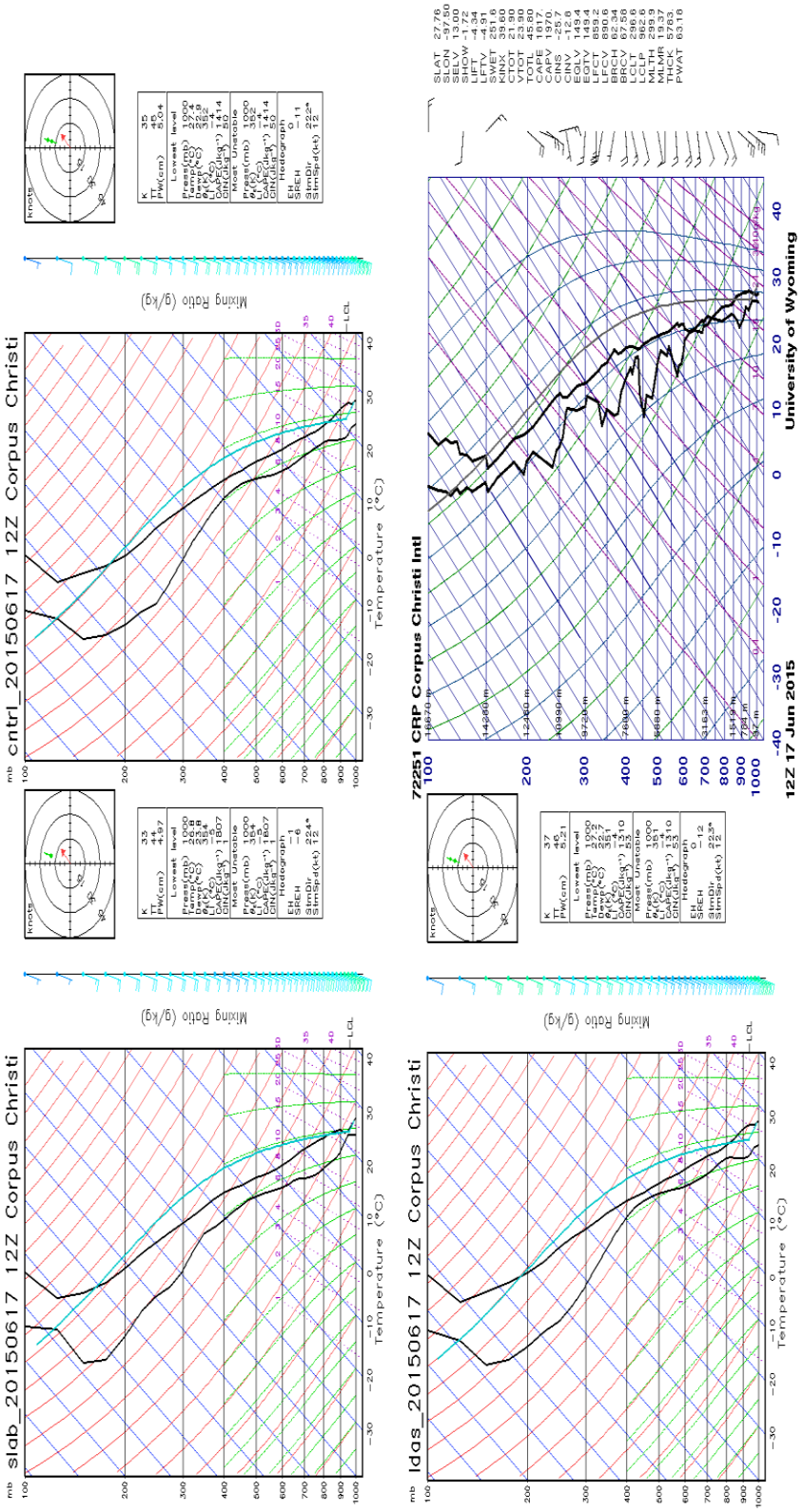

Figure 6.42 Sounding profiles at Corpus Christi, TX at 1712Z for Slab, CTRL and LDAS and compared with University of Wyoming sounding data.

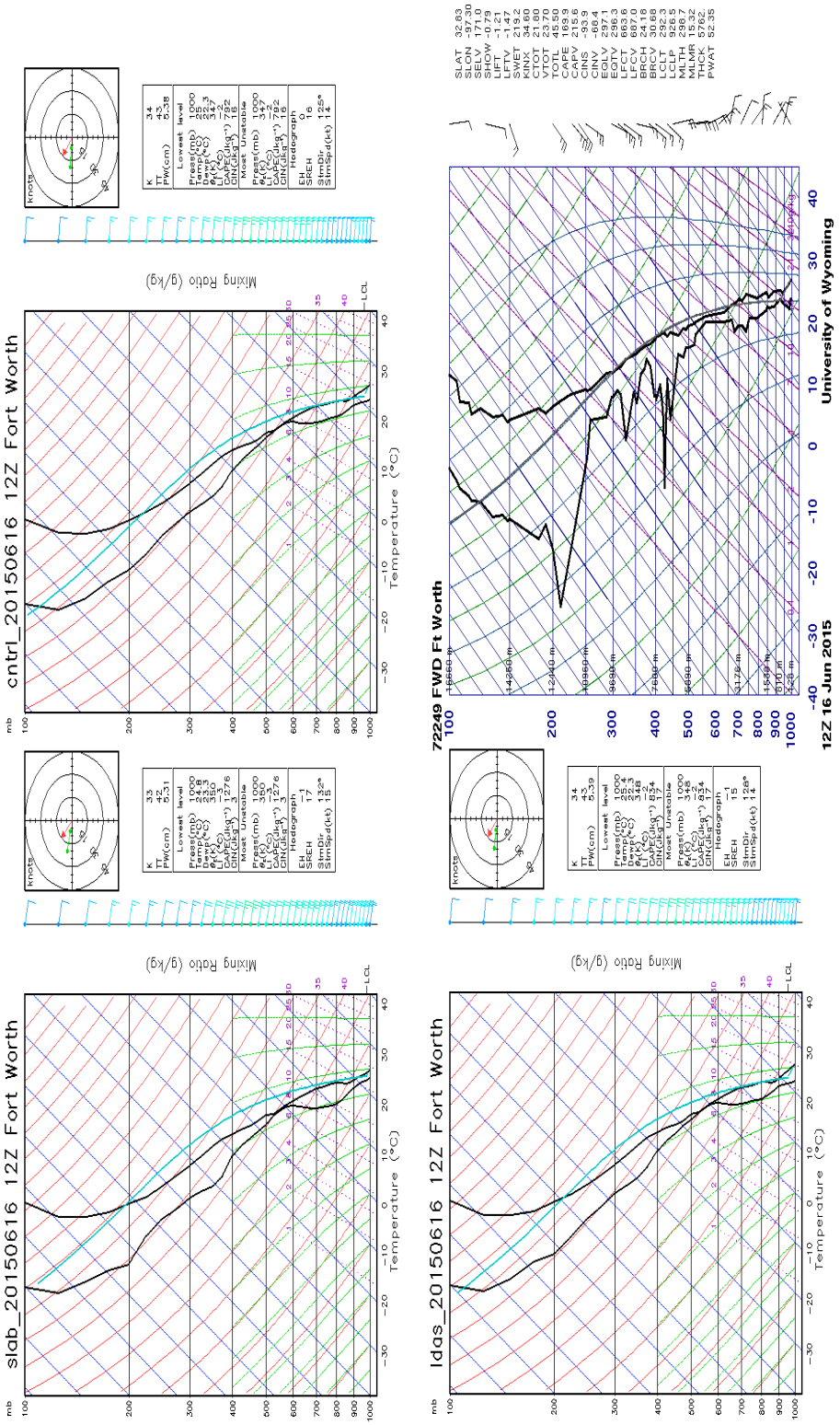

Figure 6.43 Sounding profiles at Houston, TX at 1612Z for Slab, CTRL and LDAS and compared with University of Wyoming sounding data.

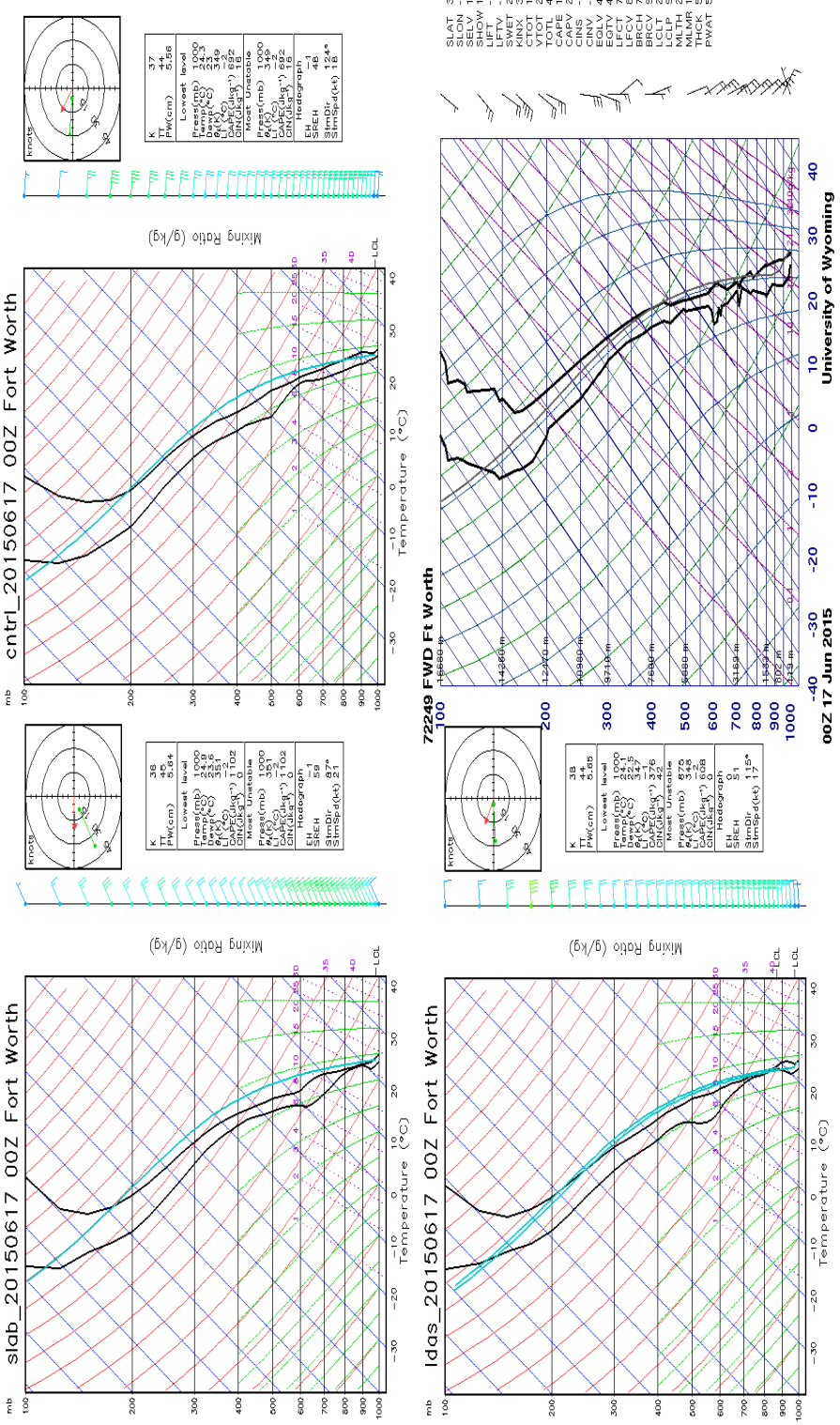

Figure 6.44 Sounding profiles at Houston, TX at 1700Z for Slab, CTRL and LDAS and compared with University of Wyoming sounding data.

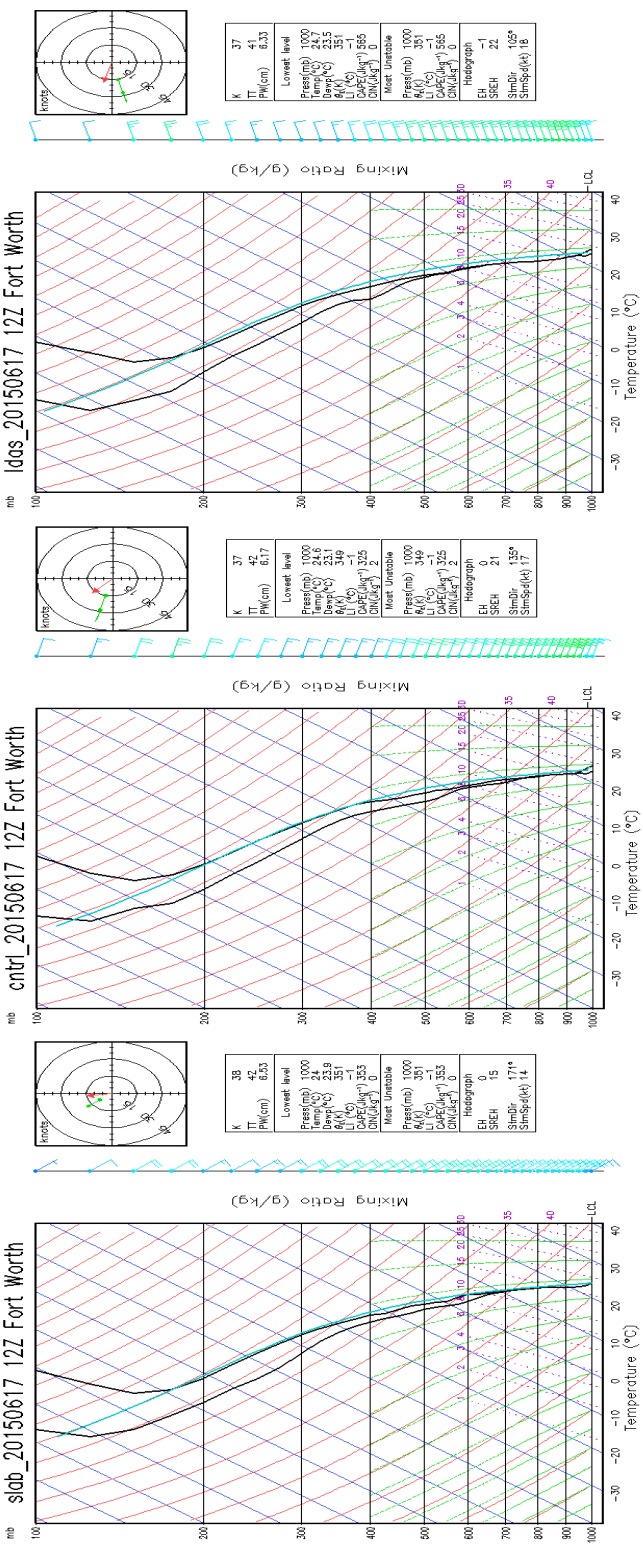

Figure 6.45 Sounding profiles at Houston, TX at 1712Z for Slab, CTRL and LDAS experiments. UWyo sounding data was unavailable for this time point.

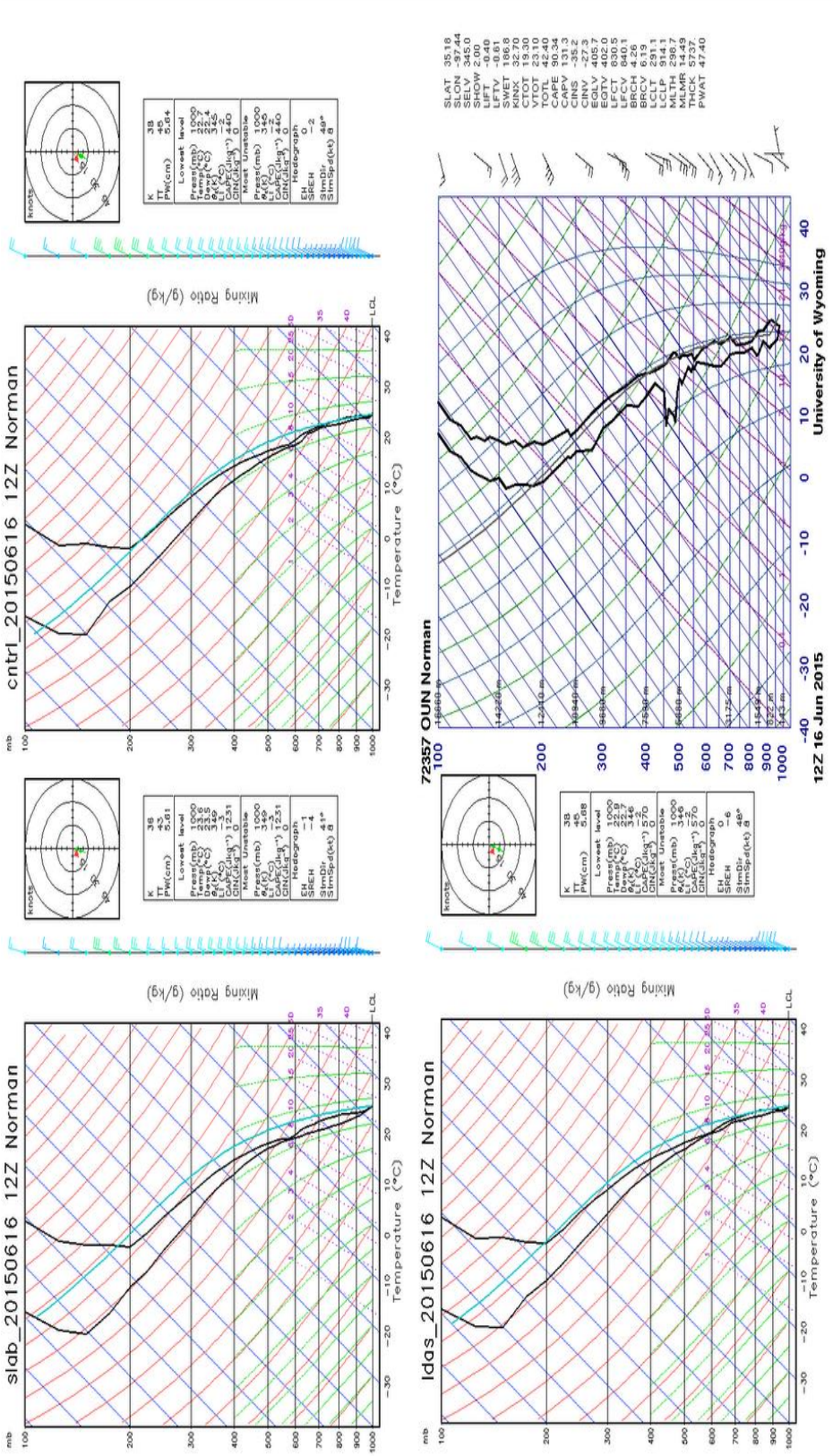

Figure 6.46 Sounding profiles at Norman, OK at 1612Z for Slab, CTRL and LDAS experiments and UWyo sounding data.

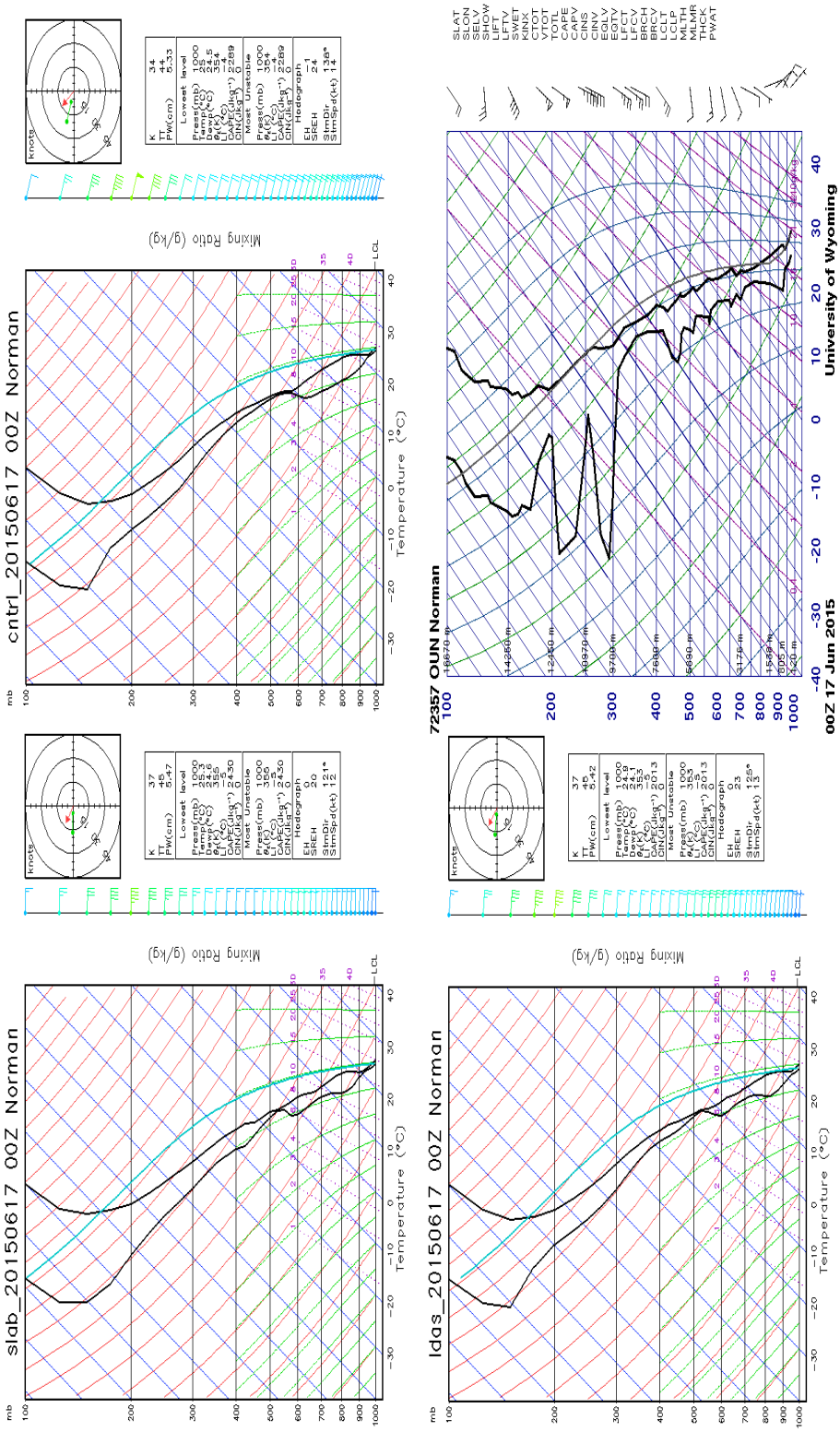

Figure 6.47 Sounding profiles at Norman, OK at 1700Z for Slab, CTRL and LDAS experiments and UWyo sounding data.

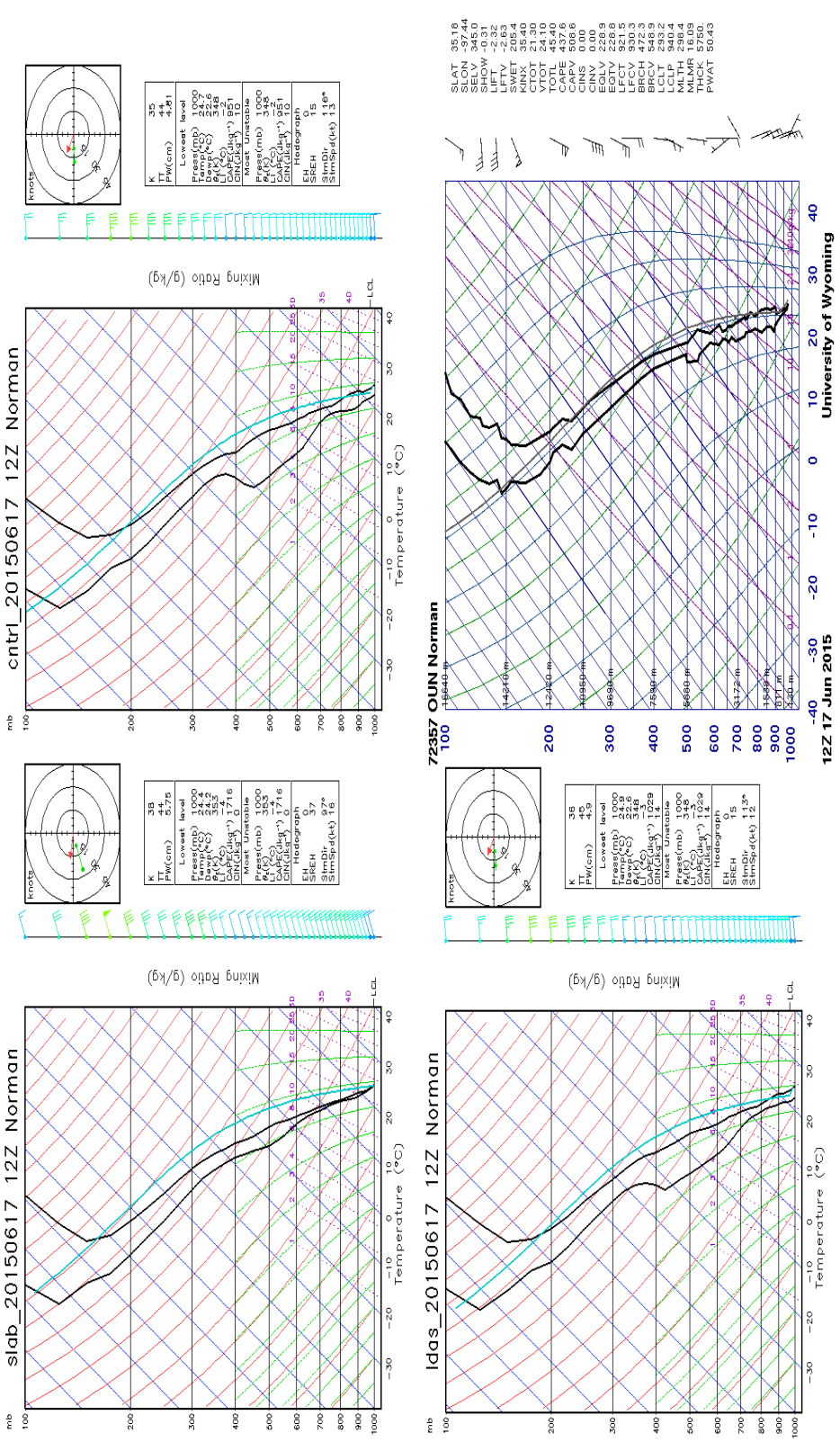

Figure 6.48 Sounding profiles at Norman, OK at 1712Z for Slab, CTRL and LDAS experiments and UWyo sounding data.

6.7 Discussion

Results suggest that improvements in the land models, land surface schemes as well as fields, surface field initialization, and the coupling between the land - atmosphere holds potential for enhancing landfalling TC predictions. Indeed, for the cases seen, limited to no difference was observed between HWRF using GFDL Slab and Noah LSM. This is expected for the operational modeling system where a large number of variables interact and constrain the outcome. Yet, the differences in rainfall for similarity in track is interesting. The surface latent and sensible heat fluxes are estimated by the difference between surface moisture and temperature and air moisture and temperature at the first model level (Flerchinger et al., 1998). Chang et al. (2009) demonstrated that the stronger gradient of heat fluxes at the surface (e.g., warmer, wetter land surface) can help to sustain the boundary layer instability and improve rainfall simulation associated with TCs. The experiments show that model performance was comparable when HWRF was runs with Noah land model in place of Slab. Indeed, the overall performance of HWRF in rainfall estimation remains to be enhanced when compared to observation. By design, these experiments were run with land atmospheric component and not with the added confounding expected with GSI or the POM-TC. Future experiments to show the impact with and without GSI and/ or POM-TC for Slab, Noah would be of interest. Other studies over India have demonstrated considerable improvement in timing and amount of rainfall through using improved initial conditions and improved LSM formulations (Osuri et al. 2015). Modeling runs involving ARW and heavy rain events have shown that land atmospheric coupling coefficients have a direct influence on the model rainfall predictions. Similar studies would be derived with the HWRF system. The results do

suggest that the atmospheric component is potentially weakly coupled with the land model or in other words, HWRF being an operational model has been over calibrated to show the impact of surface layer formulations. This is understandable given that the priority for hurricane models have always been to predict the track and intensity and during the last decade and considerable efforts have been invested to improve these metrics. Now that we start reviewing the rainfall predictions, the model framework needs to be reviewed further. This is also evident from the efforts underway at NOAA/ HRD and NCEP where in the recent years, Slab LSM has been replaced with Noah LSM and diagnostic products have been added to the operational model to improve the prediction of tornado induced by cyclones (e.g. VORTEX-SE). There is also considerable research activity in improving the LSM and surface layer formulation (this study is an example) and many Research to Operations programs to support and focus on landfalling cyclone studies.

6.8 References

Alapaty, K., D. Niyogi, F. Chen, P. Pyle, A. Chandrasekar, and N. Seaman, 2008: Development of the flux-adjusting surface data assimilation system for mesoscale models. *Journal of Applied Meteorology and Climatology*, **47,** 2331-2350.

Alavi, N., J. S. Warland, and A. A. Berg, 2009: Assimilation of soil moisture and temperature data into land surface models: a survey. *Data Assimilation for Atmospheric, Oceanic and Hydrologic Applications*, Springer, 429-448.

Anthes, R. A., and S. W. Chang, 1978: Response of the hurricane boundary layer to changes of sea surface temperature in a numerical model. *Journal of the Atmospheric Sciences*, **35,** 1240-1255.

Bister, M., and K. A. Emanuel, 1998: Dissipative heating and hurricane intensity. *Meteorology and Atmospheric Physics*, **65,** 233-240.

Bosilovich, M. G., and Coauthors, 2012: Report of the 4th World Climate Research Programme International Conference on Reanalyses.

Bozeman, M. L., D. Niyogi, S. Gopalakrishnan, F. D. Marks Jr, X. Zhang, and V. Tallapragada, 2012: An HWRF-based ensemble assessment of the land surface feedback on the post-landfall intensification of Tropical Storm Fay (2008). *Natural hazards*, **63,** 1543-1571.

Braun, S. A., and W.-K. Tao, 2000: Sensitivity of high-resolution simulations of Hurricane Bob (1991) to planetary boundary layer parameterizations. *Monthly Weather Review*, **128,** 3941-3961.

Chang, H. I., and Coauthors, 2009: Possible relation between land surface feedback and the post-landfall structure of monsoon depressions. *Geophysical Research Letters*, **36**.

Chen, F., and J. Dudhia, 2001: Coupling an advanced land surface-hydrology model with the Penn State-NCAR MM5 modeling system. Part I: Model implementation and sensitivity. *Monthly Weather Review*, **129,** 569-585.

Chen, F., and Coauthors, 1996: Modeling of land surface evaporation by four schemes and comparison with FIFE observations. *Journal of Geophysical Research: Atmospheres*, **101,** 7251-7268.

——, 2007: Description and evaluation of the characteristics of the NCAR high-resolution land data assimilation system. *Journal of applied Meteorology and Climatology*, **46,** 694-713.

Crow, W. T., and E. F. Wood, 2003: The assimilation of remotely sensed soil brightness temperature imagery into a land surface model using ensemble Kalman filtering: A case study based on ESTAR measurements during SGP97. *Advances in Water Resources*, **26,** 137-149.

Crow, W. T., W. P. Kustas, and J. H. Prueger, 2008: Monitoring root-zone soil moisture through the assimilation of a thermal remote sensing-based soil moisture proxy into a water balance model. *Remote Sensing of Environment*, **112,** 1268-1281.

Dastoor, A., and T. Krishnamurti, 1991: The landfall and structure of a tropical cyclone: The sensitivity of model predictions to soil moisture parameterizations. *Boundary-Layer Meteorology*, **55,** 345-380.

Ek, M., and Coauthors, 2003: Implementation of Noah land surface model advances in the National Centers for Environmental Prediction operational mesoscale Eta model. *Journal of Geophysical Research: Atmospheres*, **108**.

Emanuel, K., 2003: Tropical cyclones. *Annual Review of Earth and Planetary Sciences*, **31,** 75.

——, 2004: Tropical cyclone energetics and structure. *Atmospheric turbulence and mesoscale meteorology***,** 165-191.

Emanuel, K., J. Callaghan, and P. Otto, 2008: A Hypothesis for the Redevelopment of Warm-Core Cyclones over Northern Australia*. *Monthly Weather Review*, **136,** 3863-3872.

Emanuel, K. A., 1988: The maximum intensity of hurricanes. *Journal of the Atmospheric Sciences*, **45,** 1143-1155.

——, 1995: Sensitivity of tropical cyclones to surface exchange coefficients and a revised steady-state model incorporating eye dynamics. *Journal of the Atmospheric Sciences*, **52,** 3969-3976.

Evans, C., R. S. Schumacher, and T. J. Galarneau Jr, 2011: Sensitivity in the overland reintensification of Tropical Cyclone Erin (2007) to near-surface soil moisture characteristics. *Monthly Weather Review*, **139,** 3848-3870.

Gopalakrishnan, S. G., F. Marks Jr, J. A. Zhang, X. Zhang, J.-W. Bao, and V. Tallapragada, 2013: A study of the impacts of vertical diffusion on the structure and intensity of the tropical cyclones using the high-resolution HWRF system. *Journal of the Atmospheric Sciences*, **70,**524-541.

Hill, K. A., and G. M. Lackmann, 2009: Analysis of idealized tropical cyclone simulations using the Weather Research and Forecasting model: Sensitivity to turbulence parameterization and grid spacing. *Monthly Weather Review*, **137,** 745-765.

Holt, T. R., D. Niyogi, F. Chen, K. Manning, M. A. LeMone, and A. Qureshi, 2006: Effect of land-atmosphere interactions on the IHOP 24-25 May 2002 convection case. *Monthly Weather Review*, **134,** 113-133.

Hong, X., S. W. Chang, S. Raman, L. K. Shay, and R. Hodur, 2000: The interaction between Hurricane Opal (1995) and a warm core ring in the Gulf of Mexico. *Monthly Weather Review*, **128,** 1347-1365.

Kellner, O., D. Niyogi, M. Lei, and A. Kumar, 2012: The role of anomalous soil moisture on the inland reintensification of Tropical Storm Erin (2007). *Natural hazards*, **63,** 1573-1600.

Kimball, S. K., 2008: Structure and evolution of rainfall in numerically simulated landfalling hurricanes. *Monthly Weather Review*, **136,** 3822-3847.

Kishtawal, C. M., D. Niyogi, A. Kumar, M. L. Bozeman, and O. Kellner, 2012: Sensitivity of inland decay of North Atlantic tropical cyclones to soil parameters. *Natural hazards*, **63,** 1527-1542.

Lonfat, M., F. D. Marks Jr, and S. S. Chen, 2004: Precipitation distribution in tropical cyclones using the Tropical Rainfall Measuring Mission (TRMM) microwave imager: A global perspective. *Monthly Weather Review*, **132,** 1645-1660.

Marchok, T., R. Rogers, and R. Tuleya, 2007: Validation schemes for tropical cyclone quantitative precipitation forecasts: Evaluation of operational models for US landfalling cases. *Weather and forecasting*, **22,** 726-746.

Mitchell, K. E., and Coauthors, 2004: The multi-institution North American Land Data Assimilation System (NLDAS): Utilizing multiple GCIP products and partners in a continental distributed hydrological modeling system. *Journal of Geophysical Research: Atmospheres*, **109**.

Montgomery, M. T., R. K. Smith, and S. V. Nguyen, 2010: Sensitivity of tropical-cyclone models to the surface drag coefficient. *Quarterly Journal of the Royal Meteorological Society*, **136,** 1945-1953.

Niyogi, D., T. Holt, S. Zhong, P. C. Pyle, and J. Basara, 2006: Urban and land surface effects on the 30 July 2003 mesoscale convective system event observed in the southern Great Plains. *Journal of Geophysical Research: Atmospheres*, **111**.

Noilhan, J., and S. Planton, 1989: A simple parameterization of land surface processes for meteorological models. *Monthly Weather Review*, **117,** 536-549.

Nolan, D. S., D. P. Stern, and J. A. Zhang, 2009a: Evaluation of Planetary Boundary Layer Parameterizations in Tropical Cyclones by Comparison of In Situ Observations and High-Resolution Simulations of Hurricane Isabel (2003). Part II: Inner-Core Boundary Layer and Eyewall Structure. *Monthly Weather Review*, **137,** 3675-3698.

Nolan, D. S., J. A. Zhang, and D. P. Stern, 2009b: Evaluation of planetary boundary layer parameterizations in tropical cyclones by comparison of in situ observations and high-resolution simulations of Hurricane Isabel (2003). Part I: Initialization, maximum winds, and the outer-core boundary layer. *Monthly weather review*, **137,** 3651-3674.

Osuri, K. K., U. Mohanty, A. Routray, M. Mohapatra, and D. Niyogi, 2013: Real-time track prediction of tropical cyclones over the North Indian Ocean using the ARW model. *Journal of Applied Meteorology and Climatology*, **52,** 2476-2492.

Persing, J., M. T. Montgomery, and R. E. Tuleya, 2002: Environmental interactions in the GFDL hurricane model for Hurricane Opal. *Monthly weather review,* **130,** 298-317.

Pielke, R. A., 2001: Influence of the spatial distribution of vegetation and soils on the prediction of cumulus convective rainfall. *Reviews of Geophysics,* **39,** 151-177.

Reichle, R., W. Crow, R. Koster, H. Sharif, and S. Mahanama, 2008: Contribution of soil moisture retrievals to land data assimilation products. *Geophysical Research Letters*, **35**.

Reichle, R. H., D. Entekhabi, and D. B. McLaughlin, 2001: Downscaling of radio brightness measurements for soil moisture estimation: A four-dimensional variational data assimilation approach. *Water Resources Research*, **37,** 2353-2364.

Rhome, J. R., and S. Raman, 2006: Environmental influences on tropical cyclone structure and intensity: a review of past and present literature. *Indian Journal of Marine Sciences*, **35,** 61-74.

Rienecker, M. M., and Coauthors, 2011: MERRA: NASA's modern-era retrospective analysis for research and applications. *Journal of Climate*, **24,** 3624-3648.

Rogers, R., F. Marks, and T. Marchok, 2009: Tropical cyclone rainfall. *Encyclopedia of hydrological sciences*.

Smith, R. K., and G. L. Thomsen, 2010: Dependence of tropical-cyclone intensification on the boundary-layer representation in a numerical model. *Quarterly Journal of the Royal Meteorological Society*, **136,** 1671-1685.

Stewart, S. R., and J. L. Beven II, 2009: Tropical Cyclone Report Tropical Storm Fay (AL062008) 15-26 August 2008. *National Hurricane Center*.

Subramanian, S., S. Gopalakrishnan, G.R. Halliwell Jr. and D. Niyogi, 2014: Idealized Study of Land Surface Impacts on TC Intensity Predictions Using the HWRF Modeling System. 15A.8A presented at 31st Conference on Hurricanes and Tropical Meteorology March 30-April 04, 2014.

Trier, S. B., F. Chen, and K. W. Manning, 2004: A study of convection initiation in a mesoscale model using high-resolution land surface initial conditions. *Monthly weather review*, **132,** 2954-2976.

Tuleya, R. E., 1994: Tropical storm development and decay: Sensitivity to surface boundary conditions. *Monthly Weather Review*, **122,** 291-304.

Tuleya, R. E., and Y. Kurihara, 1978: A numerical simulation of the landfall of tropical cyclones. *Journal of the Atmospheric Sciences*, **35,** 242-257.

Walker, J. P., and P. R. Houser, 2001: A methodology for initializing soil moisture in a global climate model: Assimilation of near-surface soil moisture observations. *Journal of Geophysical Research*, **106,** 11761-11774.

Wang, Y., and C.-C. Wu, 2004: Current understanding of tropical cyclone structure and intensity changes–a review. *Meteorology and Atmospheric Physics*, **87,** 257-278.

Warner, T. T., 2009: *Desert meteorology*. Cambridge University Press.

Zhang, J. A., R. F. Rogers, D. S. Nolan, and F. D. Marks Jr, 2011: On the characteristic height scales of the hurricane boundary layer. *Monthly Weather Review*, **139,** 2523-2535.

CHAPTER 7. DEVELOPMENT AND APPLICATION OF HWRF COUPLED RIVER ROUTING MODEL

7.1 Introduction

Flooding related to storm surge and rainfall account for more than 75% of damages caused by TCs (Rappaport 2009, 2014). Emergency planning agencies and mitigative efforts are often dependent on streamflow forecasts. Benefits of accurate forecasts helps in preparing for imminent flood by utilizing upstream reservoirs, minimizing flood losses through emergency interventions to reduce flood impacts (sand bags, bunds, levees) and effect quick evacuations. With the gains being made in track and intensity forecasts, the focus continues to evolve to the rainfall prediction, and in particular the land surface effects on landfalling TCs and inland rain and floods have emerged as critical aspects to coordinate risk and disaster management operations. This issue has attained greater urgency after Superstorm Sandy (2012) where considerable damage was caused by coastal flooding complicated by both inland rainfall and storm surge (HFIP 2015). With significant advancements in satellite, in-situ land data collection, in addition to traditional atmospheric products and computational capacity, data assimilation techniques have been developed to improve the representation of land state in numerical models (Chen et al. 2007). There has also been considerable push to incorporate hydrology products for modeling flood and streamflow. This has resulted in adopting a more advanced land model – Noah in place of GFDL Slab model. Surface runoff and baseflow are important

hydrology products that are produced by Noah (Ek et al. 2003) and this change has made available an opportunity to couple a river routing model with HWRF to produce streamflow predictions. Developing this link and demonstrating the opportunity is the primary motivation for this chapter.

Streamflow depend on soil moisture saturation, channel precipitation, surface runoff and baseflow. With increased precipitation, soil moisture gets increasingly saturated and the infiltration capacity of soils are reduced. This results in increased surface water which seeks to find the path of low resistance to reach channels of water flow. This flow is impacted by the land use and soil condition, topography and antecedent land conditions. A schematic of streamflow and related contributors to streamflow as considered in the HWRF model is depicted in Figure 7.1.

7.2 Distributed River Routing Model

The distributed river routing model as developed by Lohmann et al. (1998) is currently part of the operational NLDAS-1 and NLDAS-2 framework that produces daily deviations from mean streamflow values for the entire continental US region. The inputs to the river routing models are surface flow and baseflow as calculated by a meteorological model. In NLDAS, the atmospheric forcing is through Global Data Assimilation System (GDAS) and a Noah model (VIC and Mosaic LSM also possible) that calculate the surface flow and baseflow for different land surfaces. Hydrographs are already present in the model and form the basis on which streamflow is predicted. The transport rules set down eight directions in which water in a grid box can flow given by

the river flow direction mask. The equation for the transport is based on St. Venant equation for river transport (Lohmann et al. 1998, 2004).

The study hypothesis that improved initial land state will improve simulations of hydrology products and can be used to drive streamflow models will be tested. In the previous chapters, the idea that land model can change rainfall prediction is already presented and tested. Indeed, the soil moisture and storage terms are also changed. Flooding and inundation are major concerns for the TC prediction and response community and a research effort in this direction is expected to be valuable.

7.3 Experimental Setup

Two sets of experiments were run; one with GFS initial condition and another with NLDAS initial conditions for soil moisture and temperature. Distributed River Routing Model is coupled with HWRF which runs Noah LSM as its land model and produces both surface runoff and baseflow as input for the streamflow model. A schematic of the one-way coupling achieved between HWRF and river routing model is given in Figure 7.2. HWRF runs of TS BILL were used to drive the streamflow model. The meteorological history of TS BILL has already been discussed in the previous chapter. This cyclone was chosen because of HWRF's ability to predict the track of the storm relatively well. In addition to If not the precipitation totals, the distribution of the precipitation is quite critical to rainfall distribution and hence streamflow. Observed archive map of streamflow over US on June 16 and June 17, 2015 is given in Figure 7.3. Bill made landfall on June 16 at 1645UTC.

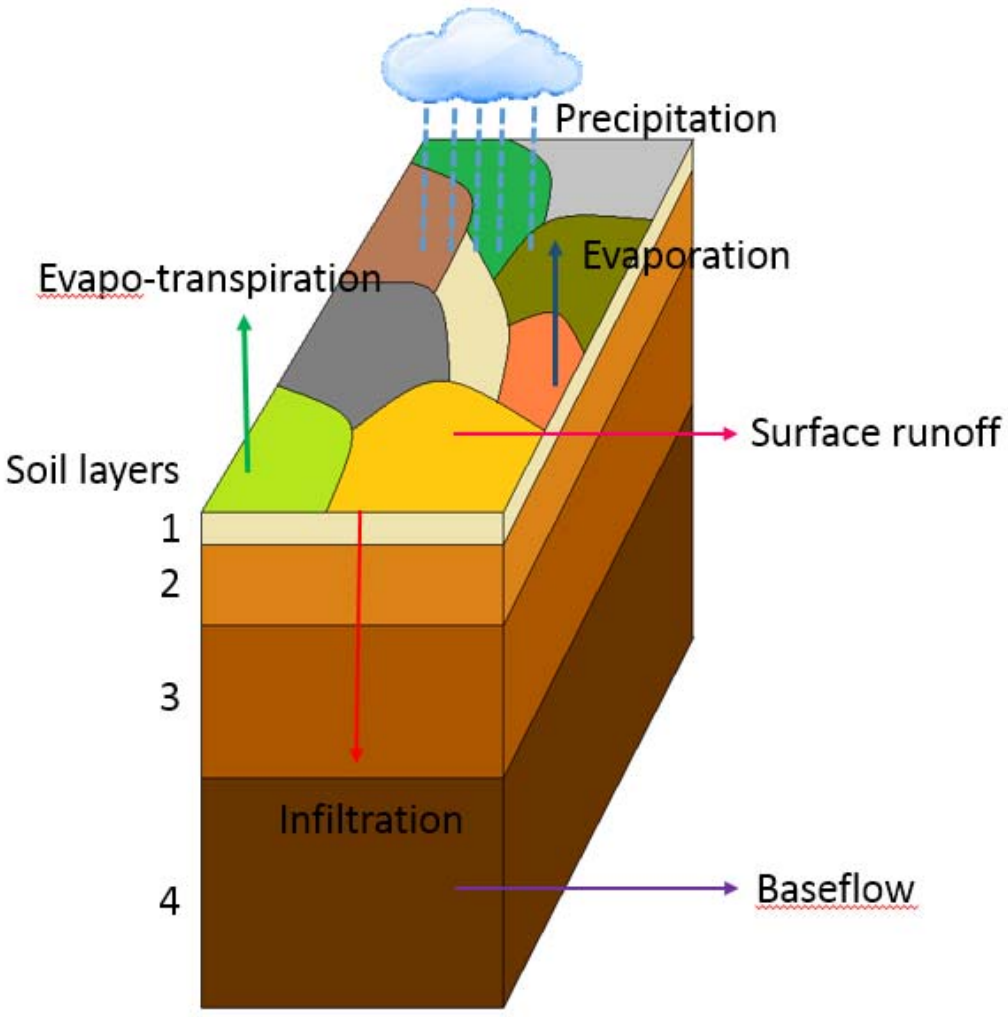

Figure 7.1 Schematic of Streamflow explained.

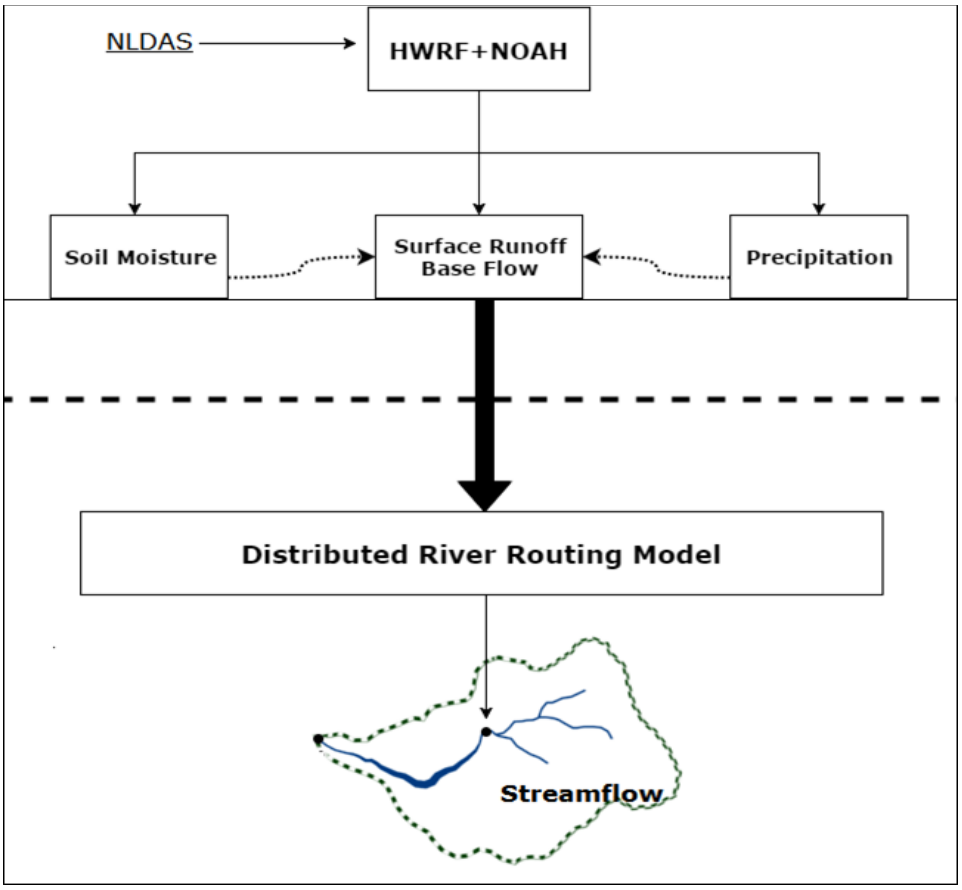

Figure 7.2 Schematic of coupled Distributed River Routing Model with HWRF.

7.4 Results

Tropical storm BILL and its precipitation characteristics have already been discussed in detail in the last chapter. A brief summary of the precipitation plot for Noah (control HWRF) and LDAS (HWRF_NLDAS) experiments compared to Stage IV precipitation is given in Figure 7.4. Both HWRF and HWRF_NLDAS experiments capture the spatial variability and rainfall totals reasonably well. The top soil moisture and the deep soil moisture plot is also shown in Figure 7.5 and Figure 7.6 and compared to NLDAS soil moisture products. Two things can be highlighted. (i) HWRF does not capture the soil

moisture's spatial distribution but follows very closely, the initial soil moisture supplied to the model through GFS, and (ii) HWRF_NLDAS experiment over estimates the soil moisture over the Southern Great Plains and the lower Mississippi region but the spatial distribution is broadly similar to NLDAS soil moisture.

The performance of the two runs in simulating the deep soil moisture is however quite different. In Noah, deep soil moisture (100-200 cm) is over predicted and there is a large area in the domain (SGP, LMV, UMV and Midwest) where deep soil moisture is quite high compared to the NLDAS dataset. With the LDAS run, the variability and the soil moisture values are well captured. The deep soil moisture layer is critical to model sub surface flow and if the deep soil layer is saturated, the excess water is channeled as baseflow producing high streamflow values. This is expected to affect the streamflow values for HWRF experiment and is expected to be high.

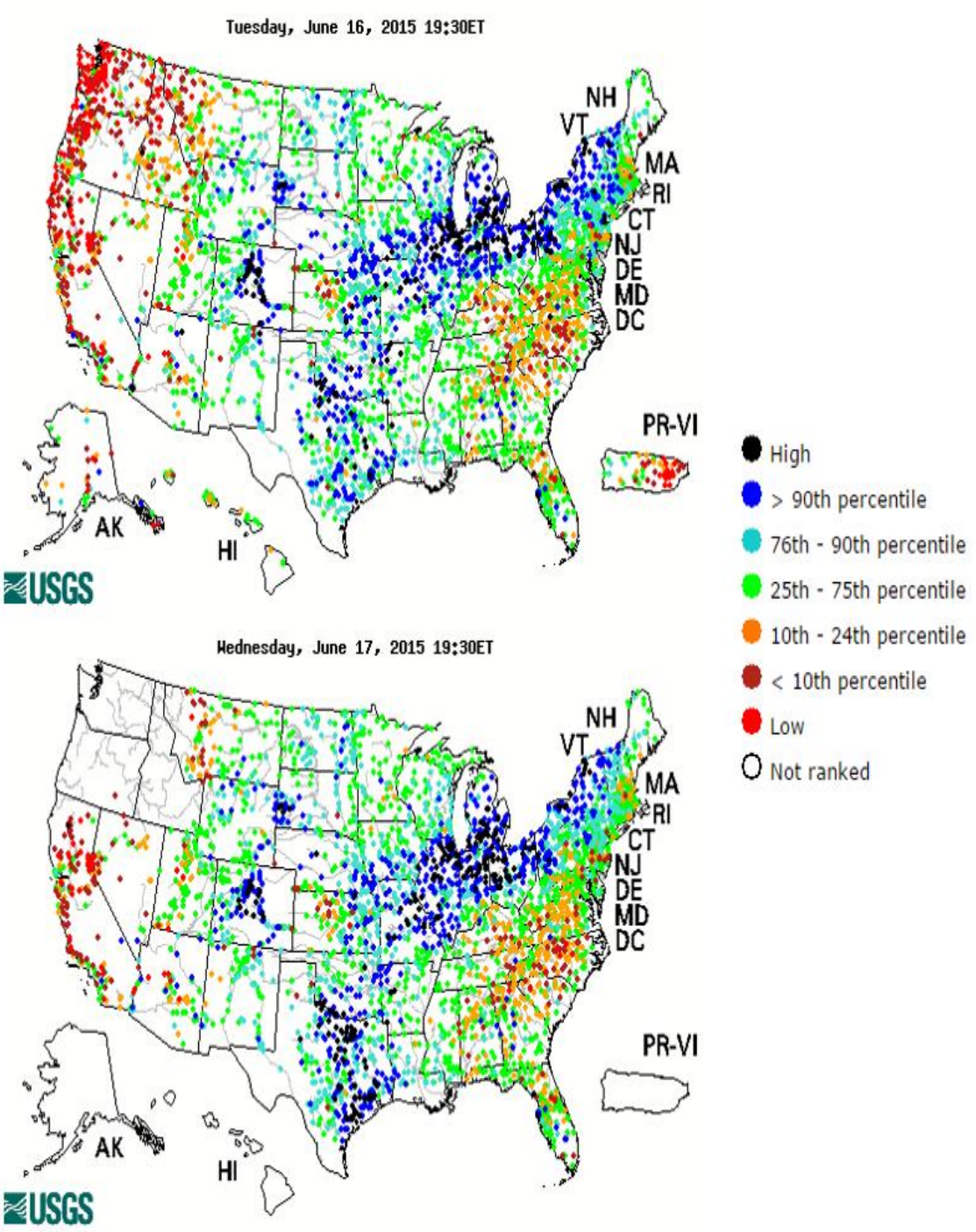

Figure 7.3 Observed Streamflow map for US on 16th and 17th June, 2015. The colors represent the streamflow conditions compared to 30 year averages.

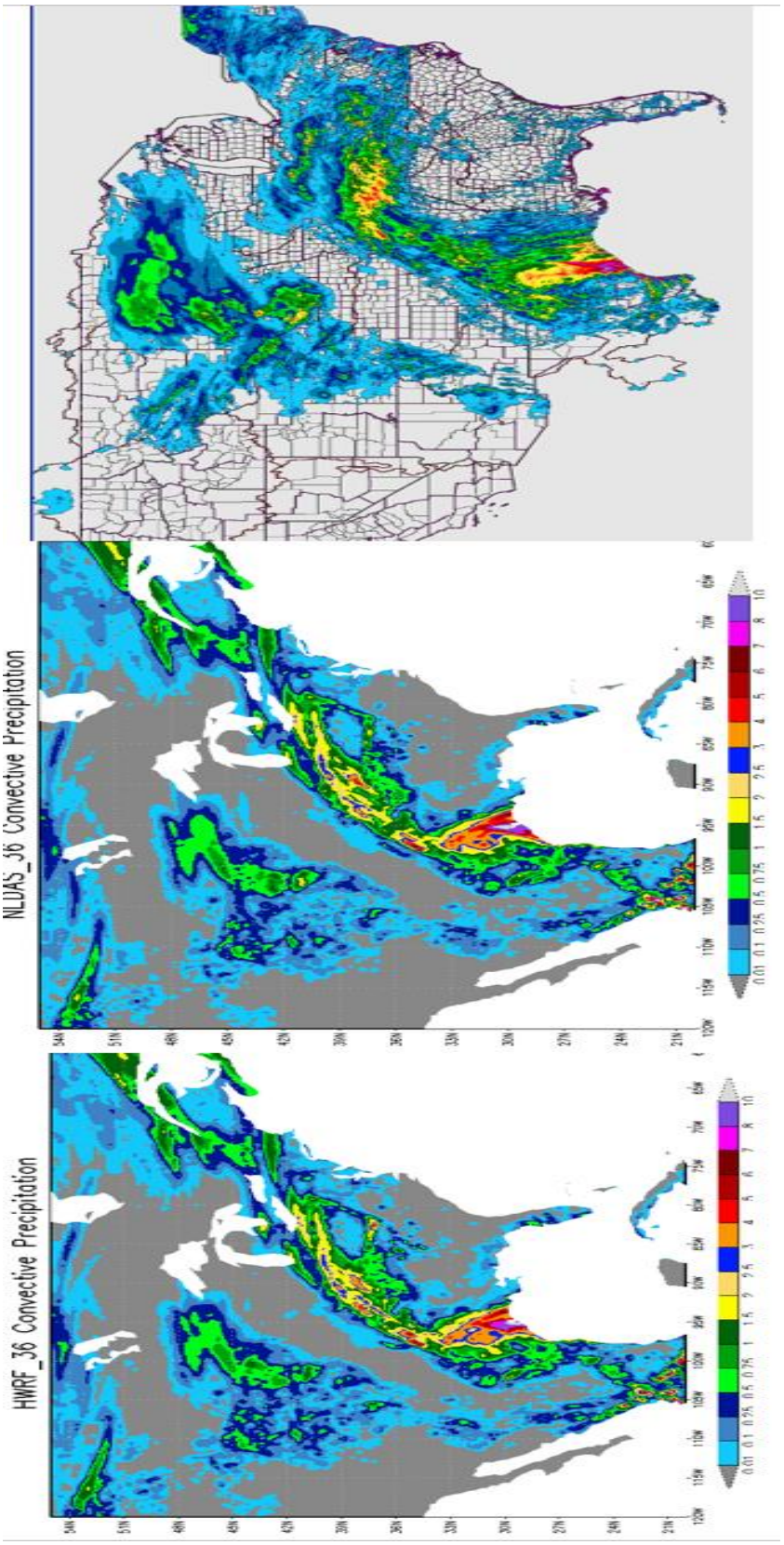

Figure 7.4 Accumulated 1-day precipitation for period ending 2016061712 in inches for HWRF, HWRF_NLDAS and Stage IV observations.

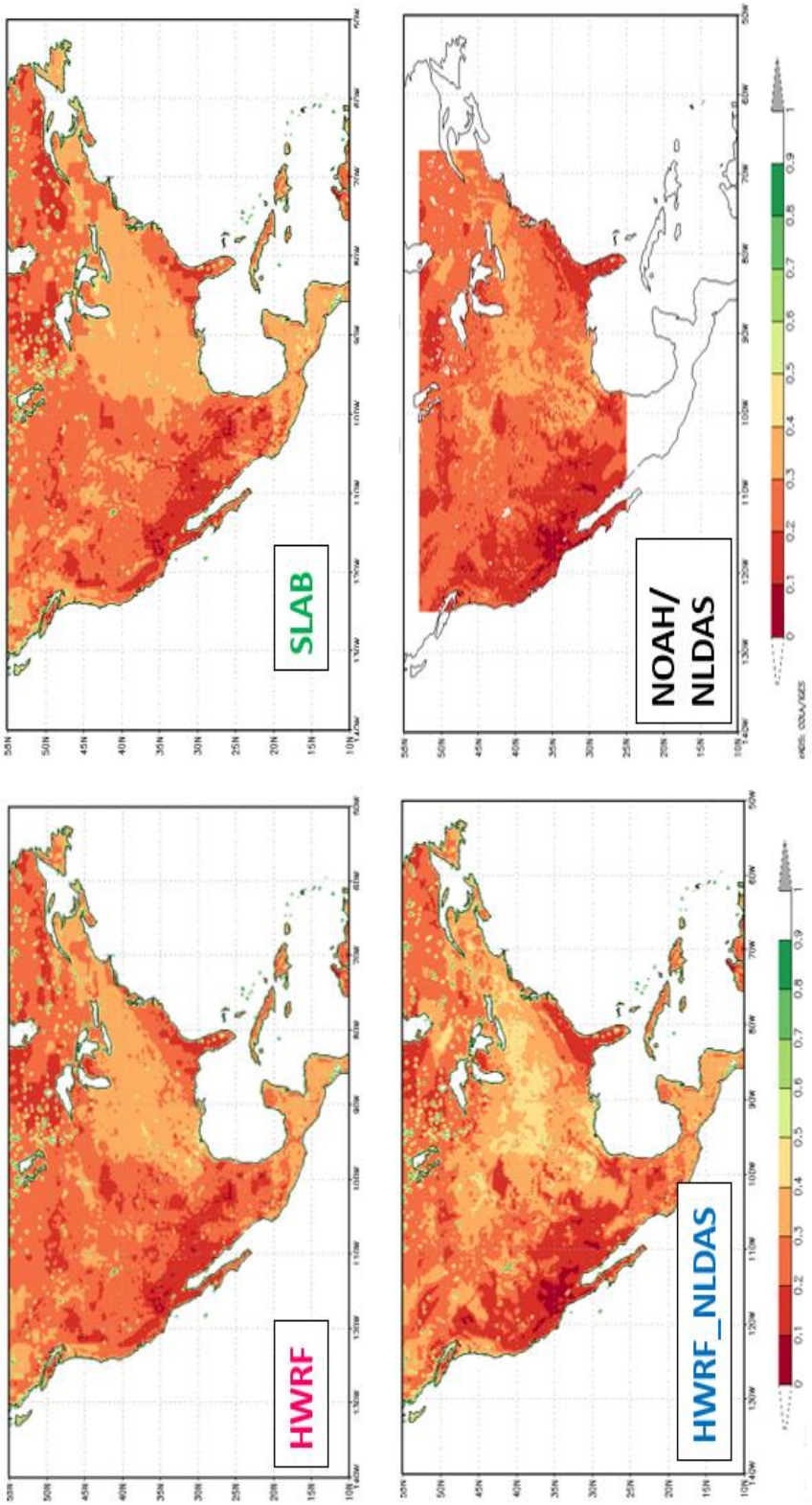

Figure 7.5 Domain plot for top soil moisture (0-10 cm, in m^3/m^3) for HWRF, Slab, HWRF_NLDAS and NLDAS datasets. Slab (by design) does not change throughout the simulation. The initial GFS soil moisture supplied to the model is kept constant and is also the initial soil moisture supplied to the HWRF experiment.

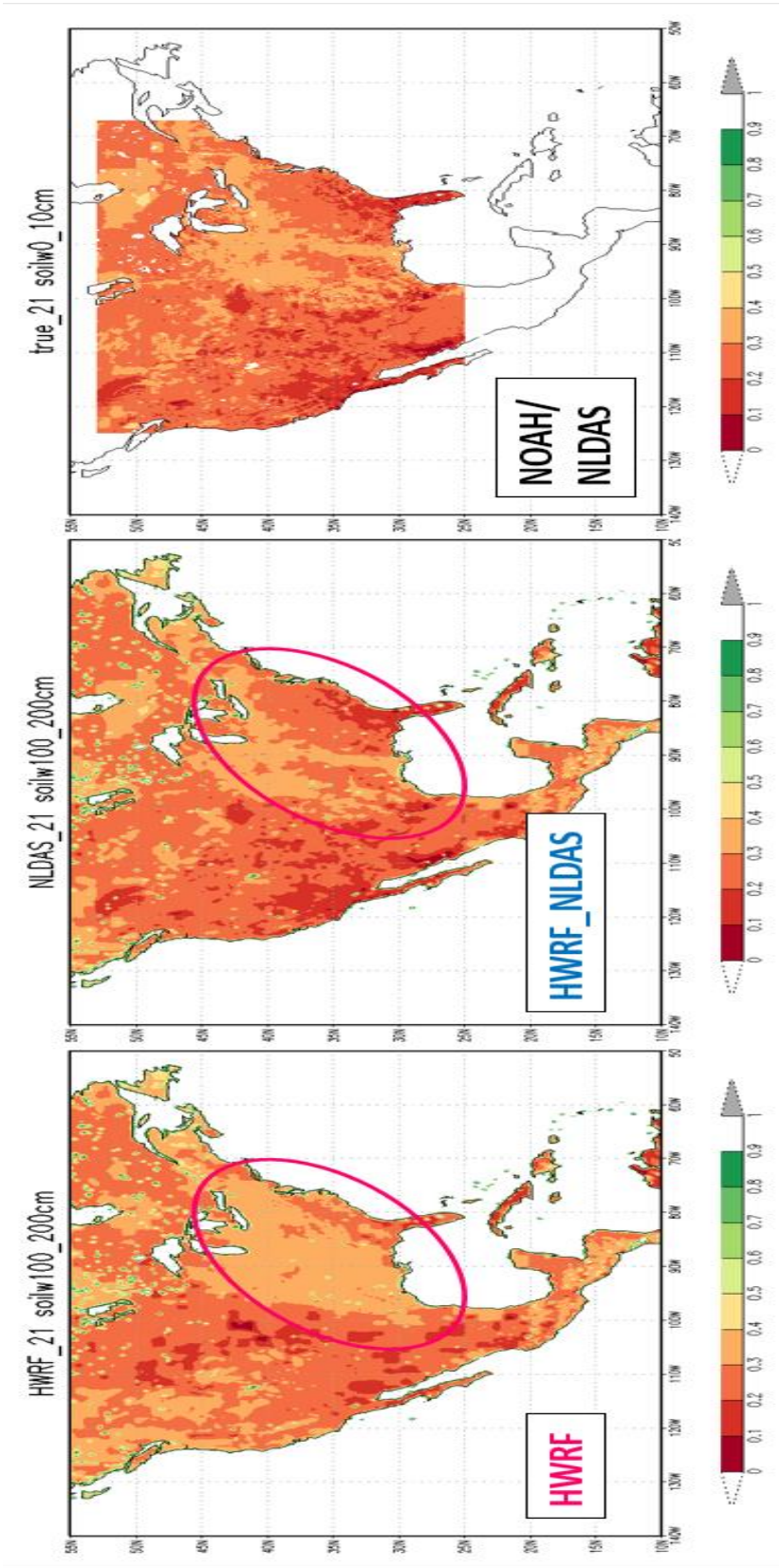

Figure 7.6 Domain plot of HWRF deep layer (100-200 cm) soil moisture (m^3/ m^3) for HWRF, HWRF_NLDAS and NLDAS (true) datasets. The region of large moisture variability between the models is highlighted.

A 3-hourly plot for the first 12 hours of simulation for the Lower Mississippi Valley is given in Figure 7.7 and shows the evolution of streamflow values from HWRF and HWRF_NLDAS. The plots indicate over prediction of streamflow values in HWRF as expected due high deep layer soil moisture. By hour 9, HWRF run starts exhibiting high streamflow values in the lower delta region when compared to HWRF_NLDAS and NLDAS streamflow values due to saturated deep soil layer. A comparison plot for the entire CONUS grid for hour 0 and 23 is shown in Figure 7.8.

Point observations of streamflow from USGS were also compared with the model run results and a time series plot for one day is given for a few select sites in Texas and Oklahoma where flooding impacts due to TS Bill were significant (Figure 7.9). Results, again indicate that streamflow in of both HWRF and NLDAS were over predicted in most locations except Ganado, TX where HWRF_NLDAS values are comparable to observations. In all other locations, the streamflow model performance is poorly. This is likely due to errors in initial soil moisture that was provided to the HWRF models. The top soil moisture data for TS BILL was compared to point observations in chapter 6 and is reproduced here as Figure 7.10. The results indicate that both HWRF and LDAS (HWRF_NLDAS) performance was impacted by rainfall/ soil moisture saturation. The considerable differences in precipitation patterns (already discussed in chapter 6) lead to observe such negative results for streamflow comparison.

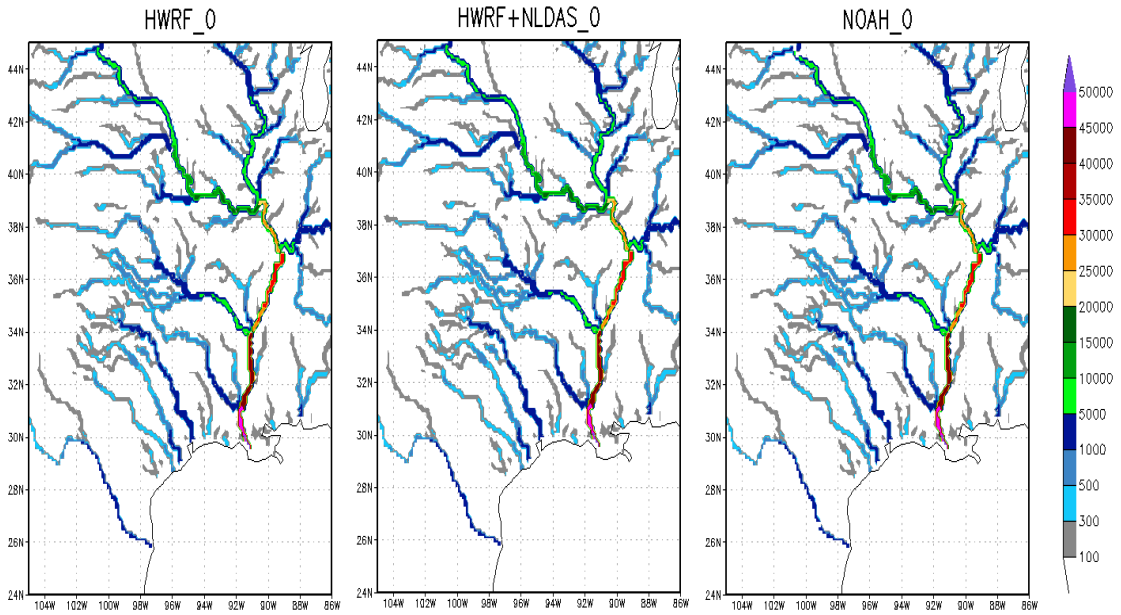

Figure 7.7 Streamflow plot at hour 0. Measured in m^3/s

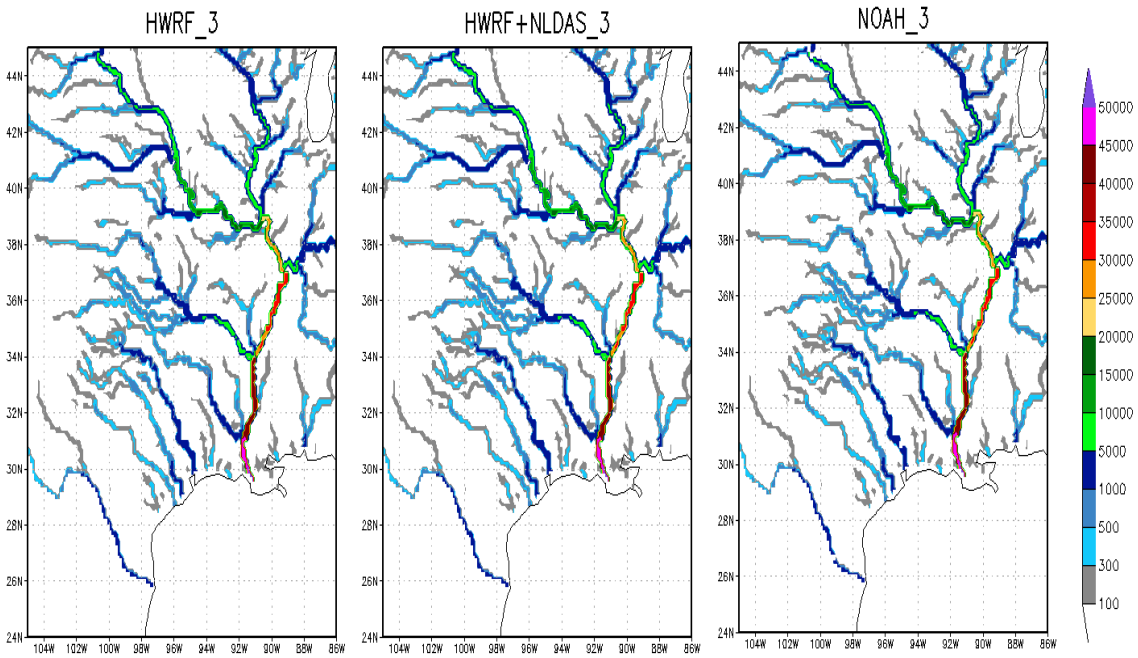

Figure 7.8 Streamflow plot at hour 3. Measured in m^3/s

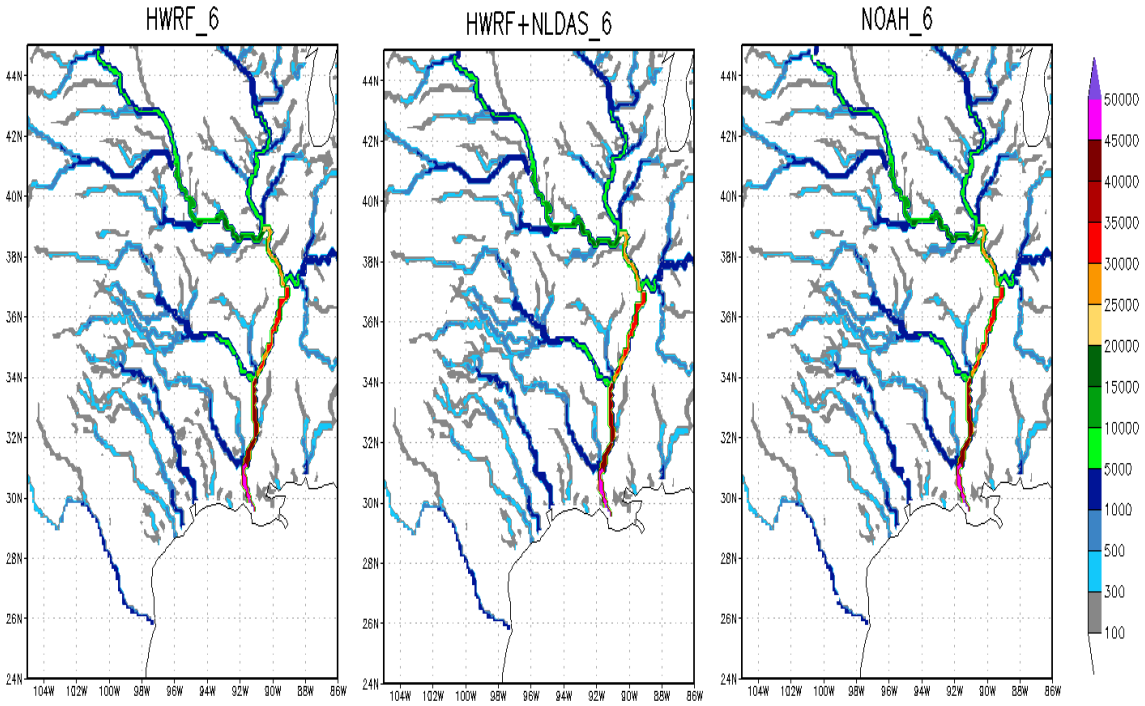

Figure 7.9 Streamflow plot at hour 6. Measured in m^3/s

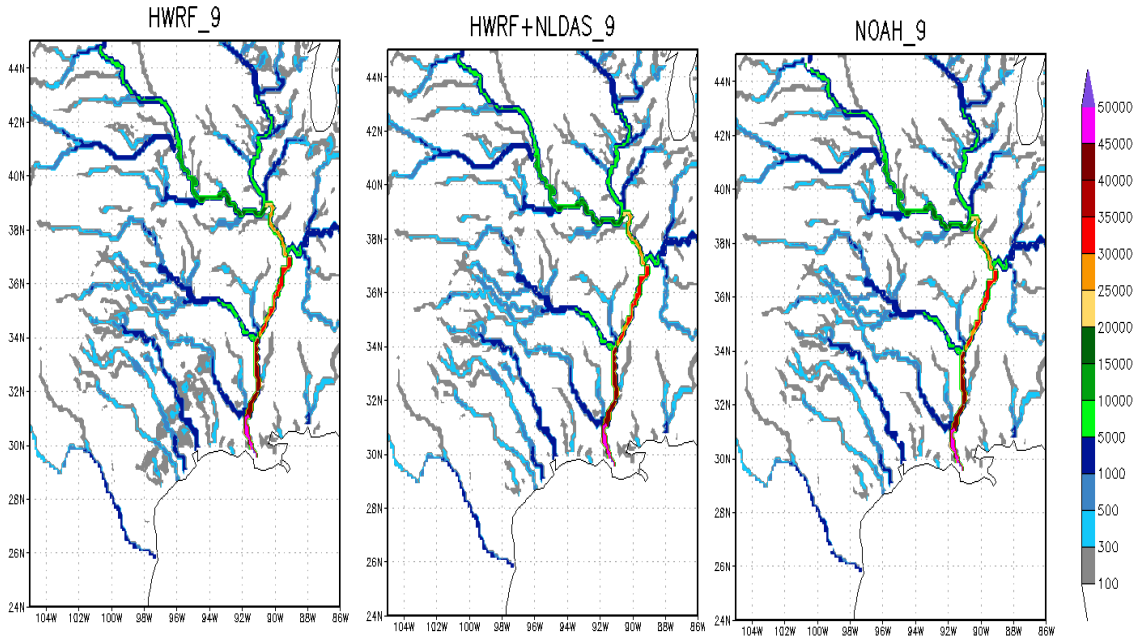

Figure 7.10 Streamflow plot at hour 9. Measured in m^3/s

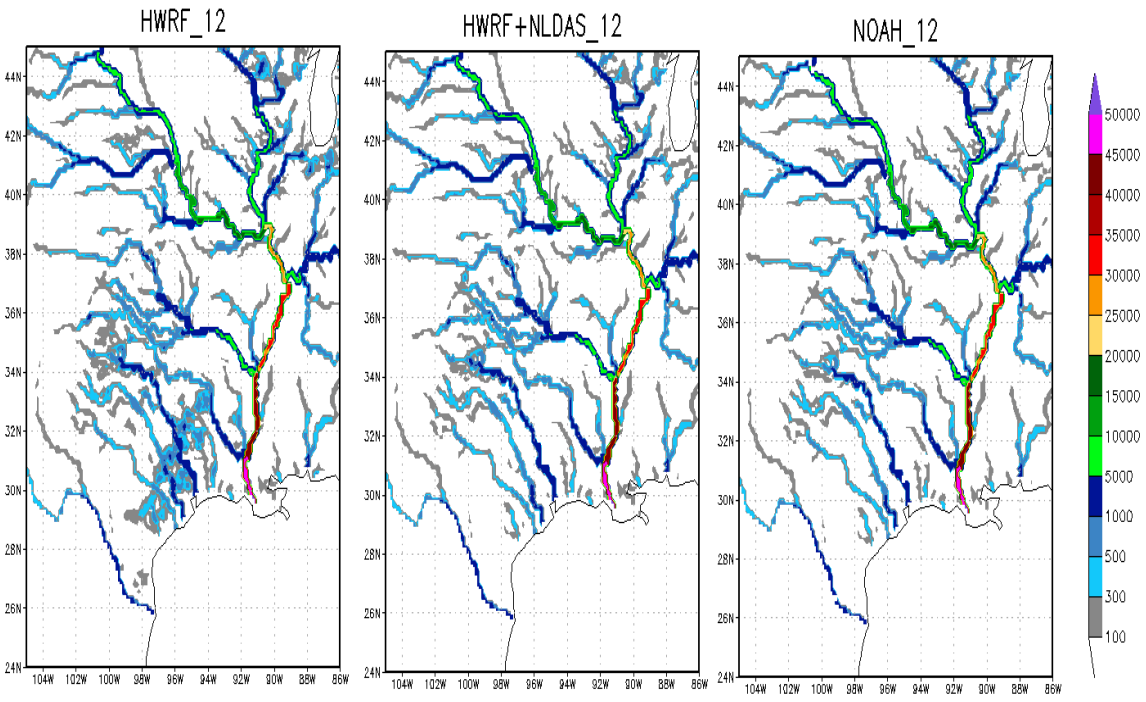

Figure 7.11 Streamflow plot at hour 12. Measured in m^3/s

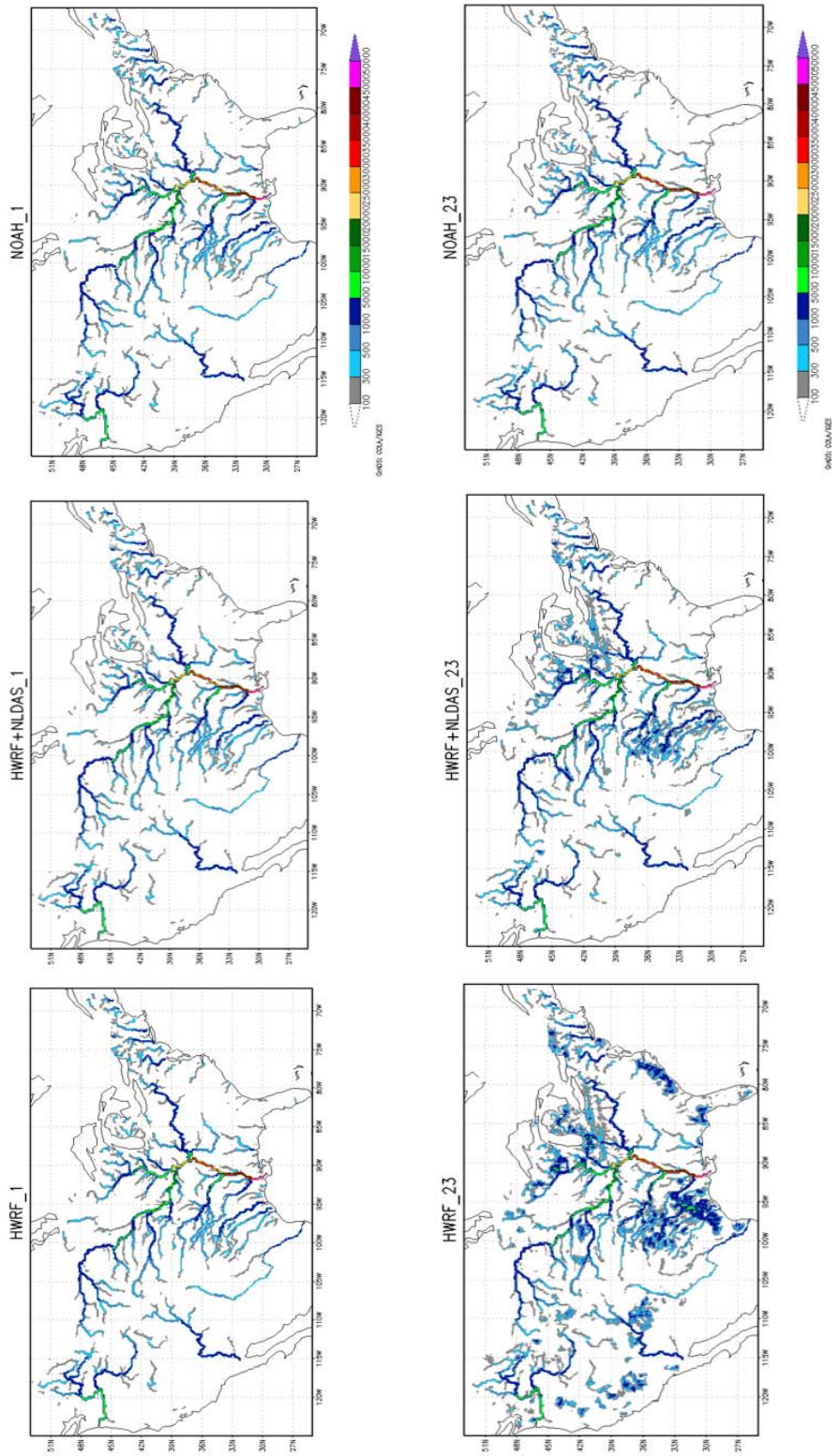

Figure 7.12 Full CONUS plot of streamflow (m^3/s) for HWRF and HWRF_NLDAS experiments and Noah (NLDAS) true dataset for the 1st hour and the 23rd hour of simulation.

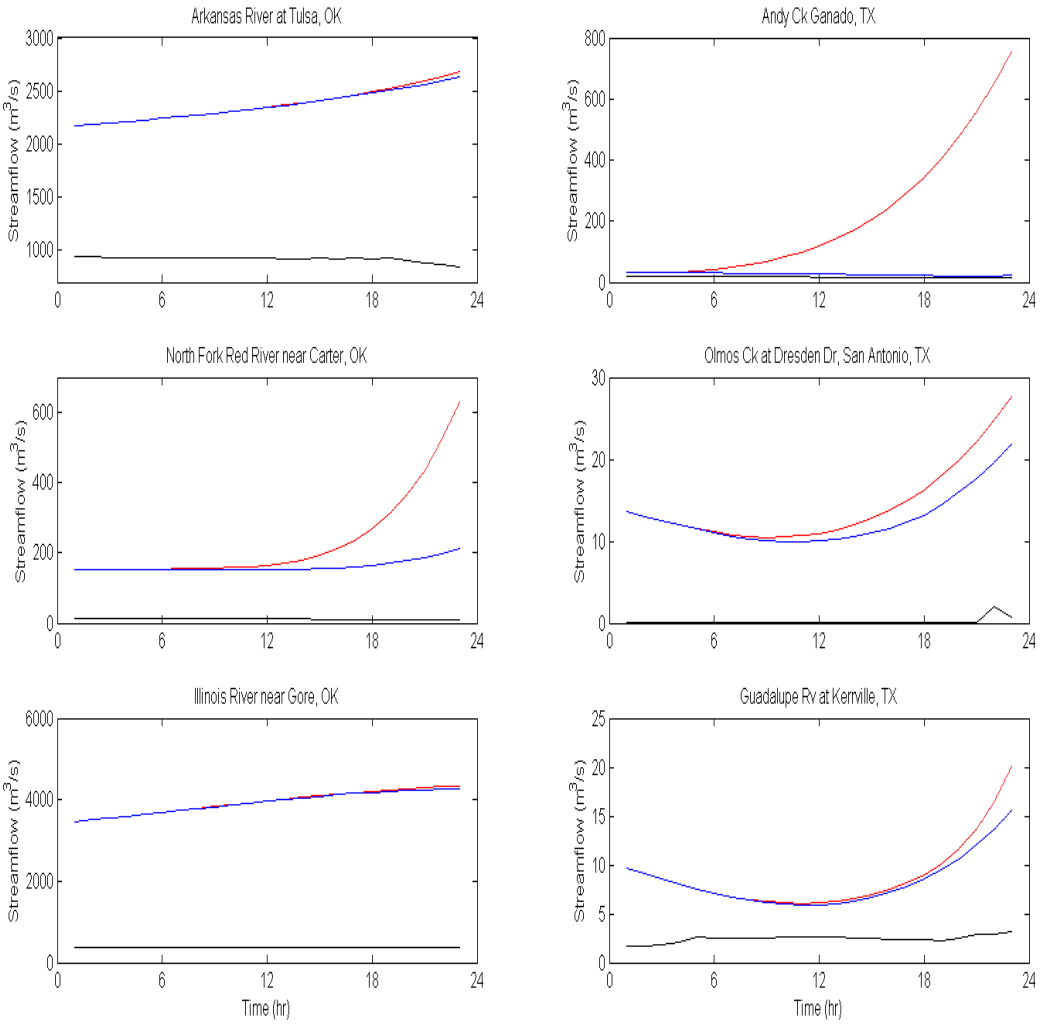

Figure 7.13 Time series plot for 24 hours for modeled streamflow (HWRF – red and HWRF_NLDAS – blue) against observations in black. All streamflow values are plotted with m^3/s unit.

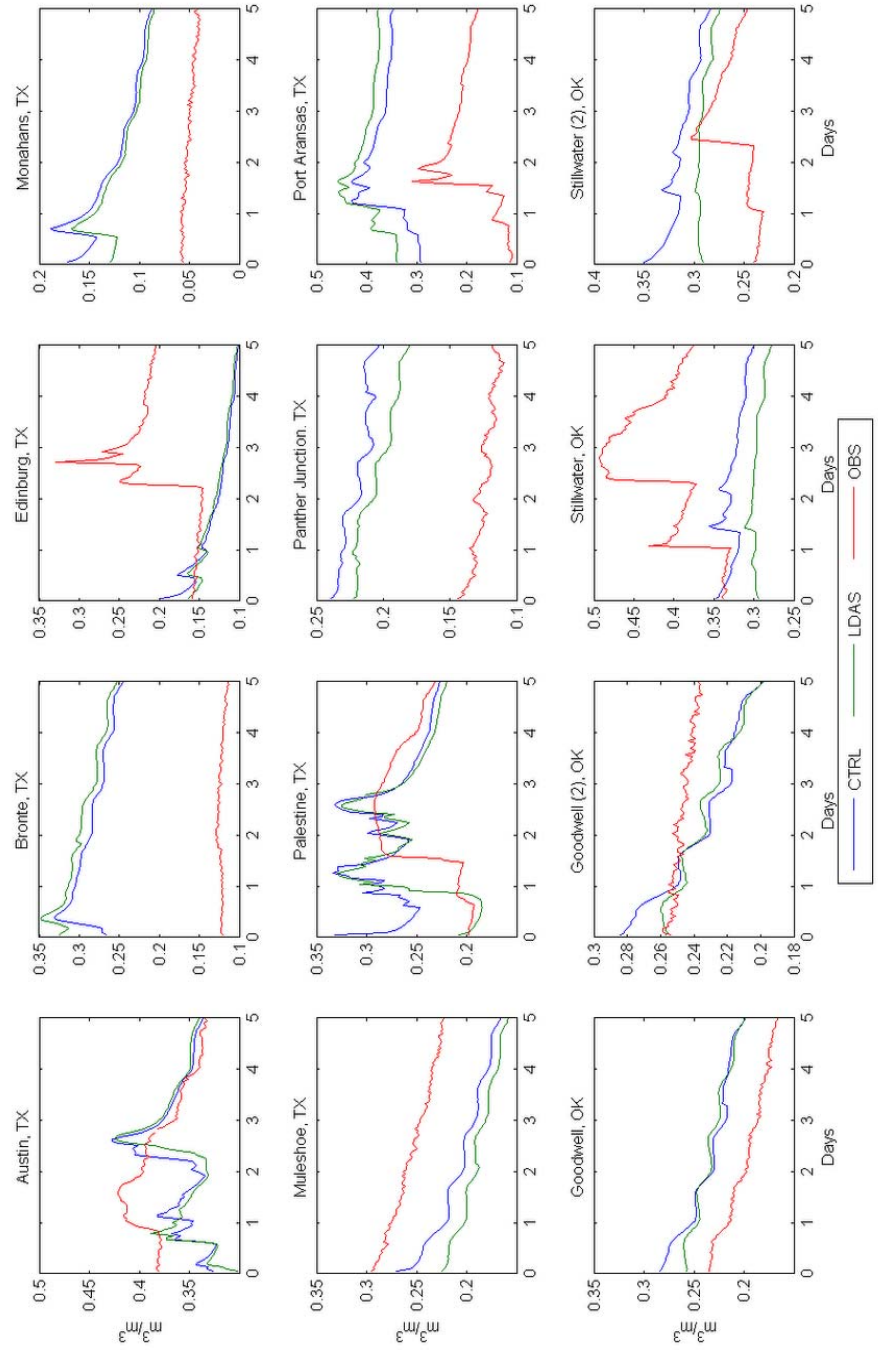

Figure 7.14 Time series plot of top soil moisture (0-10cm) in m^3/m^3 for HWRF cycle 2015061600 and experiment values are plotted against in-situ observations.

7.5 Discussion

Many severe weather phenomena are associated with high rainfall that leads to coastal and inland flooding. The enhancements being made in the modeling system via coupling of land models shows potential for improving rainfall simulations. In this chapter, the further capability of making usable products that can be used by the research and educational community to develop inundation and flood threat model, provide adequate information and forecast to the emergency planning and mitigation teams is highlighted. The incorporation of Noah LSM in HWRF creates the framework for a TC landfall coupled streamflow model output with HWRF. The current coupled model does need major calibration as large errors exists in modeling streamflow due to HWRF dependent interactive representations of land surface states and rainfall. The uncertainties in the land surface fields used to initialize HWRF also translate in the outcome. Though the streamflow predictions are still not realistic and have errors when compared to observations, the output and result highlights the capability and importance of LSMs and the coupled feedback between land surface, boundary layer, modeled precipitation and surface hydrological feedbacks

7.6 References

Chen, F., and Coauthors, 2007: Description and evaluation of the characteristics of the NCAR high-resolution land data assimilation system. *Journal of applied Meteorology and Climatology*, **46,** 694-713.

Ek, M., and Coauthors, 2003: Implementation of Noah land surface model advances in the National Centers for Environmental Prediction operational mesoscale Eta model. *Journal of Geophysical Research: Atmospheres*, **108**.

Lohmann, D., and Coauthors, 1998: The Project for Intercomparison of Land-surface Parameterization Schemes (PILPS) phase 2 (c) Red–Arkansas River basin experiment:: 3. Spatial and temporal analysis of water fluxes. *Global and Planetary Change*, **19,** 161-179.

——, 2004: Streamflow and water balance intercomparisons of four land surface models in the North American Land Data Assimilation System project. *Journal of Geophysical Research: Atmospheres*, **109**.

Marks, F. D., and L. K. Shay, 1998: Landfalling tropical cyclones: Forecast problems and associated research opportunities. *Bulletin of the American Meteorological Society*, **79,** 305-323.

Rappaport, E. N., 2014: Fatalities in the United States from Atlantic tropical cyclones: New data and interpretation. *Bulletin of the American Meteorological Society*, **95,** 341-346.

Rappaport, E. N., and Coauthors, 2009: Advances and challenges at the National Hurricane Center. *Weather and Forecasting*, **24,** 395-419.

CHAPTER 8. SYNTHESIS

8.1 Key Points

This dissertation was not a traditional one in the sense that work and projects that enabled these chapters were not confined to the research community realm only. It involved extensive interaction and working with the operational community and testing of operational hurricane models, development of code modules to improve understanding the physical processes involved in the evolution of TCs post landfall and enabling application such as a coupled streamflow model to improve flood predictions for the community. It was highly collaborative, mindful of operational community needs and lofty in its goals to understand the role of land surface processes and LSMs in TC predictions.

The role of antecedent land surface conditions was analyzed in an idealized framework and it was found that surface temperature fields could be an important factor contributing to storm's intensity over land if favorable synoptic environment exists to support a cyclone. An enthalpy analysis was conducted to identify pathways that enabled a thermodynamic assessment. The results highlight that high surface temperatures provide enough surface heat fluxes to the storm interacting with sufficient radial inflow along with increased low level convergence and divergence atop. A real case analysis was also undertaken with TS Erin that exhibited re-intensification over land and results are

identical to that obtained using the idealized framework. In conclusion, soil temperature, followed by soil texture, soil moisture, surface roughness and orographic features are identified as primary variable critical to evaluate the role of land surface on TCs. As a means to conduct such a study, a landfalling capability in HWRF idealized framework was developed. This capability as a product from this work has been added to Developmental Testbed Center code repository for community assimilation.

Most of TC studies in the past have dealt with hurricane studies over the open seas and broadly concentrated on improving track and intensity. The primary goal of TC operational community has been to accurately predict genesis, track, intensification processes and structural analysis to close the gap between observed and modeled cyclones. In the last decade, studies to improve track and intensity and achieving high accuracy, the focus has shifted to related problems such as rainfall, evolution of TCs over land and hurricane induced tornadoes. With increasing hurricane damage being caused due to storm surge or inland rainfall, the interest continues to address these topics. One of such efforts is the Research 2 Operations NOAA/ NSF Visiting Scientist Program that enabled work with the operational community and the transition of knowledge both ways. During this project, major effort was undertaken to successfully transition HWRF from using GFDL Slab land model to an updated and advanced Noah LSM. Extensive tests and calibrations was undertaken to make the HWRF model stable and able to deliver accurate surface temperature values that are critical to improve surface flux calculations. In addition to this, efforts were undertaken to deliver a precipitation analysis. It was shown that improved representation of land surface process and initial conditions would

improve prediction of convective processes. Results show a need to improve by calibrating across different verification regions and calibration and correction of convective schemes in the model. In the current framework, the track and intensity predictions did not show significant difference between the land models considered. This is likely due to multiple reasons. As the first aspect it needs to be highlighted that when introducing a new land model, the expectation is to be able to come close to the default scheme, not exceed the scheme's performance. This is because the model has many parameters and couplings which are often tuned and calibrated to the default.

i. The atmospheric model is potentially designed to be less sensitive to the lower boundary that is land surface and the model is so tuned that differences in land surface conditions are ignored in favor of large scale dynamics.

ii. Increased complexity reduces system's ability to be tuned. Though formulations in Noah are more representative of realistic feedbacks, it also brings with it a number of current uncertainties (prediction of multi-layer soil moisture, soil temperature etc.) can dampen the initial gains of a more realistic land model until further calibration is done.

iii. The role of initial conditions in a meso scale model is critical. Since, numerical weather prediction problems are initial value problems, the performance is dependent on the accuracy of the initial surface fields. The uncertainty/ errors in initial surface conditions are impacted surface energy balance that affects boundary layer evolution, stability of the atmosphere. Cloud and convective processes are critically linked to surface conditions.

iv. The lack of accurate gridded observation datasets to verify, test and tune land models to improve simulations of land surface conditions has led to a situation where models perform well only in certain regions whose data is used to calibrate the model.

The R2O opportunity offered a unique opportunity to learn, hypothesize and implement necessary parameterizations to improve simulation of land surface in HWRF models. The transition to Noah land model in HWRF followed community thrusts to improve hydrology and precipitation forecasts. The first step for which was to evaluate the current performance of HWRF to predict rainfall spatially, temporally and quantitatively. The second step was to identify potential to use the hydrology products in an application to help improve flood and inundation models. Thus, efforts were undertaken to couple a river routing model with HWRF to improve nowcast of streamflow predictions. This work also highlighted the importance of accurate representation of land surface as streamflow modeling depends on antecedent soil moisture, soil temperature conditions across soil layers in addition to topography, land use, vegetation and soil maps. The importance of streamflow modeling has become doubly important for landfalling storms responsible for both coastal and inland flooding. This dissertation lays emphasis on initialization and prediction of soil temperature, soil types and land use, soil moisture and land surface roughness and in that order to accurately simulate tropical cyclones and related hydrometeorological forecasts for effective disaster management and increased resiliency for communities affected by tropical cyclones.

8.2 Limitations

All studies are not without limitations, especially when dealing with a weather phenomenon that has not yet been fully understood.

i. The principal limitation of this study is the use of a single modeling tool – HWRF. Ensemble studies would have resulted in significant time delays to learn, run other models and normalize the results from each of them to test the principal hypothesis of land affecting TC evolution.

ii. Numerical modeling study is always limited by computational resources available and this study was no different. Currently, all experiments are run at the operational configuration's grid resolution at 18/6/2 km. At finer resolutions, TCs may exhibit higher sensitivities to land surface due to increased coupling between the land and the atmosphere. Computational resources were also a serious consideration when deciding to frame the study topic to involve only the atmospheric component of the HWRF system. Running the HWRF model with data assimilation and the coupled ocean model would have resulted in huge time delays and use of large computational time blocks and a thus a trade-off was made to run only the atmospheric component.

iii. It was a steep learning curve to work with the operational version of HWRF and all experiments described in this dissertation has used the latest HWRF community code. Care needed to be taken to keep abreast of model enhancements and translating those model developments into improved performance in cyclone simulations. Thus, many experiments were run and rerun with the latest model to keep up with operational research centers such as NCEP and HRD and be aligned

to their research priorities as well was a balancing act and took up considerable time and effort but also resulted in significant learning.

iv. Land surface studies are intimately tied together with surface layer formulation and this dissertation was limited to using the choices that was available within the operational HWRF framework. The dependencies on surface exchange coefficients and other land surface parameterizations might be a limiting factor in either exaggerating or damping/ muting the effect of land surface on TCs.

v. The absence of field campaign data for TCs continue to be a limiting factor. Such datasets for land surface will be a treasure trove when studying the coupled feedbacks between the land and cyclone. The theories and results of this dissertation should be revisited and tested when such surface data becomes available.

vi. Land surface heterogeneity impact, aerosol impact and topography effects have not been studied in this dissertation but could have huge impacts on TC evolution and its energetics. Heterogeneity in land surface can create convergence zones that may affect the precipitation. Aerosol have been known to impact the genesis of tropical cyclones over the Atlantic Ocean and the contribution of increased aerosol concentration over land may affect condensation in clouds and thus rainbands in tropical cyclones. It is one topic that warrants a comprehensive analysis.

vii. The absence of gridded land surface observations of the likes of precipitation datasets was a considerable limitation to the study. The quality of point land surface data sets was also hard to identify to analyze model results. Observation

data access issues and the unavailability of enough atmospheric and land surface data in the Indian Monsoon Region (IMR) led to change in focus region from IMR to the north Atlantic Basin.

viii. The importance and the effect of land surface on the weather phenomena depends on the region itself. While one region might show increased sensitivity to land surface conditions, another might now. All of the work in this dissertation except the idealized study was over the Atlantic Ocean basin and may or may not apply to other TC basins. This is an important caveat of the study.

Having listed these limitation, the emerging theme is within the constraints of TC cases, models, configurations, the optimal use of resources in a creative manner did lead to the development of new techniques, in creation of new tools, a rounded educational experience and more importantly a robust improvement in our understanding of the impact of land surface conditions on post landfall TC characteristics. It now allows the problem to be placed in a larger context that could be built upon and taken to the next level for broader impacts and implications for the community.

8.3 Future work

The study of land surface on TC is in a very nascent stage. Tremendous potential and opportunities exist to improve TC simulations and associated rainfall along with proving accurate hydrology predictions for catastrophe modeling. Continuing on this work, an observational analysis of landfalling storms that re-intensify emerges to be important and relevant in the larger scheme of things. A preliminary analysis has been conducted and

the Great Desert in Australia emerges to be a hotspot for re-intensifying cyclones. This may be due to anomalously dry and warm surface conditions that aid re-intensification under specific circumstances as outlined in Chapter 4. In addition to land surface impacts on TCs post landfall, impact of landfall approaching cyclones should be analyzed. Dry and warm land masses are known to produce dry air intrusion that disrupt organized convection of TC and impede development. The alternate hypothesis of whether moist land surfaces produces synoptic scale circulations that air in rapid development of cyclones remains to be tested. As land cover and land use change become increasingly important and increased urban foot print near the coastal regions, the effect of large cities on TCs and vice versa is a topic of interest that merits future studies. An initial literature review of the impact of LCLUC on rainfall characteristics over South East Asia is also part of this dissertation and is available in the Appendix section. When does city become important and at what city size would affect tropical cyclones emerges to be an important focus for studies in the future. As large amounts of satellite datasets and gridded land surface datasets become available, machine learning techniques could be applied to intuitively understand the closed and evolving feedbacks between land, atmosphere and TCs.

APPENDICES

Appendix A Secondary Circulation

Sawyer-Eliassen Framework for Secondary Circulation

The Sawyer-Eliassen non-linear balance framework enables us to analytically describe the structure of secondary circulation as a function of the structure of the TC and its environment. Furthermore, it also enables us to describe how this circulation evolved to the imposition of external heat (e.g., latent heat release) or momentum (e.g., trough interaction) forcing. In the following, we derive this equation from first principles of the atmosphere in a radial coordinate system.

The heat forcing is given by a prescribed heating Q. The momentum forcing is given by a prescribed momentum source (or sink) F. Both Q and F can take any desired from; however, in most analytical studies of the TCs. We will consider several structures for both Q and F when considering solutions to the Sawyer-Eliassen diagnostic equation. We introduce the governing equation. These are the governing equations represented in a two-dimensional (z, r) cylindrical coordinate system. In this regard, we view the secondary circulation as an axisymmetric feature. The governing equations are as follows–

$$m^2 = r^3 \frac{\partial \phi}{\partial r} \quad \ldots(A1)$$

$$\frac{dm^2}{dt} = F \quad \ldots(A2)$$

$$\frac{\partial \Phi}{\partial z} = \frac{g}{\theta_0}\theta \quad \ldots(A3)$$

$$\frac{1}{r}\frac{\partial}{\partial r}(ru) + \frac{\partial w}{\partial z} = 0 \quad \ldots(A4)$$

$$\frac{\partial \theta}{\partial t} = Q \quad \ldots(A5)$$

$$\Phi = \phi + \frac{f^2 r^2}{8} \quad \ldots(A6)$$

$$z = \left[1 - \left(\frac{\rho}{\rho_0}\right)^K\right]\frac{c_p \theta_0}{g} \quad \ldots(A7)$$

$$\frac{1}{r^3}\frac{\partial m^2}{\partial z} = \frac{g}{\theta_0}\frac{\partial \theta}{\partial r} \quad \ldots(A8)$$

Equation (A1) reflects gradient wind balance. Recalling that angular momentum is a function of the tangential wind v, equation (A2) is thus a generic form of the tangential momentum equation. Equation (A3) is the hydrostatic equation. Equation (A4) is the flux form of the continuity equation. Equation (A5) is the thermodynamic equation representing prescribed heating; i.e., this heating is diabatic in nature, and potential temperature does not change following the flow in the absence of this heating. Equation (A6) is the definition of the geopotential. Equation (A7) defines the pseudo height vertical coordinate, used to simplify the mathematics of the system and interpretation thereof. The exponent K is equal to R_d/c_p. Finally, equation (A8) is the thermal wind

relationship in this coordinate system, relating the vertical wind shear to horizontal temperature gradients. Except as described above, all variables have their standard meaning. Subscripts 0 denote base-state values.

First, expand the total derivatives in (A2) and (A5) to obtain:

$$\frac{\partial m^2}{\partial t} + u\frac{\partial m^2}{\partial r} + w\frac{\partial m^2}{\partial z} = F \qquad \ldots(A9)$$

$$\frac{\partial \theta}{\partial t} + u\frac{\partial \theta}{\partial r} + \frac{\partial \theta}{\partial w} = Q \qquad \ldots(A10)$$

Taking the partial derivative of (A9) with respect to z and multiply the results by $1/r^3$:

$$\frac{\partial}{\partial t}\left(\frac{1}{r^3}\frac{\partial m^2}{\partial z}\right) + \frac{\partial}{\partial z}\left(u\frac{1}{r^3}\frac{\partial m^2}{\partial r} + w\frac{1}{r^3}\frac{\partial m^2}{\partial z}\right) = \frac{1}{r^3}\frac{\partial F}{\partial z} \qquad \ldots(A11)$$

Similarly, taking the partial derivative of (A10) with respect to r and multiply the result by g/θ_0:

$$\frac{\partial}{\partial t}\left(\frac{g}{\theta_0}\frac{\partial \theta}{\partial r}\right) + \frac{\partial}{\partial r}\left(u\frac{g}{\theta_0}\frac{\partial \theta}{\partial r} + w\frac{g}{\theta_0}\frac{\partial \theta}{\partial z}\right) = \frac{g}{\theta_0}\frac{\partial Q}{\partial r} \qquad \ldots(A12)$$

Note that in obtaining (A11) and (A12), the partial derivatives with respect to time have been commuted with the partial derivatives with respect to z and r, respectively. Defining additional terms as:

$$N^2 = \frac{g}{\theta_0}\frac{\partial \theta}{\partial z} \qquad \ldots(A13)$$

$$B = -\frac{g}{\theta_0}\frac{\partial \theta}{\partial r} = -\frac{1}{r^3}\frac{\partial m^2}{\partial z} \qquad \ldots(A14)$$

$$I = \frac{1}{r^3}\frac{\partial m^2}{\partial r} = \left(f + \frac{1}{r}\frac{\partial (rv)}{\partial r}\right)\left(f + \frac{2v}{r}\right) \quad \ldots(A15)$$

Equation (A13) defines the static stability. Equation (A14) defines baroclinicity. Equation (A15) defines the inertial stability. Applying these definitions to (A11) and (A12), we get

$$\frac{\partial}{\partial t}(-B) + \frac{\partial}{\partial z}(Iu - Bw) = \frac{1}{r^3}\frac{\partial F}{\partial z} \quad \ldots(A16)$$

$$\frac{\partial}{\partial t}(-B) + \frac{\partial}{\partial r}(-Bu + N^2 w) = \frac{g}{\theta_0}\frac{\partial Q}{\partial r} \quad \ldots(A17)$$

Subtracting (A16) from (A17), we get

$$\frac{\partial}{\partial r}(N^2 w - Bu) + \frac{\partial}{\partial z}(Bw - Iu) = \frac{g}{\theta_0}\frac{\partial Q}{\partial r} - \frac{1}{r^3}\frac{\partial F}{\partial z} \quad \ldots(A18)$$

Equation (A18) describes the response in the zonal and vertical motion fields to imposed heat and/ or momentum forcing. However, as there are two unlinked unknowns given by u and w, this equation is difficult to solve. To link these two variables and thus make solving the diagnostic equation simpler, the definition of the stream function is used. The definition of the stream function in this coordinate system is given by

$$u = -\frac{\partial \psi}{\partial z}; w = \frac{1}{r}\left(\frac{\partial (r\psi)}{\partial r}\right) \quad \ldots(A19)$$

Substituting (A19) into (A18) results in the following

$$\frac{\partial}{\partial r}\left(N^2 \frac{1}{r}\left(\frac{\partial (r\psi)}{\partial r}\right) + B\frac{\partial \psi}{\partial z}\right) + \frac{\partial}{\partial z}\left(B\frac{1}{r}\left(\frac{\partial (r\psi)}{\partial r}\right) + I\frac{\partial \psi}{\partial z}\right) \quad \ldots(A20)$$

$$= \frac{g}{\theta_0}\frac{\partial Q}{\partial r} - \frac{1}{r^3}\frac{\partial F}{\partial z}$$

Equation (A20) is the Sawyer-Eliassen nonlinear secondary circulation diagnostic equation. It highlights the relationship between the specified heating Q, momentum forcing F, and the stream function ψ as modulated by coefficients representing static stability, inertial stability and baroclinicity. The stream function attempts to restore the thermal wind balance that the specified heating and/ or momentum forcing destroys. While thermal wind balance restoration is never truly achieved, the concept of balance destruction and restoration nevertheless enable us to consider how radial and vertical motions (i.e., the strengthen of the secondary circulation) are impacted by prescribed heating and/ or momentum forcing.

Appendix B Idealized Framework in HWRF with Landfalling Capability

Land surface definition

Land surface in the idealized framework is prescribed through a namelist file *"land.nml"*. The contents of the namelist file can be changed depending upon the need of the experiment

The namelist file references both vegparm.tbl and soilparm.tbl that characterizes the land surface in HWRF model. Both the contents of the table are given below.

Namelist file: land.nml

```
&init_land
mvland = .true.                 !true=land or false=only ocean
imin = 260                      !setup the land strip for motion
imax = 288
jmin = 0
jmax = 576
logic_temp = .false.            !true=initial surface temperature thru s_temp. false=default (first level tmp)
s_temp = 308.0                  !initial surface temperature for the land strip
VEG_ID = 19                     !land surface vegetaion parameter ID. refer VEGPARM.TBL
SOIL_ID = 1                     !land surface soil parameter ID. refer SOILPARM.TBL
/

&param_land
DIRN = 1                        !1=W-E direction, 2=E-W direction
VEG_ID = 19                     !same as above. Has to be set. Do not leave it blank
SOIL_ID = 1                     !same as above. Has to be set. Do not leave it blank
land_emiss = 0.90               !emissivity for radiation phys. Refer VEGPARM.TBL for indicative values (0-1)
land_albedo = 0.25              !albedo for radiation physics. Refer VEGPARM.TBL for indicative values (0-1)
land_vgfrac = 0.20              !vegetation fraction (0-0.99)
land_z0 = 0.01                  !surface roughness. Refer VEGPARM.TBL
land_smc = 0.02                 !soil moisture. Refer SOILPARM.TBL
/
```

VEGPARM.TBL

```
Vegetation Parameters
MODIFIED_IGBP_MODIS_NOAH
20,1, 'SHDFAC NROOT   RS      RGL      HS      SNUP  MAXALB   LAIMIN  LAIMAX   EMISSMIN EMISSMAX ALBEDOMIN ALBEDOMAX   Z0MIN    Z0MAX'
1       .70,   4,    125.,    30.,   47.35,   0.08,    52.,    5.00,   6.40,   .950,    .950,     .12,      .12,      .50,     .50,
2,      .95,   4,    150.,    30.,   41.69,   0.08,    35.,    3.08,   6.48,   .950,    .950,     .12,      .12,      .50,     .50,
3,      .70,   4,    150.,    30.,   47.35,   0.08,    54.,    1.00,   5.16,   .930,    .940,     .14,      .15,      .50,     .50,
4,      .80,   4,    100.,    30.,   54.53,   0.08,    58.,    1.85,   3.31,   .930,    .930,     .16,      .17,      .50,     .50,
5,      .80,   4,    125.,    30.,   51.93,   0.08,    53.,    2.80,   5.50,   .930,    .970,     .17,      .25,      .20,     .50,
6,      .70,   3,    300.,   100.,   42.00,   0.03,    60.,    0.50,   3.66,   .930,    .930,     .25,      .30,      .01,     .05,
7,      .70,   3,    170.,   100.,   39.18,  0.035,    65.,    0.60,   2.60,   .930,    .950,     .22,      .30,      .01,     .06,
8,      .70,   3,    300.,   100.,   42.00,   0.03,    60.,    0.50,   3.66,   .930,    .930,     .25,      .30,      .01,     .05,
9,      .50,   3,     70.,    65.,   54.53,   0.04,    50.,    0.50,   3.66,   .920,    .920,     .20,      .20,      .15,     .15,
10,     .80,   3,     40.,   100.,   36.35,   0.04,    70.,    0.52,   2.90,   .920,    .960,     .19,      .23,      .10,     .12,
11      .60,   2,     70.,    65.,   55.97   0.015     59.,    1.75,   5.72,   .950,    .950,     .14,      .14,      .30,     .30,
12,     .80,   3,     40.,   100.,   36.25,   0.04,    66.,    1.56,   5.68,   .920,    .985,     .17,      .23,      .05,     .15,
13,     .10,   1,    200.,   999.,   999.0,   0.04,    46.,    1.00,   1.00,   .880,    .880,     .15,      .15,      .50,     .50,
14      .80,   3,     40.,   100.,   36.25,   0.04,    68.,    2.29,   4.29,   .920,    .980,     .18,      .23,      .05,     .14,
15,     .00,   1,    999.,   999.,   999.0,   0.02,    82.,    0.01,   0.01,   .950,    .950,     .55,      .70,     0.001,   0.001,
16,     .01,   1,    999.,   999.,   999.0,   0.02,    75.,    0.10,   0.75,   .900,    .900,     .38,      .38,      .01,     .01,
17,     .00,   0,    100.,    30.,   51.75,   0.01,    70.,    0.01,   0.01,   .980,    .980,     .08,      .08,     0.0001,  0.0001,
18,     .60,   3,    150.,   100.,   42.00,  0.025,    55.,    0.41,   3.35,   .930,    .930,     .15,      .20,      .30,     .30,
19,     .60,   3,    150.,   100.,   42.00,  0.025,    60.,    0.41,   3.35,   .920,    .920,     .15,      .20,      .15,     .15,
20,     .30,   2,    200.,   100.,   42.00,   0.02,    75.,    0.41,   3.35,   .900,    .900,     .25,      .25,      .05,     .10,
```

SOILPARM.TBL

```
Soil Parameters
STAS
19,1   'BB      DRYSMC      F11     MAXSMC   REFSMC   SATPSI  SATDK       SATDW     WLTSMC  QTZ    '
1,     2.79,    0.010,    -0.472,   0.339,   0.236,   0.069,  1.07E-6,  0.608E-6,   0.010,  0.92, 'SAND'
2,     4.26,    0.028,    -1.044,   0.421,   0.383,   0.036,  1.41E-5,  0.514E-5,   0.028,  0.82, 'LOAMY SAND'
3,     4.74,    0.047,    -0.569,   0.434,   0.383,   0.141,  5.23E-6,  0.805E-5,   0.047,  0.60, 'SANDY LOAM'
4,     5.33,    0.084,     0.162,   0.476,   0.360,   0.759,  2.81E-6,  0.239E-4,   0.084,  0.25, 'SILT LOAM'
5,     5.33,    0.084,     0.162,   0.476,   0.383,   0.759,  2.81E-6,  0.239E-4,   0.084,  0.10, 'SILT'
6,     5.25,    0.066,    -0.327,   0.439,   0.329,   0.355,  3.38E-6,  0.143E-4,   0.066,  0.40, 'LOAM'
7,     6.66,    0.067,    -1.491,   0.404,   0.314,   0.135,  4.45E-6,  0.990E-5,   0.067,  0.60, 'SANDY CLAY LOAM'
8,     8.72,    0.120,    -1.118,   0.464,   0.387,   0.617,  2.04E-6,  0.237E-4,   0.120,  0.10, 'SILTY CLAY LOAM'
9,     8.17,    0.103,    -1.297,   0.465,   0.382,   0.263,  2.45E-6,  0.113E-4,   0.103,  0.35, 'CLAY LOAM'
10,   10.73,    0.100,    -3.209,   0.406,   0.338,   0.098,  7.22E-6,  0.187E-4,   0.100,  0.52, 'SANDY CLAY'
11,   10.39,    0.126,    -1.916,   0.468,   0.404,   0.324,  1.34E-6,  0.964E-5,   0.126,  0.10, 'SILTY CLAY'
12,   11.55,    0.138,    -2.138,   0.468,   0.412,   0.468,  9.74E-7,  0.112E-4,   0.138,  0.25, 'CLAY'
13,    5.25,    0.066,    -0.327,   0.439,   0.329,   0.355,  3.38E-6,  0.143E-4,   0.066,  0.05, 'ORGANIC MATERIAL'
14,     0.0,      0.0,       0.0,     1.0,     0.0,     0.0,      0.0,       0.0,      0.0,  0.60, 'WATER'
15,    2.79,    0.006,    -1.111,    0.20,    0.17,   0.069,  1.41E-4,  0.136E-3,   0.006,  0.07, 'BEDROCK'
16,    4.26,    0.028,    -1.044,   0.421,   0.283,   0.036,  1.41E-5,  0.514E-5,   0.028,  0.25, 'OTHER(land-ice)'
17,   11.55,    0.030,   -10.472,   0.468,   0.454,   0.468,  9.74E-7,  0.112E-4,   0.030,  0.60, 'PLAYA'
18,    2.79,    0.006,    -0.472,   0.200,    0.17,   0.069,  1.41E-4,  0.136E-3,   0.006,  0.52, 'LAVA'
19,    2.79,     0.01,    -0.472,   0.339,   0.236,   0.069,  1.07E-6,  0.608E-6,    0.01,  0.92, 'WHITE SAND'
```

Code block changes

1. module_initialize_tropical_cyclone.F

This module is used to initialize the domain. Depending upon values from the namelist *"land.nml"*, this module initializes the ocean and the land. The surface temperature is applied based on whether the user has chosen first level air temperature or a temperature value given by the user.

```
!!BEGIN: LSM changes for LANDFALL: Subashini 7/27/2016
 INTEGER                         :: imin,jmin,imax,jmax,proceed,VEG_ID,SOIL_ID
 LOGICAL                         :: mvland, logic_temp
 REAL                           :: s_temp
 NAMELIST / init_land /imin,jmin,imax,jmax,proceed,VEG_ID,SOIL_ID,mvland,logic_temp,s_temp
!! END: LSM changes for LANDFALL : Subashini 7/27/2016
```

```
!
!  SET UP IDEAL CONDITIONS
!
!!BEGIN: LSM changes for LANDFALL: Subashini 7/27/2016

   open (7,FILE='land.nml')
   read (UNIT=7, NML=init_land)
   close (UNIT=7)

   do l = 1,num_veg_cat
    do j = jts, MIN(jte,jde-1)
     do i = its, MIN(ite,ide-1)
!      create land patch that will move from W2E
       if(mvland .and. (i .ge. imin .and. i .le. imax .and. j .ge. jmin .and. j.le. jmax))then
         if(l==VEG_ID)THEN
            landusef_out(i,j,l)=1              ! barren land
         else
            landusef_out(i,j,l)=0
         endif
       else                    ! original ocean world
         if(l==16)THEN
           landusef_out(i,j,l)=1     ! create ocean elsewhere
         else
           landusef_out(i,j,l)=0
         endif
       endif
     enddo
    enddo
   enddo
```

```
   do l = 1,num_soil_top_cat
    do j = jts, MIN(jte,jde-1)
     do i = its, MIN(ite,ide-1)
!      create land patch that will move from W2E
       if(mvland .and. (i .ge. imin .and. i .le. imax .and. j .ge. jmin .and. j.le. jmax))then
         if(l==SOIL_ID)THEN
          soilctop_out(i,j,l)=1      ! sandy soil
         else
          soilctop_out(i,j,l)=0
         endif
       else                          ! original ocean world
         if(l==14)THEN
           soilctop_out(i,j,l)=1     ! create ocean everywhere
         else
           soilctop_out(i,j,l)=0
         endif
       endif
     enddo
    enddo
   enddo

  do l = 1,num_soil_bot_cat
    do j = jts, MIN(jte,jde-1)
     do i = its, MIN(ite,ide-1)
!      create land patch that will move from W2E
       if(mvland .and. (i .ge. imin .and. i .le. imax .and. j .ge. jmin .and. j.le. jmax))then
         if(l==SOIL_ID)THEN
           soilcbot_out(i,j,l)=1      ! sandy soil
         else
           soilcbot_out(i,j,l)=0
         endif
       else                          ! original ocean world
         if(l==14)THEN
           soilcbot_out(i,j,l)=1      ! create ocean everywhere
         else
           soilcbot_out(i,j,l)=0
         endif
       endif
     enddo
    enddo
   enddo
```

```
   landusef_gc=landusef_out      !=landusef_gc
   soilcbot_gc=soilcbot_out     !=soilcbot_gc
   soilctop_gc=soilctop_out     !=soilctop_gc

   do j = jts, MIN(jte,jde-1)
    do i = its, MIN(ite,ide-1)
     xice_gc(i,j)=0.
     ht_gc(i,j)=0.                    ! uniform terrain
     ght_gc(i,j,1)=0.                 ! uniform gpm at level 1
!    create land patch that will move from W2E
     if(mvland .and. (i .ge. imin .and. i .le. imax .and. j .ge. jmin .and.j.le. jmax)) then
      if(logic_temp .eq. .true.) then
      tsk_gc(i,j)=s_temp              ! uniform land temperature or first level temperature
      else
      tsk_gc(i,j)= t_gc(i,j,1)
      endif
     else
      tsk_gc(i,j)=302.0               ! uniform SSTs
     endif
    enddo
   enddo

!! END: LSM changes for LANDFALL: Subashini 7/27/2016
```

module_BNDRY_COND.F

This module is used to update the domain boundaries with the varying/ moving sea mask variable and is given in the next page.

```
!!BEGIN: LSM changes for LANDFALL: Subashini 7/27/2016
#ifdef IDEAL_NMM_TC
    REAL,DIMENSION(IMS:IME,1,SPEC_BDY_WIDTH)                    &
   &                    ,INTENT(INOUT) :: SM_BYS, SM_BYE      &
   &                                    ,SM_BTYS,SM_BTYE
    REAL,DIMENSION(JMS:JME,1,SPEC_BDY_WIDTH)                    &
   &                    ,INTENT(INOUT) :: SM_BXS, SM_BXE      &
   &                                    ,SM_BTXS,SM_BTXE
    REAL,DIMENSION(IMS:IME,JMS:JME),INTENT(INOUT) :: SM,TH
#endif
!!END: LSM changes for LANDFALL : Subashini 7/27/2016
...
...
       DO J=MAX(JTS-1,JDS+3-1),MIN(JTE+1,JDE-2)
        IF(MOD(J,2)==1)THEN
         PD_BXS(J,1,IB)=PD_BXS(J,1,IB)+PD_BTXS(J,1,IB)*DT
         PD(II,J)=PD_BXS(J,1,IB)
!!BEGIN: LSM changes for LANDFALL: Subashini 7/27/2016
#ifdef IDEAL_NMM_TC
         IF(GRIDID.GT.1)THEN
          SM(II,J)=SM_BXS(J,1,IB)   ! for W-E motion
         ENDIF
#endif
!!END: LSM changes for LANDFALL : Subashini 7/27/2016
        ENDIF
       ENDDO
...
...
       DO J=MAX(JTS-1,JDS+3-1),MIN(JTE+1,JDE-2)
        IF(MOD(J,2)==1)THEN
         PD_BXE(J,1,IB)=PD_BXE(J,1,IB)+PD_BTXE(J,1,IB)*DT
         PD(II,J)=PD_BXE(J,1,IB)
!!BEGIN: LSM changes for LANDFALL: Subashini 7/27/2016
#ifdef IDEAL_NMM_TC
         IF(GRIDID.GT.1)THEN
          SM(II,J)=SM_BXE(J,1,IB)    ! for E-W motion
         ENDIF
#endif
!!END: LSM changes for LANDFALL : Subashini 7/27/2016
        ENDIF
       ENDDO
```

```
!***  ONE ROW EAST OF WESTERN BOUNDARY
!
    IF(W_BDY)THEN
     DO J=4,JM-3,2
!
       IF(W_BDY.AND.J>=MY_JS_GLB-JBPAD1                    &
    &          .AND.J<=MY_JE_GLB+JTPAD1)THEN
         CWK=PD(1,J)
         JJ=J
         PD(1,JJ)=0.25*(PD(1,JJ-1)+PD(2,JJ-1)+PD(1,JJ+1)+PD(2,JJ+1))
...
...

!!BEGIN: LSM changes for LANDFALL: Subashini 7/27/2016
#ifdef IDEAL_NMM_TC
        IF(GRIDID.GT.1)THEN
         SM(1,JJ)=0.5*(SM(1,JJ-1)+SM(1,JJ+1))  ! updates only along W Boundary
!         TH(IIM-1,JJ)=0.5*(TH(IIM,JJ-1)+TH(IIM,JJ+1))
        ENDIF
#endif
!!END: LSM changes for LANDFALL : Subashini 7/27/2016
!
!***  NESTING TEST
!
         IF(ABS(CWK-PD(1,JJ))>300.)THEN
          WRITE(message,*)'PSEUDO HYDROSTATIC IMBALANCE AT THE WESTERN BOUNDARY
AT',1,JJ,'GRID #',GRIDID
          CALL wrf_message(trim(message))
          WRITE(message,*)'          ',CWK/100.
          CALL wrf_message(trim(message))
          WRITE(message,*)PD(1,JJ+1)/100.,'          ',PD(2,JJ+1)/100.
          CALL wrf_message(trim(message))
          WRITE(message,*)'          ',PD(1,JJ)/100.
          CALL wrf_message(trim(message))
          WRITE(message,*)PD(1,JJ-1)/100.,'          ',PD(2,JJ-1)/100.
          CALL wrf_message(trim(message))
          CALL wrf_message('  ')
         ENDIF

       ENDIF
!
     ENDDO
    ENDIF
```

```
!***  ONE ROW WEST OF EASTERN BOUNDARY
!
    IF(E_BDY)THEN
      DO J=4,JM-3,2
!
        IF(E_BDY.AND.J>=MY_JS_GLB-JBPAD1                    &
   &          .AND.J<=MY_JE_GLB+JTPAD1)THEN
          CWK=PD(IIM-1,J)
          JJ=J
          PD(IIM-1,JJ)=0.25*(PD(IIM-1,JJ-1)+PD(IIM,JJ-1)          &
   &                    +PD(IIM-1,JJ+1)+PD(IIM,JJ+1))
...
...
!!BEGIN: LSM changes for LANDFALL: Subashini 7/27/2016
#ifdef IDEAL_NMM_TC
        IF(GRIDID.GT.1)THEN
          SM(IIM-1,JJ)=0.5*(SM(IIM,JJ-1)+SM(IIM,JJ+1))  ! updates only along E Boundary
!         TH(IIM-1,JJ)=0.5*(TH(IIM,JJ-1)+TH(IIM,JJ+1))
        ENDIF
#endif
!!END: LSM changes for LANDFALL : Subashini 7/27/2016
!
!***  NESTING TEST
!
          IF(ABS(CWK-PD(IIM-1,JJ))>300.)THEN
           WRITE(message,*)'PSEUDO HYDROSTATIC IMBALANCE AT THE EASTERN BOUNDARY AT',IIM-
1,JJ,'GRID #',GRIDID
           CALL wrf_message(trim(message))
           WRITE(message,*)'          ',CWK/100.
           CALL wrf_message(trim(message))
           WRITE(message,*)PD(IIM-1,JJ+1)/100.,'          ',PD(IIM,JJ+1)/100.
           CALL wrf_message(trim(message))
           WRITE(message,*)'          ',PD(IIM-1,JJ)/100.
           CALL wrf_message(trim(message))
           WRITE(message,*)PD(IIM-1,JJ-1)/100.,'          ',PD(IIM,JJ-1)/100.
           CALL wrf_message(trim(message))
           CALL wrf_message('   ')
          ENDIF

        ENDIF
!
      ENDDO
    ENDIF
!
!-----------------------------------------------------------------------
```

solve_nmm.F

This is the solver module where from all the physics within the HWRF model is called. It also called another user defined function to move the sea mask variable after each time step to realize movement of land underneath the cyclone vortex.

```
!!BEGIN: LSM changes for LANDFALL: Subashini 7/27/2016
     integer :: move_land_time, SOIL_ID, VEG_ID, DIRN
     real :: land_albedo, land_emiss, land_vgfrac, land_smc, land_z0
     NAMELIST/param_land/SOIL_ID, VEG_ID, DIRN, land_albedo, land_emiss, land_vgfrac,
land_smc,land_z0
!! END: LSM changes for LANDFALL : Subashini 7/27/2016
..
..
!!BEGIN: LSM changes for LANDFALL: Subashini 7/27/2016
#ifdef IDEAL_NMM_TC

    IF(grid%NTSD==0 .and. grid%id .gt. 1)THEN  ! Initialize some variables
        call wrf_debug(1,'NESTS INITIALIZED TO WATER WORLD')
        grid%sm=1.0    ! Initialize a water world in the nests
    ENDIF
    move_land_time=nint(1200./30) ! This needs to be changed for different parent domain
!resolution & dt.  Subashini V1.0 7.13.2016: Speed of land movement

    IF(MOD(grid%NTSD,move_land_time)==0)THEN    ! n_print_time

     call wrf_debug(1,'LAND ADVECTED W2E FOR IDEALIZED LSM')

#ifdef DM_PARALLEL
#    include "HALO_NMM_INIT_3.inc"
#endif
!open ideal_land.nml for namelist values

     open(8,FILE='land.nml')
     read(UNIT=8,NML=param_land)
     close(UNIT=8)

CALL MOVE_LAND (grid%SM, grid%NTSD,IDS,IDE,JDS,JDE,KDS,KDE, IMS,IME,JMS,JME,KMS,KME    &
                ,ITS,ITE,JTS,JTE,KTS,KTE,DIRN)

...
```

```
    IF(DIRN == 1) THEN
     DO J = JMS, JME
      DO I = IMS,IME
       if(grid%SM(I,J) .le. 0.5)then
        grid%nmm_tsk(I,J)=grid%nmm_tsk(I-1,J)
        grid%albedo(I,J)=land_albedo
        grid%epsr(I,J)=land_emiss
        grid%isltyp(I,J)=SOIL_ID
        grid%ivgtyp(I,J)=VEG_ID
        grid%vegfrc(I,J)=land_vgfrac
        grid%z0(I,J)=land_z0
        DO K = 1,grid%num_soil_layers
        grid%smc(I,K,J)=land_smc
        ENDDO
       endif
      ENDDO
     ENDDO
     ELSE IF(DIRN == 2) THEN
     DO J = JMS, JME
      DO I = IME,IMS, -1
       if(grid%SM(I,J) .le. 0.5)then
        grid%nmm_tsk(I,J)=grid%nmm_tsk(I+1,J)
        grid%albedo(I,J)=land_albedo
        grid%epsr(I,J)=land_emiss
        grid%isltyp(I,J)=SOIL_ID
        grid%ivgtyp(I,J)=VEG_ID
        grid%vegfrc(I,J)=land_vgfrac
        grid%z0(I,J)=land_z0
        DO K = 1,grid%num_soil_layers
        grid%smc(I,K,J)=land_smc
        ENDDO
       endif
      ENDDO
     ENDDO
    ELSE
    CALL wrf_error_fatal ('Choose between 1 or 2 in land.nml')
    ENDIF

    ENDIF

#endif
!!END: LSM changes for LANDFALL : Subashini 7/27/2016
```

module_NEST_UTIL.F

This module contains the function to move the land surface. This function *move_land()* is called from the solver.

```
!!BEGIN: LSM changes for LANDFALL: Subashini 7/27/2016
#ifdef IDEAL_NMM_TC
SUBROUTINE MOVE_LAND (SM,NTSD,IDS,IDE,JDS,JDE,KDS,KDE    &
              ,IMS,IME,JMS,JME,KMS,KME,ITS,ITE,JTS,JTE,KTS,KTE,DIRN)

    USE MODULE_MODEL_CONSTANTS
    USE MODULE_DM
    IMPLICIT NONE

!   global variables
    INTEGER,INTENT(IN)                          :: NTSD,DIRN
    INTEGER,INTENT(IN)                          :: IDS,IDE,JDS,JDE,KDS,KDE,IMS,IME,JMS,JME,KMS, &
                                                   KME,ITS,ITE,JTS,JTE,KTS,KTE, NTSD, DIRN
    REAL, DIMENSION(IMS:IME,JMS:JME),       INTENT(INOUT) :: SM

!   local variables

    INTEGER                                 :: I,J,K
!   Note: make appropriate changes for boundary condition updates in
!   d02 and d03 by adding "i01rhd=(DownNear)f=(BdyNear)" for SM in the
!   Registry.NMM_HWRF. Also module_BNDRY_COND.F needs to be updated
!   for SM. This is subashini's doing for advecting land surface in
!   idealized framework
!
   IF(DIRN == 1) THEN
    DO J = MAX(JTS,2), MIN(JTE,JDE-1)
     DO I = MIN(ITE,IDE),MAX(ITS,2),-1
       SM(I,J)=SM(I-1,J)        ! Motion of land (0) from West to East
     ENDDO
    ENDDO
   ELSE
    DO J = MAX(JTS,2), MIN(JTE,JDE-1)
     DO I = ITS, MIN(ITE,IDE-1)
       SM(I,J)=SM(I+1,J)        ! Motion of land (0) from East to west
     ENDDO
    ENDDO
   ENDIF
END SUBROUTINE MOVE_LAND
#endif
!!END: LSM changes for LANDFALL : Subashini 7/27/2016
!-----------------------------------------------------------------------
```

Registry.NMM

To update the status of the sea mask variable (SM), the registry entry for SM was modified in the Registry.NMM file. This ensures SM variable update across the entire model and across all domains.

```
state  real sm ijb dyn_nmm 1 - i01rhd=(DownNear)f=(BdyNear) "SM" "Sea mask;=1 for sea, =0 for land" ""
```

Appendix C Model Configuration Studies

Experiments with different models and different initial conditions were conducted in a test mode for the Indian Domain. These studies were done in an exploratory and investigative manner to develop a modeling framework for configuration, domain size, vortex initialization method and the modeling tool itself.

HWRF was eventually selected for the research topic for its robustness, superior vortex initialization procedures and the ability to accurately simulate cyclones.
It was also aided by the close collaboration with operational communities in NCEP and IMD and research partnership with HRD and ongoing research priorities of the hurricane community.

These experiments also helped in developing an expertise in the area of modeling TCs and important learnings were achieved through hand-on experience in running different models and working with different datasets.

These results are not a comprehensive analysis on the performance of TC models but are provided for the sake of completeness and to simply trace the evolution of this research work.

Comparing different Initial and Boundary Conditions for TC simulations over India using Advanced Hurricane WRF (AHW)

Results:

1. NCEP-FNL was found to be the better dataset of IC/BC with the least error for the Indian Ocean domain and for use with the AHW modeling system.

2. AHW had significant errors in predicting the cyclone track and intensity.

Five cyclones were studied: Cyclone Laila (2010), Cyclone Phet (2010), Gonu (2007), Phyan (2009), Nargis (2008), Sidr (2007), Jal (2007)

Three IC/BC data set were compared: NCEP-FNL, NASA MERRA, ERA-Interim

The Track plots are given in the Figure C.1.

Track forecast error was calculated based on error metrics depicted in Figure C.2.

The track forecast errors were calculated and plotted against time for each of the error parameters given in Figure C.3.

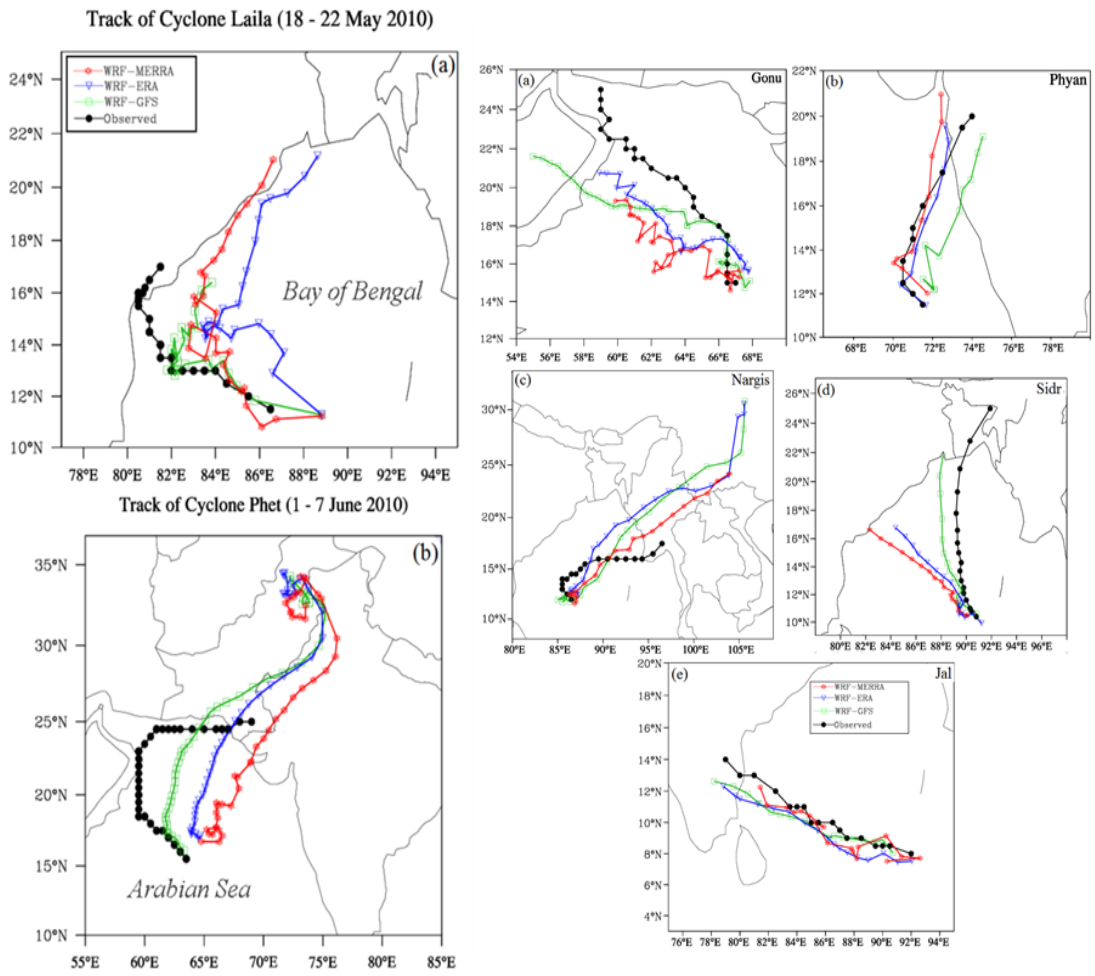

Figure C.1 Composite plots of TCs with different initial and boundary conditions

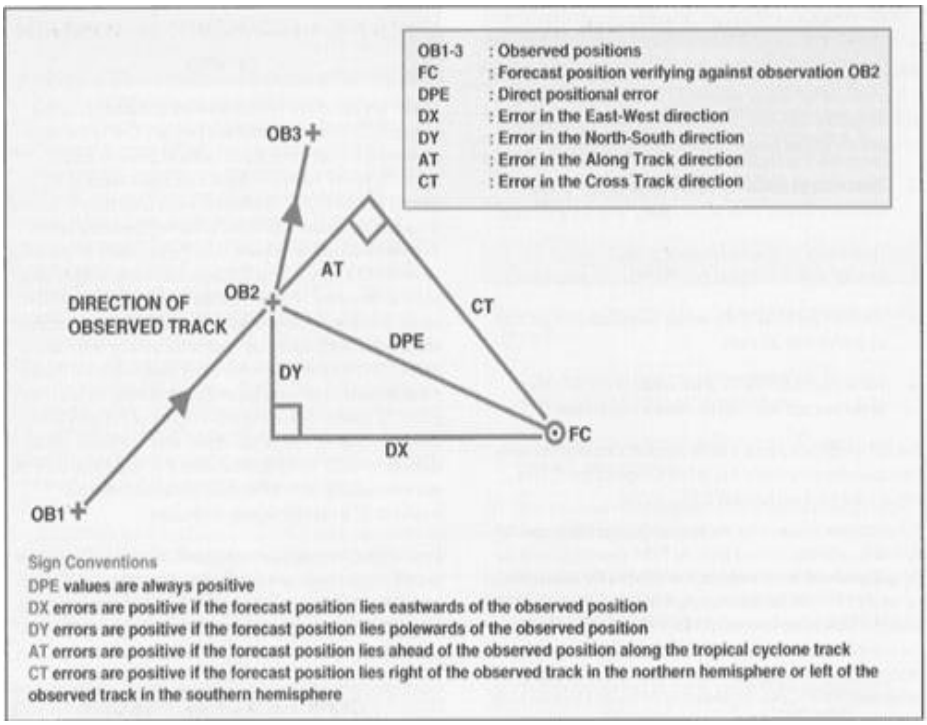

Figure C.8.1 Diagram depicting the calculation methodology of track error metrics (Source: http://www.metoffice.gov.uk/weather/tropicalcyclone/method)

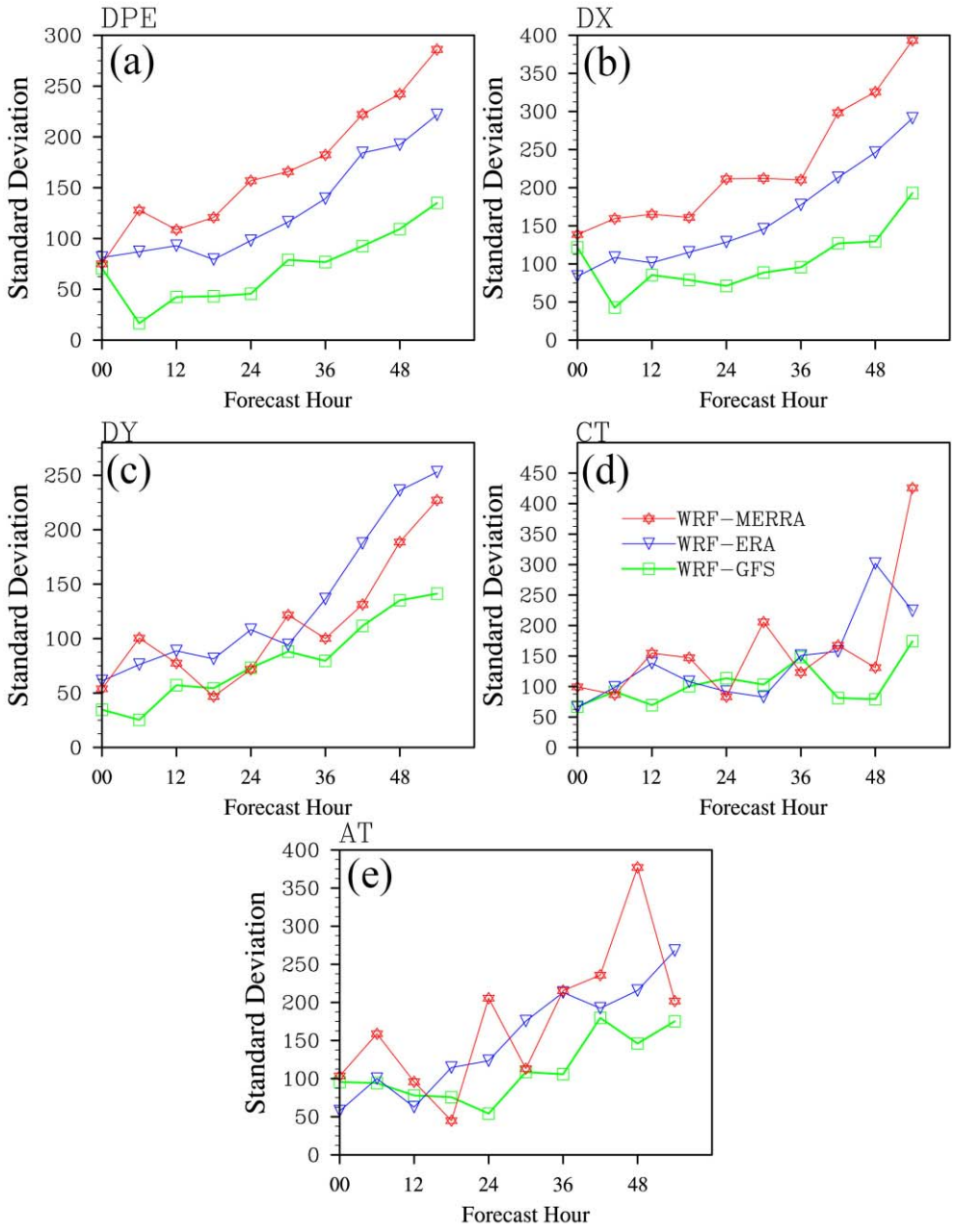

Figure C.8.2 (a) Standard deviation of Direct Positional Error (DPE) from the best track positions for a period of 54 hours, (b) standard deviation of DX errors from the best track positions, (c) standard deviation of DY errors from the best track positions, (d) standard deviation of CT errors from the best track positions, and (e) standard deviation of AT errors from the best track positions.

North Indian Ocean TC simulations using WRF-ARW model and NCEP-FNL IC/BC

Results:

1. Tracks were substantially different from the observed track.

2. The vortex initialization of TCs in ARW significantly under performed in estimating the intensity of the storm.

Following the previous study, NCEP-FNL was used to conduct the experiments for the following TCs with WRF-ARW –

Aila (2007), Jal (2007), Laila (2010), Nisha (2008), Phet (2010), Sidr (2007), Thane (2011).

Tracks for cyclones with GFDL Slab and Noah LSM were plotted and given in Figure C.4.

The track error metrics were calculated separately for Bay of Bengal and Arabian Sea domain and is given in Figure C.5 for BoB and AS.

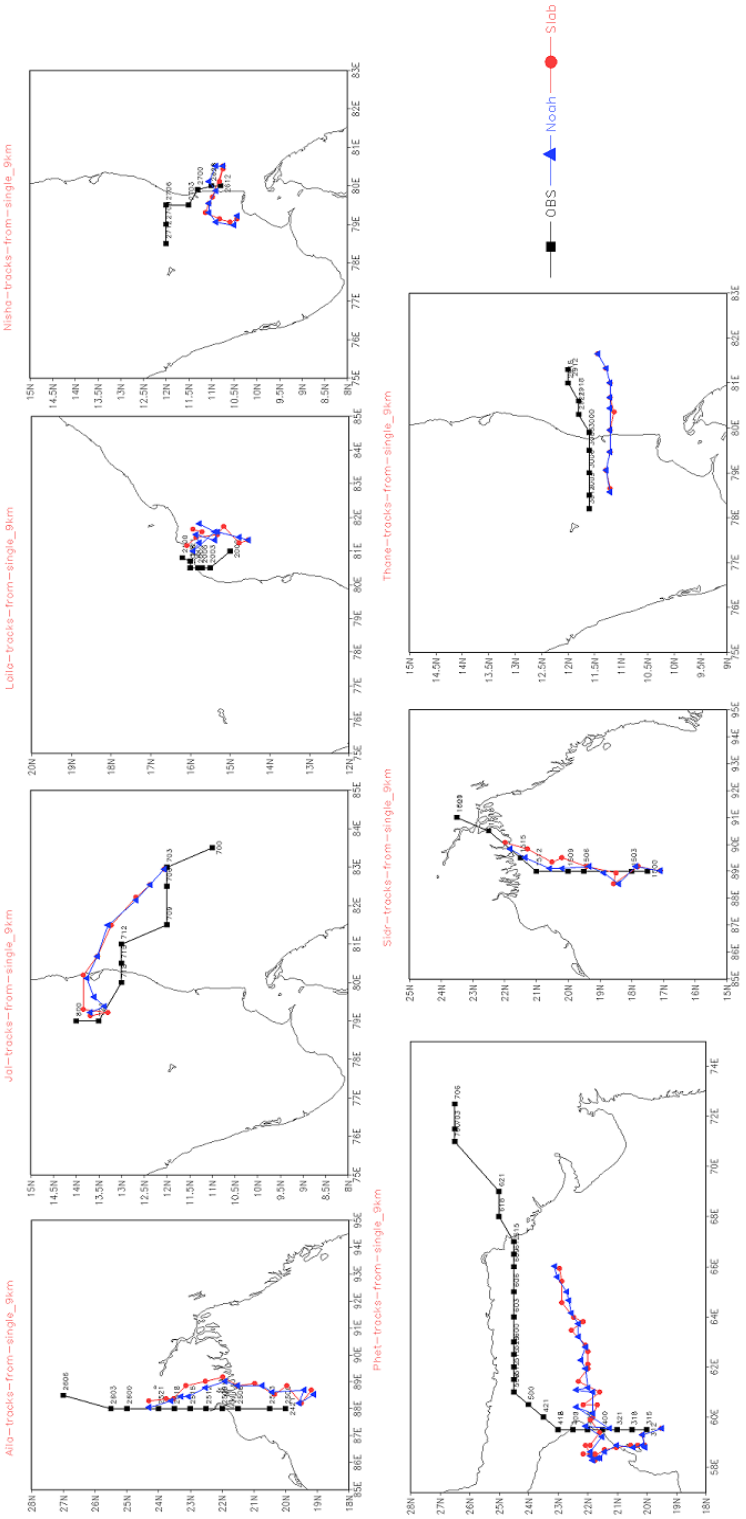

Figure C.8.3 Tracks of cyclone over the north Indian Ocean domain.

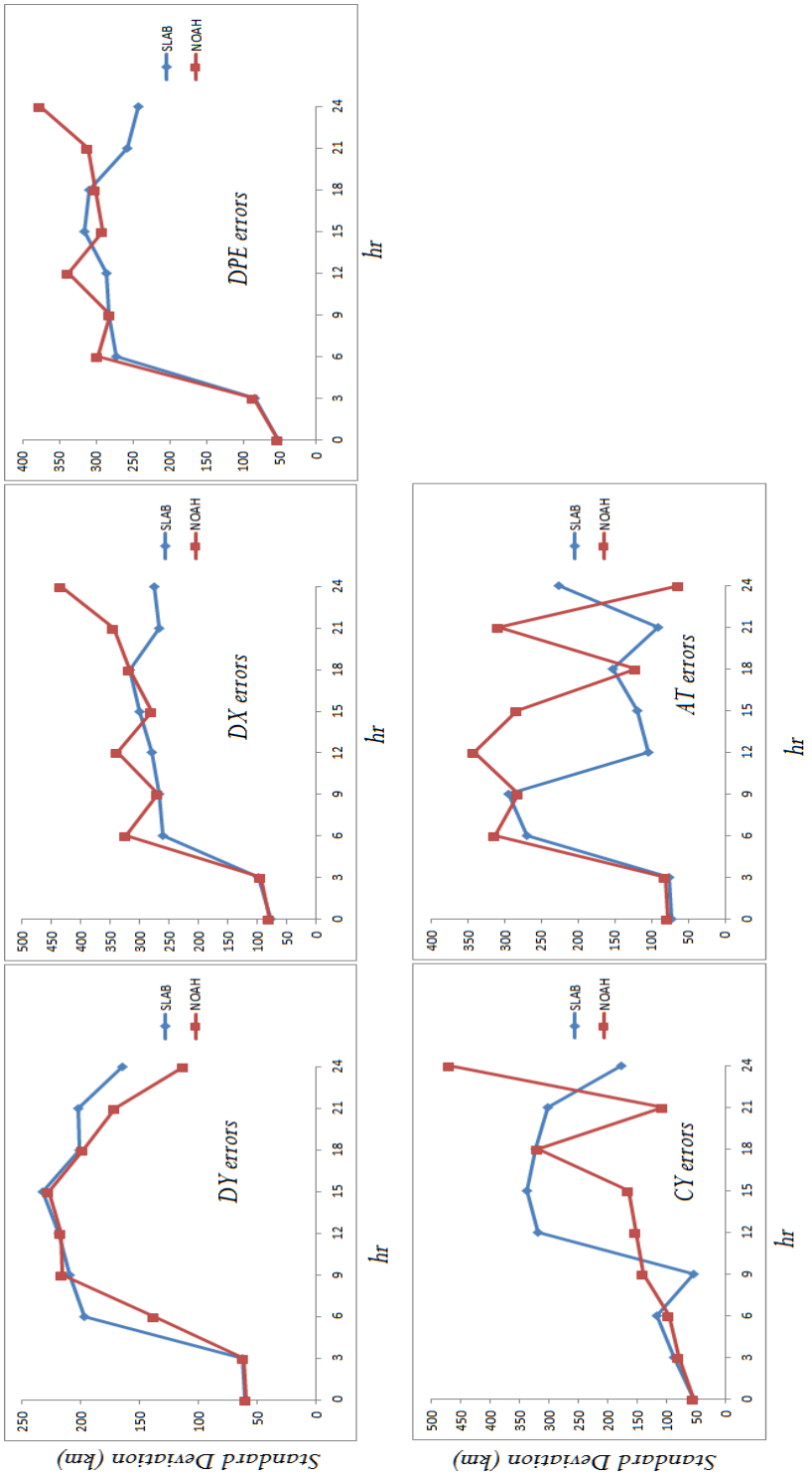

Figure C.8.4 Track error metrics for BoB domain

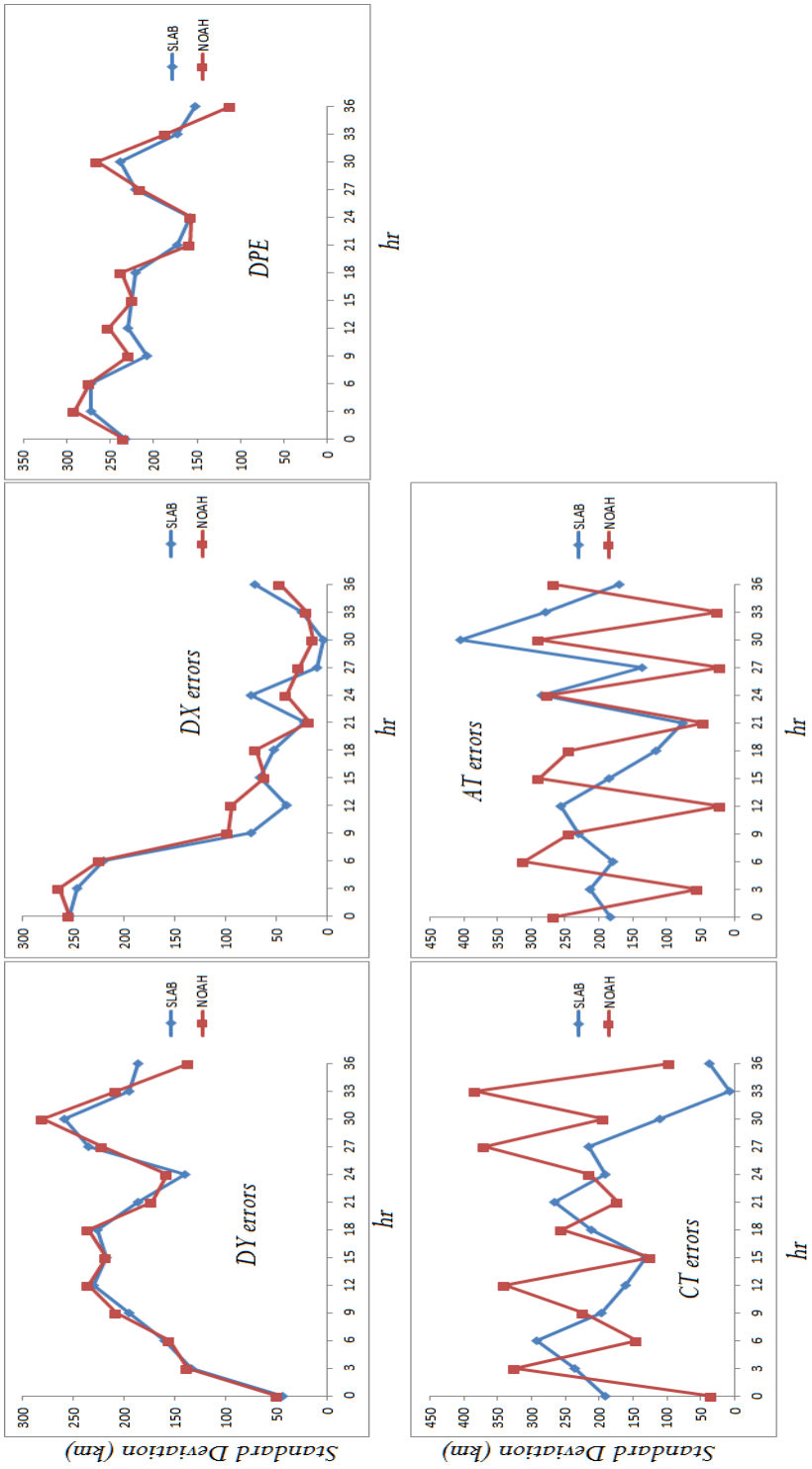

Figure C.6. Track error metrics for AS domain

Appendix D Perspectives on the Impact of Land Cover and Land Use Change on the Indian Monsoon Region Hydroclimate

D.1. Introduction

Almost a third of the population in southeast (SE) Asia, which includes India and China, are urban dwellers. This was not the case just a few decades back, and the region is experiencing one of the fastest land transformation globally. In China, for example, urban land cover has increased from 20 to 50% in last three decades. These LCLUC changes are unparalleled in the documented history of the region. As an example, Figure D.1A-D provides the anthropogenic biomes of Asia spanning the last three centuries (1770–2000). Anthropogenic biomes, (also known as anthromes or human biomes), describe the terrestrial biosphere as, human-altered form using ecosystem units defined by global patterns of sustained direct human interaction with ecosystems.

The land changes in SE Asia are indicative of the human migration and land management that continue to accelerate each year. For example, India has seen steady urban migration and consequently, its urban population exploded from being less than 10% of the total population at start of the 20th century to being nearly half of the total population by the end of the century. Population growth has led to increased urbanization and the resulting

land cover (LC)[2] land use (LU)[1] changes (LCLUC) are a significant anthropogenic forcing for environmental changes including weather and climate (Cotton and Pielke 1995; Pielke et al. 2011; Seto et al. 2010). Figure D.2 is shown as change in area of different land use/ land cover types between 1880 and 2010 (as obtained from Tian et al. 2014). Overall, grassland and forest land area have decreased, area of cropland has increased by over 50% and the built-up area has increased almost five-folds. This change (Figure D.3A-C) showing LCLUC maps of India for the years 1985, 1995 and 2005 respectively is consistent with the population growth that saw the need for growth in cropland and the increasing urban migration. Figure D.3C in particular shows major urban growth centers in India during the past decade (and continues). There is clear indication of urban growth in northwest India for regions such as Punjab (Figure D.4A), western India for regions like Maharashtra whose state capital Mumbai continues to be an economic capital of the region (Figure D.4B) and southern peninsular India (Figure D.4B). In addition to the urbanization changes, Figure D.5 highlights the significant changes in plantation area over peninsular India (Figure D.5A) and Western Himalaya (Figure D.5B) between the years 1985 and 2005.

These LCLU changes resulting from rapid urbanization and agricultural intensification in the emerging economies can be contended as two important drivers and examples of land cover changes. The land transformation noted in the last few decades can be extrapolated for the next decade highlighting the continued pattern of migration to urban areas leading

[2] Land use changes refers to changes in land like growing agriculture/vegetation, cutting forests/trees, or building cities) and land cover changes refers to the differences in physical characteristics of land surface such as grass, vegetation, clay, sand or concrete.

to dense population. In addition, many coastal areas are also experiencing rapid growth and continue to be important seats of LCLUC. According to Schneider et al. (2011), in Japan and South Korea, 3–5% of country's land area has highly urbanized populations of ~80–90%. Cities of all sizes are growing in China, Indonesia, the Philippines, and Thailand, with higher rates of population growth for small cities during the last decade (Schneider et al. 2011). Urban areas with dense population are also impacted by air pollution due to industrialization, increased vehicular emissions and consumption of natural resources. Further, the population in these region of land transformation will face a variety of significant environmental risks in terms of health, air and water quality (Munich Re Group, 2004; Sailor 1995; Gaffen and Ross 1998; Walsh 2000; Arnfield 2003). For example, cities are warmer (urban heat island) and impacted by more number of heat waves than the rural or countryside areas. A recent survey by the World Health Organization (WHO) indicated that 10 out of 15 most polluted cities in the world were in Indian subcontinent (WHO, 2014) As the number and the size of urban cities continue to grow (urban expansion), more than 90% of increase (in environmental extremes/risks) will occur in the emerging economies of the world (World Cities Report, 2016). Thus, the LCLUC feature and associated environmental changes are a notable characteristic of the biogeography of the region.

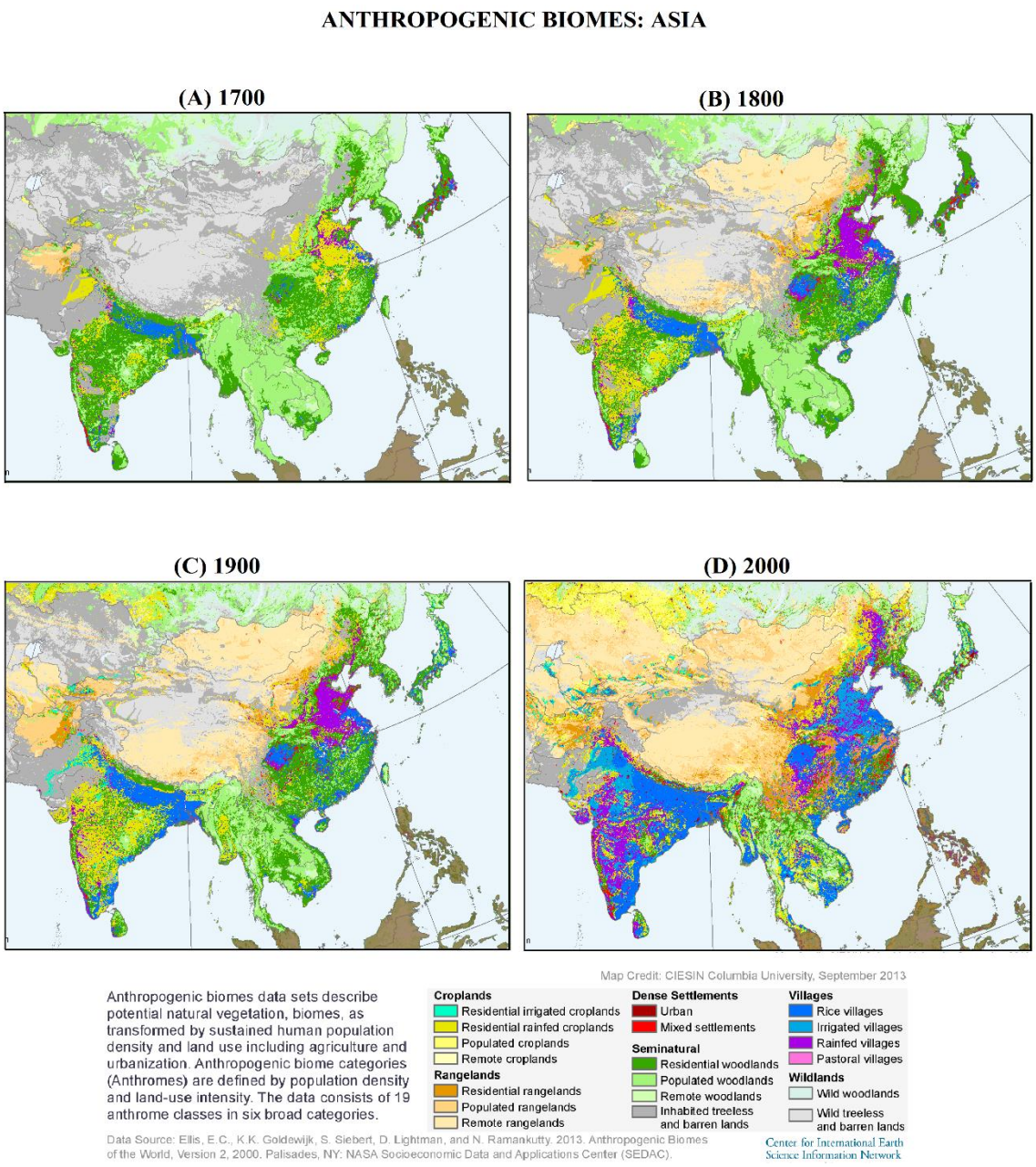

Figure D.1 Anthropogenic biomes of Asia for the year (A) 1700, (B) 1800, (C) 1900 and (D) 2000. (Open Sourced from NASA Socioeconomic Data and Applications Center (SEDAC))

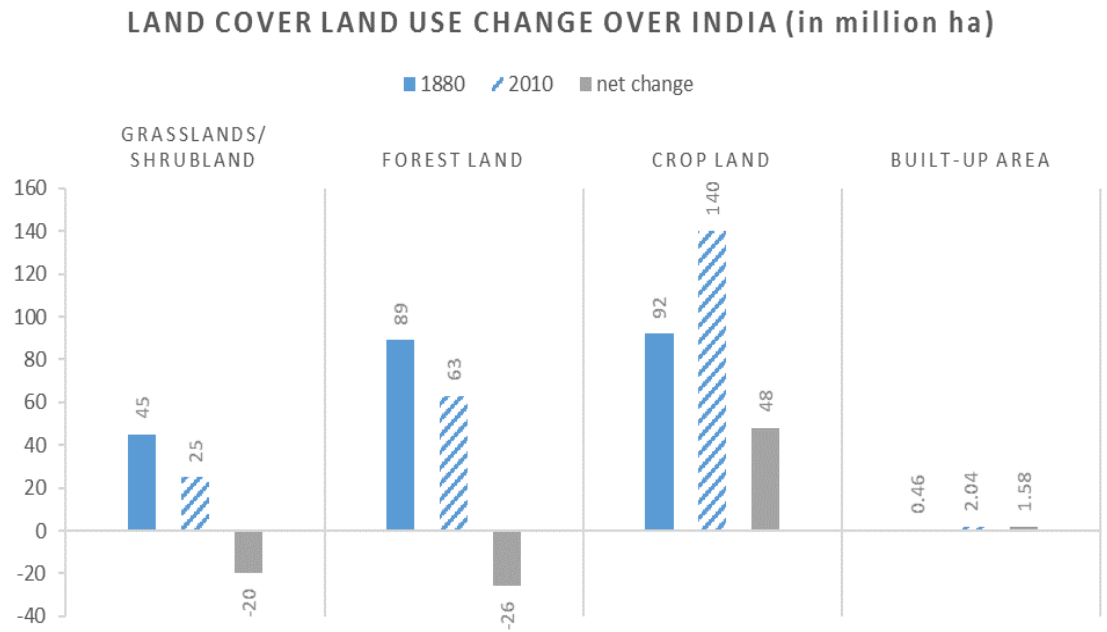

Figure D.2 Land use and change in LCLUC over India between 1880 and 2010 in million hectares (Data Source: Tian et al. 2014). While grasslands and forest land area have decreased, area of cropland has increased by over 50% and the built-up (urban) area has increased by almost 5 times.

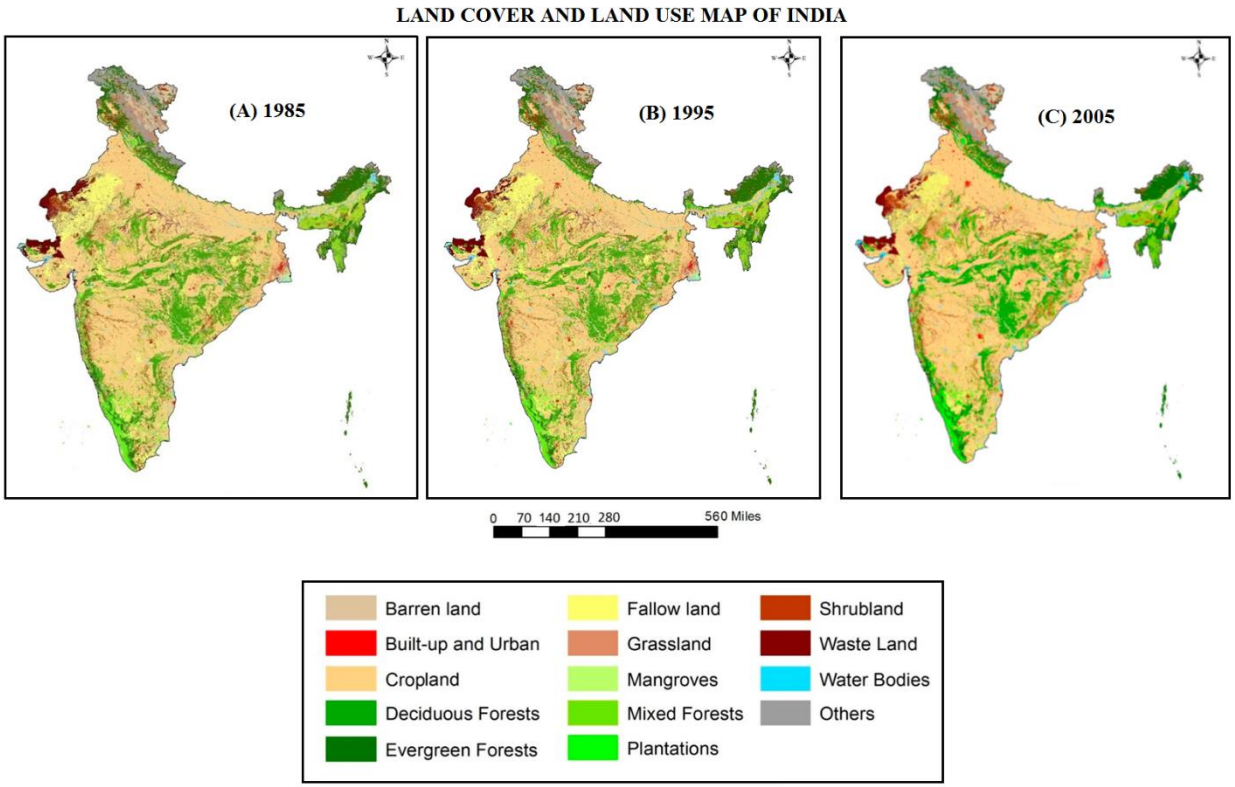

Figure D.3 Land cover and land use map of India prepared using satellite remote sensing data sets for the years (A) 1985, (B) 1995 and (C) 2005. (Openly Sourced from Roy et al. 2015)

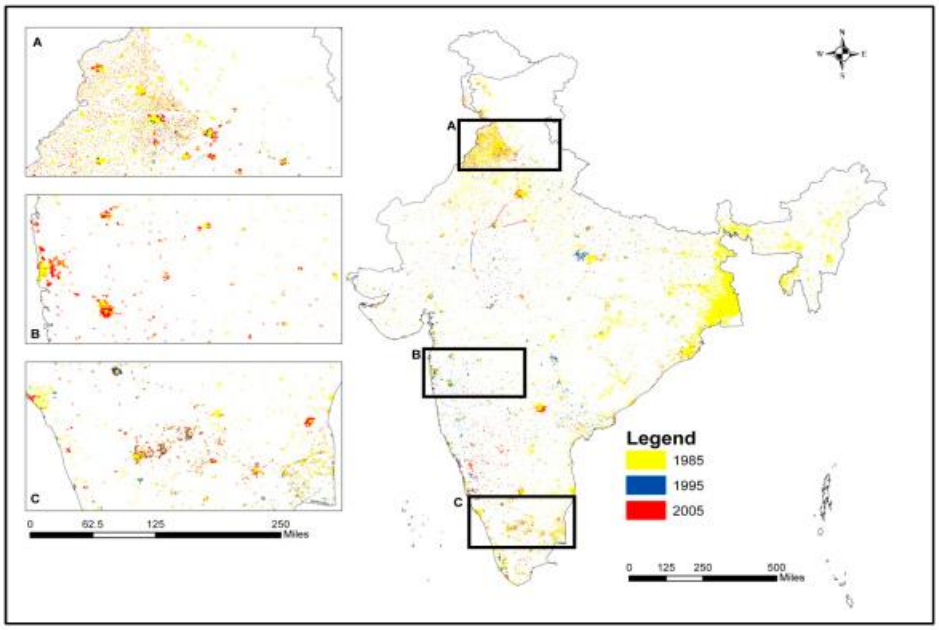

Figure D.4 Map showing urban growth during the years 1985, 1995 and 2005. Major urban growth centers include (A) north- west Punjab, (B) western India around Mumbai region and (C) Southern India. (Openly sourced from Roy et al. 2015)

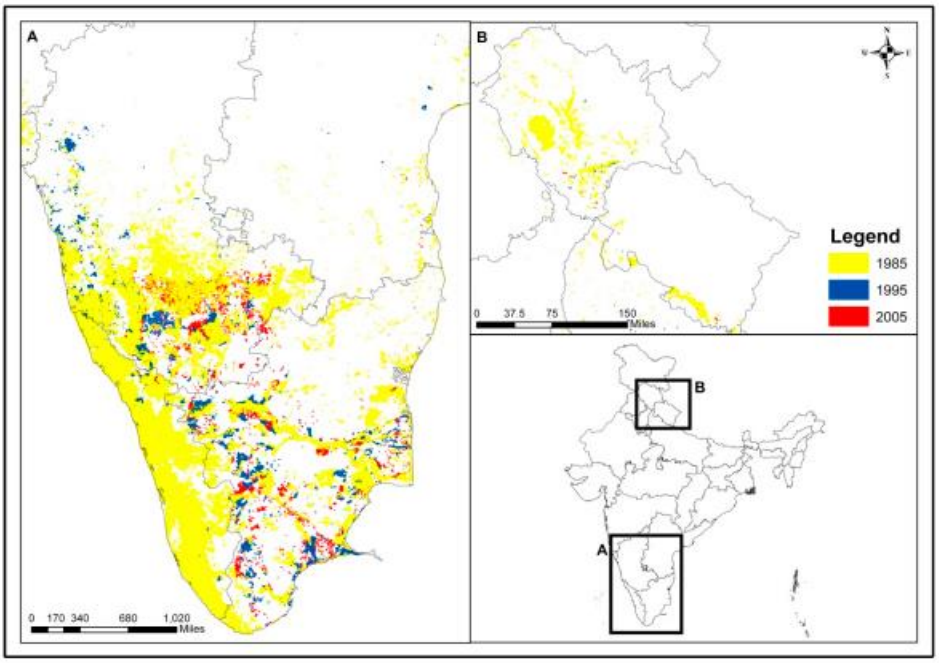

Figure D.5 Significant changes in plantation area in (A) Peninsular India and (B) Western Himalaya between the years 1985 and 2005. (Openly Sourced from Roy et al. 2015)

Also related to the LCLUC trajectories underway, the southeast Asia region, and the IMR in particular, has witnessed a large number of high impact, extreme weather events. For example, the July 26, 2005 Mumbai heavy rains resulted in over 944 mm of rains within 24h over a localized region causing intense flooding and significant human and property damage (Kumar et al. 2008). There was a similar rainfall (>340 mm) on 17 June 2013 in the state of Uttarakhand (between 28.72°–31.45°N and 77.57°–81.03°E) in the Western Himalayas, which is 375% more than the daily normal (65.9 mm) rainfall during monsoon. In November 2015, Chennai, a major city in southern parts of India, received record-breaking rainfall of 1049 mm (three times the monthly mean for November). Rapid LCLUC and alteration of the cities hydrological settings have been cited as reasons for increased flood risk (Gupta and Nair, 2010, Mujumdar et al. 2015). Similar intense heavy rain events with extreme intensities have occurred in other megacities in India and other tropical counties (e.g. May 2006 rains in Hong Kong / Guangdong province in China). A recent study by Chen et al. (2007) demonstrated that the afternoon/evening thunderstorm activity in urban area such as Taipei, Taiwan is increased by 67% compared to rural sites, and 77% increase in associated rainfall. The mean surface temperature over China is increasing at 0.05° C decade^{-1}, according to Zhou et al. (2004) and is attributed to urbanization. Thus, there is a growing need to understand the regional weather extremes in the context of LCLUC, an extreme of which is being manifested through urbanization and urban floods.

In wake of these LCLUC underway and the meteorological extremes expected to continue, the meteorological modeling community today has a necessary and critical

challenge of considering LCLUC for improving model predictions and confidence. As a result, following three immediate challenges can be posed:

i. How to assess the effect of LCLUC changes (including the impact on landscape soil moisture, radiative properties) on the land surface response (thermodynamic as well as hydrological)?

ii. How to represent these land surface feedbacks in the numerical weather prediction and regional climate models that are seamlessly integrative at multiple scales (i.e. micro, urban, regional and continental scales)?

iii. How to demonstrate and attribute the dynamical impact of the improvement in the physical land surface representation on the meteorological model performance for weather forecasting regional climate; and the monsoon rains especially the extremes and anomalous rains that can cause floods or droughts?

In this chapter, it is postulated that, explicitly considering the role of land-surface processes is critical in improving the model predictions over the monsoon domain. The lack of frontal and synoptic activities (in the absence of active monsoons) makes the local surface interactions a dominant forcing for the atmospheric boundary-layer processes (Zheng et al. 2015). The surface temperatures and fluxes are also typically high further making the land surface feedback important for the regions. The objective of this chapter thus is to provide a perspective and summary of the recent findings on this topic within the context of utilizing the emerging LCLU for the predictive or synthesis models over the IMR. There is also a growing need to develop weather and climate models at finer scales to resolve scales the scale interactions from processes which are smaller than ~1

km and spanning greater than ~100 km. Incorporation of these LCLU changes into these models and proper response of surface physics parameterization to these changes are also of growing interest.

D.3 Impacts on Surface Energy Balance

One of the primary consequences of LCLUC is the alteration to energy balance of the region. Depending on the datasets available for analyzing LCLUC, over India for example the percentage of agricultural land has remained constant over the years but the amount of irrigated landscape has significantly expanded. Increase in the amount of satellite cities[3] around megacities and expanding urbanization in coastal regions of India have also contributed to altering the regional surface energy balance. Increased dryland desertification, intensive agricultural practices, unsustainable land use changes (particularly in mountain regions) and explosive population growth have also altered surface energy balance (Abrol and Venkateshwaralu, 1995; Bai et al. 2008; Faroda 1998; Kumar et al 2007; Narayan and Kar 2006; Purohit 2009; Sathaye et al. 2006; Saxena et al. 1997).

Surface radiative fluxes are expected to change via partitioning between the net longwave and short wave radiation reaching the earth surface. From the perspective of surface energy balance and day time land cover interaction, the short wave radiation becomes one of the dominant elements of the energy budget. Incoming shortwave radiation can also be classified into direct and diffused radiation, which also depends on the aerosols and cloud

[3] Satellite cities are smaller cities that are near to a large city that is the center of a metropolitan area. Satellite cities could be separate cities outside of the larger metropolitan areas.

characteristics (Niyogi et al. 2007). For a typical clear sky condition, the direct shortwave radiation is the dominant radiative vector that will be interacting with the land surface. The net radiative flux (Rn) is partitioned into sensible, latent and ground heat flux. This partitioning is function of landscape and radiation interaction and can be represented as

$$Rn = \textit{Sensible heat flux } (H_S) + \textit{Latent heat flux } (H_L) + \textit{Ground heat flux } (H_G)$$

For instance, vegetated landscape utilizes the radiation for photosynthesis, part of which is used towards water use and transpiration as a cost function associated with the photosynthesis process. Transpiration from vegetation and evaporation from the ground surface together lead to a change of state of water from liquid to vapor state (into atmospheric moisture) and into the atmosphere as latent heat flux, LHF (Figure D.6A). The resultant of the energy fluxes is then stored as ground heat flux (GHF) and the rest used as sensible heat flux (SHF) resulting in heating of the atmosphere. This then results in the changes to the land skin temperature as well as changes in the ground/ soil temperature which then translates into surface air temperature change.

The changes in the surface energetics is expected to affect the overall atmospheric radiative balance and dynamics over that particular landscape. The characteristics of surface land cover, hydrology, and vegetation density affect partitioning of net radiation into latent and sensible heat fluxes (McGuffie et al. 1995). Figure D.6B and D.6C provides portioning of radiation into radiative fluxes for different land cover or land use. Figure 6B shows the energy partition for arid land area in summer. Majority of the net radiation is partitioned into SHF while the LHF is almost negligible. In contrast, the partitioning into LHF increased over needle leaf forest area (Figure D.6C). The ratio of

SHF to the LHF is known as Bowen ratio. The change in Bowen ratio reflects the availability of energy in the atmosphere. Typical average values of Bowen ratio are 0.1 for tropical oceans, 0.1–0.3 for tropical wet forests, 0.4–0.8 for grasslands, 0.75–2 for urban areas with lawns and trees, and >2 reaching extreme value of 6 for dry urban areas (Oke, 1978). The ground heat flux component is also expected to increase in urbanized areas. In many land models the ground heat flux is taken as 10% of the Rn for simplicity (Noilhan and Planton, 1989).

Thus, changes in land use/ land cover introduce changes in physical, thermal, and aerodynamic properties that determine the radiation and thermal characteristics of the surface. Albedo, emissivity, thermal conductivity, specific heat capacity, density, and roughness length are important factors that need to be represented accurately for that land cover. The literature suggests that thermal conductivity and specific heat are lower, and aerodynamic roughness lengths are higher, in urban or bare soil landscapes compared to agricultural region (Arya, 2001; Oke, 1978). Aerodynamic roughness of the land change is reported to reduce the wind speed by 25% which increases the convective efficiency. As summarized in a number of studies including Pielke et al. (2011) and Kellner and Niyogi (2014), the cascade of energy balance and energetics from the surface can start organizing and affect the dynamical processes at different scales.

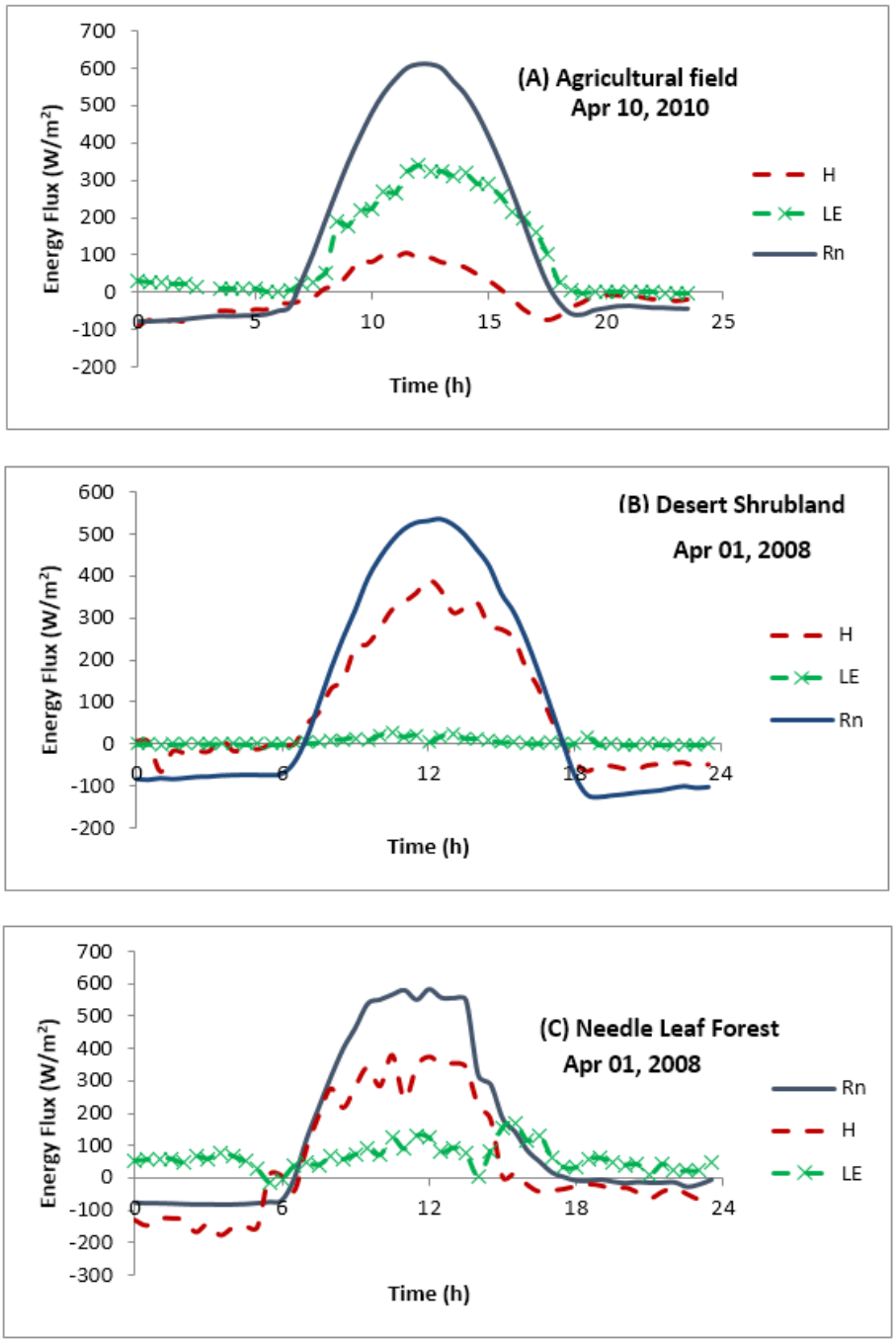

Figure D.6 Observed diurnal energy budget for different land use. (A) An agricultural field in Oklahoma, USA on Apr 10, 2010, (B) Sevilleta Desert Shrubland in Apr 01, 2008 and (C) a needle leaf forest in Niwot Ridge, Colorado, USA, on Apr 01, 2008. (data source: Ameriflux)

D.4 Impact on Large scale rainfall in IMR

The dynamical feedbacks of different scales (micro to synoptic) on associated LCLUC and their understanding remains unexplored and is an emergent area in this region. Recent study by Roxy et al. (2015) utilized large-scale model simulations and concluded that the reduction in the monsoonal rainfall can be attributed, in part, to the modification of land – sea temperature contrast. Rainfall characteristics such as timing as well as the magnitude were reported to have shifted from control when LCLUC was considered in the simulations. This study is part of a growing number of reports that highlight the coherent manner through which the LCLU heterogeneity could create an atmospheric feedback that can be akin to the SST changes.

Majority of large scale Global Climate Model (GCM) studies have prominently studied deforestation / afforestation impacts on large scale rainfall and temperature patterns. Takata et al. (2009) studied the impact of LCLUC across centuries and identified that LCLUC during the period of the first industrial revolution (1700-1850) contributed most to the decreased Asian Summer Monsoon intensities. In more contemporary studies, Gupta et al. (2005) studied the impact of deforestation in Africa and South East Asia and found that rainfall decreased over those regions and northern India but resulted in increased rain rate over southern India. Devaraju et al. (2015) undertook a large scale LCLUC experiment and concluded that global deforestation resulted in tropical northern hemisphere rainfall decrease and an increase in southern hemisphere tropics. Another important result of this study is the degree of response of the global climate to the location of deforestation/ afforestation. Rainfall showed high sensitivity to mid-latitude

deforestation compared to negligible effects on rainfall due to deforestation in the tropics. This suggests that planned and controlled LCLUC (deforestation and reforestation efforts) can offset the large scale impacts. Halder et al. (2015) used an embedded regional climate model to analyze LCLUC over India. They conclude that the recent LCLUC has contributed to a moderate weakening of Indian Summer Monsoon due to the decrease of moisture convergence over the Indian peninsular region. They also found regional warming over central India by about 1- 1.2 °C, over central India with an increase in average daily temperature extremes. Similar surface temperature increases have been noted by Lejeune et al. (2014), Mahmood et al. (2014), Lawrence and Vandecar (2015) where global deforestation has led to an increase in surface temperature due to the loss of evapotranspiration. All of these studies and more have shown varying degrees of impact of LCLUC and while there is a strong sense that LCLUC has a notable impact on the SE Asia climate via local and teleconnections, there is still lack of consensus related to the impacts, and the mechanisms. This is possibly because of the limitations to compare different studies which use different GCMs, and the inherent model uncertainties, biases and variations. Indeed, some studies also consider unrealistic and hypothetical LCLUC scenarios that may or may not exaggerate the impacts. Thus, there is an urgent need for more studies that comprehensively analyze results from multiple GCMs and incorporate sensible and realistic changes in land use to ass the impact of LCLUC on long term climate, changes in large scale temperature and precipitation patterns and, remote teleconnections.

Note that there is often a perception that the LCLUC impact is much more of a localized feature affecting micro or mesoscale process as this feature has been relatively well documented (e.g. Pielke 2001). The LCLUC effects are extensively documented for local scales where energy balance change is the principal effect. At the regional or larger scales, the effect is on convection, and rainfall changes. The synthesis of LCLUC feedbacks on the larger scales however, is relatively difficult (Pielke et al. 2011). Essentially, the effect/ feedback depends not only on what is the land transformation but also on the land cover that is being replaced. Further, the effect of changes is also dependent on other variables such as soil texture and soil moisture. Another factor that makes the detection difficult is that the change in convection and rainfall can be over a region that is different than where the LCLUC occurs.

A study by Kumar et al. (2013) provides a perspective and a possible methodology to look at the LCLUC feedbacks on the hydroclimatology as well as monsoonal features taking the different global climate model runs as an example. The CMIP5 results were analyzed over different large river basin including Gangetic, Brahmaputra and other river basins in India. Study showed that LCLUC effects can be detected and modified to include a detectable climate forcing signature for the contemporary and future climate. The mechanisms associated with the LCLUC processes impacting the monsoonal characteristics in the SE Asia have been studied in detail in studies such as Chase et al. (2003), Lee et al. (2009), Niyogi et al. (2009) and more recently, Saha et al. (2015) using a combination of observation, satellite datasets, reanalysis datasets**.**

Niyogi et al. (2010) identified a lagged temporal relation between the climatology of soil moisture, NDVI and rainfall anomalies. The implication of early greening and irrigation induced LCLUC has also been discussed in their study. Specifically, it has been shown using causal statistical analysis, that the summer monsoon (July) rainfall anomalies could be attributed to the anomaly in spring greenness. In other words, a change in vegetation green fraction (VGF) could lead to a change in the overall memory of soil and surface temperature and regional entropy associated with sensible heating. That is, the changes associated with greening modifies the thermal contrast in the region which is a necessary condition for the monsoonal low to propagate from southern India into the northern region. As a result, this leads to reduced intensity of monsoon (June-July rainfall) in the northwest India region. These features were also analyzed and found in the studies of Lee et al. (2009, 2011) where changes in agricultural and irrigation practices resulted in a weakening of the monsoon flow due to alteration of surface energy partition (more LHF and less SHF) that lead to decrease in tropospheric temperature and lowering of tropospheric height (See Figure D.7 for the flowchart). Krishnamurti et al. (2012) report that the isochrones that track the monsoon propagation post onset, can be modulated by the vegetation greenness and soil moisture availability. As a follow up to the results presented in Niyogi et al. (2010) and Lee et al. (2009), Saha et al. (2015) conducted a series of global model runs and their assessment are also supportive of the perspective that anomalies in the early Spring LCLU could result in the modification of June-July summer monsoon rainfall over the Indian monsoon region. As a result, the findings that winter or early spring LCLUC feedback, particularly in the VGF through a series of cascade of scales could eventually start affecting the land sea temperature contrast. The

summer time rainfall modulation via spring greening appears to be a consistent feature in a number of studies and an indicator of the pathway in which LCLUC in the SE Asia region is affecting the large-scale monsoon system.

Similarly, LCLUC feature was also studied in a NDVI assessment over the northern India region and it was noted that with the access to irrigation water for agriculture, the landscape in northern India has changed. This change in irrigation resulted in the modification of agricultural practices in the northwest India region. As a result, that area has started to experience the greening earlier than the monsoonal greening associated with the landscapes. A satellite data analysis study by Singh et al. (2006) has shown that for every decade since 1981, the region has been greening by approximately one week earlier compared to the previous decade. The synthesis shows that with increase in irrigation over this region, there is a decrease in rainfall amounts, which is consistent with the dynamic pathway that was outlined before. In other words, a consistent and coherent picture has emerged indicating that LCLUC alters the spatial thermal characteristics and the regional circulation which in turn modifies the strength of the regional low that is required for the monsoon to advance as well as for rainfall intensity over this region. These aspects, while typically noted from the large scale analysis, has its signature embedded in the series of processes, and are summarized next.

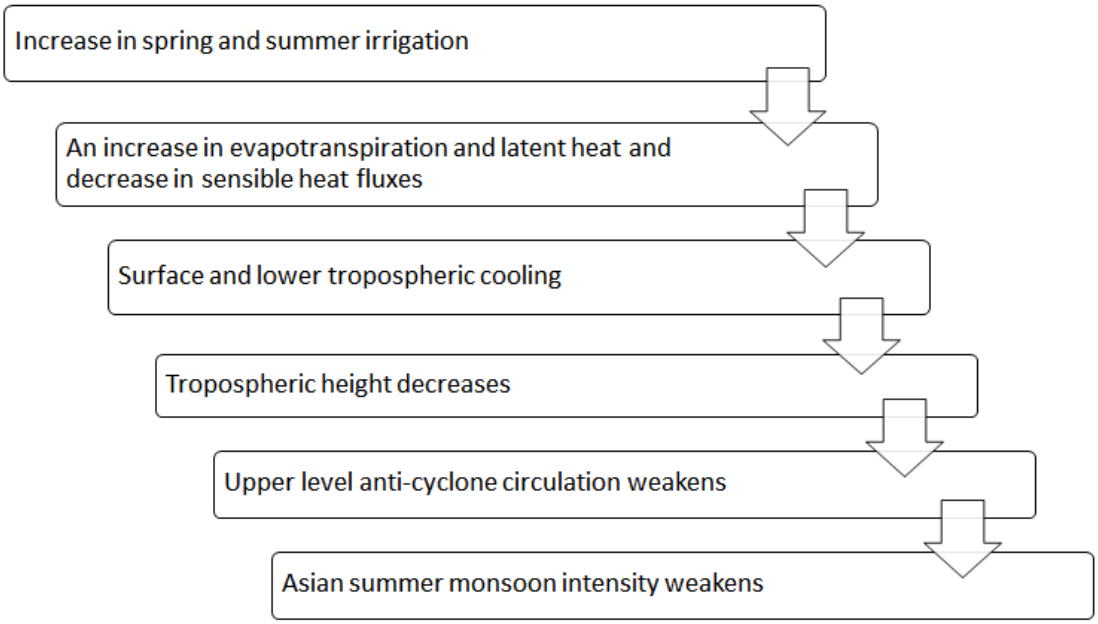

Figure D.7 Pathway connecting changes in agricultural practices to weakening of Asian jet in summer. (Source: Niyogi et al. 2010 and Lee et al. 2011)

D.5 Impact of LCLUC on Mesoscale events

In the following sections, some examples of the mesoscale studies that have been undertaken to understand the role of LCLUC in the context of SE Asia and the monsoonal changes in particular is discussed. A study by Douglas et al. (2009) looked at potential versus current land cover on mesoscale rainfall changes. They applied a mesoscale model to simulate a typical rainfall event occurring during summer monsoon. Their analysis showed that because of the changes in land cover characteristics, there were changes in albedo, emissivity and roughness which changed the associated temperature patterns, humidity and CAPE which resulted in changes in location and timing of convection and rainfall characteristics over the monsoon region.

The role of LHF in modulating the monsoon climate is of particular interest in the LCLUC arena because of the efficiency associated with certain land covers in transferring moisture to the atmosphere compared to other landscapes. Resulting changes could occur in surface temperature, humidity as well as moisture characteristics associated with any system. For example, Roy et al. (2007) showed two different regimes in temperature characteristics by considering two epochs of agricultural practices in India, i.e., traditional agricultural practices (pre-green revolution) and the biotechnology aided Green Revolution (post-green revolution). Similarly, Paul et al. (2016) conducted model analysis to simulate impacts due to contemporary deforestation over the IMR. They concluded that the changes in the LHF and recycling component of precipitation affect the rainfall patterns and weakening of the monsoons. A modeling study by Halder et al. (2015) over Western Ghats has also concluded that LCLUC causes daily mean temperature extremes to exceed by 1-1.2 C and, significantly reduces the summer time

monsoonal rainfall. These changes in the temperature or rainfall are embedded within the largescale impact of human intervention on landscape characteristics causing changes in regional temperature and humidity over the India region.

Another approach used in assessing the impact of LCLUC on the SE monsoonal characteristics is through the so-called ‘Observed Minus Reanalysis (OMR)’ framework proposed by Kalnay and Cai (2003). The basis of the OMR is that most of the reanalysis data do not account for the changes in local land cover characteristics and as a result the temporal changes do not account for the changes that could be attributed to land cover characteristics changes at a much smaller scale (Pielke et al. 2009). Thus, for observations impacted by the meso and microscale changes in the landscape characteristics the OMR values in those grids show a notable (sometimes dramatic) deviation in terms of trends and magnitude of parameters/indices compared between the observed and gridded reanalysis dataset. Nayak and Mandal (2012) conducted such an analysis over India, where modest but coherent changes in temperature and rainfall patterns could be linked to LCLUC identified over IMR.

These studies provide a glimpse of the kind of changes in the atmosphere that LCLUC induces over the IMR. The initial feature seen in Nayak and Mandal (2012) and Roy et al. (2007) is that of temperature feedbacks. There is, however, a strong and well-known effect on humidity characteristics too. The resulting changes in dew point and specific humidity in the region is linked with changes associated with atmospheric stability that could be altered by LCLUC. This feature was reviewed in Pielke et al. (2007) and also in Pielke et al. (2011) as part of a synthesis paper for LCLUC impacts on the IMR. With the

changes in temperature and humidity, it is not surprising that the regional entropy as well as convectively available potential energy also changes. The challenge remains in linking the coherent and co-located changes in the temperature characteristics with the broader changes in humidity and in the energy balance due to changes in LCLU characteristics. Nonetheless, if the data are appropriately analyzed and the confounding due to dynamical features considered, it is often noted that the changes in land cover affects local to mesoscale processes in a nonlinear but detectable manner (Kishtawal et al. 2009). Reviewing the reanalysis dataset as well as synthesis of different model runs has helped develop a perspective that rainfall patterns are changing in response to changes in land cover characteristic. There are theoretically and observationally viable and verifiable changes in the temperature characteristics, which are generally better detected, followed by humidity, CAPE and ultimately rainfall characteristics- in that order. Note that, the challenge in understanding the effect on temperature and rainfall changes as a result of LCLUC is not straightforward. As an example, a region that was not urbanized before but has started to become urban area would show changes in thermal characteristics and storages resulting in heating of the area with a creation of so called “urban heat island” with signature changes in temperature characteristics. However, the humidity parameters and in particular rainfall changes are a result of both temperature modifications and the interaction associated with roughness and the gradients in the surface radiative fluxes. These flux gradients create boundaries, aiding mesoscale convection which can be advected away from the location. As a result, there is often a lack of coherency or consistency in the detection of rainfall changes that can be attributed to land cover changes in a straight forward manner (as compared to temperature changes) over the

region. It can be asserted that, if proper dynamical considerations are made, such as to assess the wind direction, advection and stability, that reduce the confounders and data is properly spatially transposed, it is possible to show changes in LCLU and rainfall characteristics to be causatively linked (Niyogi et al. 2016). On the other hand, if the data is analyzed in a geospatial framework that only bins data under urban versus nonurban grids, then the results can also often produce a flawed conclusion that rainfall changes are not as a result of land cover changes (e.g. Ali et al. 2015). Therefore, caution is needed in examining the impact of LCLUC on hydroclimatic changes. This challenge is particularly notable when looking at the case of extremes, and is described in the following section.

D.6 Effect of LCLUC on Extremes

A number of studies show that the Indian monsoon is becoming more extreme (Goswami et al. 2006). These studies highlight increased occurrences of heavy to extremely heavy rainfall events with modest, to no changes, in the mean rainfall characteristics. While the change in the extremes has been subsequently well documented, the causes for these extremes continues to be researched. Indeed, a body of literature such as Goswami et al. (2006) concludes the rainfall changes could be in response to the large-scale features associated with climate change. A second body of literature examines the potential role of aerosol and dust characteristics in this region which could be interacting with cloud microphysics through the atmospheric brown clouds as well as changes in the radiative feedbacks (Ramanathan et al. 2001; Ramanathan and Carmichael 2008; Kulkarni et al. 2012). Both direct and indirect feedbacks could eventually lead to the changes in the rainfall characteristics over the region. Indeed, Niyogi et al. (2007) argued that the

change in land use and aerosol could be inter-related. A change in land use could also lead to changes in aerosol distribution and characteristics, and can combine to create a much more complex feedback in the atmosphere. Yet, this feature, though being quite important, is much more regional in nature, particularly where there is high growth in aerosol concentration such as in parts of China, India and many other regions of the emerging economies. For example, aerosol and land surface continues to be explored and considered important in numerical prediction of weather extremes.

Following the perspective that the LCLUC contributes to changes in rainfall distribution, the study by Kishtawal et al. (2010) addressed the question that whether LCLUC due to urbanization maybe an attributable factor for changes in extreme monsoonal rainfall. In their study, the same rainfall data as in Goswami et al. (2006) study was analyzed. To assess the urbanization impacts the first step was to develop a classification for urbanization that is reflective of the domain, and the need for disassociating the confounders. For example, if the data was analyzed simply as urban vs. non-urban grids using some of the traditional definitions such as population that is being used in NOAA's Global Historical Climate Network (GHCN) dataset, then the signal associated with the difference is relatively small. But, it was recognized that population alone is not the indicator over SE Asia where population density is already high as compared to many European and North American landscapes. So, the land cover characteristics such as emissivity and albedo were also mapped and considered as part of the urban demarcation. The analysis also considered the observations from satellite sources such as TRMM and Optical Line Scan data to develop a thermal imagery map over urban areas. The need for thermal analysis builds off the understanding that the LCLUC and thermal changes are

often co-located. Once this was undertaken, it was possible to develop a robust conclusion regarding the changes in LC characteristics and the rainfall changes. In other words, comparing the rainfall distribution for urban vs. non-urban areas, the probability density functions for urban areas showed much higher peak indicating higher potential for extremes in the dataset. When a time series analysis was conducted for the gridded urban vs. non-urban dataset, it could be clearly identified that only those areas where LCLUC was noted are also the areas in which the increasing trend in rainfall extremes is observed. In other words, LCLUC can be considered if not the causal aspect, at least the locale, where occurrences of extremes are noted. Thus detection of these zones become an important aspect in the hydro climatic perspective. This feature of changes in extremes due to LCLUC has been concluded in multiple studies and the role of land cover feedback is an emergent important factor. Following the work of Kishtawal et al. (2010) more recently Ghosh et al. (2012) as well as Sashtri et al. (2015) and other studies have noted similar signature associated with urbanization. In fact, recent studies have also concluded that the non-stationarity noted in the IMR observations cannot be simulated unless LCLUC is explicitly considered. These studies further highlight the need for explicit LCLUC considerations in developing improved predictions over the IMR.

An important point that needs to be noted is that even when LCLUC is being highlighted as pathway for the changes in rainfall extremes, it does not negate other anthropogenic forcings that are also involved. In fact, changes in LCLUC can synergize the impact of other such changes. For example, the changes in urban area could also lead to a change in aerosol distribution. So, the combination of surface LCLU and the atmospheric aerosols can work in tandem to change the boundary layer heating rates, the cloud microphysics,

magnitude and intensity of regional rainfall extremes (Schmid and Niyogi 2015). So, the question should not be posed as whether LCLUC or aerosols or if the large scale climatic changes are the cause, rather it is important to look at combination of these factors as interlinked features within in the earth system framework. The mechanism of how aerosols could advect or entrain into clouds or the role of LCLU could be seen through the increased availability of cloud condensation nuclei (CCN) that could be impacted by the circulation caused by thermal gradients due to LCLUC or the emission from the LCLUC. Indeed, the other pathway is through diffuse radiation, which could eventually change the landscapes efficiency for evapotranspiration and photosynthesis/net productivity and alter the VGF (Niyogi et al. 2009). These features are interlinked and studies need to consider them more synergistically than what has reported until now (Schmid and Niyogi 2016).

D.7 Additional studies on the impact of LCLUC on weather and climate:

Indeed, a large number of studies, both observational and modeling based, exist that highlight the role of LCLUC as one of the important aspect influencing land-atmosphere interactions. The feedbacks are manifested through changes in the surface heat fluxes, evapotranspiration and exchange of land surface characteristics to surface/boundary layer that can significantly changes the boundary-layer dynamics influencing weather and climate.

At a larger scale, land state studies indicate that surface characteristics can affect the movement, intensity and rainfall of offshore atmospheric vortices such as TCs and

monsoon depressions (MDs) when they approach or move inland. Studies undertaken by Kishtawal et al. (2012), Subramanian et al. (2014), and Chang et al. (2009) suggest that the availability of antecedent soil moisture could affect the summer time rainfall. The availability of soil moisture two week prior to the onset of monsoon depression could lead to a weaker but longer sustained MDs leading to a wide spread rainfall. On the other hand, dryer landscape conducive to higher evaporation rates could lead to a much stronger cyclonic system albeit a shorter one with intense rainfall experienced over a smaller spread of area. These features also manifest in the regional rainfall climatology (Krishnamurti et al. 2012; Dastoor and Krishnamurti 1991). While majority of these studies are for the Bay of Bengal basin, Chandrasekar et al. (2009) has shown that the realistic land surface representation and surface data assimilation improved simulation of surface variables (surface fluxes, precipitation, moisture and temperature) associated with weather phenomena such as off-shore trough over the Arabian Sea.

Experiments with different LSMs indicated that precipitation over land is sensitive to the representation of land surface conditions. Thus is a significant conclusion, since almost quarter of the rainfall experienced in the region is due to monsoonal activity and is essential to the agriculture, water resources, and the regional economy and sustained development. Other studies that have been conducted for this region for heat wave could also be linked to LCLUC though the effect has been relatively modest but remains to be studied further (Niyogi et al. 2016).

Other examples beyond the monsoon rainfall effect include studies such as by Cui and Graf (2009) that studied the effect of land cover changes on the Tibetan plateau. They

identified that the permafrost and snow melting is directly impacted by the recent warming trends in the plateau which in turn impacts local ecosystem. The increased human activities on the plateau in the last few decades modify land use which include permafrost and grassland degradation, urbanization, deforestation and desertification. This resulted in modifying local climate and regional hydrology, leading to floods at the upper reaches of Yangtze River and droughts along the middle and lower reaches of Yellow River.

A study on wintertime land surface characteristics was conducted by Dimri and Niyogi (2013) with a 22-year regional climate model simulation for the western Himalayas. The results brought out the role of land change/ land representation on systematic biases in precipitation and temperature fields over the western Himalayan domain. Realistic topography and land state representation within model significantly improved the winter precipitation simulation. Model simulations using detailed land-use classification reduced the bias in the temperature and rain occurrence at higher elevations. Similarly, Chawla and Mujumdar (2015) have shown that streamflow characteristics simulated by VIC model in the upper Ganga River basin are highly sensitivity to LCLUC in urban areas and moderate sensitivity to cropland area changes. Once again highlighting that the LCLUC representation is important for both the summer as well as wintertime hydroclimatic simulations over the IMR.

At the other extreme geographical locale, Kharol et al. (2013) studied the LCLUC influence on atmospheric dynamics over the arid/ desert region of Rajasthan, India. Satellite observations (Landsat MSS for 1972–73 and IRS-P6 AWiFS for 2006–07)

suggested that there is considerable LCLUC over this region. With the access to irrigation resources, an increase of about 57% and 68% is seen in crop-land and vegetated areas over the eastern and western Rajasthan, respectively. This increase in agriculture, results indicate, has modified the land-atmosphere fluxes, with increase in atmospheric humidity and latent heat and reduction in sensible heat in this region. On the other hand, the analyses of inter-annual variability (1951–2007) of annual rainfall and total number of rainy days have exhibited a slight increasing trend over arid western Rajasthan with the increase in the agricultural land use. Their results show that precipitation variability is primarily influenced by the large scale monsoon circulations followed by local phenomena such as LCLUC. Similarly, Ranjan et al. (2006) studied the effects of climate and land use changes on groundwater resources in this region. Their analysis concluded that in case of arid areas, the fresh groundwater loss is increasing with the increase of forest cover while the groundwater recharge is increasing in arid, deforested areas due to reduction in evapotranspiration.

More broadly across the SE Asia, increased population resulted in widespread land degradation and rapid changes in upland farming systems. Valentin et al. (2008) studied the runoff and sediment losses in Southeast Asia (Indonesia, Laos, Philippines, Thailand, and Vietnam) with reference to rapid land use changes. They found LCLUC has strong influence on the soil erosion predominantly followed by the environmental characteristics. Similarly, a study by Paiboonvorachat and Oyana (2011), the forest area is mainly converted to agricultural and urban areas under mountainous conditions. It is noted that there is an increase in soil erosion in Nan watershed due to deforestation.

Model predictions also showed that the forecast areas are like to convert agriculture/crop lands and north/eastern parts of watershed is like to have high risk of soil erosion. A detailed review on hydrological investigations of forest disturbance and land cover impacts in South–East Asia can be found in Douglas (2009). That review focuses on the relationships between rainfall and runoff with the land cover and forecast area changes in most of the countries.

Land use changes have large impacts on water resources and its quantification is a challenging problem in the present growing population scenario. Stonestrom et al. (2009) presented possible impacts of land use changes on water resources. Petchprayoon et al. (2010) also demonstrated the hydrological impacts of land use/land cover change in a large river basin in central–northern Thailand using a 15-year period observational and modeling analysis. For their study region, urban area is increased by 132% (from 210 sq. km in 1990 to 488 sq. km in 2006). The long term trend of river discharge shows significant increase. However, the rate of discharge increase was significantly greater in downstream of the rapid urbanization than the upstream area. The LCLU changes led to systematic increase in rate of change in discharge over the 15-year period. A study by Bharati and Jayakody (2011) focused on the changes in water balance in the Gorai River Catchment in the Bangladesh delta before and after operationalization of Farakka Barrage. Land use changes in catchment area decreased runoff. Yang et al. (2010) showed urban representation in hydroclimatic land models for runoff assessments is not just a function of prescribing the urban fraction correctly but also the spatial distribution right. In fact, their result, further updated by Yang et al. (2015), suggests that there is a

minimal threshold of about 10% coverage or so that is required before the model grid outcome "detects" it. Thus, LCLUC representation is important for simulating virtually all aspects of the hydroclimatic cycles and studies have shown there are significant impacts on all aspects of the SE Asia hydroclimatology.

D.8 Conclusions

Our understanding of the interactions between tropical surface and atmosphere exchanges is still relatively limited compared to that in the mid-latitudes. This is due to the lack of detailed field studies, as well as the extreme nature of the hydrological cycle (drought and flooding) in the tropics. The monsoonal systems are large scale events and synoptic in nature. However, embedded within these large scale features are a variety of scales that result in terms of regional mesoscale factors as well as microscale feedbacks which can regulate weather extremes. The emergent conclusion of this work and the current understanding of the community is that LCLUC feedbacks can affect the monsoonal characteristics by a variety of scale interactions. Land surface feedbacks manifest their role by changes in surface energetics, boundary layer processes, and organized convection which could even impact or retard the larger scale feedback associated with monsoon features, and future projections as well as current improvements in the monsoon climate including rains will need to have a concerted and continued effort for developing, incorporating and synthesizing the role of land surface feedbacks in the monsoon forecasts and is part of ongoing monsoon mission projects in Indian (NMM, 2016).

D.9 References

Abrol, I., and J. Venkateswarlu, 1995: Sustainable development of arid areas in India with particular reference to Western Rajasthan. *Land Degradation and Desertification in Asia and the Pacific Region***,** 135-153.

Academy, I. N. S., and Z. K. X. yuan, 2001: *Growing populations, changing landscapes: studies from India, China, and the United States.* National Academies Press.

Ali, H., V. Mishra, and D. Pai, 2014: Observed and projected urban extreme rainfall events in India. *Journal of Geophysical Research: Atmospheres*, **119**.

Arnfield, A. J., 2003: Two decades of urban climate research: a review of turbulence, exchanges of energy and water, and the urban heat island. *International journal of climatology*, **23,** 1-26.

Arya, P. S., 2001: *Introduction to micrometeorology*. Vol. 79, Academic press.

Bai, Z., D. Dent, L. Olsson, and M. Schaepman, 2008: Global assessment of land degradation and improvement. 1. Identification by remote sensing. *Wageningen: International Soil Reference and Information Centre (ISRIC)*.

Bharati, L., and P. Jayakody, 2011: Hydrological impacts of inflow and land-use changes in the Gorai River catchment, Bangladesh. *Water international*, **36,** 357-369.

Chandrasekar, A., D. Niyogi, and K. Alapaty, 2009: Impact of land surface representation and surface data assimilation on the simulation of an off-shore trough over the Arabian Sea. *Global and Planetary Change*, **67,** 104-116.

Chang, H. I., and Coauthors, 2009: Possible relation between land surface feedback and the post-landfall structure of monsoon depressions. *Geophysical Research Letters*, **36**.

Chase, T., R. Pielke, T. Kittel, M. Zhao, A. Pitman, S. Running, and R. Nemani, 2001: Relative climatic effects of landcover change and elevated carbon dioxide combined with aerosols: A comparison of model results and observations. *Journal of Geophysical Research: Atmospheres*, **106,** 31685-31691.

Chawla, I., and P. Mujumdar, 2015: Isolating the impacts of land use and climate change on streamflow. *Hydrology and Earth System Sciences*, **19,** 3633-3651.

Chen, C.-S., Y.-L. Chen, C.-L. Liu, P.-L. Lin, and W.-C. Chen, 2007: Statistics of heavy rainfall occurrences in Taiwan. *Weather and Forecasting*, **22,** 981-1002.

Cotton, W. R., and R. A. Pielke Sr, 2007: *Human impacts on weather and climate*. Cambridge University Press.

Cui, X., and H.-F. Graf, 2009: Recent land cover changes on the Tibetan Plateau: a review. *Climatic Change*, **94,** 47-61.

Dabberdt, W. F., and Coauthors, 2000: Forecast issues in the urban zone: report of the 10th prospectus development team of the US weather research program. *Bulletin of the American Meteorological Society*, **81,** 2047-2064.

Dastoor, A., and T. Krishnamurti, 1991: The landfall and structure of a tropical cyclone: The sensitivity of model predictions to soil moisture parameterizations. *Boundary-Layer Meteorology*, **55,** 345-380.

Devaraju, N., G. Bala, and R. Nemani, 2015: Modelling the influence of land-use changes on biophysical and biochemical interactions at regional and global scales. *Plant, cell & environment*, **38,** 1931-1946.

Diem, J. E., and T. L. Mote, 2005: Interepochal changes in summer precipitation in the southeastern United States: evidence of possible urban effects near Atlanta, Georgia. *Journal of Applied Meteorology*, **44,** 717-730.

Dimri, A., 2012: Wintertime land surface characteristics in climatic simulations over the western Himalayas. *Journal of earth system science*, **121,** 329-344.

Dimri, A., and U. Mohanty, 2009: Simulation of mesoscale features associated with intense western disturbances over western Himalayas. *Meteorological Applications*, **16,** 289-308.

Dimri, A., and D. Niyogi, 2013: Regional climate model application at subgrid scale on Indian winter monsoon over the western Himalayas. *International Journal of Climatology*, **33,** 2185-2205.

Dixon, P. G., and T. L. Mote, 2003: Patterns and causes of Atlanta's urban heat island-initiated precipitation. *Journal of Applied Meteorology*, **42,** 1273-1284.

Douglas, E., A. Beltrán-Przekurat, D. Niyogi, R. Pielke, and C. Vörösmarty, 2009: The impact of agricultural intensification and irrigation on land–atmosphere interactions and Indian monsoon precipitation—A mesoscale modeling perspective. *Global and Planetary Change*, **67,**117-128.

Douglas, I., 1999: Hydrological investigations of forest disturbance and land cover impacts in South–East Asia: a review. *Philosophical Transactions of the Royal Society of London B: Biological Sciences*, **354,** 1725-1738.

Faroda, A., 1999: Desertification control: Recent technologies in the Indian context. *Desertification Control in the Arid Ecosystem of India for Sustainable Development*, 36-47.

Gaffen, D. J., and R. J. Ross, 1998: Increased summertime heat stress in the US. *Nature*, **396,** 529-530.

Ghosh, S., D. Das, S.-C. Kao, and A. R. Ganguly, 2012: Lack of uniform trends but increasing spatial variability in observed Indian rainfall extremes. *Nature Climate Change*, **2,** 86-91.

Goswami, B. N., V. Venugopal, D. Sengupta, M. Madhusoodanan, and P. K. Xavier, 2006: Increasing trend of extreme rain events over India in a warming environment. *Science*, **314,** 1442-1445.

Government of India, 2006: Report of the National Forest Commission. Ministry of Environment and Forests.

Gupta, A. K., and S. S. Nair, 2010: Flood risk and context of land-uses: Chennai city case. *Journal of Geography and Regional Planning*, **3,** 365.

Halder, S., S. Saha, P. Dirmeyer, T. Chase, and B. Goswam, 2015: Investigating the impact of land-use land-cover change on Indian summer monsoon daily rainfall and temperature during 1951-2005 using a regional climate model. *Hydrology & Earth System Sciences Discussions*,**12**.

Henderson-Sellers, A., K. McGuffie, and A. Pitman, 1996: The project for intercomparison of land-surface parametrization schemes (PILPS): 1992 to 1995. *Climate Dynamics*, **12,** 849-859.

Henderson-Sellers, A., A. Pitman, P. Love, P. Irannejad, and T. Chen, 1995: The project for intercomparison of land surface parameterization schemes (PILPS): Phases 2 and 3. *Bulletin of the American Meteorological Society*, **76,** 489-503.

Kalnay, E., and M. Cai, 2003: Impact of urbanization and land-use change on climate. *Nature*, **423,** 528-531.

Kellner, O., and D. Niyogi, 2014: Land Surface Heterogeneity Signature in Tornado Climatology? An Illustrative Analysis over Indiana, 1950–2012*. *Earth Interactions*, **18,** 1-32.

Kharol, S. K., D. Kaskaoutis, K. Badarinath, A. R. Sharma, and R. Singh, 2013: Influence of land use/land cover (LULC) changes on atmospheric dynamics over the arid region of Rajasthan state, India. *Journal of arid environments*, **88,** 90-101.

Kishtawal, C. M., D. Niyogi, M. Tewari, R. A. Pielke, and J. M. Shepherd, 2010: Urbanization signature in the observed heavy rainfall climatology over India. *International Journal of Climatology*, **30,** 1908-1916.

Kishtawal, C. M., D. Niyogi, A. Kumar, M. L. Bozeman, and O. Kellner, 2012: Sensitivity of inland decay of North Atlantic tropical cyclones to soil parameters. *Natural hazards*, **63,** 1527-1542.

Krishnamurti, T., and Coauthors, 2012: Modeling of forecast sensitivity on the march of monsoon isochrones from Kerala to New Delhi: the first 25 days. *Journal of the Atmospheric Sciences*, **69,** 2465-2487.

Kulkarni, J., and Coauthors, 2012: The cloud aerosol interactions and precipitation enhancement experiment (CAIPEEX): overview and preliminary results. *Curr. Sci*, **102,** 413-425.

Kumar, A., J. Dudhia, R. Rotunno, D. Niyogi, and U. Mohanty, 2008: Analysis of the 26 July 2005 heavy rain event over Mumbai, India using the Weather Research and Forecasting (WRF) model. *Quarterly Journal of the Royal Meteorological Society*, **134,** 1897-1910.

Kumar, P., P. Kapuria, N. Sengupta, A. Shah, and K. Chopra, 2007: National Capacity Needs Self-Assessment (NCSA) in Land Degradation in India. Institute of Economic Growth, Delhi. http://ncsa.undp.org/docs/593.pdf (Accessed July 2016)

Kumar, S., P. A. Dirmeyer, V. Merwade, T. DelSole, J. M. Adams, and D. Niyogi, 2013: Land use/cover change impacts in CMIP5 climate simulations: A new methodology and 21st century challenges. *Journal of Geophysical Research: Atmospheres*, **118,** 6337-6353.

Landsberg, H. E., 1970: Man-made climatic changes. *Science*, **170,** 1265-1274.

Lawrence, D., and K. Vandecar, 2015: Effects of tropical deforestation on climate and agriculture. *Nature climate change*, **5,** 27-36.

Lee, E., W. J. Sacks, T. N. Chase, and J. A. Foley, 2011: Simulated impacts of irrigation on the atmospheric circulation over Asia. *Journal of Geophysical Research: Atmospheres*, **116**.

Lee, E., T. N. Chase, B. Rajagopalan, R. G. Barry, T. W. Biggs, and P. J. Lawrence, 2009: Effects of irrigation and vegetation activity on early Indian summer monsoon variability. *International Journal of Climatology*, **29,** 573-581.

Lejeune, Q., E. L. Davin, B. P. Guillod, and S. I. Seneviratne, 2015: Influence of Amazonian deforestation on the future evolution of regional surface fluxes, circulation, surface temperature and precipitation. *Climate Dynamics*, **44,** 2769-2786.

Mahmood, R., and Coauthors, 2014: Land cover changes and their biogeophysical effects on climate. *International Journal of Climatology*, **34,** 929-953.

McGuffie, K., A. Henderson-Sellers, H. Zhang, T. Durbidge, and A. Pitman, 1995: Global climate sensitivity to tropical deforestation. *Global and Planetary change*, **10,** 97-128.

Munich Re Group Annual Report, 2004: https://www.munichre.com/site/corporate/get/documents/mr/assetpool.shared/Documents/0_Corporate%20Website/_Publications/302-04331_en.pdf. (Accessed July 2016)

Narayan, P. and Kar, A., 2006: Desertification and its control in India. International Center for Agricultural Research in the Dry Areas (ICARDA). http://researchsea.com/html/article.php/aid/737/cid/6 (Accessed July 2016)

Nayak, S., and M. Mandal, 2012: Impact of land-use and land-cover changes on temperature trends over Western India. *Current Science(Bangalore)*, **102,** 1166-1173.

Niyogi, D., R. Mahmood, and J. O. Adegoke, 2009: Land-use/land-cover change and its impacts on weather and climate. *Boundary-layer meteorology*, **133,** 297-298.

Niyogi, D., C. Kishtawal, S. Tripathi, and R. S. Govindaraju, 2010: Observational evidence that agricultural intensification and land use change may be reducing the Indian summer monsoon rainfall. *Water Resources Research*, **46**.

Niyogi, D., H.-I. Chang, F. Chen, L. Gu, A. Kumar, S. Menon, and R. A. Pielke Sr, 2007: Potential impacts of aerosol–land–atmosphere interactions on the Indian monsoonal rainfall characteristics. *Natural Hazards*, **42,** 345-359.

NMM, 2016: National Monsoon Mission accessible at http://www.tropmet.res.in/monsoon/. (Accessed July 2016)
Noilhan, J., and S. Planton, 1989: A simple parameterization of land surface processes for meteorological models. *Monthly Weather Review*, **117,** 536-549.

Oke, T., 1978: Surface heat fluxes and the urban boundary layer. *WMO Boundary Layer Phys. Appl. to Specific Probl. of Air Pollution p 63-69(SEE N 79-16393 07-45)*.

Organization, W. H., 2014: Ambient (outdoor) air pollution in cities database 2014. *World Health Organization, Geneva*.

Paiboonvorachat, C., and T. J. Oyana, 2011: Land-cover changes and potential impacts on soil erosion in the Nan watershed, Thailand. *International journal of remote sensing*, **32,** 6587-6609.

Paul, S., S. Ghosh, R. Oglesby, A. Pathak, A. Chandrasekharan, and R. Ramsankaran, 2016: Weakening of Indian Summer Monsoon Rainfall due to Changes in Land Use Land Cover. *Scientific Reports*, **6**.

Petchprayoon, P., P. D. Blanken, C. Ekkawatpanit, and K. Hussein, 2010: Hydrological impacts of land use/land cover change in a large river basin in central–northern Thailand. *International Journal of Climatology*, **30,** 1917-1930.

Pielke, R., and Coauthors, 2007: An overview of regional land-use and land-cover impacts on rainfall. *Tellus B*, **59,** 587-601.

Pielke, R. A., 2001: Influence of the spatial distribution of vegetation and soils on the prediction of cumulus convective rainfall. *Reviews of Geophysics*, **39,** 151-177.

Pielke, R. A., and Coauthors, 2011: Land use/land cover changes and climate: modeling analysis and observational evidence. *Wiley Interdisciplinary Reviews: Climate Change*, **2,** 828-850.

Pitman, A., and A. Henderson-Sellers, 1998: Recent progress and results from the project for the intercomparison of landsurface parameterization schemes. *Journal of Hydrology*, **212,** 128-135.

Pohit, S., 2009: Land degradation and trade liberalization: an Indian perspective. *Available at SSRN 1457666*.

Ramanathan, V., and G. Carmichael, 2008: Global and regional climate changes due to black carbon. *Nature geoscience*, **1,** 221-227.

Ramanathan, V., P. Crutzen, J. Kiehl, and D. Rosenfeld, 2001: Aerosols, climate, and the hydrological cycle. *science*, **294,** 2119-2124.

Ranjan, S. P., S. Kazama, and M. Sawamoto, 2006: Effects of climate and land use changes on groundwater resources in coastal aquifers. *Journal of Environmental Management*, **80,** 25-35.

Roxy, M. K., K. Ritika, P. Terray, R. Murtugudde, K. Ashok, and B. Goswami, 2015: Drying of Indian subcontinent by rapid Indian Ocean warming and a weakening land-sea thermal gradient. *Nature communications*, **6**.

Roy, S. S., and Coauthors, 2007: Impacts of the agricultural Green Revolution–induced land use changes on air temperatures in India. *Journal of Geophysical Research: Atmospheres*, **112**.

Saha, S. K., P. A. Dirmeyer, and T. N. Chase, 2016: Investigating the impact of land-use land-cover change on Indian summer monsoon daily rainfall and temperature during 1951-2005 using a regional climate model. *Hydrology and Earth System Sciences*, **20,** 1765.

Saha, S. K., K. Sujith, S. Pokhrel, H. S. Chaudhari, and A. Hazra, 2015: Predictability of global monsoon rainfall in NCEP CFSv2. *Climate Dynamics***,** 1-23.

Sailor, D. J., 1995: Simulated urban climate response to modifications in surface albedo and vegetative cover. *Journal of applied meteorology*, **34,** 1694-1704.

Sathaye, J., P. Shukla, and N. Ravindranath, 2006: Climate change, sustainable development and India: Global and national concerns. *CURRENT SCIENCE-BANGALORE-*, **90,** 314.

Saxena, S., K. Sharma, and B. Sharma, 1997: Rehabilitation of mined wastelands in Indian arid ecosystem. *Desertification Control in the Arid Ecosystem of India for Sustainable Development***,** 334-341.

Schneider, U. A., and Coauthors, 2011: Impacts of population growth, economic development, and technical change on global food production and consumption. *Agricultural Systems*, **104,** 204-215.

Seto, K. C., R. Sánchez-Rodríguez, and M. Fragkias, 2010: The new geography of contemporary urbanization and the environment. *Annual review of environment and resources*, **35,** 167-194.

Shastri, H., S. Paul, S. Ghosh, and S. Karmakar, 2015: Impacts of urbanization on Indian summer monsoon rainfall extremes. *Journal of Geophysical Research: Atmospheres*, **120,** 496-516.

Shepherd, J. M., 2005: A review of current investigations of urban-induced rainfall and recommendations for the future. *Earth Interactions*, **9,** 1-27.

Singh, R., S. Oza, and M. Pandya, 2006: Observing long-term changes in rice phenology using NOAA-AVHRR and DMSP-SSM/I satellite sensor measurements in Punjab, India. *CURRENT SCIENCE-BANGALORE-*, **91,** 1217.

Stonestrom, D. A., B. R. Scanlon, and L. Zhang, 2009: Introduction to special section on impacts of land use change on water resources. *Water resources research*, **45**.

Subramanian, S., S. Gopalakrishnan, G. Halliwell, and D. Niyogi, 2014: Idealized Study of Land Surface Impacts on TC Intensity Predictions Using the HWRF Modeling System. 15A.8A presented at 31st Conference on Hurricanes and Tropical Meteorology March 30-April 04, 2014.

Takata, K., K. Saito, and T. Yasunari, 2009: Changes in the Asian monsoon climate during 1700–1850 induced by preindustrial cultivation. *Proceedings of the National Academy of Sciences*, **106,** 9586-9589.

Tian, H., K. Banger, T. Bo, and V. K. Dadhwal, 2014: History of land use in India during 1880–2010: Large-scale land transformations reconstructed from satellite data and historical archives. *Global and Planetary Change*, **121,** 78-88.

UN-HABITAT, 2016: World Cities Report: Urbanization and Development – Emerging Futures, UN Habitat, 262pp.

Unnikrishnan, C., M. Rajeevan, S. V. B. Rao, and M. Kumar, 2013: Development of a high resolution land surface dataset for the South Asian monsoon region. *Current Science*, **105,** 1235-1246.

Valentin, C., and Coauthors, 2008: Runoff and sediment losses from 27 upland catchments in Southeast Asia: Impact of rapid land use changes and conservation practices. *Agriculture, Ecosystems & Environment*, **128,** 225-238.

Walsh, C. J., 2000: Urban impacts on the ecology of receiving waters: a framework for assessment, conservation and restoration. *Hydrobiologia*, **431,** 107-114.

Yang, G., L. C. Bowling, K. A. Cherkauer, B. C. Pijanowski, and D. Niyogi, 2010: Hydroclimatic response of watersheds to urban intensity: an observational and modeling-based analysis for the White River Basin, Indiana. *Journal of Hydrometeorology*, **11,** 122-138.

Yang, L., F. Tian, and D. Niyogi, 2015: A need to revisit hydrologic responses to urbanization by incorporating the feedback on spatial rainfall patterns. *Urban Climate*, **12,** 128-140.

Zheng, Y., A. Kumar, and D. Niyogi, 2015: Impacts of land–atmosphere coupling on regional rainfall and convection. *Climate Dynamics*, **44,** 2383-2409.

Zhong, S., and J. Doran, 1995: A modeling study of the effects of inhomogeneous surface fluxes on boundary-layer properties. *Journal of the atmospheric sciences*, **52,** 3129-3142.

Zhou, L., and Coauthors, 2004: Evidence for a significant urbanization effect on climate in China. *Proceedings of the National Academy of Sciences of the United States of America*, **101,** 9540-9544.

VITA

VITA

SUBASHINI SUBRAMANIAN

EDUCATION

Purdue University West Lafayette, IN
- Ph.D. Atmospheric Science December 2016
- Dissertation: Impact of Antecedent Land Surface Conditions on Post Landfall Characteristics of Tropical Cyclones
- **Awards & Honors:** NOAA/ DTC Visiting Fellow • NSF/ NOAA visiting scientist award • Young Scientist award to attend Indo – US Advanced Training and Workshop on Tropical Cyclones and Data Assimilation (India)

University of Madras (Madras Christian College) Chennai (India)
- M.Sc. in Physics May 2010
- Thesis: Wind Tunnel Studies to Understand the Impact of Horizontal Electric Fields on Cloud Droplet Break-up
- **Award & Honors:** 1st Class with Distinction • Summer and Winter Research Fellow

University of Madras (Women's Christian College) Chennai (India)
- B.Sc. in Physics; Minor in Chemistry and Mathematics May 2006
- **Awards & Honors:** 1st Class with Distinction

RESEARCH EXPERIENCE

Purdue University **West Lafayette, IN**
Ph.D. Research Assistant at Indiana State Climate Office Aug 2011 – present
- Investigating how land surface affects hurricanes and implementing techniques to improve hurricane track, intensity and rainfall predictions in hurricane models.
- Exploring how land use land cover change affects large scale and meso scale weather.
- On-going collaborations with scientists and research teams from national labs such as NOAA, NCEP, NCAR, Space Application Center (ISRO, India) and Indian Institute of Technology (IIT Delhi/ Bhubaneshwar)

Developmental Testbed Center Visiting Fellow (Boulder, CO) Jul 2016- Jun 2017
- Awarded an invited grant to implement hurricane land fall capability in idealized version of HWRF.
- Model will be available in the public domain for assimilation into research community and related businesses.

NSF/NOAA Visiting Scientist (College Park, MD) Oct 2014 – present

- Awarded the first ever NSF/ NOAA funding for Ph.D. students to work in operational environment.
- Improved hurricane forecasts by implementing a new land physics within the operational hurricane forecast model.
- Enhanced flood prediction and a risk assessment for hurricane affected areas by implementing new method in the operational hurricane model.

Indian Institute of Tropical Meteorology **Pune (India)**
Research Fellow May – Dec 2009

- Won a competitive fellowship jointly awarded by Indian Academy of Sciences, Indian National Science Academy and The National Academy of Sciences in India.
- Studied the effect of pollutants on cloud droplets in thunderstorms that led to a peer reviewed publication.

WORK EXPERIENCE

Krannert School of Business (Purdue University) West Lafayette, IN
Experiential Learning Initiative – Consultant Pioneer Oil Company Jan–May 2016

- Designed and developed a Monte Carlo based financial tool for Pioneer Oil to assess the financial viability of initiating chemical Enhanced Oil Recovery (cEOR) over the Illinois oil basin.
- This tool also assists in price negotiation and quantization of risk for a project.

Kuiper Research & Educational Services Pvt. Ltd Bangalore (India)
Scientific Officer – Academics Oct 2010 – May 2011

- Initiated redesign of high school science curriculum with do-it-yourself experiments and developed activity based programs to supplement textbooks which were adopted by several schools in Bangalore and Hyderabad.
- Engaged in Science Outreach in astronomy and space science. Promoted science education and tourism.

Wipro Technologies Chennai (India)
Student – Computer Applications Oct 2006 – May 2008

- Managed a team to support a mobile auditing application of Johnson Diversey Inc., that had over 500 end users.
- Selected to attend training in Racine, Wisconsin (USA) to develop and manage mobile applications.
- Studied Point of Sale systems for Wipro's Retail IT Solutions division.

TEACHING EXPERIENCE

Purdue University West Lafayette, IN
Teaching Assistant – Physics of Climate Jan – May 2014

- Instructed weekly review sessions and hands-on lab sessions for 25 students. Graded 3 exams and 8 lab exercises.
- Received 4.5/5 for effective presentation and accessibility in student evaluation.

Women's Christian College Chennai (India)
Teaching Associate July – Oct 2010

- Courses: Electricity and Magnetism, Probability & Statistics, Physics of Sound
- Designed the course curriculum and mid semester exams for all the 3 courses.
- Instructed 3 courses with 30 students each on basic concepts in undergraduate level physics.

TEAMWORK & LEADERSHIP EXPERIENCE

Madras Christian College Chennai (India)
Chairperson - Physics Society July 2009 – Apr 2010

- Revived a 5-part lecture series named 'Vistas in Physics' to engage students on the latest avenues in physics.
- Organized an annual physics conference for students to share and exchange ideas. The conference was extremely successful and saw participants from physics departments across the country.

Bhumi –NPO/ NGO Bangalore (India)
Lead Volunteer Oct 2010 – May 2011

- Organized night sky observations and activity based programs to encourage science education for children through Bhumi's "Little Einsteins" program.
- As a team, raised $2000 to install a small community center in Bangalore with computers, books and other learning material to spread computer literacy among under privileged students in the society.

PRODUCTS

- Landfalling capability in Idealized HWRF framework – Implemented at DTC. Release Oct 2016
- HWRF coupled Streamflow model – NCEP/ EMC.

PUBLICATIONS

- Bhalwankar R, **Subramanian S**, and AK Kamra (2014) Laboratory simulation of spontaneous breakup of polluted water drops in the horizontal electric field. Journal of Atmospheric and Solar-Terrestrial Physics: 147-152.

- **Subramanian S**, Gopalakrishnan S, Tuleya R, and Niyogi D (2016) Impact of Antecedent Land State on Post Landfall Tropical Cyclone Sustenance. Geophysical Research Letters: (In Revision)
- **Subramanian S**, Tallapragada V, Ek MB, Gopalakrishnan S, Marks F and Niyogi D (2016) Impact of Improved Land Surface Representation on Hurricane Rainfall. Monthly Weather Review (Manuscript in submission)
- **Subramanian S**, Xia Y, Yihua Wu Y, Ek MB, Tallapragada V and Niyogi D (2016) Development and Application of HWRF coupled River Routing Model. (2016) Journal of Hydrometeorology (Manuscript in submission)

BOOK CHAPTERS

- Niyogi D, **Subramanian S**, and Osuri K (2016) The Role of Land Surface Processes on Tropical Cyclones: Introduction to Land Surface Models. Advanced Numerical Modeling and Data Assimilation Techniques for Tropical Cyclone Predictions, Capital Publishing Co., India and Springer, Germany
- Niyogi D, Osuri K and **Subramanian S** (2016) The Role of Land-Surface Processes on Extreme Weather Events: Land Data Assimilation. Advanced Numerical Modeling and Data Assimilation Techniques for Tropical Cyclone Predictions, Capital Publishing Co., India and Springer, Germany
- Niyogi D, **Subramanian S**, Mohanty UC, Osuri K, Kishtawal CM, Ghosh S, Nair US, Ek M and Rajeevan M (2016) Perspectives on the Impact of Land Cover and Land Use Change on the Indian Monsoon Region Hydroclimate

CONFERENCE POSTERS & PROCEEDINGS

- **Subramanian S**, Xia Y, Wu Y, Ek MB, Tallapragada V, and Niyogi D (2016) Impact of improved initial land surface conditions on HWRF simulations and HWRF coupled streamflow routing model. 14B.4 presented at 32st Conference on Hurricanes and Tropical Meteorology, San Juan, PR.
- **Subramanian S**, Gopalakrishnan S, Halliwell G, and Niyogi D (2014) Idealized Study of Land Surface Impacts on Tropical Cyclone Intensity Predictions Using the HWRF Modeling System. 15A.8A presented at 31st Conference on Hurricanes and Tropical Meteorology, San Diego, CA.
- **Subramanian S**, Gopalakrishnan S, Niyogi D, and Marks Jr. F (2012) Effect of Land and its Surface Characteristics on Tropical Cyclone Intensity and Structure – An idealized study using HWRF. A41E-0033 presented at 2012 Fall Meeting, AGU, San Francisco, CA.
- **Subramanian S**, Kumar A, Niyogi D (2012) Impact of Reanalysis Forcing Data – NCEP-FNL, NASA-MERRA and ECMWF-ERA Interim on Tropical Cyclone Forecasts: An Analysis over the North Indian Ocean, UA-36 presented at 4th WCRP International Conference on Reanalysis, Silver Spring, MD.